



รายงานวิจัยฉบับสมบูรณ์

โครงการ การพัฒนากระบวนการปรับปรุงคุณภาพพลังงาน เชื้อเพลิงจากสารชีวมวลด้วยตัวเร่งปฏิกิริยาซีโอไลต์นาโนชีท

> โดย ดร. จุฬารัตน์ วัฒนกิจ สถาบันวิทยสิริเมธี

เดือน ปี ที่เสร็จโครงการ กุมภาพันธ์ 2561

สัญญาเลขที่ MRG5980114

รายงานวิจัยฉบับสมบูรณ์

โครงการ การพัฒนากระบวนการปรับปรุงคุณภาพพลังงาน เชื้อเพลิงจากสารชีวมวลด้วยตัวเร่งปฏิกิริยาซีโอไลต์นาโนชีท

> ผู้วิจัยดร. จุฬารัตน์ วัฒนกิจ สังกัด สำนักวิชาวิทยาการพลังงาน สถาบันวิทยสิริเมธี

สนับสนุนโดยสำนักงานกองทุนสนับสนุนการวิจัยและ ต้นสังกัด

(ความเห็นในรายงานนี้เป็นของผู้วิจัย สกว. และต้นสังกัดไม่ จำเป็นต้องเห็นด้วยเสมอไป)

เอกสารแนบหมายเลข 2 รหัสโครงการ : MRG5980114	
ชื่อโครงการ :การพัฒนากระบวนการปรับปรุงคุณภาพพลังงานเชื้อเพลิงจากสารชีวมวล ด้วยตัวเร่งปฏิกิริยาซีโอไลต์นาโนชีท	l
ชื่อหักวิจัย และสถาบัน : ดร. จุฬารัตน์ วัฒนกิจ สังกัด สำหักวิชาวิทยาการพลังงางสถาบันวิทยสิริเมธี	И
E-mail Address : chularat.w@vistec.ac.th	
Project Period : 2 킵	
Keywords: Chemistry/ Heterogeneous catalysis/Bio-oil upgrading/Hierarchical zeolites/Nanosheets	

Output จากโครงการวิจัยที่ได้รับทุนจาก สกว

- 1. ผลงานตีพิมพ์ในวารสารวิชาการนานาชาติ (ระบุชื่อผู้แต่ง ชื่อเรื่อง ชื่อวารสาร ปี เล่มที่ เลขที่ และหน้า) หรือผลงานตามที่คาดไว้ในสัญญาโครงการ
 - Wattanakit, C*.; Yutthalekha, T.; Assavapanumat, S.; Lapeyre, V.; Kuhn, A.*, "Pulsed electroconversion for highly selective enantiomer synthesis", Nature Communications, 2017, 8:2087, doi: 10.1038/s41467-017-02190-z.
 - Yutthalekha, T.; Suttipat, D.; Salakhum, S.; Thivasasith, A.; Nokbin, S.; Limtrakul J.; Wattanakit, C.*, "Aldol condensation of biomass-derived platform molecules over amine-grafted hierarchical FAU-type zeolite nanosheets featuring basic sites", Chemical Communications, 2017, 53, 12185—12188 (Back cover page).
 - 3. Salakhum, S.; Yutthalekha, T.; Chareonpanich, M.; Limtrakul J.; **Wattanakit, C.***, "Synthesis of hierarchical faujasite nanosheets from corn cob ash-derived nanosilica as efficient catalysts for hydrogenation of lignin-derived alkylphenols", Microporous and Mesoporous Materials, 2018, 258, 141-150.
 - Wattanakit, C.*, "Chiral metals as electrodes", Current Opinion in Electrochemistry, 2017, 7:54–60.
 - Rodponthukwaji, K.; Wattanakit, C.*; Yutthalekha, T.; Assavapanumat, S.; Warakulwit, C.; Wannapakdee, W.; Limtrakul, J., "Catalytic upgrading of carboxylic acids as bio-oil models over hierarchical ZSM-5 obtained via an organosilane approach", RSC Advances, 2017, 7, 35581-35589.
 - 6. Yutthalekha, T.; **Wattanakit, C.**; Warakulwit, C.; Wannapakdee, W.; Rodponthukwaji, K.; Witoon, T.; Limtrakul, J.*, "Hierarchical FAU-type zeolite nanosheets as green and sustainable catalysts for Benzylation of Toluene", Journal of Cleaner Production, 2017, 142 (3), 1244-1251.

2. การนำผลงานวิจัยไปใช้ประโยชน์

- เชิงวิชาการ

ผลที่ได้จากการศึกษาของโครงการ "การพัฒนากระบวนการปรับปรุงคุณภาพ พลังงานเชื้อเพลิงจากสารชีวมวลด้วยตัวเร่งปฏิกิริยาซีโอไลต์นาโนชีท" สามารถนำเสนอ ได้สองลักษณะคือ 1. การเตรียมตัวเร่งปฏิกิริยาซีโอไลต์ที่มีโครงสร้างแบบนาโนชีท เพื่อ ใช้เป็นตัวเร่งปฏิกิริยาเคมีที่สำคัญ และ 2. การศึกษากระบวนการเร่งปฏิกิริยาของซี โอไลต์ที่ได้ทำการเตรียมขึ้นและพร้อมทั้งศึกษากลไกการเร่งปฏิกิริยาที่เกิดขึ้น จาก ผลงานวิจัยที่ได้ทำให้มีการนำองค์ความรู้ที่ได้จากพัฒนาตัวเร่งปฏิกิริยาซีโอไลต์นาโน ซีทดังกล่าวไปใช้ต่อยอดในการศึกษาเชิงลึกเกี่ยวกับความสัมพันธ์ทางคุณสมบัติทาง เคมีและกายภาพที่มีผลต่อกลไกการเกิดปฏิกิริยาเคมีในระดับโมเลกุล รวมทั้งความรู้

ดังกล่าวสามารถช่วยต่อยอดให้กับทั้งทางภาคการศึกษาและภาคอุตสาหกรรม กล่าวคือ สำหรับภาคการศึกษาได้มีการเชื่อมโยงกับสถาบันการศึกษาเช่น Department of Chemical Engineering and Chemistry, Eindhoven University of Technology (TU/e) ประเทศเนเธอร์แลนด์ ได้มีความสนใจนำตัวเร่งปฏิกิริยาที่ได้พัฒนาขึ้น ไปศึกษา ในเชิงโครงสร้างเชิงลึกเพื่อต่อยอดความรู้ต่อไป นอกจากนี้ในภาคอุตสาหรกรรมเคมีได้ นำความรู้พื้นฐานในการพัฒนาตัวเร่งปฏิกิริยาดังกล่าวเพื่อนำมาใช้ในการต่อยอดการ พัฒนาตัวเร่งปฏิกิริยาเพื่อใช้ในประเทศต่อไปในภายภาคหน้า

สารบัญ

สารบัญ	หน้า
กิตติกรรมประกาศ	1
บทคัดย่อ	2
บทนำ	4
วัตถุประสงค์ของโครงการและแผนดำเนินการวิจัย	6
เอกสารและงานวิจัยที่เกี่ยวข้อง	8
ระเบียบวิธีวิจัย	11
ผลการวิจัย	12
สรุปและวิจารณ์ผลการวิจัย	30
เอกสารอ้างอิง	31
ภาคผนวก	36

กิตติกรรมประกาศ

เนื่องด้วยโครงการวิจัยนี้ "โครงการ การพัฒนากระบวนการปรับปรุงคุณภาพพลังงานเชื้อเพลิง จากสารชีวมวลด้วยตัวเร่งปฏิกิริยาซีโอไลต์นาโนซีท" ได้รับการสนับสนุนจากสำนักงานกองทุน สนับสนุนการวิจัย (สกว) และสำนักงานคณะกรรมการการอุดมศึกษา (สกอ) เป็นอย่างดี ดิฉัน ขอขอบคุณในความกรุณาสำหรับทุนสนับสนุนดังกล่าวซึ่งทำให้งานวิจัยนี้สำเร็จลุล่วงได้เป็น อย่างดี นอกจากนี้ขอขอบคุณสำนักวิชาวิทยาการพลังงาน และ Frontier Research Center (FRC) สถาบันวิทยสิริเมธี สำหรับการสนับสนุนเกี่ยวกับเครื่องมือวิจัยที่เกี่ยวข้อง และ ขอขอบคุณ ศาสตราจารย์จำรัส ลิ้มตระกูล ที่ปรึกษานักวิจัย สำหรับการให้คำปรึกษาและ คำแนะนำในการทำวิจัยมาโดยตลอด

จุฬารัตน์ วัฒนกิจ

บทคัดย่อ

การพัฒนาแหล่งพลังงานเชื้อเพลิงทางเลือกและสารเคมีที่สำคัญจากสารชีวมวลและ อนุพันธ์ชีวมวล มีความสำคัญอย่างมากต่อประเทศ ทั้งทางภาคการศึกษา ชุมชน และ ภาคอุตสาหกรรม ในปัจจุบันนี้มีการพัฒนางานวิจัยต่อยอดเกี่ยวข้องกับการปรับปรุงคุณภาพ ของสารที่ได้จากชีวมวลและสารอนุพันธ์ชีวมวลได้หลายกระบวนการ เช่น การใช้วิธีทาง กายภาพ และทางเคมี โดยวิธีหนึ่งที่มีประสิทธิภาพสูงและเป็นที่นิยมคือ เทคนิคการเพิ่ม ประสิทธิภาพของสารดังกล่าวโดยใช้ตัวเร่งปฏิกิริยาเคมี (Catalytic upgrading processes) ซึ่ง กระบวนการนี้สามารถถูกเร่งปฏิกิริยาได้ด้วยตัวเร่งปฏิกิริยหลายประเภท เช่น ซีโอไลต์ (Zeolite) โลหะบนตัวซัพพอร์ต (Metal supported on solid support) เป็นตัน

ซีโอไลต์เป็นตัวเร่งปฏิกิริยาวิวิธพันธุ์ ซึ่งเป็นสารประกอบชนิดอะลูมิโนซิลิเกตที่มี ความสามารถในการเร่งปฏิกิริยาได้หลากหลาย รวมถึงการนำมาประยุกต์ใช้ในการเร่งปฏิกิริยา สำหรับกระบวนการปรับปรุงคุณภาพของสารชีวมวลและอนุพันธ์ชีวมวล อย่างไรก็ตามการนำซี โอไลต์แบบดั้งเดิมมาใช้งานนี้ มักมีข้อจำกัดหลายประการ เช่น ไม่สามารถนำมาเร่งปฏิกิริยาที่ เกี่ยวข้องกับสารตั้งต้นขนาดใหญ่ได้ และบ่อยครั้งมักพบการเสื่อมสภาพอย่างรวดเร็วของตัวเร่ง ปฏิกิริยาดังกล่าว ดังนั้นการพัฒนาคุณภาพของตัวเร่งปฏิกิริยาดังกล่าวจึงเป็นหัวข้อหนึ่งที่มี ความน่าสนใจ

การปรับปรุงคุณภาพของตัวเร่งปฏิกิริยาซีโอไลต์สามารถทำได้หลายวิธี เช่น การ สังเคราะห์ซีโอไลต์ที่มีผลึกขนาดเล็ก และการเติมรูพรุนขนากลางและขนาดใหญ่เข้าไปใน โครงสร้างของซีโอไลต์ซึ่งโดยทั่วไปประกอบไปด้วยรูพรุนขนาดเล็ก ดังนั้นซีโอไลต์ที่ได้จึง ประกอบไปด้วยรูพรุนขนาดเล็ก และขนาดกลาง เป็นต้น ดังนั้นซีไอไลต์ใหม่ที่ได้รับการพัฒนาขึ้น จึงมีชื่อเรียกว่า Hierarchical zeolite หรือซีโอไลต์ที่ ประกอบไปด้วยรูพรุนลำดับขั้น อย่างไรก็ตามในการพัฒนาตัวเร่งปฏิกิริยาดังกล่าวเพื่อมาใช้งาน จริงโดยเฉพาะสำหรับการนำมาใช้เป็นตัวเร่งปฏิกิริยาที่สำคัญของกระบวนการปรับปรุงคุณภาพ ของสารที่ได้จากชีวมวลและสารอนุพันธ์ชีวมวลยังมีข้อจำกัด ดังนั้นในงานวิจัยนี้จึงมีความ มุ่งเน้นที่จะทำการพัฒนากระบวนการปรับปรุงคุณภาพของสารดังกล่าวโดยผ่านตัวเร่งปฏิกิริยา ซีโอไลต์ที่ประกอบไปด้วยรูพรุนลำดับขั้นที่มีโครงสร้างแบบนาโนซีท

กล่าวโดยสรุปได้ว่าโครงการวิจัยนี้ส่งผลกระทบต่อการพัฒนาประเทศทั้งในเชิง การศึกษาและทางพาณิชย์ กล่าวคือทำให้สามารถพัฒนาองค์ความรู้พื้นฐานสำหรับการ สังเคราะห์ตัวเร่งปฏิกิริยาที่มีประสิทธิภาพสูงสำหรับการนำมาใช้ประโยชน์ได้จริงในกระบวนการ ปรับปรุงคุณภาพสารชีวมวลและอนุพันธ์ชีวมวลต่อไป

Abstract

Bio-oils are promising alternative energy sources replacing to fossil fuels. There are many possible ways to produce the bio-oils. One possibility for the production of bio-oils is the catalytic pyrolysis of biomass. Lignin is one of the most abundant components of a biomass and the major by-product from the paper industry. It is also available in massive quantities from biomass-to-ethanol processes and other bio-refineries. However, the produced bio-oils from the lignin compose of a high oxygen content (20-50 wt%) and acidity (pH=2.5-3), resulting in the poor quality of produced fuels derived from bio-oils due to low thermal and chemical stabilities, low heating value, high corrosiveness and immiscibility with hydrocarbon fuels. To improve the quality of fuels and chemicals derived from bio-oils, the bio-oil has been predominantly performed via catalytic upgrading processes by one of two following approaches: (i) the hydrodeoxygenation (HDO); (ii) zeolite-catalyzed processes to remove oxygen components. Nevertheless, the most important problem is a very short catalyst lifetime, for example, when zeolites are used as catalysts. This proposal will focus on the development of novel hierarchical zeolites acting as bifunctional catalysts for the bio-oil upgrading processes via hydrodeoxygenation (HDO) and esterification. The research scope of this work is the design of new bifunctional hierarchical zeolites for the catalytic upgrading of bio-oils to transportation fuels. The efficiency of the fuels would be improved by catalytic upgrading processes using the novel designed hierarchical zeolites. Furthermore, the novel synthesis will be optimized in terms of cost, time, and efficiency for applying in the large-scale synthesis. The development of such bio-fuel and fine chemical productions from a biomass will deliver the new basic knowledge, leading to the utilization in the petroleum industry in future for the production of alternative energies and fine chemicals from biomass.

บทน้ำ

การพัฒนาแหล่งพลังงานเชื้อเพลิงทางเลือกจากสารชีวมวล (Biomass) มีความสำคัญ อย่างมากต่อประเทศ ทั้งทางภาคการศึกษา ชุมชน และภาคอุตสาหกรรม โดยทั่วไปมีการนำ เทคโนโลยีหลากหลายมาประยุกต์ใช้ในการผลิตแหล่งพลังงานเชื้อเพลิงทางเลือก เช่น การ ผลิตใบโอเอทานอล และใบโอดีเซล เป็นต้น ลิกโนเซลลูโลสยังเป็นอีกหนึ่งแหล่งวัตถุดิบจาก ธรรมชาติที่สามารถนำมาใช้ในการผลิตพลังงานเชื้อเพลิงทางเลือกได้อีกด้วย โดยที่ลิกโน เซลลุโลสเป็นสารประกอบเชิงซ้อนของลิกนิน เฮมิเซลลุโลส และเซลลุโลส ซึ่งเป็นองค์ประกอบ หลักของผนังเซลล์พืช ซึ่งการนำสารประกอบลิกโนเซลลูโลสนี้มาใช้เป็นแหล่งพลังงานเชื้อเพลิง ทดแทนนี้นับว่ามีข้อดี เนื่องจากเป็นวัตถุดิบที่หาได้ง่าย และยังเป็นวัตถุดิบที่ได้มาจากของเสีย ของอุตสาหกรรมการผลิตกระดาษ และยังเป็นการช่วยลดปัญหาการนำพืชอาหารที่ใช้บริโภคไป ใช้ในการผลิตพลังงานเชื้อเพลิงทดแทน โดยทั่วไปการแปลงสารชีวมวลของสารประกอบลิกโน เซลลูโลสสามารถทำผ่านกระบวนการเคมีความร้อนที่เรียกว่า ไพโรไลซิส จนได้เป็นน้ำมันที่ เรียกว่าไบโอออยล์ (Bio oil) ในการนำไบโอออยล์ดังกล่าวไปใช้ประโยชน์เป็นแหล่งพลังงาน เชื้อเพลิงทดแทนนั้น จำเป็นต้องผ่านกระบวนการปรับปรุงคุณภาพของไบโอออยล์ เนื่องจากไบ โอออยล์ที่ได้จากกระบวนการดังกล่าวมีสารประกอบของออกซิเจน (Oxygenate Compound) เป็นส่วนประกอบอยู่ในปริมาณมาก (20-50 เปอร์เซ็นต์โดยน้ำหนัก) ซึ่งทำให้มีคุณสมบัติที่ไม่ เหมาะสมสำหรับการนำไปใช้เป็นแหล่งพลังงานเชื้อเพลิง เช่น มีความเป็นกรดสูง มีค่าความร้อน ของการเผาใหม้ต่ำ และมีความหนืดสูง เป็นต้น

ในปัจจุบันนี้สามารถทำการปรับปรุงคุณภาพของไบโอออยล์ได้หลายวิธี เช่น การใช้วิธี ทางกายภาพ และทางเคมี โดยวิธีหนึ่งที่มีประสิทธิภาพสูงและเป็นที่นิยมคือ เทคนิคการเพิ่ม ประสิทธิภาพของไบโอออยล์โดยใช้ตัวเร่งปฏิกิริยา (Catalytic upgrading processes) ซึ่ง กระบวนการนี้สามารถถูกเร่งปฏิกิริยาได้ด้วยตัวเร่งปฏิกิริยหลายประเภท เช่น ซีโอไลต์ (Zeolite) โลหะบนตัวซัพพอร์ต (Metal supported on solid support) เป็นต้น

ซีโอไลต์เป็นตัวเร่งปฏิกิริยาวิวิธพันธุ์ ซึ่งเป็นสารประกอบชนิดอะลูมิโนซิลิเกตที่มี ความสามารถในการเร่งปฏิกิริยาได้หลากหลาย รวมถึงการนำมาประยุกต์ใช้ในการเร่งปฏิกิริยา สำหรับกระบวนการปรับปรุงคุณภาพของไบโอออย์ อย่างไรก็ตามการนำซีโอไลต์แบบดั้งเดิมมา ใช้งานนี้ มักมีข้อจำกัดหลายประการ เช่น ไม่สามารถนำมาเร่งปฏิกิริยาที่เกี่ยวข้องกับสารตั้งต้น ขนาดใหญ่ของไบโอออยล์ได้ และบ่อยครั้งมักพบการเสื่อมสภาพอย่างรวดเร็วของตัวเร่ง ปฏิกิริยาดังกล่าว ดังนั้นการพัฒนาคุณภาพของตัวเร่งปฏิกิริยาดังกล่าวจึงเป็นหัวข้อหนึ่งที่มี ความน่าสนใจ

การปรับปรุงคุณภาพของตัวเร่งปฏิกิริยาซีโอไลต์สามารถทำได้หลายวิธี เช่น การ สังเคราะห์ซีโอไลต์ที่มีผลึกขนาดเล็ก และการเติมรูพรุนขนากลางและขนาดใหญ่เข้าไปใน โครงสร้างของซีโอไลต์ ซึ่งโดยทั่วไปประกอบไปด้วยรูพรุนขนาดเล็ก ดังนั้นซีโอไลต์ที่ได้จึง ประกอบไปด้วยรูพรุนหลายขนาด เช่น ประกอบไปด้วยรูพรุนขนาดเล็ก และขนาดกลาง เป็นต้น ดังนั้นซีไอไลต์ใหม่ที่ได้รับการพัฒนาขึ้น จึงมีชื่อเรียกว่า Hierarchical zeolite หรือซีโอไลต์ที่ ประกอบไปด้วยรูพรุนลำดับขั้น อย่างไรก็ตามในการพัฒนาตัวเร่งปฏิกิริยาดังกล่าวเพื่อมาใช้งาน จริง โดยเฉพาะสำหรับการนำมาใช้เป็นตัวเร่งปฏิกิริยาที่สำคัญของกระบวนการปรับปรุงคุณภาพ ของไบโอออยล์ยังมีข้อจำกัด ดังนั้นในงานวิจัยนี้จึงมีความมุ่งเน้นที่จะทำการพัฒนากระบวนการ ปรับปรุงคุณภาพของไบโอออยล์โดยผ่านตัวเร่งปฏิกิริยาซีโอไลต์ที่ประกอบไปด้วยรูพรุนลำดับ ขั้น ที่มีโครงสร้างแบบนาโนซีท

กล่าวโดยสรุปได้ว่าโครงการวิจัยนี้ส่งผลกระทบต่อการพัฒนาประเทศทั้งในเชิงการศึกษา
และทางพาณิชย์ทั้งทางตรงและทางอ้อม ในทางตรงคือทำให้สามารถพัฒนาเทคโนโลยีการ
สังเคราะห์ตัวเร่งปฏิกิริยาที่มีประสิทธิภาพสูงสำหรับการนำมาใช้ประโยชน์ได้จริงในกระบวนการ
ปรับปรุงคุณภาพไบโอออยล์ นอกจากนี้องค์ความรู้ใหม่ที่ได้จากโครงการวิจัยนี้ ผู้วิจัยเห็น
ศักยภาพอย่างชัดเจนในการจดสิทธิบัตร และการตีพิมพ์เผยแพร่ในวารสารนานาชาติ ส่วน
ประโยชน์ในทางอ้อมคือโครงการวิจัยนี้สามารถสนับสนุนการผลิตบุคลากรที่มีความรู้
ความสามารถในด้านนาโนเทคโนโลยี เน้นทางด้านการพัฒนาตัวเร่งปฏิกิริยาสำหรับการนำมา
ประยุกต์ใช้ในการผลิตแหล่งพลังงานทดแทน และเพิ่มขีดความสามารถในการแข่งขันด้าน
งานวิจัยทางด้านนาโนเทคโนโลยีที่เกี่ยวกับการพัฒนาตัวเร่งปฏิกิริยาได้เป็นอย่างดี

วัตถุประสงค์ของโครงการและแผนดำเนินการวิจัย

วัตถุประสงค์ของโครงการ

- 1. เพื่อพัฒนากระบวนการผลิตแหล่งพลังงานเชื้อเพลิงทางเลือกจากแหล่งวัตถุดิบชีวมวล
- 2. เพื่อพัฒนาเทคโนโลยีสำหรับกระบวนการปรับปรุงคุณภาพของไบโอออยล์ด้วยเทคนิคทาง เคมี
- 3. เพื่อพัฒนาตัวเร่งปฏิกิริยาเคมีที่ประกอบไปด้วยรูพรุนลำดับขั้นที่มีประสิทธิภาพสูง
- 4. เพื่อสร้างองค์ความรู้ใหม่สำหรับการออกแบบตัวเร่งปฏิกิริยา และกระบวนการปรับปรุง คุณภาพของไบโอออยล์
- 5. เพื่อผลิตบุคลากรที่มีความรู้ความสามารถในด้านนาโนเทคโนโลยี และเพิ่มขีด ความสามารถในการแข่งขันด้านงานวิจัยทางด้านนาโนเทคโนโลยีที่เกี่ยวกับการพัฒนา แหล่งพลังงานทางเลือก

แผนดำเนินการวิจัย

ตารางที่ 1 แสดงแผนการดำเนินงานวิจัยตลอดโครงการ

รายละเอียด	เดือนที่				หมายเหตุ
	1-6	7-12	13-18	19-24	
1) การเตรียมตัวเร่งปฏิกิริยาซีโอไลต์ที่มี โครงสร้างแบบนาโนชีท และประกอบไป ด้วย Metallic active sites					
2) วิเคราะห์คุณสมบัติทางกายภาพและทาง เคมีของตัวเร่งปฏิกิริยาที่ได้ทำการ สังเคราะห์ขึ้น					
3) ศึกษากระบวนการเร่งปฏิกิริยาของตัวเร่ง ปฏิกิริยาที่ทำการสังเคราะห์ขึ้นสำหรับการ ปรับปรุงคุณภาพของไบโอออยล์ โดยใช้ Model reaction					
4) เตรียม Manuscript สำหรับการตีพิมพ์ใน วารสารนานาชาติ					

ตารางที่ 1 แสดงแผนการดำเนินงานวิจัยตลอดโครงการ (ต่อ)

รายละเอียด	เดือนที่				หมายเหตุ
	1-6	7-12	13-18	19-24	
5) ศึกษากระบวนการเร่งปฏิกิริยาของตัวเร่ง ปฏิกิริยาที่ทำการสังเคราะห์ขึ้นสำหรับการ ปรับปรุงคุณภาพของไบโอออยล์ โดยใช้ สารตั้งตันจาก Biomass					
6) . ศึกษากระบวนการเร่งปฏิกิริยาของตัวเร่ง ปฏิกิริยาที่ทำการสังเคราะห์ขึ้นสำหรับการ ปรับปรุงคุณภาพของไบโอออยล์ ด้วย ระเบียบวิธีการคำนวณทางเคมี คอมพิวเตอร์					
7).เตรียม Manuscript สำหรับการตีพิมพ์ใน วารสารนานาชาติ					

จากแผนการดำเนินการวิจัยได้ตั้งเป้าหมายในการทำงานวิจัยคือ การเตรียมตัวเร่ง ปฏิกิริยาซีโอไลต์ที่มีโครงสร้างแบบนาโนซีท และประกอบไปด้วย Metallic active sites รวมทั้ง วิเคราะห์คุณสมบัติทางกายภาพและทางเคมีของตัวเร่งปฏิกิริยาที่ได้ทำการสังเคราะห์ขึ้น และ ศึกษากระบวนการเร่งปฏิกิริยาของตัวเร่งปฏิกิริยาที่ทำการสังเคราะห์ขึ้นสำหรับการปรับปรุง คุณภาพของไบโอออยล์ โดยใช้ Model reaction ซึ่งปัจจุบันในกรอบแผนงานดังกล่าวได้ ดำเนินการลุล่วงเป็นอย่างดี ดังแสดงรายละเอียดได้จากผลงานที่ได้รับการตีพิมพ์ในวารสาร นานาชาติ ทั้งสิ้น 6 ผลงานดังแสดงในส่วน Output

เอกสารและงานวิจัยที่เกี่ยวข้อง

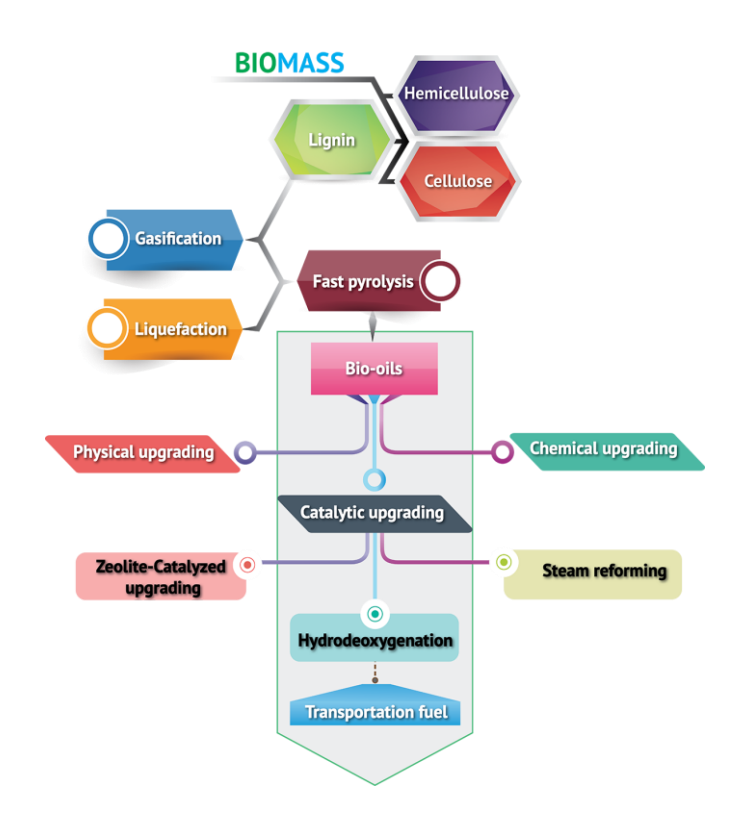
สารประกอบซีโอไลต์เป็นสารประกอบอะลูมิโนซิลิเกตที่ประกอบไปด้วยซิลิกาหรืออะลูมิ นาที่เป็นทรงสี่หน้ามาเชื่อมต่อกันจนได้โครงสร้างที่ประกอบไปด้วยรูพรุนจำนวนมาก โดยที่รู พรุนของซีโอไลต์มีขนาดเล็กกว่า 2 นาโนเมตร จึงจัดซีโอไลต์เป็นสารประเภทไมโครพอร์ (Microporous materials) อย่างไรก็ตามการประกอบไปด้วยรูพรุนขนาดเล็กของซีโอไลต์ส่งผล เสียในการเร่งปฏิกิริยากล่าวคือทำให้เกิดข้อจำกัดของการถ่ายโอนมวลสารของสารตั้งต้นและ ผลิตภัณฑ์ผ่านเข้าออกจากผลึกซีโอไลต์ ดังนั้นในปัจจุบันมีคณะผู้วิจัยจำนวนหนึ่งได้มีความ พยายามปรับปรุงโครงสร้างของซีโอไลต์โดยการทำเป็นนาโนซีโอไลต์ และซีโอไลต์ที่ประกอบไปด้วยรูพรุนแบบลำดับขั้น

สำหรับการสังเคราะห์นาโนซีโอไลต์สามารถทำได้ด้วย 2 เทคนิคด้วยกัน สำหรับวิธีแรก เป็นการสังเคราะห์โดยใช้สารละลายใสหรือเจลภายใต้สภาวะการทดลองที่เหมาะสมเพื่อควบคุม การเติบโตของผลึก สำหรับวิธีที่สองสามารถสังเคราะห์นาโนซีโอไลต์ได้โดยใช้สารแม่แบบ กำหนดขอบเขตของการเติบโตของผลึก สารที่ใช้เป็นสารกำหนดแม่แบบเช่น อนุภาคของ คาร์บอน คาร์บอนนาโนทิวบ์ และเครือข่ายของสารประกอบประเภทพอลิเมอร์ โดยที่สาร แม่แบบดังกล่าวสามารถทำหน้าที่กำหนดขอบเขตการโตของผลึกขนาดเล็ก และสามารถกำจัด ออกได้ง่ายภายหลังจากการสังเคราะห์นาโนซีโอไลต์โดยใช้เทคนิคการเผาภายใต้อากาศ อย่างไรก็ตามเนื่องจากข้อจำกัดของนาโนซีโอไลต์ กล่าวคือขนาดผลึกมีขนาดเล็ก ดังนั้นจึงทำให้กระบวนการแยกตัวเร่งปฏิกิริยานาโนซีโอไลต์ออกจากสารผสมหลังจากการเร่งปฏิกิริยาเคมี ทำได้ยาก

เพื่อให้การปรับปรุงคุณภาพตัวเร่งปฏิกิริยาประเภทซีโอไลต์มีประสิทธิภาพมากขึ้น นักวิจัยได้มีความพยายามพัฒนาซีโอไลต์ที่มีชื่อเรียกว่า ซีโอไลต์ที่ประกอบไปด้วยรูพรุนลำดับขั้น (Hierarchical zeolites) สำหรับการสังเคราะห์ซีโอไลต์ประเภทนี้สามารถทำได้ด้วย 2 เทคนิค คือ การปรับปรุงคุณภาพหลังการสังเคราะห์ (Post-synthesis treatment) และการสังเคราะห์โดยตรง (Direct synthesis method) สำหรับกระบวนการสังเคราะห์ด้วยการปรับปรุงคุณภาพหลังการสังเคราะห์สามารถทำได้โดยใช้วิธีดึงซิลิกาหรืออะลูมินาออกจากโครงสร้างของซีโอไลต์ดั้งเดิมโดยใช้สารละลายของกรดหรือเบสเป็นตัวช่วย สำหรับวิธีการสังเคราะห์โดยตรงทำได้โดยการใช้สารแม่แบบกำหนดโครงสร้างของรูพรุนขนาดกลางเช่น อนุภาคคาร์บอน และพอลิเมอร์ เป็นตัน

นอกจากนี้ซีโอไลต์ที่ประกอบด้วยรูพรุนลำดับขั้นที่มีโครงสร้างแบบนาโนชีทสามารถ สังเคราะห์ขึ้นได้โดยใช้สารลดแรงตึงผิว (Diquaternary ammonium-type surfactants) เป็นสาร กำหนดโครงสร้าง ในปี 2006 งานวิจัยของ Choi และคณะ (Nature, 2009, 461 246-249) ได้ ทำการศึกษาการเตรียมซีโอไลต์นาโนชีทที่มีความบางในระดับอะตอมโดยใช้สารลดแรงตึงผิว ดังกล่าว จากการศึกษาพบว่าสามารถควบคุบการเติบโตของผลึกในระนาบสองมิติได้โดยใช้หมู่ ไฮโดรโฟบิกขัดขวางการเจริญเติบโตของผลึก นอกจากนี้งานวิจัยของ Zhang และคณะ (Science, 2012, 336, 1684-1687) ได้ทำการศึกษาผลของของการเกิดซีโอไลต์นาโนชีทโดยใช้ สารเตตระบิวทิลฟอสฟอเนียมไฮดรอกไซด์ (TBPOH) เป็นตัวกำหนดโครงสร้าง จาก เอกสารอ้างอิงดังกล่าวทำให้เห็นว่ามีนักวิจัยที่ได้ให้ความสนใจในการปรับปรุงคุณภาพซีโอไลต์ นาโนชีทอย่างหลากหลาย แต่อย่างไรก็ตามยังพบข้อจำกัดในการนำซีโอไลต์ดังกล่าวมาใช้ ประโยชน์ในการเร่งปฏิกิริยาเคมี

สำหรับการประยุกต์ใช้ตัวเร่งปฏิกิริยาซีโอไลต์ในกระบวนการปรับปรุงคุณภาพไบโอ ออยล์ (Catalytic upgrading processes) ในกระบวนการเปลี่ยนแปลงสารชีวมวลสามารถทำได้ โดยผ่านกระบวนการเคมีความร้อนที่เรียกว่า ไพโรไลซิส จนได้เป็นน้ำมันที่เรียกว่าไบโอออยล์ (Bio oil) อย่างไรก็ตามไบโอออยล์ที่ได้ ยังมีข้อจำกัดในด้านประสิทธิภาพสำหรับการนำไปใช้ ประโยชน์เป็นแหล่งพลังงานเชื้อเพลิงทดแทน ซึ่งจำเป็นต้องผ่านกระบวนการปรับปรุงคุณภาพ ของไบโอออยล์ก่อนการนำไปใช้งาน โดยกระบวนการปรับปรุงคุณภาพไบโอออยล์ สามารถทำ ได้โดยใช้เทคนิคทางเคมี และเทคนิคทางกายภาพ ดังแสดงในแผนภาพที่ 1 ซึ่งกระบวนการ ปรับปรุงคุณภาพใบโอออยล์โดยใช้ตัวเร่งปฏิกิริยา (Catalytic upgrading processes) เป็น เทคนิคหนึ่งที่นิยมใช้เนื่องจากเป็นเทคนิคที่มีความจำเพาะเจาะจงสำหรับการเลือกเกิดสาร ผลิตภัณฑ์ที่ต้องการได้ โดยในกระบวนการปรับปรุงคุณภาพไบโอออยล์โดยใช้ตัวเร่งปฏิกิริยา สามารถทำได้สองวิธีด้วยกันคือ การเร่งปฏิกิริยาโดยใช้ตัวเร่งปฏิกิริยาประเภทซีโอไลต์ (Zeolite-catalyzed upgrading) และการเร่งปฏิกิริยาไฮโดรดีออกซีจีเนชัน (Hydrodeoxygenation, HDO) อย่างไรก็ตามพบปัญหาว่าคุณภาพไบโอออยล์ที่ได้จากสอง เทคนิคนี้มีคุณภาพต่ำเมื่อเทียบกับน้ำมันที่ได้จากแหล่งฟอสซิล ซึ่งในปัจจุบันได้มีการพัฒนา กระบวนการปรับปรุงคุณภาพใบโอออยส์โดยใช้ตัวเร่งปฏิกิริยาหลายวิธีด้วยกัน เช่น ในปี 2015 Wang และคณะ (ACS Catal., 2015, 5, 2727-2734) ได้ทำการศึกษาการเร่งปฏิกิริยาการ ปรับปรุงคุณภาพของใบโอออยล์โดยใช้ตัวเร่งปฏิกิริยาโลหะแพลตินัมและรูที่เนียม บนตัวซัพ พอร์ตประเภทซีโอไลต์ ซึ่งตัวเร่งปฏิกิริยานี้สามารถเพิ่มประสิทธิภาพของไบโอออยล์ได้อย่างดี เยี่ยม แม้ว่าตัวเร่งดังกล่าวจะให้ผลการเร่งปฏิกิริยาเป็นที่น่าพอใจ อย่างไรก็ตามยังคงพบปัญหา การเสื่อมสภาพอย่างรวดเร็วของตัวเร่งปฏิกิริยา ประกอบกับการเร่งปฏิกิริยาดังกล่าวอาศัย สภาวะที่รุนแรง คือใช้ความดันและอุณหภูมิสูง และยังพบว่าในการเร่งปฏิกิริยาดังกล่าวต้อง อาศัยการเติมไฮโดรเจนเพื่อช่วยในการเร่งปฏิกิริยา จึงเป็นการเพิ่มต้นทุนในกระบวนการ ดังกล่าวดังนั้นในการพัฒนางานวิจัยที่เกี่ยวกับกระบวนการปรับปรุงคุณภาพไบโอออยล์ดัวย กระบวนการที่มีประสิทธิภาพสูง ราคาถูก และมีความปลอดภัย จึงเป็นสิ่งที่น่าสนใจที่จะทำการ พัฒนาต่อไป เพื่อให้เกิดประโยชน์ในการนำไปใช้งานได้จริงในอนาคต



แผนภาพที่ 1 แสดงกระบวนการปรับปรุงคุณภาพใบโอออยล์

โดยปกติแล้วการนำตัวเร่งปฏิกิริยาซีโอไลต์มาใช้ในกระบวนการดังกล่าวพบข้อจำกัด ของการเสื่อมสภาพของตัวเร่งปฏิกิริยาเนื่องจากการเกิดการสะสมตัวของสารประกอบ ไฮโดรคาร์บอนขนาดใหญ่ งานวิจัยของ Nimmanwudipong และคณะได้ทำการศึกษาการ เปลี่ยนแปลงของสารประกอบ guaiacol บนตัวเร่งปฏิกิริยาซีโอไลต์พบว่าร้อยละการ เปลี่ยนแปลงดังกล่าวลดลงประมาณร้อยละ 50 หลังจากการเร่งปฏิกิริยาโดยใช้โลหะแพลตินัม บนซีโอไลต์ชนิด HY ไปเพียง 1 ชั่วโมง (Energy Fuels, 2011, 25, 3417–3427)

ดังนั้นในงานวิจัยนี้จึงเห็นความสำคัญในการพัฒนาตัวเร่งปฏิกิริยาซีโอไลต์ที่มี ประสิทธิภาพสูงเพื่อใช้ประโยชน์ในกระบวนที่เกี่ยวข้องกับการปรับปรุงคุณภาพใบโอออยล์ ดังนั้นในงานวิจัยนี้ได้ทำการศึกษาการเร่งปฏิกิริยาที่เกี่ยวข้องด้วยกัน 3 แนวทาง คือ การเร่ง ปฏิกิริยาสำหรับกระบวนการปรับปรุงคุณภาพของไบโอออยล์ผ่านกระบวนการ Esterification ของสารประกอบแอลกอฮอล์และกรดอินทรีย์ การเร่งปฏิกิริยาสำหรับกระบวนการปรับปรุง คุณภาพของไบโอออยล์ผ่านกระบวนการ Hydrogenation ของอนุพันธ์ของสารประกอบ Phenol ซึ่งเป็นอนุพันธ์หนึ่งที่พบมากในไบโอออยล์ และการเร่งปฏิกิริยาสำหรับกระบวนการปรับปรุง คุณภาพของไบโอออยล์ผ่านกระบวนการ Aldol condensation ของสารประกอบ Aldehyde และ Ketone

ระเบียบวิธีวิจัย

- 1. การออกแบบตัวเร่งปฏิกิริยาซีโอไลต์นาโนชีทชนิดต่างๆ เช่น FAU และ ZSM5 ด้วย เทคนิค hydrothermal processes และมีการใช้สารแม่แบบเพื่อกำหนดโครงสร้าง นอกจากนี้ยังทำการศึกษาผลของเวลาและอุณหภูมิที่ใช้ในการตกผลึก รวมถึงปริมาณ สารแม่แบบที่ใช้เพื่อกำหนดโครงสร้างนาโนชีท
- 2. ทดสอบคุณสมบัติทางเคมีและกายภาพของตัวเร่งปฏิกิริยาซีโอไลต์นาโนซีท ด้วย เทคนิค X-ray diffraction (XRD), Physisorption/Chemisorption techniques, Nuclear magnetic resonance (NMR), Fourier transform infrared (FTIR) spectroscopy, Scanning Electron Microscopy Energy Dispersive X-Ray Spectroscopy (SEMEDS), Transmission electron microscopy (TEM), elemental analysis, H₂ chemisorption และ NH₃ temperature programmed desorption (TPD)
- 3. ศึกษาคุณสมบัติการเร่งปฏิกิริยาของสารที่ทำการสังเคราะห์ขึ้นสำหรับกระบวนการ กระบวนการปรับปรุงคุณภาพพลังงานเชื้อเพลิงจากสารชีวมวล โดยผ่านกระบวนการ หลากหลาย เช่น การเร่งปฏิกิริยาสำหรับกระบวนการปรับปรุงคุณภาพของใบโอออยล์ ผ่านกระบวนการ Esterification ของสารประกอบแอลกอฮอล์และกรดอินทรีย์ การเร่ง ปฏิกิริยาสำหรับกระบวนการปรับปรุงคุณภาพของใบโอออยล์ผ่านกระบวนการ Hydrogenation ของอนุพันธ์ของสารประกอบ Phenol ซึ่งเป็นอนุพันธ์หนึ่งที่พบมาก ในไบโอออยล์ และการเร่งปฏิกิริยาสำหรับกระบวนการปรับปรุงคุณภาพของใบโอออยล์ ผ่านกระบวนการ Aldol condensation ของสารประกอบ Aldehyde และ Ketone โดย ใช้ Batch และ Fixed-bed reactor และวิเคราะห์สารองค์ประกอบด้วยเทคนิค Gas Chromatography

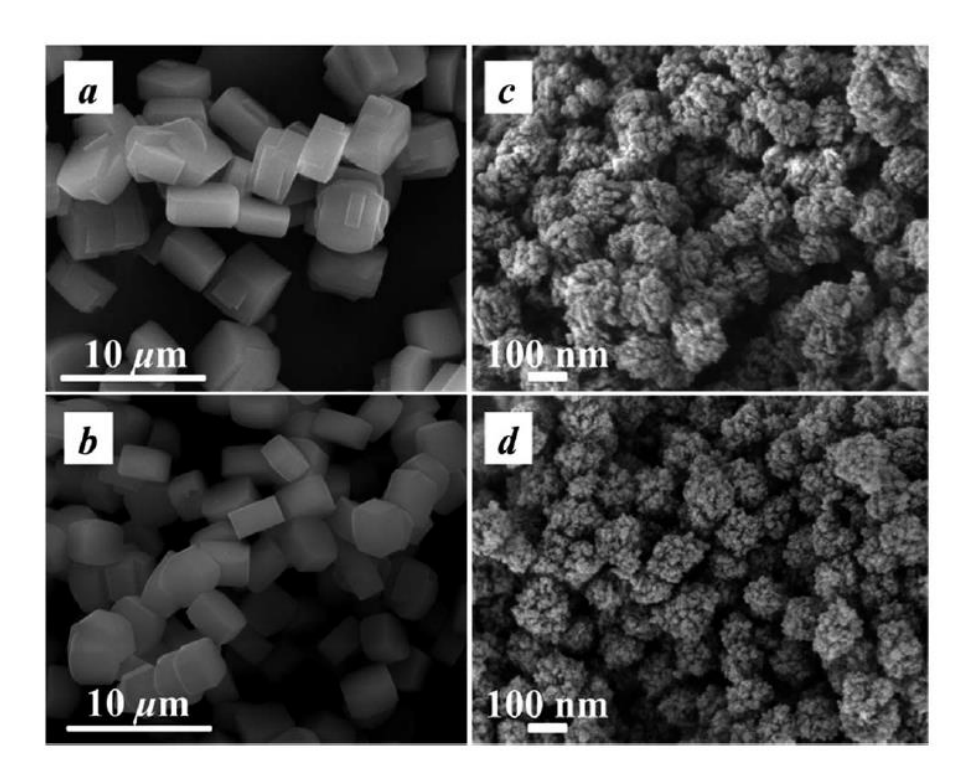
ผลการวิจัย

จากการดำเนินการในโครงการ ได้รับความประสบความสำเร็จในการการเตรียมตัวเร่ง ปฏิกิริยาซีโอไลต์ที่มีโครงสร้างแบบนาโนซีท และประกอบไปด้วย Metallic active sites รวมทั้ง การวิเคราะห์คุณสมบัติทางกายภาพและทางเคมีของตัวเร่งปฏิกิริยาที่ได้ทำการสังเคราะห์ขึ้น และศึกษากระบวนการเร่งปฏิกิริยาของตัวเร่งปฏิกิริยาที่ทำการสังเคราะห์ขึ้นสำหรับการ ปรับปรุงคุณภาพของไบโอออยล์ โดยมีรายละเอียดดังนี้

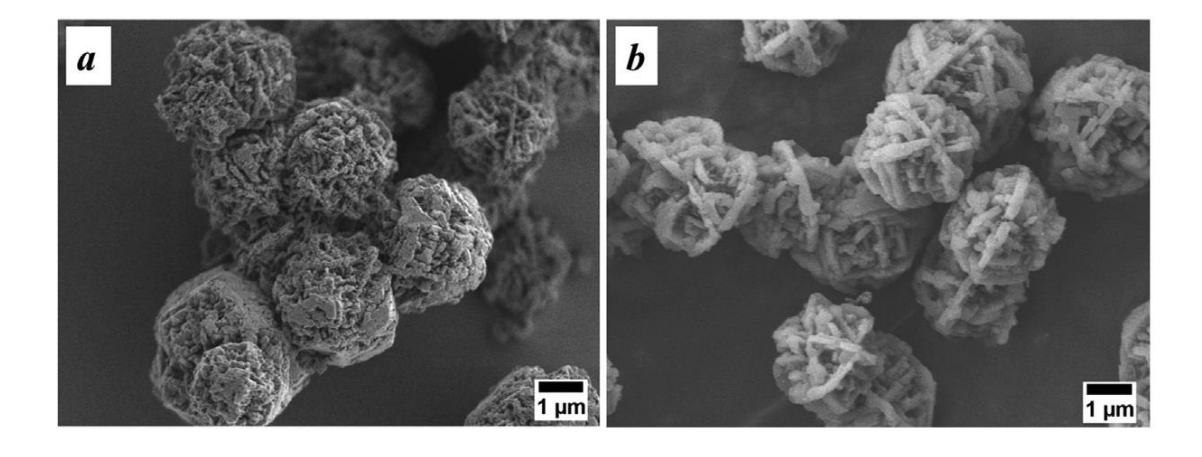
การออกแบบและการทดสอบคุณสมบัติทางเคมีและกายภาพของตัวเร่งปฏิกิริยา ซีโอไลต์หาโนชีทที่ประกอบไปด้วยบริเวณเร่งสองแบบ (Design of hierarchical zeolite nanosheets having bifunctional active sites by novel hydrothermal processes)

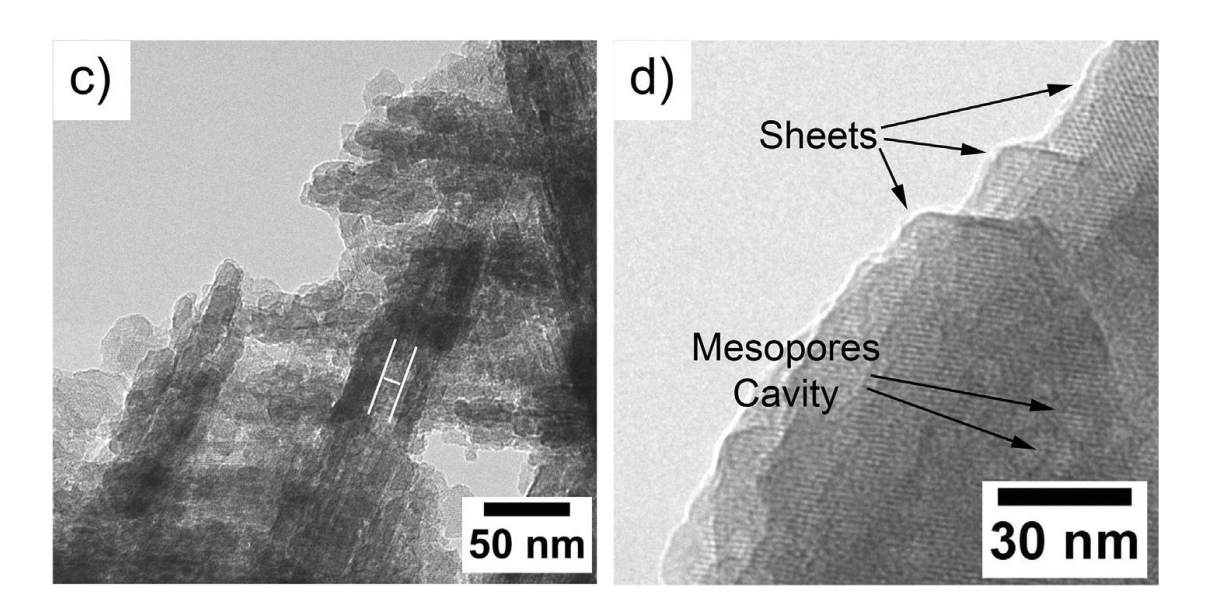
ทางคณะผู้วิจัยได้ประสบความสำเร็จในการเตรียมตัวเร่งปฏิกิริยาซีโอไลต์นาโนซีทชนิด ต่างๆ เช่น Hierarchical mesoporous HZSM-5, HZSM-5 nanosheets, FAU nanosheets ด้วยเทคนิค Hydrothermal synthesis โดยใช้แหล่งกำเนิดของซิลิกาที่มีความหลากหลาย รวมทั้งใช้แหล่งซิลิกาที่มาจากสารชีวมวล เป็นต้น และนอกจากนี้ยังทำการศึกษาผลของการใช้ สารกำหนดโครงสร้างหรือสารแม่แบบ Structure-directing agent (SDA) ในปริมาณแตกต่างกัน ซึ่งมีผลต่อโครงสร้างของซีโอไลต์นาโนซีท และคุณสมบัติทางกายภาพโดยเฉพาะปริมาณพื้นที่ ผิวของซีโอไลต์นาโนซีทที่แตกต่างกัน นอกจากการสังเคราะห์สารตัวอย่างดังกล่าวทาง คณะผู้วิจัยได้ทำการทดสอบคุณสมบัติทางเคมีและกายภาพของตัวเร่งปฏิกิริยาที่ทำการ สังเคราะห์ขึ้น (Investigation of physical and chemical properties of designed hierarchical zeolites) ตัวยเทคนิคดังนี้ X-ray diffraction (XRD), scanning electron microscopy (SEM), X-ray fluorescence (XRF), N2 physisorption, and Fourier transform infrared spectroscopy (FTIR), TEM, และ AI NMR เป็นตัน

ทางคณะผู้วิจัยได้ทำการเตรียมตัวเร่งปฏิกิริยาซีโอไลต์นาโนชีทชนิด HZSM-5 และ FAU ซึ่งเมื่อดูลักษณะของพื้นผิวของตัวเร่งปฏิกิริยาดังกล่าวด้วยเทคนิคทาง Scanning Electron Microscopy ได้ผลแสดงดังรูปที่ 1 และ 2 สำหรับซีโอไลต์นาโนชีทชนิด HZSM-5 และ FAU ตามลำดับ



ร**ูปที่ 1** a และ b แสดงลักษณะผลึกของซีโอไลต์แบบดั้งเดิมชนิด และ c-d แสดงลักษณะผลึก ของซีโอไลต์แบบนาโนชีทชนิด HZSM-5 ซึ่งได้ทำการสังเคราห์ขึ้นด้วยเทคนิค Hydrothermal synthesis สังเกตได้ด้วยเทคนิค Scanning Electron Microscopy

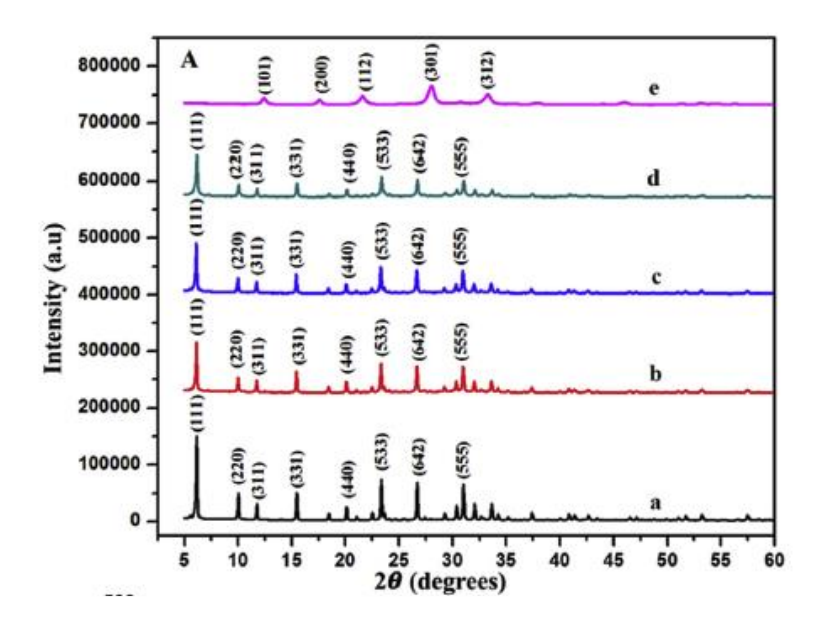




รูปที่ 2 a และ b แสดงลักษณะผลึกของซีโอไลต์นาโนชีทชนิด FAU ซึ่งได้ทำการสังเคราห์ขึ้น ด้วยเทคนิค Hydrothermal synthesis โดยใช้แหล่งกำเนิดของซิลิกาที่มีความหลากหลาย รวมทั้งใช้แหล่งซิลิกาที่มาจากสารชีวมวล สังเกตได้ด้วยเทคนิค Scanning Electron Microscopy (SEM) และ c และ d แสดงลักษณะผลึกของซีโอไลต์นาโนชีทชนิด FAU ที่สังเกต ได้จากเทคนิค Transmission electron microscope (TEM) (Microporous and Mesoporous Materials, 2018, 258, 141-150)

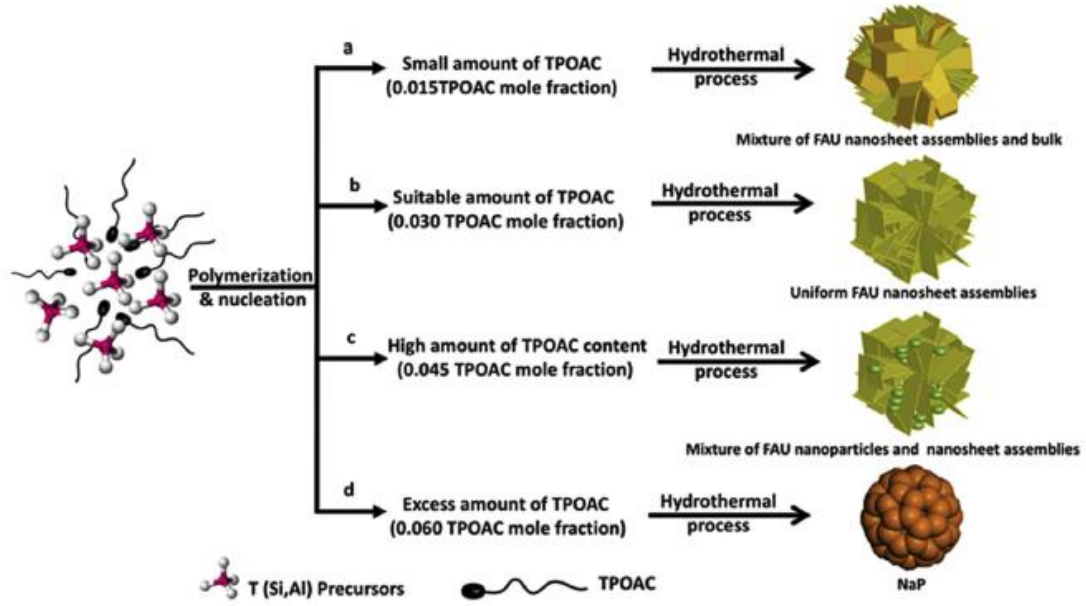
เพื่อทำการยืนยันลักษณะผลึกที่ได้ ทางคณะผู้วิจัยได้ทำการทดสอบลักษณะทาง โครงสร้างของตัวเร่งปฏิกิริยาที่สังเคราะห์ได้ด้วยเทคนิค Transmission electron microscope (TEM) ดังแสดงดังรูปที่ 2 c และ d จากผลการศึกษา ยืนยันได้อย่างแน่ชัดถึงการเกิดโครงสร้าง ที่มีลักษณะแบบนาโนชีทและเมื่อพิจารณาภายในผลึกของแต่ละชั้นของนาโนชีทพบว่าประกอบ ไปด้วยรูพรุนขนาดกลาง (Mesopores) เป็นจำนวนมาก

นอกจากนี้ทางคณะผู้วิจัยได้ทำการยืนยันคุณลักษณะพื้นฐานของโครงสร้างซีโอไลต์ ชนิดต่างๆ ดังเช่นตัวอย่างแสดงในรูปที่ 3 แสดงลักษณะ Pattern ที่สังเกตได้จากเทคนิค X-ray diffraction (XRD) จากผลการทดลองดังกล่าวทางคณะผู้วิจัยได้ทำการศึกษาผลของการ เปลี่ยนแปลงปริมาณสารแม่แบบที่ใช้ในการกำหนดโครงสร้างแบบนาโนซีท จากผลการทดลอง แสดงให้เห็นว่าเราสามารถสังเคราะห์ซีโอไลต์แบบนาโนซีทชนิด FAU ได้เมื่อทำการใช้ปริมาณ สารแม่แบบที่เหมาะสม อย่างไรก็ตามถ้าทำการเติมสารแม่แบบในปริมาณมากเกินไปจะมีผลทำ ให้เกิดของผสมของซีโอไลต์หนิดอื่นขึ้น



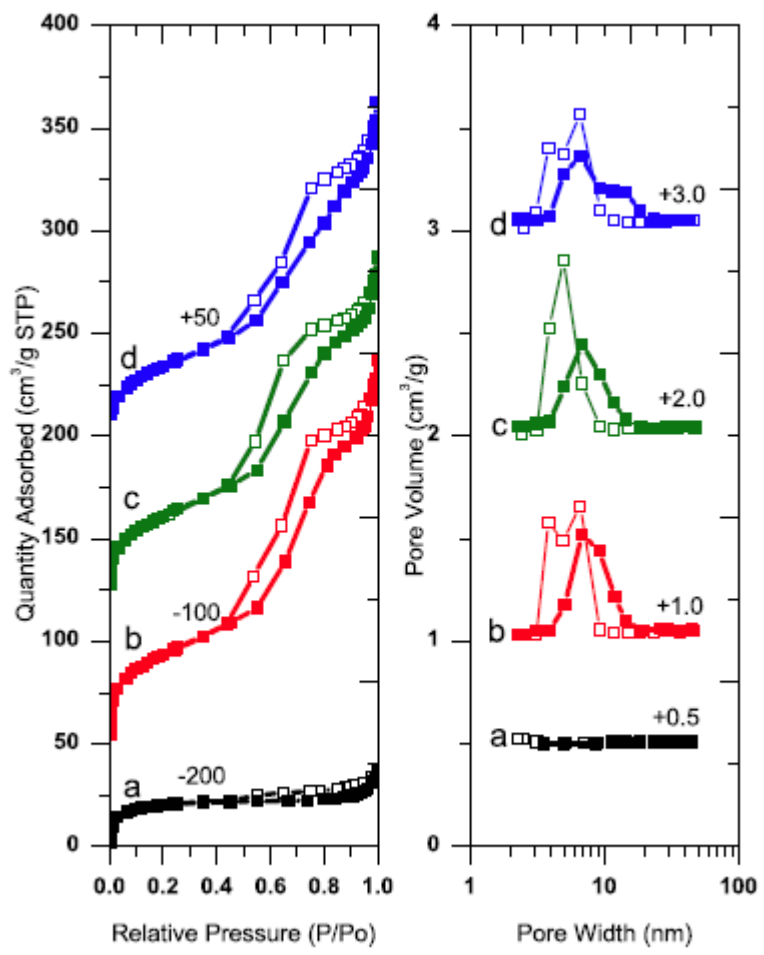
ร**ูปที่ 3** แสดงผลของ XRD patterns ของสารตัวอย่างซีโอไลต์นาโนชีทชนิด FAU ที่เตรียมด้วย สารแม่แบบในปริมาณแตกต่างกัน ดังนี้ (a) FAU-CON-85C-0T, (b) FAU-NS-85C-0.015T, (c) FAU-NS-85C-0.030T, and (d) FAU-NS-85C-0.045T, and (e) FAU-NS-85C-0.06T (NaP) (Microporous and Mesoporous Materials, 2018, 258, 141-150)

ดังนั้นจากผลการทดลองการสังเคราะห์ซีโอไลต์นาโนชีทด้วยการปรับเปลี่ยนปริมาณ ของสารแม่แบบทำให้สรุปเป็นแผนผังการเกิดซีโอไลต์รูปแบบต่างๆ ดังแสดงดังรูปที่ 4 จากผล การศึกษาพบว่าเมื่อทำการใช้สารแม่แบบในปริมาณน้อยเป็นผลทำให้เกิดของผสมระหว่างซี โอไลต์แบบนาโนชีทและซีโอไลต์ดั้งเดิม อย่างไรก็ตามเมื่อใช้สารแม่แบบในปริมาณที่เหมาะสม สามารถควบคุมการเกิดผลึกซีโอไลต์นาโนชีทแบบสวยงามได้



ร**ูปที่ 4** แสดงแผนผังสรุปการเกิดซีโอไลต์นาโนชีทชนิด FAU เมื่อทำการปรับเปลี่ยนปริมาณของ สารแม่แบบ (Microporous and Mesoporous Materials, 2018, 258, 141-150)

เมื่อพิจารณาเพิ่มเติมเกี่ยวกับพื้นที่ผิวจำเพาะของตัวเร่งปฏิกิริยาซีโอไลต์นาโนซีทที่ทำการสังเคราะห์ขึ้น สามารถแสดงให้เห็นดังรูปที่ 5 แสดงให้เห็นไอโซเทอมของการดูดซับแก๊ส ในโตรเจน จากการทดลองพบว่าซีโอไลต์แบบดั้งเดิมแสดงลักษณะไอโซเทอมของการดูดซับใน ลักษณะเป็น type 1 ซึ่งเป็นลักษณะเฉพาะของสารที่ประกอบไปด้วยรูพรุนขนาดเล็ก (Microporous material) อย่างไรก็ตามไอโซเอมของการดูดซับเปลี่ยนไปอย่างเห็นได้ชัดสำหรับ ตัวอย่างซีโอไลต์แบบนาโนซีทซึ่งแสดให้เห็นลักษณะของไอโซเทอมผสมของ type 1 และ 4 เป็น การยืนยันอย่างชัดเจนถึงการมีอยู่ของรูพรุนขนาดกลางบนตัวเร่งปฏิกิริยาซีโอไลต์นาโนซีท



ร**ูปที่ 5** แสดงไอโซเทอมการดูดซับแก๊สไนโตรเจนและการกระจายตัวของขนาดของรูพรุน (BJH pore size distribution) บนตัวเร่งปฏิกิริยาซีโอไลต์นาโนชีทชนิด FAU ซึ่งได้จากการปรับเปลี่ยน ปริมาณสารแม่แบบ และอุณหภูมิดังนี้ a) 0 โมลของสารแม่แบบและตกผลึกที่ 75 องศา เซลเซียส b) 0.01 โมลของสารแม่แบบและตกผลึกที่ 65 องศาเซลเซียส c) 0.02 โมลของสาร แม่แบบและตกผลึกที่ 65 องศาเซลเซียส และ d) 0.06 โมลของสารแม่แบบและตกผลึกที่ 75 องศาเซลเซียส (Journal of Cleaner Production, 2017, 142, 1244-1251)

2. ศึกษาคุณสมบัติการเร่งปฏิกิริยาของตัวเร่งปฏิกิริยาชีโอไลต์นาโนชีทสำหรับใช้ ในกระบวนการปรับปรุงคุณภาพพลังงานเชื้อเพลิงจากสารชีวมวล (Study of the catalytic properties of the catalytic upgrading of bio-oils to transportation fuels over designed hierarchical zeolite nanosheets by using a model reaction)

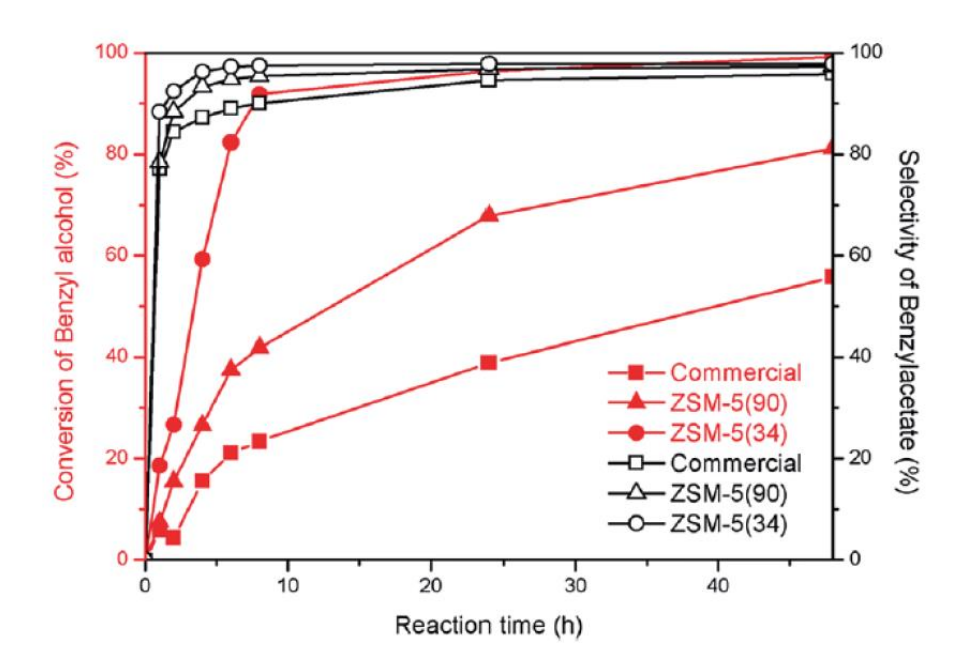
ในโครงการวิจัยนี้เกี่ยวข้องกับการศึกษาเบื้องต้นสำหรับการนำตัวเร่งปฏิกิริยาซีโอไลด์ นาโนชีทที่สังเคราะห์ขึ้นได้มาใช้ในกระบวนการปรับปรุงคุณภาพพลังงานเชื้อเพลิงจากสารชีว มวล โดยกิจกรรมที่ทำเป็นการนำตัวเร่งปฏิกิริยาดังกล่าวมาประยุกต์ใช้ในกระบวนการปรับปรุง คุณภาพพลังงานเชื้อเพลิงผ่านปฏิกิริยา Esterification ของสารประกอบแอลกอฮอล์และกรด อินทรีย์ เนื่องจากเป็นการลดค่าความเป็นกรดของไบโอออยล์ได้ นอกจากนั้นยังนำตัวเร่ง ปฏิกิริยาซีโอไลด์นาโนซีทมาประยุกต์ใช้ในการเร่งที่ประกอบไปด้วยบริเวณเร่งสองแบบ มาใช้ใน การเร่งปฏิกิริยา Hydrogenation อนุพันธ์ของสารประกอบ Phenol ซึ่งเป็นอนุพันธ์หนึ่งที่พบ มากในไบโอออยล์ โดยปฏิกิริยานี้เป็นขั้นตอนแรกที่เกิดขึ้นในกระบวนการปรับปรุงคุณภาพ ของไบโอออยล์ นอกจากการศึกษาคุณสมบัติการเร่งปฏิกิริยาผ่านกระบวนการ Esterification และ Hydrogenation ของ bio-oil model compounds นอกจากนี้ทางคณะนักวิจัยยังได้ ทำการศึกษาคุณสมบัติการเร่งปฏิกิริยาผ่านทางปฏิกิริยา Aldol condensation ของสารประกอบ Aldehyde และ Ketone ที่เป็นองค์ประกอบที่สำคัญของไบโอออยล์ รวมถึงเป็นขั้นตอนหนึ่งของ การผลิต Bio-oil derived jet fuels ซึ่งคณะผู้วิจัยได้มีความคืบหน้าที่ได้ตีพิมพ์งานวิจัยที่ เกี่ยวข้องกับงานดังกล่าวเป็นที่เรียบร้อย ภายใต้การได้รับทุนสนับสนุนจากสกว จำนวนทั้งลิ้น 6 ผลงาน

1.1. ศึกษาการเร่งปฏิกิริยาสำหรับกระบวนการปรับปรุงคุณภาพของไบโอออยล์ผ่าน กระบวนการ Esterification ของสารประกอบแอลกอฮอล์และกรดอินทรีย์

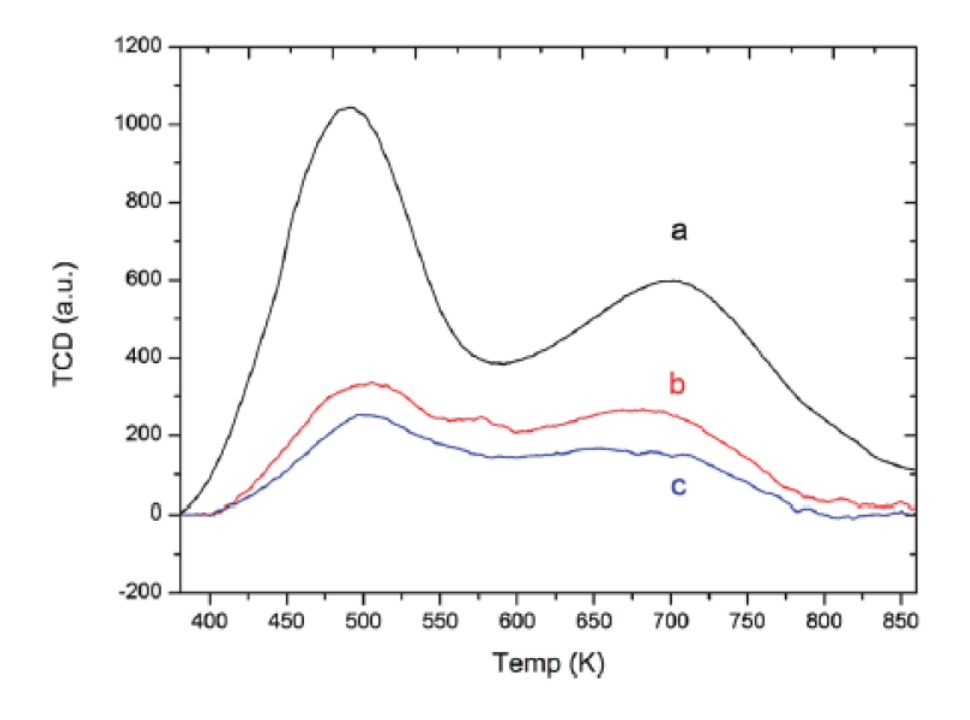
ตัวอย่างหนึ่งของงานวิจัยที่เกี่ยวข้องกับการปรับปรุงคุณภาพสารชีวมวล ทางคณะวิจัยได้ ประยุกต์ใช้ตัวเร่งปฏิกิริยาที่สังเคราะห์ได้ดังกล่าวข้างต้นเพื่อใช้ในการปรับปรุงคุณภาพสารชีว มวลผ่านปฏิกิริยา Esterification ของสารประกอบแอลกอฮอล์และกรดอินทรีย์ เพื่อเป็นการลด ค่าความเป็นกรดของสารประกอบเนื่องจากการมีกรดอินทรีย์เป็นองค์ประกอบ ดังแสดงดังรูปที่

ร**ูปที่ 6** แสดงปฏิกิริยา Esterification ของสารประกอบแอลกอฮอล์และกรดอินทรีย์เพื่อใช้เป็น Model reaction (RSC Advances, 2017, 7, 35581–35589)

ในส่วนนี้ทางคณะผู้วิจัยได้ทำการศึกษาประสิทธิภาพตัวเร่งปฏิกิริยาที่ได้ทำการ สังเคราะห์ขึ้น ในการเร่งปฏิกิริยา Esterification ของสารประกอบแอลกอฮอล์และกรดอินทรีย์ รูปที่ 7 แสดงความสัมพันธ์การเร่งปฏิกิริยา Esterification ของสารประกอบแอลกอฮอล์และกรด อินทรีย์ โดยแอลกอฮอล์ที่เลือกใช้ในครั้งนี้คือ Benzyl alcohol และ กรดอินทรีย์คือ Acetic acid บนตัวเร่งปฏิกิริยาซีโอไลต์ที่ทำการดัดแปลงเทียบกับซีโอไลต์แบบตั้งเดิม จากการทดลองพบว่า ซีโอไลต์ที่ทำการสังเคราะห์ขึ้นสามารถเพิ่มประสิทธิภาพได้มากถึงสามเท่าเมื่อเทียบกับซีโอไลต์ แบบดั้งเดิม นอกจากนี้ทางคณะผู้วิจัยได้ทำการศึกษาผลของอัตราส่วน Si/Al ที่มีผลต่อความ เป็นกรดของตัวเร่งปฏิกิริยา ดังแสดงในรูปที่ 8 ซึ่งผลดังกล่าวส่งผลกระทบต่อการเร่งปฏิกิริยา อีกด้วย กล่าวคือตัวเร่งปฏิกิริยาที่มีอัตราส่วน Si/Al ต่ำจะมีผลให้ได้ค่าความเป็นกรดที่สูงและ สามารถนำมาใช้เร่งปฏิกิริยานี้ได้อย่างดี



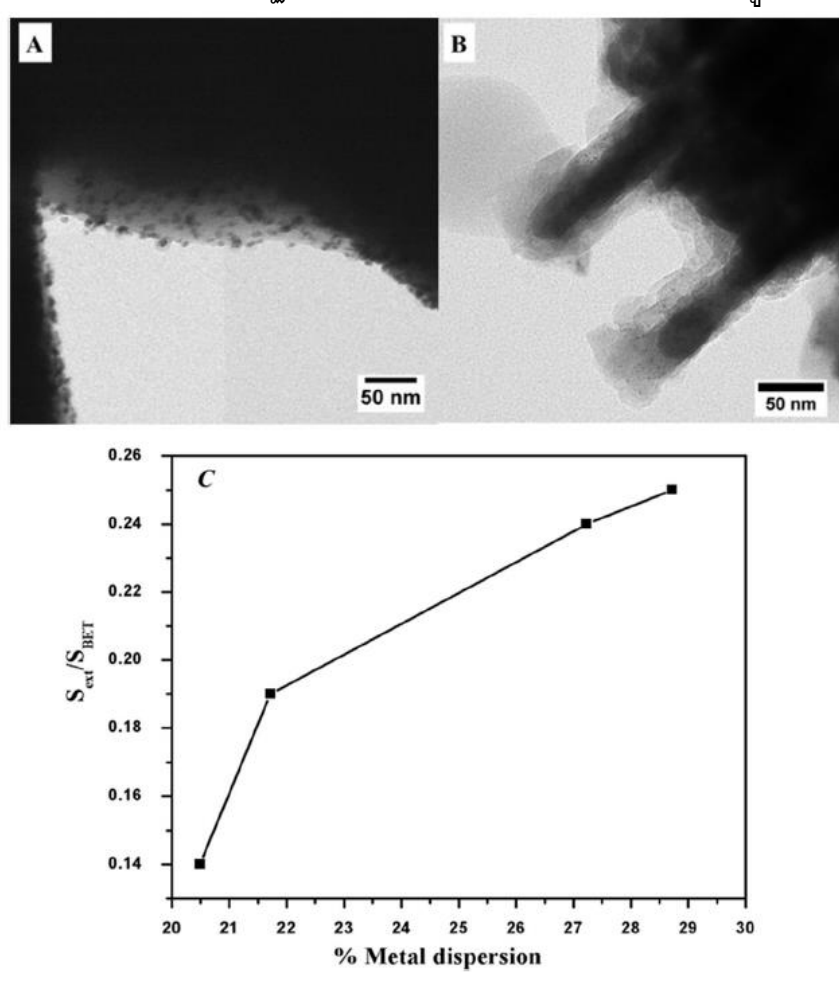
ร**ูปที่ 7** แสดงความสัมพันธ์ร้อยละการเปลี่ยนแปลงของสารตั้งต้นและเวลาในการเกิดปฏิกิริยา บนตัวเร่งปฏิกิริยาซีโอไลต์ชนิดต่างๆ (RSC Advances, 2017, 7, 35581–35589)



รูปที่ 8 แสดงกราฟของ NH₃-TPD ของตัวเร่งปฏิกิริยาต่างๆ a) Commercial ZSM-5, (b) Hierarchical ZSM-5(34), and (c) Hierarchical ZSM-5(90) (RSC Advances, 2017, 7, 35581–35589)

2.2 ศึกษาการเร่งปฏิกิริยาสำหรับกระบวนการปรับปรุงคุณภาพของไบโอออยล์ผ่าน กระบวนการ Hydrogenation ของอนุพันธ์ของสารประกอบ Phenol ซึ่งเป็น อนุพันธ์หนึ่งที่พบมากในไบโอออยล์

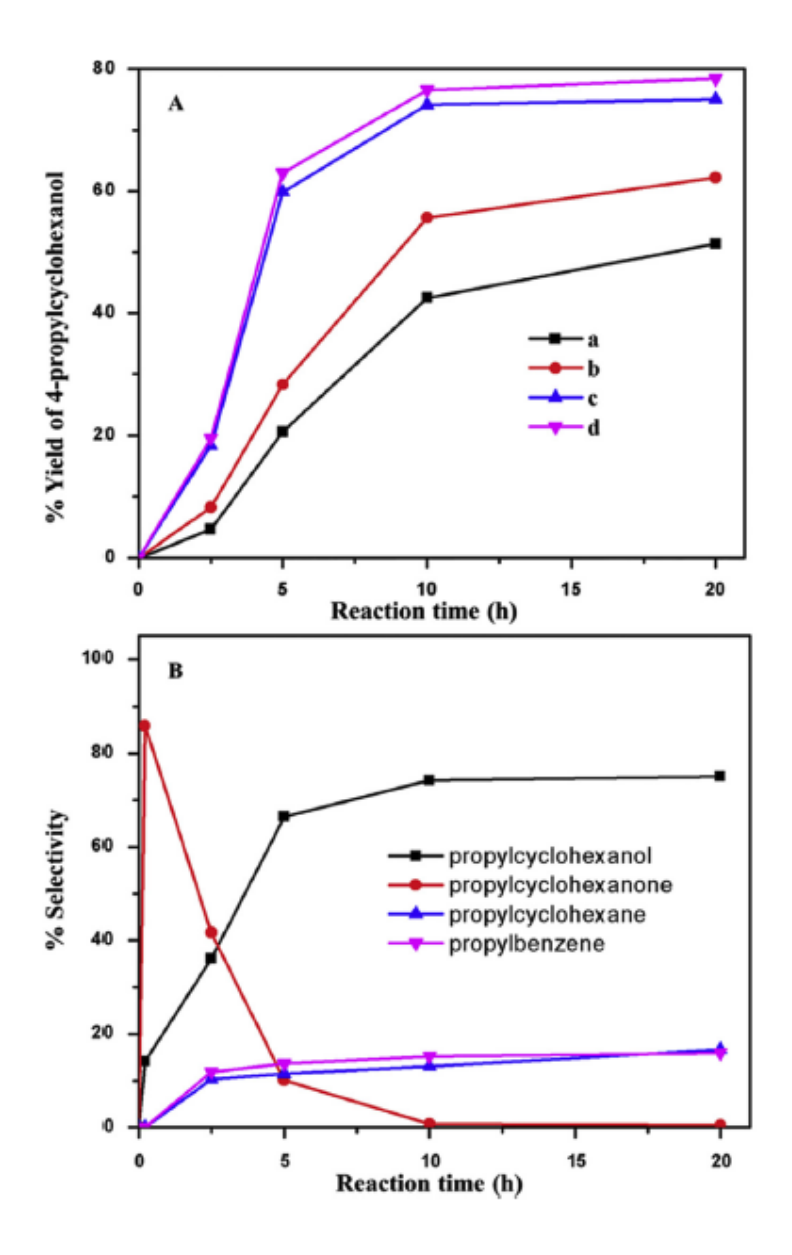
สำหรับงานวิจัยในส่วนนี้ทางคณะผู้ทำวิจัยได้ทำการศึกษากระบวนการเร่งปฏิกิริยาสำหรับ กระบวนการปรับปรุงคุณภาพของไบโอออยล์ผ่านกระบวนการ Hydrogenation ของอนุพันธ์ของ สารประกอบ Phenol ซึ่งเป็นอนุพันธ์หนึ่งที่พบมากในไบโอออยล์โดยใช้ตัวเร่งปฏิกิริยาซีโอไลต์ นาโนชีทที่ได้ทำการสังเคราะห์ขึ้น โดยซีโอไลต์ที่ใช้ในกระบวนการนี้มีการเติมบริเวณเร่ง (Active site) เพิ่มเติม โดยใช้โลหะแพลตินัมเป็นบริเวณเร่ง ซึ่งเป็นที่น่าสนใจในการเติมโลหะ บริเวณเร่งดังกล่าวบนตัวเร่งปฏิกิริยาซีโอไลต์แบบนาโนชีทสามารถเพิ่มการกระจายตัวของโลหะ แพลตินัมเมื่อเทียบกับการใช้ตัวเร่งปฏิกิริยาซีโอไลต์แบบดั้งเดิม ดังแสดงได้ดังรูปที่ 9



ร**ูปที่ 9** แสดงภาพ TEM ของโลหะแพลตินัมบนตัวเร่งปฏิกิริยาซีโอไลต์ประเภทต่างๆ a) บน ตัวเร่งปฏิกิริยาซีโอไลต์แบบดั้งเดิม b) บนตัวเร่งปฏิกิริยาซีโอไลต์นาโนซีท c) แสดง ความสัมพันธ์ระหว่างการกระจายตัวของโลหะแพลตินัมและพื้นที่ผิวจำเพาะภายนอกของซีโอไลต์

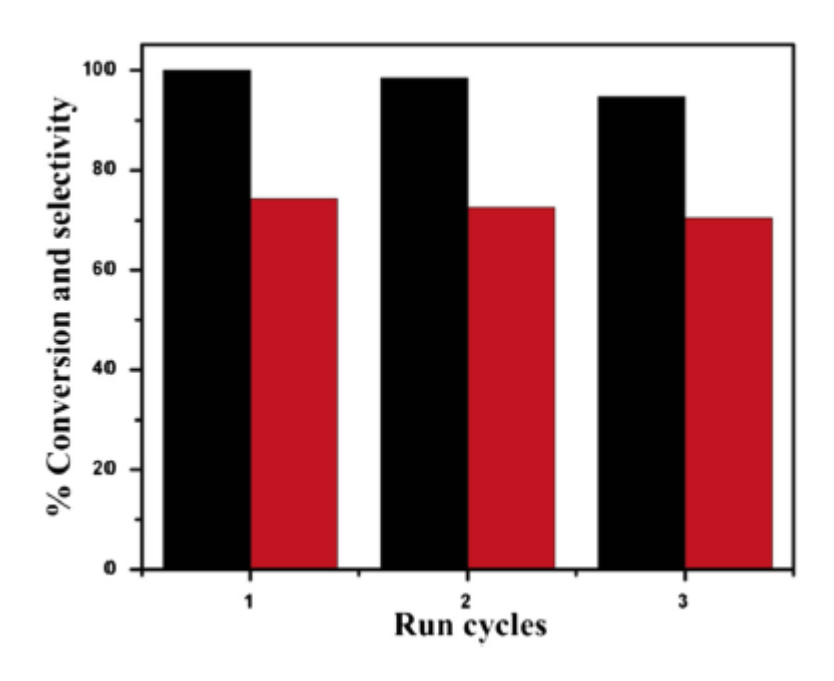
สำหรับงานวิจัยในส่วนนี้ทางคณะผู้วิจัยได้ศึกษาการเร่งปฏิกิริยา Hydrogenation ของ สารประกอบ 4-propylphenol ไปเป็น 4-propylcyclohexanol เพื่อใช้ในการศึกษาเบื้องต้น ดัง แสดงในรูปที่ 10 จากการศึกษากระบวนเร่งปฏิกิริยานี้มีความน่าสนใจเป็นการยืนยันการเกิด สารประกอบ 4-propylcyclohexanol จากสารประกอบ 4-propylcyclohexanone ซึ่งเป็นสาร Intermediate ดังแสดงในรูปที่ 11B นอกจากนี้ตัวเร่งปฏิกิริยาซีโอไลต์นาโนซีทที่ทำการ สังเคราะห์ขึ้นมานี้สามารถเพิ่มประสิทธิภาพในการเร่งปฏิกิริยาเมื่อเทียบกับตัวเร่งปฏิกิริยาซีโอไลต์แบบดั้งเดิม

ร**ูปที่ 10** แสดงปฏิกิริยา Hydrogenation ของสารประกอบ 4-propylphenol ไปเป็น 4-propylcyclohexanol บนตัวเร่งปฏิกิริยาโลหะแพลตินัมบนซีโอไลต์ (Microporous and Mesoporous Materials, 2018, 258, 141-150)



ร**ูปที่ 11** A) แสดงร้อยละผลิตภัณฑ์ของสาร 4-propylcyclohexanol ที่ได้บนตัวเร่งปฏิกิริยา a-b) แพลตินัมบนซีโอไลต์ดั้งเดิมชนิด FAU c-d) แพลตินัมบนซีโอไลต์นาโนซีท B) แสดงร้อยละของ สารผลิตภัณฑ์ต่างๆ บนตัวเร่งปฏิกิริยาแพลตินัมบนซีโอไลต์นาโนซีท (Microporous and Mesoporous Materials, 2018, 258, 141-150)

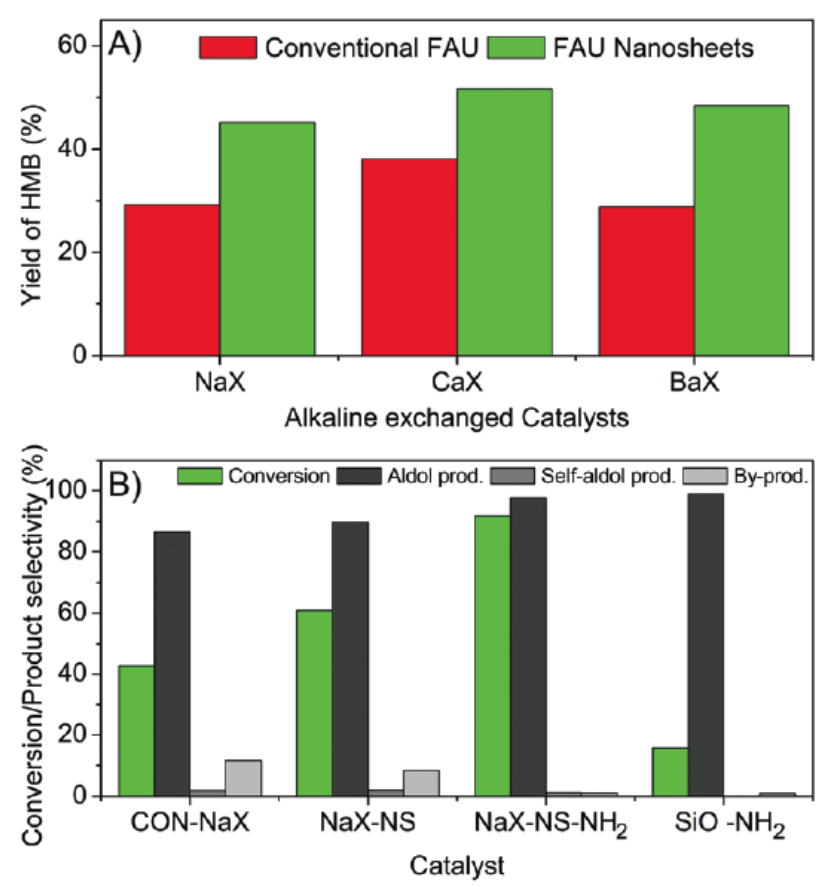
นอกจากนี้ทางคณะผู้วิจัยได้ทำการศึกษาคุณสมบัติเพิ่มเติมของการนำตัวเร่งปฏิกิริยา นำกลับมาใช้ใหม่ได้ จากการศึกษาพบว่าตัวเร่งปฏิกิริยาที่เตรียมขึ้นมีคุณสมบัติที่ดีเยี่ยมที่สมา รถนำกลับมาใช้ใหม่ได้จำนวนหลายครั้ง ดังแสดงดังรูปที่ 12



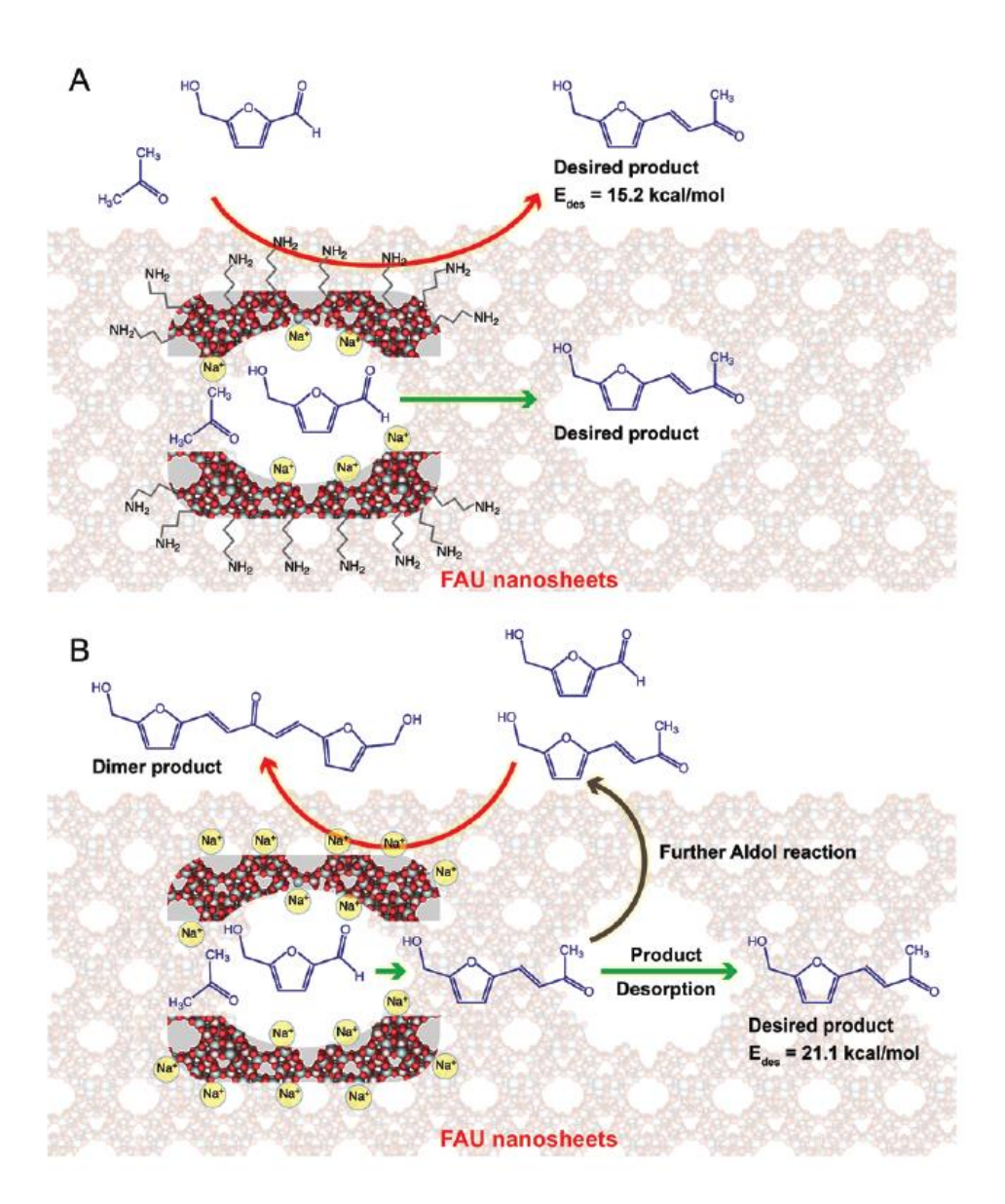
ร**ูปที่ 11** แสดงความสามารถในการนำตัวเร่งปฏิกิริยานาโนชีทกลับมาใช้ใหม่ได้ (Microporous and Mesoporous Materials, 2018, 258, 141-150)

2.3 ศึกษาการเร่งปฏิกิริยาสำหรับกระบวนการปรับปรุงคุณภาพของไบโอออยล์ผ่าน กระบวนการ Aldol condensation ของสารประกอบ Aldehyde และ Ketone

สำหรับกระบวนการปรับปรุงคุณภาพของใบโอออยล์ผ่านกระบวนการ Aldol condensation ของสารประกอบ Aldehyde และ Ketone ที่เป็นองค์ประกอบที่สำคัญของไบโอ ออยล์ รวมถึงเป็นขั้นตอนหนึ่งของการผลิต Bio-oil derived jet fuels โดยงานนี้ได้ทำการศึกษา การเร่งปฏิกิริยา Aldol condensation ของสารประกอบ 5-hydroxymethylfurfural (5-HMF) และ acetone (Ac) จากการศึกษาพบว่าการเร่งปฏิกิริยาดังกล่าวบนตัวเร่งปฏิกิริยาที่พัฒนาขึ้น สามารถทำให้ได้เปอร์เซ็นต์การผลิตของสารผลิตภัณฑ์ได้มากถึง 100 เปอร์เซ็นต์ ดังแสดงในรูป ที่ 12 นอกจากนี้ยังเป็นที่น่าสนใจอย่างยิ่งที่สามารถทำการปรับปรุงคุณสมบัติของพื้นผิวของ ตัวเร่งปฏิกิริยาโดยการใช้สารประกอบของเอมีน ดังแสดงในรูปที่ 13 แสดงถึงคุณลักษณะการ ปรับปรุงพื้นผิวด้วยสารประกอบดังกล่าวสามารถทำให้เกิดการปรับปรุงคุณภาพในการเลือกเกิด สารผลิตภัณฑ์เนื่องจากการลดพลังงานการดูดชับ (Adsorption energy) ของสารผลิตภัณฑ์บน ตัวเร่งปฏิกิริยาที่ทำการปรับปรุงพื้นที่ผิวภายนอก



ร**ูปที่ 12** A) แสดงร้อยละการผลิตของสารผลิตภัณฑ์บนตัวเร่งปฏิกิริยาซีโอไลต์แบบดั้งเดิมและซีโอไลต์แบบนาโนซีทที่มีบริเวณเร่งเป็นโลหะ Na Ca และ Ba และ B) แสดงร้อยละการ เปลี่ยนแปลงของสารตั้งต้นและร้อยละการเลือกเกิดของสารผลิตภัณฑ์บนตัวเร่งปฏิกิริยาต่าง ๆ (Chemical Communications, 2017, 53, 12185—12188)



ร**ูปที่ 1-** A) แสดงการเลือกเกิดสารผลิตภัณฑ์แบบจำเพาะเจาะจงบนตัวเร่งปฏิกิริยาซีโอไลต์นา โนชีทที่มีการปรับปรุงคุณภาพของพื้นผิวภายนอก B) แสดงการเลือกเกิดสารผลิตภัณฑ์แบบ จำเพาะเจาะจงบนตัวเร่งปฏิกิริยาซีโอไลต์แบบดั้งเดิม (Chemical Communications, 2017, 53, 12185—12188)

จากผลการศึกษาดังกล่าวทำให้สามารถตีพิมพ์งานวิจัยที่เกี่ยวข้องในวารสารวิชาการระดับ นานาชาติดังต่อไปนี้

ผลงานวิจัยที่ตีพิมพ์ในวารสารวิชาการระดับนานาชาติ

จากการดำเนินของโครงการฯ ได้รับผลงานวิจัยที่ตีพิมพ์ไปแล้วภายใต้หัวข้องานวิจัยที่ได้รับ ทุนสนับสนุนจากโครงการฯ เป็นจำนวน 6 เรื่อง และ 1 proceeding ดังนี้

- Wattanakit, C*.; Yutthalekha, T.; Assavapanumat, S.; Lapeyre, V.; Kuhn, A.*,
 "Pulsed electroconversion for highly selective enantiomer synthesis", Nature Communications, 2017, 8:2087, doi: 10.1038/s41467-017-02190-z.
- Yutthalekha, T.; Suttipat, D.; Salakhum, S.; Thivasasith, A.; Nokbin, S.; Limtrakul J.; Wattanakit, C.*, "Aldol condensation of biomass-derived platform molecules over amine-grafted hierarchical FAU-type zeolite nanosheets featuring basic sites", Chemical Communications, 2017, 53, 12185—12188 (Back cover page).
- Salakhum, S.; Yutthalekha, T.; Chareonpanich, M.; Limtrakul J.; Wattanakit, C.*, "Synthesis of hierarchical faujasite nanosheets from corn cob ash-derived nanosilica as efficient catalysts for hydrogenation of lignin-derived alkylphenols", Microporous and Mesoporous Materials, 2018, 258, 141-150.
- Wattanakit, C.*, "Chiral metals as electrodes", Current Opinion in Electrochemistry, 2017, 7:54–60.
- Rodponthukwaji, K.; Wattanakit, C.*; Yutthalekha, T.; Assavapanumat, S.;
 Warakulwit, C.; Wannapakdee, W.; Limtrakul, J., "Catalytic upgrading of carboxylic acids as bio-oil models over hierarchical ZSM-5 obtained via an organosilane approach", RSC Advances, 2017, 7, 35581-35589.
- Yutthalekha, T.; Wattanakit, C.; Warakulwit, C.; Wannapakdee, W.; Rodponthukwaji, K.; Witoon, T.; Limtrakul, J.*, "Hierarchical FAU-type zeolite nanosheets as green and sustainable catalysts for Benzylation of Toluene", Journal of Cleaner Production, 2017, 142 (3), 1244-1251.
- Shetsiri, S.; Wannapakdee, W.; Salakhum, S.; Wattanakit, C.*, "Catalytic conversion of bioethanol to light olefins over hierarchical zeolites catalysts"
 Accepted proceeding, Pure and Applied Chemistry International Conference 2017.

และผลงานวิจัยที่ตีพิมพ์ในหัวข้ออื่นๆ ดังนี้

- Yutthalekha, T.; Wattanakit, C.; Lapeyre, V.; Nokbin, S.; Warakulwit, C.; Limtrakul, J.; Kuhn, A.*, "Asymmetric synthesis using chiral encoded metal", Nature Communications, 2016, 7:12678, doi: 10.1038/ncomms12678.
- Warakulwit, C.; Yadnum, S.; Boonyuen, C.; Wattanakit, C.; Karajic, A.;
 Garrigue, P.; Mano, N.; Bradshaw, D.; Limtrakul, J.; Kuhn, A.,
 CrystEngComm, 2016, 18, 5095-5100.
- Wannapakdee, W.; Wattanakit, C.*; Paluka, V.; Yutthalekha, T.; Limtrakul, J.,
 RSC Advance, 2016, 6, 2875-2881.
- Wuamprakhon, P.; Wattanakit, C.; Warakulwit, C.; Yutthalekha, T.;
 Wannapakdee, W.; Ittisanronnachai, S.; Limtrakul, J., Microporous and Mesoporous Materials, 2016, 219, 1–9.

นอกจากนี้ยังมีผลงานอื่นๆ ที่เกี่ยวข้องที่ได้ไปเสนอผลงานในงานประชุมวิชาการและนำเสนอ ผลงานวิจัยระดับนานาชาติ

- Chularat Wattanakit, Wannaruedee Wannapakdee, Thittaya Yutthalekha, Phatsawit Wuamprakhon, Kamonlatth Rodponthukwaji, Jumras Limtrakul, "Synthesis and applications of various hierarchical zeolite nanosheets for potential petrochemical reactions", The 3rd Euro-Asia Zeolite Conference 2017 (the 3rd EAZC 2017), January 22-25, 2017, Bali Island, Indonesia (Oral presentation).
- Thittaya Yutthalekha, Saros Salakhum, Jumras Limtrakul, Chularat Wattanakit, FAU-type zeolite nanosheets as superior basic catalysts for aldol condensation", The 3rd Euro-Asia Zeolite Conference 2017 (the 3rd EAZC 2017)", January 22-25, 2017, Bali Island, Indonesia (Poster presentation).
- Saros Salakhum, Thittaya Yutthalekha, Jumras Limtrakul, Chularat Wattanakit, "Novel Design of Hierarchical Zeolite Nanosheets Using Renewable Resources", The 3rd Euro-Asia Zeolite Conference 2017 (the 3rd EAZC 2017)", January 22-25, 2017, Bali Island, Indonesia (Poster presentation).
- Chularat Wattanakit, Thittaya Yutthalekha, Veronique Lapeyre, Somkiat Nokbin, Chompunuch Warakulwit, Jumras Limtrakul, Alexander Kuhn, "Chiral recognition and asymmetric synthesis at mesoporous chiral metal surfaces", The 3rd International Congress on Advanced Materials (AM 2016), November 27-30,

- 2016, Bangkok, Thailand (Oral presentation, Outstanding oral presentation award).
- Sirawit Shetsiri, Wannaruedee Wannapakdee, Saros Salakhum, Chularat Wattanakit, "Ethylene production from dehydration of bioethanol over MFI zeolite nanosheets, The 6th International Conference on Biorefinery (ICB2017), Christchurch, New Zealand (Oral presentation).
- Duangkamon Suttipat, Sareeya Bureekaew, Wannaruedee Wannapakdee, Chularat Wattanakit, "Novel design of FAU@ZIF-8 composite in core/shell structures via a layer-by-layer method". The 6th IUPAC Conference on Green Chemistry, September 4-8, 2016 (Oral presentation).
- Wannaruedee Wannapakdee, Duangkamon Suttipat, Chularat Wattanakit, "Onepot synthesis of novel hierarchical bifunctional Ga/HZSM-5 nanosheets for
 propane aromatization", The 6th IUPAC Conference on Green Chemistry,
 September 4-8, 2016 (Oral presentation).

และใต้ไปเสนอผลงานที่ได้รับเชิญไปเป็นวิทยากร ดังนี้

- Chularat Wattanakit, Thittaya Yutthalekha, Veronique Lapeyre, Somkiat Nokbin, Chompunuch Warakulwit, Jumras Limtrakul, Alexander Kuhn, "Enantioselective recognition and asymmetric synthesis at mesoporous chiral metal surfaces", The 13th IUPAC International Conference on Novel Materials and their Synthesis (NMS-XIII), October 11-16, 2017, Nanjing, China (Invited speaker).
- Chularat Wattanakit, Thittaya Yutthalekha, Veronique Lapeyre, Somkiat Nokbin, Chompunuch Warakulwit, Jumras Limtrakul, Alexander Kuhn, " Chiral recognition and asymmetric synthesis at mesoporous chiral metal surfaces", The 12th IUPAC International Conference on Novel Materials and their Synthesis (NMS-XII), October 14-19, 2016, Changsha, China (Invited speaker).
- Chularat Wattanakit, "Hierarchical zeolites: From catalyst design to their potential applications", International Conference on Nano-Materials for Enery and Life (NanoM2017), Febuary 6-7, 2017, Rayong, Thailand. (Invited speaker).

และมีการเชื่อมโยงทางวิชาการกับนักวิชาการอื่น ๆทั้งในและต่างประเทศ สำหรับการเชื่อมงานวิจัยกับนักวิชาอื่น ๆ ในประเทศมีดังนี้

- รศ.ดร.เมตตา เจริญพานิช ภาควิชาวิศวกรรมเคมี คณะวิศวกรรมศาสตร์ มหาวิทยาลัยเกษตรศาสตร์ เหตุผล: เนื่องจากมีความเชี่ยวชาญเป็นอย่างมาก โดยเฉพาะเกี่ยวกับด้านการพัฒนาตัวเร่งปฏิกิริยาเคมี
- ดร. ธนา ไม้หอม ภาควิชาวิทยาศาสตร์ คณะศิลปศาสตร์และวิทยาศาสตร์ มหาวิทยาลัยเกษตรศาสตร์ วิทยาเขตกำแพงแสน เหตุผล: เนื่องจากมีความเชี่ยวชาญทางด้านเคมีเชิงคำนวณ เพื่อทำการศึกษา กลไกการเกิดปฏิกิริยาที่เกิดขึ้นในกระบวนการเร่งปฏิกิริยา

สำหรับการเชื่อมโยงทางงานวิจัยกับนักวิชาอื่น ๆ ต่างประเทศมีดังนี้

- Prof. Dr. Alexander Kuhn, Department of Physical Chemistry, University of Bordeaux, France
 เหตุผล: เนื่องจากมีความเชี่ยวชาญอย่างยิ่งเกี่ยวกับการวิจัยการออกแบบสารที่
 ประกอบไปด้วยรูพรุนที่มีความเป็นระเบียบสูง และการพัฒนาตัวเร่งปฏิกิริยาทาง
 เคมีไฟฟ้า ในการเชื่อมโยงดังกล่าวทำให้เกิดผลความร่วมมือทางการทำงานวิจัย
 ร่วมกันในหลายโครงการ เช่น Le Projet International de Coopération Scientifique
 (PICS) โดยได้รับการสนับสนุนจาก CNRs ประเทศฝรั่งเศส และได้มีการส่งนิสิต
 ปริญญาเอก จำนวน 1 คน เพื่อเข้าร่วมในโปรแกรม
 การผลิตบัณฑิตปริญญาเอกร่วม และได้รับเงินทุนสนับนุนจากสถาบันวิทยสิริเมธีและ
 Franco-Thai Scholarship Program จากสถานเอกอัครราชทูตฝรั่งเศสประจำประเทศ
 ไทย
- Prof. Dr. E.J.M. (Emiel) Hensen, Department of Chemical Engineering and Chemistry, Eindhoven University of Technology, The Netherlands เหตุผล: เนื่องจากมีความเชี่ยวชาญในด้านการพัฒนาตัวเร่งปฏิกิริยาประเภทซีโอไลต์ เพื่อใช้ในอุตสาหกรรมปิโตรเคมี ได้มีความร่วมมือทางการทำงานวิจัยร่วมกันใน เบื้องตันโดยการส่งนิสิตปริญญาเอก จำนวน 1 คน เข้าร่วมในงานวิจัยภายใต้การดูแล ของ Prof. Hensen เป็นระยะเวลา 1 ปี
- Prof. Dr. Johannes A. Lercher, Department of Chemistry, Technische Universität München (TUM), Germany
 เหตุผล: เนื่องจากมีความเชี่ยวชาญและมีชื่อเสียงระดับโลกในด้านการพัฒนาตัวเร่ง
 ปฏิกิริยาประเภทซีโอไลต์เพื่อใช้ในอุตสาหกรรมปิโตรเคมี ได้มีความร่วมมือทางการ
 ทำงานวิจัยร่วมกันในเบื้องต้นโดยมีการส่งนิสิตปริญญาเอก จำนวน 1 คน เข้าร่วมใน
 งานวิจัยภายใต้การดูแลของ Prof. Lercher เป็นระยะเวลา 1 ปี

สรุปและวิจารณ์ผลการวิจัย

จากการศึกษางานวิจัยนี้ได้แบ่งงานออกเป็นสองส่วน ในส่วนแรกเน้นการออกแบบและ การทดสอบคุณสมบัติทางเคมีและกายภาพของตัวเร่งปฏิกิริยาซีโอไลต์นาโนชีทที่ประกอบไป ด้วยบริเวณเร่งสองแบบ (Design of hierarchical zeolite nanosheets having bifunctional active sites by novel hydrothermal processes) ซึ่งงานในส่วนนี้ได้ทำการสังเคราะห์ตัวเร่ง ปฏิกิริยาซีโอไลต์นาโนชีทที่มีโครงสร้งหลากหลายเช่น FAU และ ZSM-5 จากการวิเคราะห์ คุณสมบัติของตัวเร่งปฏิกิริยาที่สังเคราะห์ขึ้น เป็นที่น่าสนใจว่าตัวเร่งปฏิกิริยาดังกล่าวสามารถ ปรับปรุงคุณสมบัติเช่นความเป็นกรด ความเสถียรทางความร้อน และการเพิ่มของพื้นที่ผิวได้ อย่างดีเยี่ยมเมื่อเทียบกับซีโอไลต์แบบดั้งเดิม และสำหรับงานวิจัยในส่วนที่สองเป็นการศึกษา คุณสมบัติการเร่งปฏิกิริยาของตัวเร่งปฏิกิริยาซีโอไลต์นาโนชีทสำหรับใช้ในกระบวนการปรับปรุง คุณภาพพลังงานเชื้อเพลิงจากสารชีวมวล โดยผ่านกระบวนการหลากหลาย เช่น การเร่ง ปฏิกิริยาสำหรับกระบวนการปรับปรุงคุณภาพของไบโอออยล์ผ่านกระบวนการ Esterification ของสารประกอบแอลกอฮอล์และกรดอินทรีย์ การเร่งปฏิกิริยาสำหรับกระบวนการปรับปรุง คุณภาพของใบโอออยล์ผ่านกระบวนการ Hydrogenation ของอนุพันธ์ของสารประกอบ Phenol ซึ่งเป็นอนุพันธ์หนึ่งที่พบมากในใบโอออยล์ และการเร่งปฏิกิริยาสำหรับกระบวนการปรับปรุง คุณภาพของใบโอออยล์ผ่านกระบวนการ Aldol condensation ของสารประกอบ Aldehyde และ Ketone ซึ่งจากงานวิจัยนี้เห็นว่ามีความประสบความสำเร็จในการพัฒนาตัวเร่งปฏิกิริยาดังกล่าว เพื่อใช้ในกระบวนการปรับปรุงคุณภาพของไบโอออยล์ได้หลากหลายกระบวนการ

เอกสารอ้างอิง

- 1. A. Demirbas, Applied Energy, 88 (2011) 17-28.
- 2. X. Liu, P.R. Jensen, M. Workman, Bioresour. Technol., 104 (2012) 579-586.
- T.O. Jensen, T. Kvist, M.J. Mikkelsen, P.V. Christensen, P. Westermann, J. Ind. Microbiol. Biotechnol., 39 (2012) 709-717.
- 4. S. Czernik, A.V. Bridgwater, Energy & Fuels, 18 (2004) 590-598.
- 5. M. Saidi, F. Samimi, D. Karimipourfard, T. Nimmanwudipong, B.C. Gates, M.R. Rahimpour, Energ. Environ. Sci., 7 (2014) 103-129.
- 6. M. Milina, S. Mitchell, J. Pérez-Ramírez, Catal. Today. 2014, 235, 176-183.
- 7. A. Oasmaa, S. Czernik, Energy & Fuels, 13 (1999) 914-921.
- 8. P.M. Mortensen, J.D. Grunwaldt, P.A. Jensen, K.G. Knudsen, A.D. Jensen, Appl. Catal. A: Gen, 407 (2011) 1-19.
- D. Gao, C. Schweitzer, H.T. Hwang, A. Varma, Ind. Eng. Chem. Res., 53 (2014) 18658-18667.
- 10. J. HoužviČka, S. Hansildaar, V. Ponec, J. Catal, 167 (1997) 273-278.
- 11. K. Tanabe, W.F. Hölderich, Appl. Catal A: Gen, 181 (1999) 399-434.
- 12. H.H. Kung, B.A. Williams, S.M. Babitz, J.T. Miller, W.O. Haag, R.Q. Snurr, Top. Catal., 10 (2000) 59-64.
- 13. I.E. Maxwell, Catal. Today, 1 (1987) 385-413.
- J. Rouquerol, D. Avnir, C.W. Fairbridge, D.H. Everett, J.M. Haynes, N. Pernicone,
 J.D.F. Ramsay, K.S.W. Sing, K.K. Unger, Pure Appl. Chem., 66 (1994) 1739.
- 15. Y. Tao, H. Kanoh, L. Abrams, K. Kaneko, Chem. Rev., 106 (2006) 896-910.
- C.H. Christensen, K. Johannsen, E. Törnqvist, I. Schmidt, H. Topsøe, C.H. Christensen, Catal. Today, 128 (2007) 117-122.
- 17. E.I. Ko, AlChE Journal, 42 (1996) 2993-2993.
- 18. F. Ocampo, H.S. Yun, M.M. Pereira, J.P. Tessonnier, B. Louis, Cryst. Growth. Des., 9 (2009) 3721-3729.
- 19. J. Zheng, X. Zhang, Y. Zhang, J. Ma, R. Li, Micropor. Mesopor. Mat., 122 (2009) 264-269.
- 20. D.P. Serrano, J.M. Escola, P. Pizarro, Chem. Soc. Rev., 42 (2013) 4004-4035.
- A.H. Janssen, A.J. Koster, K.P. de Jong, Angew. Chem. Int. Edit., 40 (2001) 1102-1104.

- 22. K. Möller, B. Yilmaz, R.M. Jacubinas, U. Müller, T. Bein, J. Am. Chem. Soc., 133 (2011) 5284-5295.
- F.-S. Xiao, L. Wang, C. Yin, K. Lin, Y. Di, J. Li, R. Xu, D.S. Su, R. Schlögl, T. Yokoi, T. Tatsumi, Angew. Chem. Int. Edit., 45 (2006) 3090-3093.
- 24. A. Boisen, I. Schmidt, A. Carlsson, S. Dahl, M. Brorson, C.J.H. Jacobsen, Chem. Commun., (2003) 958-959.
- 25. H. Chen, J. Wydra, X. Zhang, P.-S. Lee, Z. Wang, W. Fan, M. Tsapatsis, J. Am. Chem. Soc., 133 (2011) 12390-12393.
- 26. C. Wattanakit, C. Warakulwit, P. Pantu, B. Sunpetch, M. Charoenpanich, J. Limtrakul, Can. J. Chem. Eng., 90 (2012) 873-880.
- 27. M. Choi, H.S. Cho, R. Srivastava, C. Venkatesan, D.-H. Choi, R. Ryoo, Nat Mater, 5 (2006) 718-723.
- 28. I.I. Ivanova, E.E. Knyazeva, Chem. Soc. Rev., 42 (2013) 3671-3688.
- 29. S. Mitchell, N.-L. Michels, K. Kunze, J. Pérez-RamÃ-rez, Nat Chem, 4 (2012) 825-831.
- K. Varoon, X. Zhang, B. Elyassi, D.D. Brewer, M. Gettel, S. Kumar, J.A. Lee, S. Maheshwari, A. Mittal, C.-Y. Sung, M. Cococcioni, L.F. Francis, A.V. McCormick, K.A. Mkhoyan, M. Tsapatsis, Science, 334 (2011) 72-75.
- 31. A. Corma, V. Fornes, S.B. Pergher, T.L.M. Maesen, J.G. Buglass, Nature, 396 (1998) 353-356.
- 32. A. Corma, U. Diaz, M.E. Domine, V. Fornés, Angew. Chem. Int. Edit., 39 (2000) 1499-1501.
- 33. X. Zhang, D. Liu, D. Xu, S. Asahina, K.A. Cychosz, K.V. Agrawal, Y. Al Wahedi, A. Bhan, S. Al Hashimi, O. Terasaki, M. Thommes, M. Tsapatsis, Science, 336 (2012) 1684-1687.
- 34. W. Song, V.H. Grassian, S.C. Larsen, Chem. Commun., (2005) 2951-2953.
- 35. L. Tosheva, V.P. Valtchev, Chem. Mater., 17 (2005) 2494-2513.
- 36. V.P. Valtchev, K.N. Bozhilov, J. Am. Chem. Soc., 127 (2005) 16171-16177.
- 37. I. Schmidt, C. Madsen, C.J.H. Jacobsen, Inorg. Chem., 39 (2000) 2279-2283.
- 38. H. Wang, B.A. Holmberg, Y. Yan, J. Am. Chem. Soc., 125 (2003) 9928-9929.
- 39. K. Egeblad, C.H. Christensen, M. Kustova, C.H. Christensen, Chem. Mater., 20 (2008) 946-960.
- 40. J.C. Groen, J.A. Moulijn, J. Perez-Ramirez, J. Mater. Chem., 16 (2006) 2121-2131.

- 41. J.C. Groen, J.C. Jansen, J.A. Moulijn, J. Pérez-Ramírez, J. Phys. Chem. B, 108 (2004) 13062-13065.
- 42. F.-S. Xiao, L. Wang, C. Yin, K. Lin, Y. Di, J. Li, R. Xu, D.S. Su, R. Schlögl, T. Yokoi, T. Tatsumi, Angew. Chem., 118 (2006) 3162-3165.
- 43. M. Choi, K. Na, J. Kim, Y. Sakamoto, O. Terasaki, R. Ryoo, Nature, 461 (2009) 246-249.
- 44. A. Inayat, I. Knoke, E. Spiecker, W. Schwieger, Angew. Chem. Int. Ed., 51 (2012) 1962-1965.
- 45. P. Wuamprakhon, C. Wattanakit, C. Warakulwit, T. Yutthalekha, W. Wannapakdee, S. Ittisanronnachai, J. Limtrakul, Micropor. Mesopor. Mat., 219 (2016) 1-9.
- 46. R. Fricke, H. Kosslick, G. Lischke, M. Richter, Chem. Rev., 100 (2000) 2303-2406.
- 47. A. Jongerius, R. Jastrzebski, P. C. A. Bruijnincx, B. M. Weckhuysen, J. Catal., 285 (2012) 315-323.
- 48. Y. C. Lin, C. L. Li, H. P. Wan, H. T. Lee, C. F. Liu, Energy Fuel., 25 (2011) 890-896.
- 49. E. M. Ryymin, M. L. Honkela, T. R. Viljava, A. O. I. Krause, Appl. Catal. A Gen., 358 (2009) 42-48.
- E. M. Ryymin, M. L. Honkela, T. R. Viljava, A. O. I. Krause, Appl. Catal. A Gen., 389 (2010) 114-121.
- 51. E. Furimsky, Appl. Catal. A Gen. 199 (2000) 147-190.
- D. C. Elliott, D. Beckman, A. V. Bridgwater, J. P. Diebold, S. B. Gevert, Y. Solantausta, Energy Fuels., 5 (1991) 399-410.
- 53. C. Zhao, J. A. Lercher, Angew. Chem., Int. Ed., 51 (2012) 5935-5940.
- 54. C. Zhao, C. J. A. Lercher, ChemCatChem., 4 (2012), 64-68.
- 55. D. Y. Hong, S. J. Miller, P. K. Agrawal, C. W. Jones, Chem. Commun., 46 (2010) 1038-1040.
- 56. X. L. Zhu, L. L. Lobban, R. G. Mallinson, D. E. Resasco, J. Catal. 281 (2011) 21-
- 57. H. Ohta, H. Kobayashi, K. Hara, A. Fukuoka, Chem. Commun., 47 (2011) 12209-12211.
- 58. C. Zhao, Y. Kou, A. A. Lemonidou, X. Li, J. A. Lercher, Angew. Chem., Int. Ed., 48 (2009) 3987-3990.
- C. Zhao, J. Y. He, A. A. Lemonidou, X. B. Li, J. A. Lercher, J. Catal., 280 (2011) 8 16.

- 60. A. G. Sergeev, J. F. Hartwig, Science 332 (2011), 439-443.
- C. Zhao, Y. Kou, A. A. Lemonidou, X. B. Li, J. A. Lercher, Chem. Commun., 46 (2010) 412-414.
- 62. S. Echeandia, P. L. Arias, V. L. Barrio, B. Pawelec, J. L. Fierro, Appl. Catal. B., 101 (2010) 1-12.
- 63. D. Y. Hong, S. J. Miller, P. K. Agrawal, C. W. Jones, Chem. Commun., 46 (2010) 1038-1040.
- 64. C. Zhao, D. M. Camaioni, J. A. Lercher, J. Catal., 288 (2012) 92-103.
- 65. X. L. Zhu, L. L. Lobban, R. G. Mallinson, D. E. Resasco, J. Catal., 281 (2011) 21-29.
- 66. W. Zhang, C. Jinzhu, L. Ruliang, W. Shengpei, C. Limin, K. Li, ACS Sustainable Chem. Eng., 2 (2014) 683-691.
- 67. T. Nimmanwudipong, R. C. Runnebaum, D. E. Block, B. C. Gates, Energy Fuels, 25 (2011) 3417–3427.
- 68. Y. Wang, F. Yunming Fang, T. He, H. Hu, J. Wu, Catal. Commun., 12 (2011) 1201–1205.
- H. W. Lee, S. H. Park, J Jeon, R. Ryoo, W. Kimd, D. J. Suh, Y.-K. Park. Catal. Today., 232 (2014) 119–126.
- J. Li, X. Li, G. Zhou, W. Wang, C. Wang, S. Komarneni, Y. Wang. Applied Catalysis A: General, 470 (2014) 115–122.
- C. Zhang, J. Xing, L. Song, H. Xin, Sen. Lin, L. Xing, X. Li. Catalysis Today, 234 (2014) 145–152.
- 72. L. Wang, J. Zhang, X. Yi, A. Zheng, F. Deng, C. Chen, Y. Ji, F. Liu, X. Meng, F.-S. Xiao, ACS Catal., 5 (2015) 2727-2734.
- 73. A. Ausavasukhi, Y. Huang, A. T. To, T. Sooknoi, D. E. Resasco, J. Catal., 290 (2012) 90–100.
- 74. H. Ohta, Y. Kentaro, H. Minoru, G. Hamasak, Y. Uozumi, Y. Watanabe, Chem. Commun., 11 (2015) 17000-17003.
- 75. S. Furuta, H. Matsuhashi, K. Arata, Catal. Commun., 5 (2004) 721-723.
- 76. E. Cano-Serrano, G. Blanco-Brieva, J.M. Campos-Martin, J.L.G. Fierro, Langmuir, 19 (2003) 7621-7627.
- 77. H. Liu, N. Xue, L. Peng, X. Guo, W. Ding, Y. Chen, Catal. Commun., 10 (2009) 1734-1737.
- 78. J. Bedard, H. Chiang, A. Bhan, J. Catal., 290 (2012) 210-219.

- 79. A. Corma, H. Garcia, S. Iborra, J. Primo, J. Catal., 120 (1989) 78-87.
- 80. M. Milina, S. Mitchell, J. Pérez-Ramírez, Catal. Today. 235 (2014) 176-183.
- 81. J.C. Groen, J.C. Jansen, J.A. Moulijn, J. Pérez-Ramírez, J. Phys. Chem. B 108 (2004) 13062-13065.
- 82. J.C. Groen, J.A. Moulijn, J. Pérez-Ramírez, Microporous Mesoporous Mater. 87 (2005) 153-161.

ภาคผนวก

ผลงานตีพิมพ์ในวารสารวิชาการนานาชาติ

- 1. Wattanakit, C*.; Yutthalekha, T.; Assavapanumat, S.; Lapeyre, V.; Kuhn, A.*, "Pulsed electroconversion for highly selective enantiomer synthesis", Nature Communications, 2017, 8:2087, doi: 10.1038/s41467-017-02190-z.
- Yutthalekha, T.; Suttipat, D.; Salakhum, S.; Thivasasith, A.; Nokbin, S.; Limtrakul J.; Wattanakit, C.*, "Aldol condensation of biomass-derived platform molecules over amine-grafted hierarchical FAU-type zeolite nanosheets featuring basic sites", Chemical Communications, 2017, 53, 12185—12188 (Back cover page).
- Salakhum, S.; Yutthalekha, T.; Chareonpanich, M.; Limtrakul J.; Wattanakit, C.*,
 "Synthesis of hierarchical faujasite nanosheets from corn cob ash-derived nanosilica
 as efficient catalysts for hydrogenation of lignin-derived alkylphenols", Microporous
 and Mesoporous Materials, 2018, 258, 141-150.
- 4. Wattanakit, C.*, "Chiral metals as electrodes", Current Opinion in Electrochemistry, 2017, 7:54–60.
- Rodponthukwaji, K.; Wattanakit, C.*; Yutthalekha, T.; Assavapanumat, S.; Warakulwit, C.; Wannapakdee, W.; Limtrakul, J., "Catalytic upgrading of carboxylic acids as bio-oil models over hierarchical ZSM-5 obtained via an organosilane approach", RSC Advances, 2017, 7, 35581-35589.
- Yutthalekha, T.; Wattanakit, C.; Warakulwit, C.; Wannapakdee, W.;
 Rodponthukwaji, K.; Witoon, T.; Limtrakul, J.*, "Hierarchical FAU-type zeolite nanosheets as green and sustainable catalysts for Benzylation of Toluene",
 Journal of Cleaner Production, 2017, 142 (3), 1244-1251.

ผลงานที่อยู่ระหว่างรอการตีพิมพ์ในวารสารวิชาการนานาชาติ

Suttipat, D.; Yutthalekha, T.; Wannapakdee, W.; Bureekaew, S.; Limtrakul, J.;
 Wattanakit, C*. Hierarchical FAU/ZIF-8 nanosheet hybrid materials as highly efficient base catalysts for aldol con-densation 2018, Manuscript revision.

1



ARTICLE

DOI: 10.1038/s41467-017-02190-z

OPEN

Pulsed electroconversion for highly selective enantiomer synthesis

Chularat Wattanakit¹, Thittaya Yutthalekha¹, Sunpet Asssavapanumat^{1,2}, Veronique Lapeyre² & Alexander Kuhn²

Asymmetric synthesis of molecules is of crucial importance to obtain pure chiral compounds, which are of primary interest in many areas including medicine, biotechnology, and chemistry. Various methods have been used very successfully to increase the enantiomeric yield of reaction pathways, but there is still room for the development of alternative highly enantioselective reaction concepts, either as a scientific challenge of tremendous fundamental significance, or owing to the increasing demand for enantiopure products, e.g., in the pharmaceutical industry. In this context, we report here a strategy for the synthesis of chiral compounds, based on pulsed electrochemical conversion. We illustrate the approach with the stereospecific electroreduction of a prochiral model molecule at chiral mesoporous metal structures, resulting in an enantiomeric excess of over 90%. This change of paradigm opens up promising reaction schemes for the straightforward synthesis of high-added-value molecules.

¹ Department of Chemical and Biomolecular Engineering, School of Energy Science and Engineering, Vidyasirimedhi Institute of Science and Technology, Rayong 21210, Thailand. ² Univ. de Bordeaux, CNRS, ISM, UMR 5255, Bordeaux INP, Site ENSCBP, 16 Avenue Pey Berland, FR-33607 Pessac, France. Correspondence and requests for materials should be addressed to C.W. (email: chularat.w@vistec.ac.th) or to A.K. (email: kuhn@enscbp.fr)

olecular chirality is one of the most fascinating topics in chemical research due to its importance in many areas such as materials engineering 1-3, surface science 4-8, pharmaceutics⁹, separation science, and catalysis¹⁰. Therefore, the scientific community has made enormous efforts to obtain enantiomerically pure compounds, either based on the chiral pool^{11–13}, resolution of racemates^{14, 15}, or asymmetric synthesis¹⁶. Among them, enantioselective synthesis has been extensively developed as a controllable process^{17–19}, and successfully achieved via catalysis based on the use of chiral coordination complexes^{20, 21}, imprinted polymers^{22, 23}, and biocatalysts^{24, 25}. However, there are also potential drawbacks, such as too flexible molecular structures²⁶, low thermal and chemical stability¹⁸, and tedious catalyst preparation²⁷. Furthermore, some of the most successful strategies are based on homogeneous catalysis with inherent problems of catalyst separation from the reaction product^{28, 29}. Therefore, heterogeneous reaction schemes may have significant advantages^{30, 31}. For electrochemical reactions, electronic conductors are mandatory and in this context, the development of metals with chiral surfaces is an interesting choice to carry out heterogeneous enantioselective reactions.

Several concepts have been tested in the past such as the binding of chiral ligands to metal surfaces³², the adsorption of chiral molecules on surfaces to produce chiral metals³³, or metal oxides^{34, 35}, the cutting of high Miller index planes of metal monocrystals^{36, 37}, and the distortion of symmetrical metal structures³⁸. The design and synthesis of chiral metal structures has been explored for several of them (e.g., Pt, Pd, Ag, Au, Cu, Rh)³⁹⁻⁴⁴. Recently it has been reported that even the bulk of metals can be imprinted with chiral information^{41, 45}. Our group demonstrated that chiral cavities can be generated in mesoporous platinum, based on the electrochemical reduction of platinum ions around a self-assembled liquid crystal phase of non-ionic surfactant and chiral template molecules⁴⁶. These materials exhibit fascinating properties because they can be used to discriminate the enantiomers of an imprinted chiral molecule and other chiral molecules with analog structures^{46–48}. The reason for the remarkable chiral recognition can be attributed to the fact that a large number of chiral cavities are located at the internal surface of the mesoporous network.

In addition, theses chiral-encoded mesoporous metal surfaces have also been shown to induce a certain degree of enantioselectivity during the electrochemical synthesis of mandelic acid from its prochiral precursor⁴⁷, meaning that one of the possible stereoisomers of the molecule is formed preferentially. However, the enantiomeric excess is very modest with typical values in the few percent range. One reason for this low performance is that the external surface of the electrode is not imprinted with chiral information and therefore produces the final compound in a completely non-stereospecific way. Therefore, the product is a mixture of enantiomers produced in a quite selective way inside the mesoporous phase, and a racemate resulting from the reaction of precursor molecules at the outer surface. This intrinsically prevents from achieving high values of enantiomeric excess. A promising way to increase the ratio between precursor molecules that are transformed inside the metal matrix and those reacting at the outside is to play with the competition of transport and reaction kinetics. In this context, electrochemistry has the unique advantage of allowing a perfectly time-controlled triggering of the involved redox reactions⁴⁹. The interplay between filling the chiral cavities with precursor molecules by diffusion and intermittently transforming them by applying an appropriate potential pulse constitutes an efficient heterogeneous reaction concept which is solely possible with electrochemistry.

In the present study, we describe an application of this concept to the highly selective asymmetric synthesis of chiral molecules based on the pulsed electroconversion of a prochiral molecule with chiral-imprinted mesoporous metal. This strategy is expected to avoid almost completely the interference of reactions at non-imprinted sites. In a proof-of principle synthesis, the two enantiomers of 1-phenylethanol (PE) are successfully and selectively synthesized via pulsed electroconversion of prochiral acetophenone on chiral-imprinted mesoporous platinum (CIMP). The degree of enantioselectivity can be tuned by changing the pulse time and the amount of imprinted chiral cavities.

Results

Concept of enantioselective pulsed electrosynthesis. Conventional steady-state electroreduction of a prochiral molecule on chiral mesoporous platinum exhibits some enantioselectivity because the handedness of the product is influenced by the geometry of the chiral metal cavities⁴⁷. However, the interference

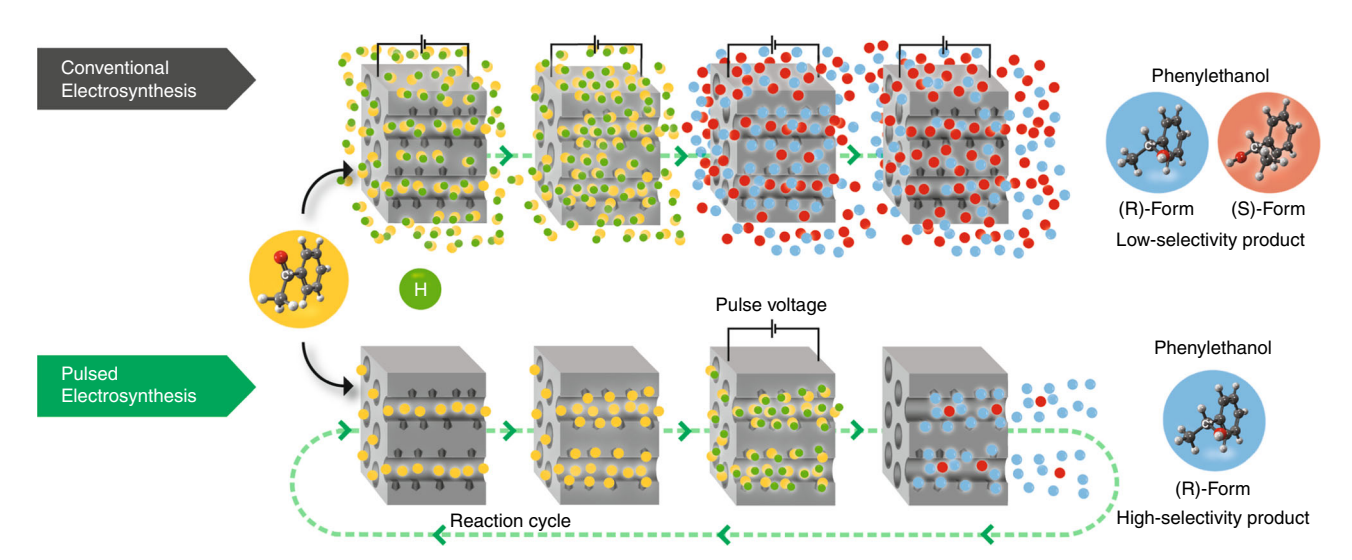


Fig. 1 Comparison of conventional and pulsed chiral electrosynthesis. Illustration of the conversion of achiral acetophenone (yellow dots) into (*R*)- and (*S*)-PE (blue and red dots, respectively) by stereoselective addition of hydrogen (green dots) during conventional and pulsed asymmetric electrosynthesis using chiral-encoded metal electrodes

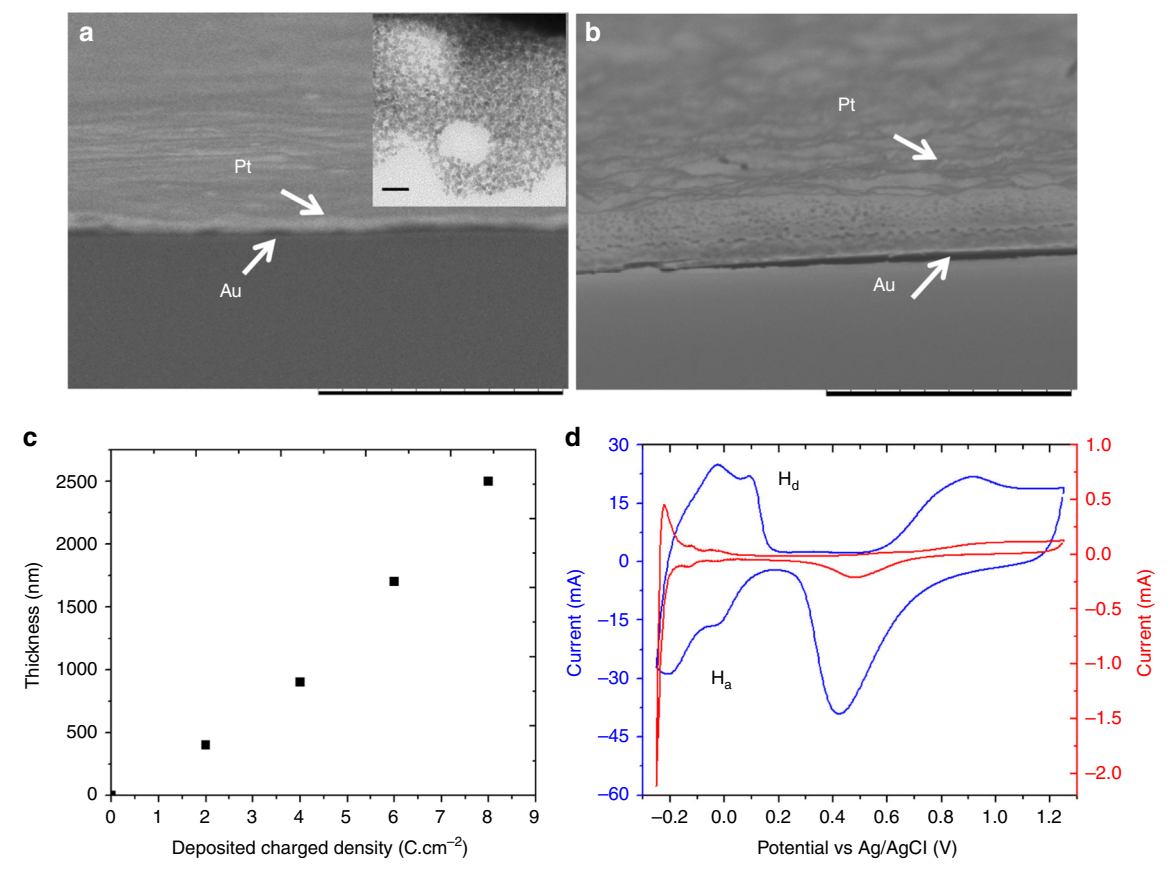


Fig. 2 Structural characterization of chiral mesoporous platinum. a, b Scanning electron microscopy images of cross sections of mesoporous metal films obtained for injected charge densities of 2 and 8 C cm⁻². Scale bar 10 μm. The inset in **a** is a TEM image of such a mesoprous structure with a scale bar of 20 nm. c Relationship between film thickness and the deposited charged density. d Cyclic voltammograms of flat platinum (red) and a chiral-imprinted mesoporous platinum film obtained by injecting a charge density of 8 C cm⁻² (blue) recorded in 0.5 M H₂SO₄ at 100 mV s⁻¹. H_a (hydrogen adsorption) and H_d (hydrogen desorption)

of concomitant reactions at non-imprinted metal located at the external electrode surface cannot be prevented and therefore leads to a decrease in overall stereoselectivity. Thus, in order to enhance the enantioselectivity, the major issue is to suppress such interferences. For this, we propose a concept allowing to improve the degree of enantioselectivity by using pulsed electrosynthesis. The differences between conventional and pulsed electroconversion of a prochiral starting molecule are illustrated in Fig. 1.

In the case of conventional electrosynthesis, carried out under steady-state conditions (i.e., constant applied potential), the achiral molecules (in this example acetophenone, symbolized by yellow dots) can combine with hydrogen (green dots) both, inside the chiral cavities and at the outermost surface of the electrode, resulting in low excess of either (R)- or (S)-PE (blue and red dots, respectively) as a function of the imprinted enantiomer. In strong contrast to this, pulsed electroconversion can lead to a very significant increase of the enantioselective properties based on the following mechanism. When no potential is applied, the prochiral educts diffuse into the mesopores and adsorb in the chiral cavities that are decorating the pore walls. Once the host matrix is filled, a potential pulse of appropriate amplitude and duration is applied to reduce the adsorbed precursor molecules in an enantioselective way. During the subsequent relaxation period at open circuit, the formed products can leave the matrix and, simultaneously, fresh precursor can enter the mesopores. Then the potential pulse is applied again. Repeating this cycle many times will lead to the gradual accumulation of the preferentially formed enantiomer in the bulk solution.

Obviously, during each potential pulse precursor molecules can also be reduced at the non-selective outer electrode surface. However, the quantity of converted molecules at the outer surface is much smaller because the internal surface area of mesoporous metals is typically two to three orders of magnitude higher compared to the external surface area⁵⁰. This means that, depending on the pulse duration, the interference of electroreduction at the external surface can be almost completely suppressed, and results in the highly selective production of one enantiomer with respect to the other.

Synthesis of chiral-encoded mesoporous platinum surfaces.

Chiral-encoded mesoporous platinum has been synthesized analog to previous reports^{46–48}. In brief, the hexagonal (H₁) structure of a lyotropic liquid crystal, obtained by the selfassembly of the surfactant Brij 56, has been used as a template to control the mesoporous structure of the metal⁵⁰. The interaction between the hydrophilic outer part of the surfactant columns and the OH groups of the chiral template leads to an oriented geometry of chiral cavities when metal is grown around these supramolecular structures⁴⁶. Several template molecules have been successfully used for controlling the shape of the chiral imprint, such as DOPA (3,4-dihydroxyphenylalanine)⁴⁶, mandelic acid⁴⁷, and PE (this work). CIMP films with different thickness have been prepared on gold-coated glass slides for the subsequent use as working electrodes in the experiments of pulsed electroconversion of the prochiral molecule (Fig. 2a, b).

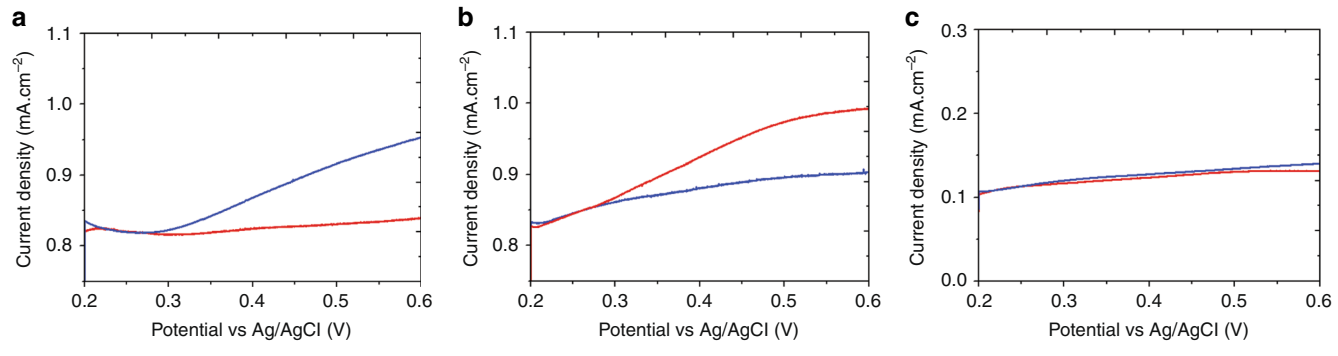


Fig. 3 Electrochemical characterization of enantioselectivity. Differential pulse voltammetry (DPV) in 4 mM (R)-PE (blue), and (S)-PE (red), using 0.2 M KNO₃ as supporting electrolyte with **a** a CIMP electrode imprinted with (R)-PE, **b** a CIMP electrode imprinted with (S)-PE, **c** a non-imprinted mesoporous platinum electrode. All electrodes were prepared using a deposition charge density of 2 C cm⁻² and a PE/PtCl₆²⁻ weight ratio of 0.05 for the imprinted ones.

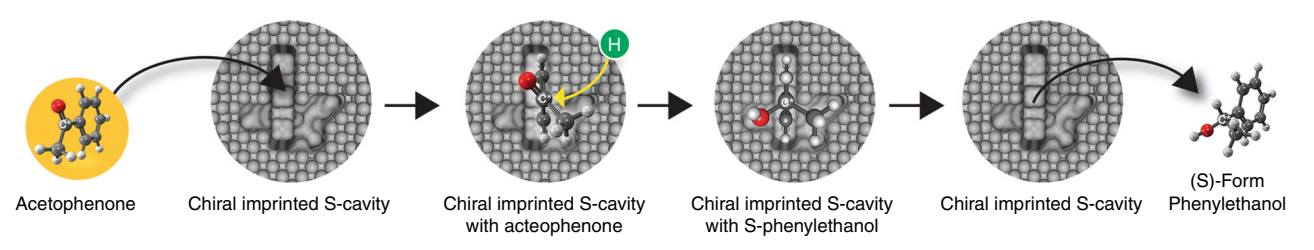


Fig. 4 Enantioselective synthesis steps. Illustration of the electrosynthesis of (S)-phenylethanol from acetophenone based on its adsorption in chiral-imprinted cavities of the mesoporous metal, followed by its stereoselective reduction and desorption

The morphology and the dimensions were uniform and similar to what has been described in previous reports^{46, 47}. The mesoporosity is clearly visible when performing transmission electron microscopy (see inset of Fig. 2a). The film thickness is proportional to the injected charge density (Fig. 2c) and various thicknesses were used for tuning the enantioselectivity, because a more pronounced selectivity can be observed when increasing the film thickness⁴⁶.

To characterize the active surface area related to the mesoporous feature, cyclic voltammetry of the porous platinum electrodes in 0.5 M of $\rm H_2SO_4$ was used (Fig. 2d and Supplementary Figure 1). The peaks between -0.20 and 0.20 V can be attributed to the hydrogen adsorption and desorption, whereas the oxidation of Pt and the reduction of PtOn occur at about 0.7 and 0.5 V, respectively. The significant enhancement of active surface area of a porous platinum film (blue) compared with flat platinum (red) is translated into a roughness factor of 33.4. No additional increase in active surface area is observed when comparing a chiral-imprinted and a non-imprinted mesoporous electrode (Supplementary Figure 1). This indicates that the high surface area is essentially due to the mesoporosity and not to the chiral cavities.

In order to verify the enantioselective properties of the soobtained surfaces, the recognition of 1-PE via electrooxidation was monitored using differential pulse voltammetry as shown in Fig. 3a–c. The explored potential window has been limited on the positive side to $+0.6 \,\mathrm{V}$ in order to avoid interference with the oxidation of platinum. When comparing the different records, a more pronounced signal for (R)-PE with respect to (S)-PE can be observed in the case of chiral mesoporous platinum imprinted by (R)-PE (Fig. 3a). In contrast, the electrode imprinted by the opposite enantiomer exhibits a higher amplitude for (S)-PE with respect to (R)-PE (Fig. 3b). It is necessary to confirm that the different signals for the two enantiomers are not artifacts; in particular they might be due to chiral template molecules remaining inside the metal after the imprinting. Therefore, the removal of the template molecules was monitored by measuring the amount of chiral molecules leaving the metal phase as a function of rinsing time using UV-Vis spectroscopy (see Supplementary Figure 2). It clearly demonstrates that no more template molecules are leaving the cavities after sufficient rinsing. As expected, no enantioselective discrimination properties are revealed for non-imprinted mesoporous platinum (Fig. 3c), meaning that no chiral information is encoded without using a chiral template molecule in the preparation mixture. These observations confirm that CIMP can be successfully prepared using this general approach with various types of a chiral templates and the so-obtained host matrix exhibits intrinsic chiral properties even after removable of the chiral template.

Pulsed enantioselective synthesis of chiral phenylethanol. The enantioselective synthesis of PE from acetophenone has been chosen as a model system because it is an interesting compound in bio-oil in which ketones are present in a large portion (27 wt%)⁵¹. Acetophenone is a very simple aromatic ketone, and therefore well-suited for first proof-of-principle studies, which then might be extended to other, more complex, ketones^{52, 53}. In addition, the conversion of this compound into a pure enantiomer of 1-PE as an important chiral building block in pharmaceutical industries can be considered as a representative example for the production of high-added-value products. The molecule is going to adsorb inside the chiral cavities present in the mesoporous structure and this will direct the synthesis preferentially towards one of the two enantiomers of phenylethanol, depending on which one has been imprinted (Fig. 4). After the reduction is accomplished, the product is desorbed and the cavity is again available for the transformation of further molecules.

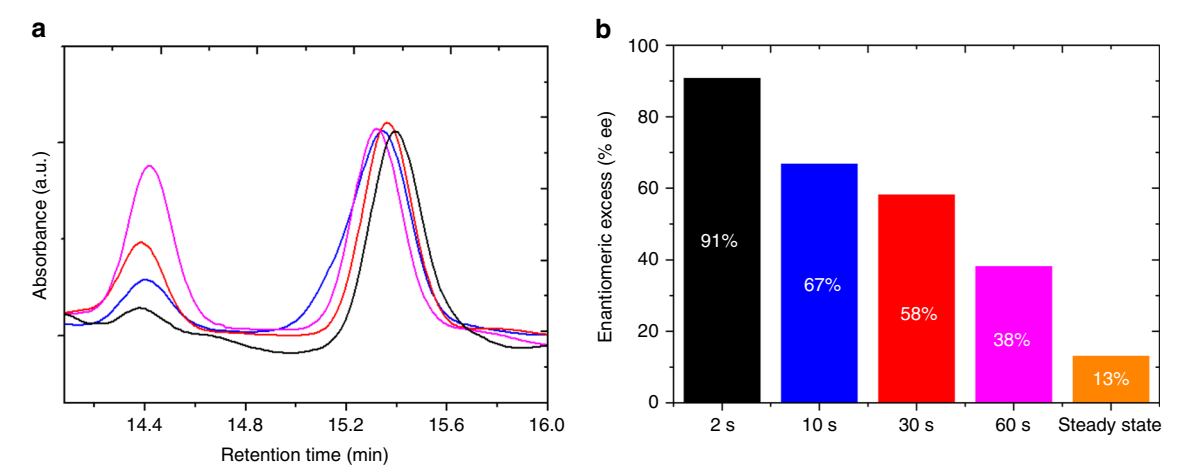


Fig. 5 Monitoring of enantioselectivity as a function of pulse time. **a** HPLC chromatograms of the electrosynthesis products obtained with an electrode imprinted with (S)-PE ((S)-PE/PtCl₆²⁻ weight ratio of 0.15) at -0.45 V for different pulse times; 60 s pulse time (pink), 30 s (red), 10 s (blue) and 2 s (black), with 120 s relaxation time in all cases. The peaks at retention times of 14.4 and 15.3 min belong to (*R*)-PE and (S)-PE, respectively; **b** Histogram of the relationship between enantiomeric excess and pulse time using the same color code and showing for comparison also the value obtained in a steady-state experiment (orange)

In order to test the described concept and optimize the different electrosynthesis parameters, such as the reduction potential, the thickness of the Pt film and the amount of imprinted chiral sites, the conventional steady-state electroreduction of acetophenone was first studied. To prevent the reduction of protons at too negative potentials, the potential has been fixed in the range of -0.40 to -0.50 V, because the carbonyl function of acetophenone starts to reduce at these potentials (see Supplementary Figure 3). Supplementary Table 1 summarizes the relationship between the enantiomeric excess and the reduction potential, the amount of chiral template, and the metal layer thickness. A more positive reduction potential can allow a slight increase of enantiomeric excess (Entries 1 and 2 in Supplementary Table 1). Increasing the weight ratio of chiral template to PtCl₆²⁻ from 0.05 to 0.15, improves the enantiomeric excess by a factor of about two (Entries 2-4 in Supplementary Table 1). A similar tendency can also be observed when using electrodes imprinted with the opposite enantiomer (Entries 5 and 6 in Supplementary Table 1). This confirms the presence of a pronounced chiral character of the metal surfaces, able to promote the transformation of a prochiral molecule into a chiral compound. As stated above, the degree of enantioselectivity is correlated with the thickness of the porous metal layer. Entries 5 and 6 in Supplementary Table 1 indicate a significant improvement of enantiomeric excess when increasing the amount of deposited metal. From these preliminary optimization experiments it is possible to identify as the best conditions for a maximized enantiomeric excess a reduction potential of -0.45 V, a PE enantiomer/PtCl₆²⁻ weight ratio of 0.15, and a metal deposition charge density of 8 C cm⁻².

These conditions were maintained identical for studying the impact of a pulsed driving force on enantioselectivity. As can be seen in Fig. 5a, pulsing the potential has a tremendous impact of the experimental outcome. The high-performance liquid chromatography (HPLC) records obtained with a chiral stationary phase column, which have been normalized with respect to the concentration of (S)-PE, clearly show that the electroreduction of acetophenone on chiral mesoporous platinum imprinted with (S)-PE produces (S)-PE with extremely high selectivity for the shortest pulses. This tendency is quantitatively summarized in Fig. 5b. For long pulses, the unspecific contribution from the acetophenone reduction at the non-chiral outer electrode surface has a strong influence and consequently leads to modest

enantiomeric excess. However, at a very short pulse time (2 s) the %ee is clearly dominated by the conversion occurring almost exclusively inside the mesoporous matrix, owing to its large internal surface area when compared with the area of the non-imprinted outer surface. In this extreme case it reaches values slightly above 90%. In all cases, the relaxation time has been chosen long enough (120 s) to allow the product to leave the metal phase by diffusion and to refill it with fresh prochiral precursor before applying again the potential. This relaxation period has been overestimated on purpose to be on the safe side, and might be easily decreased by an order of magnitude when considering classic diffusion constants. This strategy leads to an almost complete suppression of the non-selective reaction at the external surface.

This effect can be understood by analyzing more closely the chronoamperometric curves obtained during such potential pulses (Supplementary Figure 4). The experiment consists of recording a chronoamperogram with an imprinted electrode when the potential is applied immediately after immersing it in a solution containing acetophenone. In this case acetophenone is not present in the mesopores and only reacts at the outer surface producing I_{Out} as a current (Supplementary Figure 4a, red curve). In a second experiment, the same electrode is allowed to equilibrate with the solution before applying the potential. Therefore, acetophenone will be present also in the mesoporous phase and lead to a current enhancement measured as I_{Out+In} (Supplementary Figure 4a, blue curve). Plotting the ratio between these two currents (I_(In+Out)/I_(Out)) gives a good indication of the relative contribution of the conversion of molecules inside the porous phase compared with the global amount of reacting molecules (Supplementary Figure 4b). It becomes evident that for rather short times (<2 s) the current is strongly influenced by molecules reacting inside the pores in a chiral environment, whereas for longer time intervals the overall current is mostly owing to molecules converted at the outer surface, which can be more easily resupplied by diffusion, but react in a nonenantioselective way. This leads to a decrease of %ee when increasing the pulse duration. These measurements demonstrate that the characteristic time scale of diffusion from the outside into the pores is much longer than that for the electron transfer rate inside the pores. A pulse time of 2 s seems therefore to be close to optimal, because for shorter pulses not all the molecules in the pores are converted, so the yield is lower, whereas for longer pulse

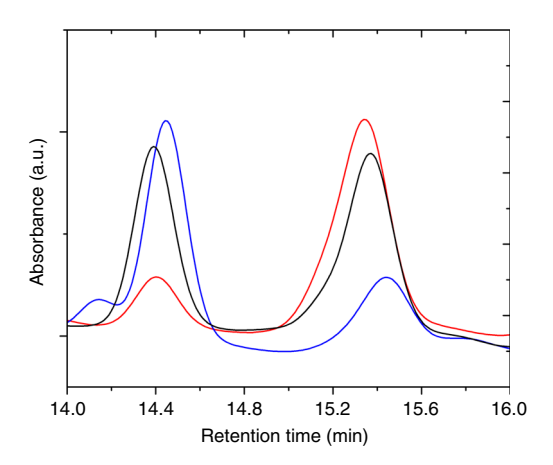


Fig. 6 Monitoring of enantioselectivity as a function of imprinted enantiomer. HPLC chromatograms of the electrosynthesis products obtained by an electrode imprinted with (S)-PE (red) and an electrode imprinted with (R)-PE (blue) (PE/PtCl₆²⁻ weight ratio of 0.15). The respective signals are compared with a racemate of PE that is obtained by electrosynthesis with an electrode imprinted with racemic PE (black). Peaks at retention times of 14.4 and 15.3 min belong to (R)-PE and (S)-PE, respectively

times the outer electrode surface starts to interfere more and more and lowers the enantiomeric excess.

An opposite selectivity is observed when using electrodes imprinted with (R)-PE (pulse time of 10 s). The (R)-PE peak area is much higher than the (S)-PE peak (Fig. 6 and Supplementary Table 2). In addition, the enantiomeric excess obtained by using the electrodes imprinted with different chiral configurations was also confirmed by the results of circular dichroism measurements (Supplementary Figure 5) of the product solutions. Opposite signals in the circular dichroism spectra were obtained for electrodes imprinted with different enantiomers. The %ee values for electrodes imprinted with opposite enantiomers are in good agreement (+60.4 and -66.9% for imprinting with (R)-PE and (S)-PE, respectively), indicating the reproducibility of the electrodes.

One important aspect of heterogeneous reactions is the reusability of the active surface. We therefore studied the stability of the retained chiral information by measuring the degree of enantioselectivity of one and the same imprinted electrode in three consecutive experiments (Supplementary Figure 6 and Supplementary Table 3). The enantioselectivity is decreasing, but even after the third run %ee values are still very significant (about 40%). Obviously, such a decrease should be kept at a minimum and might be due to a rearrangement of the chiral cavities as a consequence of the surface mobility of the metal atoms. One possibility to stabilize the structural chiral information might be to perform the synthesis at lower temperatures.

Theoretically, the amount of generated chiral metal cavities should correlate with the content of chiral template molecule in the plating mixture. Therefore, we also examined the enantios-electivity as a function of the weight ratio of chiral template/ PtCl₆²⁻. It was found that the %ee dramatically improves from 12.0 to 66.9 % when increasing the chiral template to platinum ratio from 0.05 to 0.15 for a 10 s pulse time (Supplementary Figure 7a,b). However, the %ee starts to decrease when using a too high amount of chiral template. This may be explained by the fact that the self-assembly of the lyotropic liquid crystal phase is disturbed in the presence of too much chiral template, thus preventing the formation of the mesopores. Such a morphological change of the supramolecular template leads to less efficient imprinting of chiral information.

Discussion

Highly stereoselective reduction of acetophenone with CIMP electrodes has been successfully achieved based on potential pulsed electrolysis. In conventional electrosynthesis a constant potential is applied to the working electrode. This leads to a steady-state conversion of molecules preferentially at the outer electrode surface, because diffusion into the mesopores is rather slow. As all parts of the platinum film are used as working electrode, but the chiral character is only present inside the mesopores, and not at the outer surface, the obtained enantiomeric excess is dominated by the unspecific reaction path. This eventually leads to almost a racemate even though selectivity can be slightly increased by changing the amount of chiral template in the plating mixture, the porous metal film thickness, and the reduction potential.

In order to circumvent this problem of modest stereoselectivity it is necessary to play with the competition between molecular transport efficiency into the enantioselective mesopores and reaction kinetics at the non-selective outer surface. The main strategy of this work has been to use repeatedly short potential pulses alternating with relaxation periods at open circuit. During the relaxation period the mesoporous matrix is filled with prochiral starting molecules by diffusion, which adsorb in the metal cavities bearing the chiral information. Application of a potential pulse leads to the conversion of these molecules inside the mesopores, but also of molecules at the external surface. The relative contribution of these two populations is tunable by the pulse length. To confirm this hypothesis, electroreduction experiments were carried out with varying pulse times. For long pulses the molecules in the matrix are converted immediately, but then cannot be resupplied efficiently enough during the remaining time of the pulse. For short pulses the situation is opposite, because the quantity of molecules stored and converted in the mesopores is much higher due to the very high internal surface area. Once this conversion has taken place, the potential is switched off so that the contribution of the much smaller outer surface area is almost negligible.

Interestingly, theses electrodes can be reused for several independent experiments and still show significant enantioselectivity. This demonstrates that the observed chiral features don't originate from chiral template molecules left over in the porous structure after the initial metal electrodeposition step. Optimization of all different parameters finally allows reaching a %ee of over 90 %, which is extremely high for such a heterogeneous reaction scheme and starts to be competitive with respect to more classic approaches. However, the global conversion yield for a given reaction time is still modest (Supplementary Figure 8) owing to the exagerated relaxation time, but this can be further optimized in forthcoming studies. It is also important to mention that no significant quantities of side products, for example, owing to dimerization, seem to be formed as can be judged from HPLC analysis (Supplementary Figure 9). Thus, this opens up interesting perspectives in the frame of the development of selective chiral synthesis strategies for high-added-value products, one of the key challenges in modern organic chemistry.

Methods

Chemicals. Hexachloroplatinic acid hydrate (H₂PtCl₆. xH₂O), polyoxyethylene (10) cetyl ether (Brij 56) together with (*R*)- and (*S*)-phenylethanol (PE) and MilliQ water were used to prepare the liquid crystal plating mixtures. Acetophenone was used as the prochiral reactant. Ammonium chloride was used as a supporting electrolyte. All chemicals were purchased from Sigma-Aldrich and used without further purification.

Synthesis and characterization of CIMP. CIMP was prepared following a modified literature procedure 46 . Gold-coated glass slides (1 cm 2) were used as substrates and PE enantiomer was used as a chiral template molecule. The liquid

crystal mixture composed of 42 wt% of non-ionic surfactant (Brij 56), 29 wt% of chloroplatinic acid, 29 wt% of MiliQ water and the calculated amount of the chiral template molecule, was mixed until becoming completely homogeneous. The obtained, very viscous, paste was then placed as a several millimeter thick layer on a cleaned gold-coated glass slide. After insertion of a reference (Ag/AgCl) and counter electrode (platinum grid) in the liquid crystal paste, platinum was deposited at a constant potential of $-0.1~\rm V$ while measuring and integrating the current. Depending on the desired final thickness of the mesoporous metal layer, the injected charge densities have been varied from 2 to 8 C.cm⁻². Subsequently, in order to remove the template molecules (surfactant and enantiomer), the electrodes were rinsed and soaked in MilliQ water for 24 h. Series of UV-Vis spectra of the different washing solutions were recorded to monitor the template removal as a function of rinsing time (Supplementary Figure 2).

The surface morphology and the thickness of the Pt film was characterized with a Hitachi TM-1000 tabletop electron microscope. The mesoporous nature of the deposit was studied by transmission electron microscopy (JEOL JEM-2010). In order to perform these TEM measurements, the platinum covered Au-coated glass slides were immersed in an aqueous solution of 4 wt% KI and 1 wt% $\rm I_2$ for ~ 20 mins ot that the underlying Au layer gets etched away. The mesoporous platinum film was then carefully detached from the electrode by slow immersion of the sample into DI water. The obtained floating film was finally transferred onto a TEM grid.

The electroactive surface area of CIMP was calculated from the integral of the hydrogen adsorption and desorption peaks obtained from the cyclic voltammograms of the Pt electrodes in 0.5 M $\rm H_2SO_4$ recorded at a scan rate of 100 mVs $^{-1}$ in the range from -0.25 to 1.25 V. The real surface area of Pt was estimated based on a calibration factor of 210 mC.cm $^{-2.54}$.

Pulsed electroconversion of acetophenone on CIMP. In order to optimize the experimental parameters, including the reduction potential, the amount of chiral template used in the plating mixture, and the thickness of the platinum film, conventional steady-state electrochemical reduction of acetophenone on CIMP was performed with potentials ranging from -0.40 to -0.50 V for 13 h in a stirred aqueous solution of 10 mM acetophenone and 1 M ammonium chloride as supporting electrolyte. Before starting the reaction, the system was kept for 30 min in the mixture to let the solution diffuse inside the porous network. All experiments were carried out using an Autolab PGSTAT204 equipped with Ag/AgCl (sat. KCl), a Pt mesh, and CIMP as reference, counter, and working electrodes, respectively.

In the case of pulsed electrochemical reduction, the applied potential was -0.45 V with pulse times varying from 2 to 60 s. The relaxation time was kept constant at 120 s after each voltage pulse.

Finally, the products were extracted using heptane as solvent and the organic solution was analyzed by HPLC. HPLC was performed on a Shimadzu LC-2030C3D equipped with a chiral HPLC column (CHIRALPAK IB, 250 \times 4.6 mm inner diameter) using a mobile phase containing 95% heptane/5% i-propanol at a flow rate of 0.5 ml min $^{-1}$ and an optical detection at 215 nm. The integrated peak area was measured using Lab Solution software. To calculate the total conversion of acetophenone into product, a calibration curve of product was recorded (Supplementary Figure 8). To further confirm the enantiomeric excess, circular dichroism spectroscopy was performed on a Jasco J-815 spectrometer and circular dichroism spectra were recorded at a scan rate of 50 nm min $^{-1}$ (Supplementary Figure 5).

Data availability. All relevant data that support the current findings and which are not included in the main manuscript or the Supplementary Information are available from the corresponding authors on request.

Received: 3 August 2017 Accepted: 10 November 2017 Published online: 12 December 2017

References

- Gautier, C. & Bürgi, T. Chiral gold nanoparticles. ChemPhysChem. 10, 483–492 (2009)
- Chen, W. et al. Nanoparticle superstructures made by polymerase chain reaction: Collective interactions of nanoparticles and a new principle for chiral materials. *Nano. Lett.* 9, 2153–2159 (2009).
- Liang, J., Wu, Y., Deng, X. & Deng, J. Optically active porous materials constructed by chirally helical substituted polyacetylene through a high internal phase emulsion approach and the application in enantioselective crystallization. ACS Macro Lett. 4, 1179–1183 (2015).
- Horvath, J. D., Koritnik, A., Kamakoti, P., Sholl, D. S. & Gellman, A. J. Enantioselective separation on a naturally chiral surface. *J. Am. Chem. Soc.* 126, 14988–14994 (2004).
- Balents, L. & Fisher, M. P. A. Chiral surface states in the bulk quantum hall effect. *Phys. Rev. Lett.* 76, 2782–2785 (1996).

- Gellman, A. J. Chiral surfaces: accomplishments and challenges. ACS Nano. 4, 5–10 (2010).
- Arnaboldi, S. et al. Inherently chiral electrodes: the tool for chiral voltammetry. Chem. Sci. 6, 1706–1711 (2015).
- Peng, C. & Lavrentovich, O. D. Chirality amplification and detection by tactoids of lyotropic chromonic liquid crystals. Soft Matter 11, 7257–7263 (2015).
- Farina, V., Reeves, J. T., Senanayake, C. H. & Song, J. J. Asymmetric synthesis of active pharmaceutical ingredients. *Chem. Rev.* 106, 2734–2793 (2006).
- Blaser, H.-U., Pugin, B. & Spindler, F. Progress in enantioselective catalysis assessed from an industrial point of view. J. Mol. Catal. A 231, 1–20 (2005).
- 11. Blaser, H. U. The chiral pool as a source of enantioselective catalysts and auxiliaries. *Chem. Rev.* **92**, 935–952 (1992).
- Casiraghi, G., Zanardi, F., Rassu, G. & Spanu, P. Stereoselective approaches to bioactive carbohydrates and alkaloids with a focus on recent syntheses drawing from the chiral pool. *Chem. Rev.* 95, 1677–1716 (1995).
- Nugent, W. A., RajanBabu, T. V. & Burk, M. J. Beyond nature's chiral pool: enantioselective catalysis in industry. Science 259, 479 (1993).
- Maier, N. M., Franco, P. & Lindner, W. Separation of enantiomers: needs, challenges, perspectives. J. Chromatogr. A. 906, 3–33 (2001).
- Okamoto, Y. & Ikai, T. Chiral HPLC for efficient resolution of enantiomers. Chem. Soc. Rev. 37, 2593–2608 (2008).
- Noyori, R. Asymmetric catalysis: Science and opportunities (Nobel lecture 2001). Adv. Synth. Catal. 345, 15–32 (2003).
- Heitbaum, M., Glorius, F. & Escher, I. Asymmetric heterogeneous catalysis. Angew. Chem. Int. Ed. 45, 4732–4762 (2006).
- Cornils, B. & Herrmann, W. A. Concepts in homogeneous catalysis: the industrial view. J. Catal. 216, 23–31 (2003).
- Yoon, T. P. & Jacobsen, E. N. Privileged chiral catalysts. Science 299, 1691 (2003).
- Lu, Z. & Ma, S. Metal-catalyzed enantioselective allylation in asymmetric synthesis. Angew. Chem. Int. Ed. 47, 258–297 (2008).
- Morris, R. H. Asymmetric hydrogenation, transfer hydrogenation and hydrosilylation of ketones catalyzed by iron complexes. *Chem. Soc. Rev.* 38, 2282–2291 (2009).
- Kupai, J., Rojik, E., Huszthy, P. & Szekely, G. Role of chirality and macroring in imprinted polymers with enantiodiscriminative power. ACS Appl. Mater. Interfaces 7, 9516–9525 (2015).
- Dai, C. et al. Chiral sensing of Eu(III)-containing achiral polymer complex from chiral amino acids coordination induction. J. Polym. Sci. Part A 52, 3080–3086 (2014).
- Savile, C. K. et al. Biocatalytic asymmetric synthesis of chiral amines from ketones applied to sitagliptin manufacture. Science 329, 305 (2010).
- Matsuda, T., Yamanaka, R. & Nakamura, K. Recent progress in biocatalysis for asymmetric oxidation and reduction. *Tetrahedron* 20, 513–557 (2009).
- Verendel, J. J. et al. Highly flexible synthesis of chiral azacycles via iridiumcatalyzed hydrogenation. J. Am. Chem. Soc. 132, 8880–8881 (2010).
- Xia, Q. H., Ge, H. Q., Ye, C. P., Liu, Z. M. & Su, K. X. Advances in homogeneous and heterogeneous catalytic asymmetric epoxidation. *Chem. Rev.* 105, 1603–1662 (2005).
- Funk, T. W., Berlin, J. M. & Grubbs, R. H. Highly active chiral ruthenium catalysts for asymmetric ring-closing olefin metathesis. J. Am. Chem. Soc. 128, 1840–1846 (2006).
- Noyori, R. & Ohkuma, T. Asymmetric catalysis by architectural and functional molecular engineering: Practical chemo- and stereoselective hydrogenation of ketones. Angew. Chem. Int. Ed. 40, 40–73 (2001).
- Song, F., Wang, C., Falkowski, J. M., Ma, L. & Lin, W. Isoreticular chiral metal
 —organic frameworks for asymmetric alkene epoxidation: Tuning catalytic
 activity by controlling framework catenation and varying open channel sizes. J.
 Am. Chem. Soc. 132, 15390–15398 (2010).
- 31. Jeong, K. S. et al. Asymmetric catalytic reactions by NbO-type chiral metalorganic frameworks. *Chem. Sci.* **2**, 877–882 (2011).
- Gross, E. et al. Asymmetric catalysis at the mesoscale: gold nanoclusters embedded in chiral self-assembled monolayer as heterogeneous catalyst for asymmetric reactions. J. Am. Chem. Soc. 135, 3881–3886 (2013).
- Lawton, T. J. et al. Long range chiral imprinting of Cu(110) by tartaric acid. J. Phys. Chem. C 117, 22290–22297 (2013).
- Switzer, J. A., Kothari, H. M., Poizot, P., Nakanishi, S. & Bohannan, E. W. Enantiospecific electrodeposition of a chiral catalyst. *Nature* 425, 490–493 (2003)
- Chen, C., Shi, H. & Zhao, G. Chiral recognition and enantioselective photoelectrochemical oxidation toward amino acids on single-crystalline ZnO. J. Phys. Chem. C 118, 12041–12049 (2014).
- Attard, G. A. Electrochemical studies of enantioselectivity at chiral metal surfaces. J. Phys. Chem. B 105, 3158–3167 (2001).
- Hazzazi, O. A., Attard, G. A. & Wells, P. B. Molecular recognition in adsorption and electro-oxidation at chiral platinum surfaces. *J. Mol. Catal. A* 216, 247–255 (2004).

- Garzón, I. L. et al. Chirality, defects, and disorder ingold clusters. Eur. Phys. J. D 24, 105–109 (2003).
- Farrag, M. Enantioselective silver nanoclusters: preparation, characterization and photoluminescence spectroscopy. *Mater. Chem. Phys.* 180, 349–356 (2016).
- Yan, J. et al. Asymmetric synthesis of chiral bimetallic [Ag₂₈Cu₁₂(SR)₂₄]₄-nanoclusters via ion pairing. J. Am. Chem. Soc. 138, 12751–12754 (2016).
- Durán Pachón, L. et al. Chiral imprinting of palladium with cinchona alkaloids. Nat. Chem. 1, 160–164 (2009).
- 42. Yasukawa, T., Suzuki, A., Miyamura, H., Nishino, K. & Kobayashi, S. Chiral metal nanoparticle systems as heterogeneous catalysts beyond homogeneous metal complex catalysts for asymmetric addition of arylboronic acids to α,βunsaturated carbonyl compounds. J. Am. Chem. Soc. 137, 6616–6623 (2015).
- Zhan, P., Wang, Z.-G., Li, N. & Ding, B. Engineering gold nanoparticles with DNA ligands for selective catalytic oxidation of chiral substrates. ACS Catal. 5, 1489–1498 (2015).
- Fang, Y. et al. Chiral sensing with mesoporous Pd@Pt nanoparticles. ChemElectroChem. 4, 1–5 (2017).
- 45. Behar-Levy, H., Neumann, O., Naaman, R. & Avnir, D. Chirality induction in bulk gold and silver. Adv. Mater. 19, 1207–1211 (2007).
- 46. Wattanakit, C. et al. Enantioselective recognition at mesoporous chiral metal surfaces. *Nat. Commun.* 5, 3325 (2014).
- Yutthalekha, T. et al. Asymmetric synthesis using chiral-encoded metal. Nat. Commun. 7, 12678 (2016).
- Yutthalekha, T., Warakulwit, C., Limtrakul, J. & Kuhn, A. Enantioselective recognition of DOPA by mesoporous platinum imprinted with mandelic acid. *Electroanalysis* 27, 2209–2213 (2015).
- Yoshida, J. I., Kataoka, K., Horcajada, R. & Nagaki, A. Modern strategies in electroorganic synthesis. Chem. Rev. 108, 2265–2299 (2008).
- Attard, G. S. et al. Mesoporous platinum films from lyotropic liquid crystalline phases. Science 278, 838–840 (1997).
- Valle, B., Gayubo, A. G., Aguayo, A. T., Olazar, M. & Bilbao, J. Selective production of aromatics by crude bio-oil valorization with a nickel-modified HZSM-5 zeolite catalyst. *Energy Fuels* 24, 2060–2070 (2010).
- Undri, A. et al. A simple procedure for chromatographic analysis of bio-oils from pyrolysis. J. Anal. Appl. Pyrolysis 114, 208–221 (2015).
- González, C., Marín, P., Diez, F. V. & Ordóñez, S. Hydrodeoxygenation of acetophenone over supported precious metal catalysts at mild conditions: Process optimization and reaction kinetics. *Energy Fuels* 29, 8208–8215 (2015).
- Trasatti, S. & Petrii, O. A. Real surface area measurements in electrochemistry. J. Electroanal. Chem. 327, 353–376 (1992).

Acknowledgements

This work has been supported by the CNRS through the French-Thai PICS program. A. K. acknowledges financial support from the Institut Universitaire de France. This project

has also received funding from the European Research Council (ERC) under the European Union's Horizon 2020 research and innovation program (grant agreement no. 741251, ERC Advanced grant ELECTRA). C.W. thanks for the support of scientific instruments by the Frontier Research Center and the Vidyasirimedhi Institute of Science and Technology (VISTEC). The Junior Research Fellowship program and Franco-Thai PhD scholarship program, sponsored by the French Ministry of Foreign Affairs, and the Thailand Research Fund (TRF) (MRG5980114) as well as the Office of Higher Education Commission (OHEC) are acknowledged for financial support. This work has benefited from the facilities and expertize of the Biophysical and Structural Chemistry platform (BPCS) at IECB, CNRS UMS3033, Inserm US001, Bordeaux University.

Author contributions

C.W. and A.K. conceived and designed the experiments; C.W., T.Y., S.A., and V.L. performed the experiments; C.W., T.Y. and A.K. co-produced the manuscript.

Additional information

Supplementary Information accompanies this paper at https://doi.org/10.1038/s41467-017-02190-z.

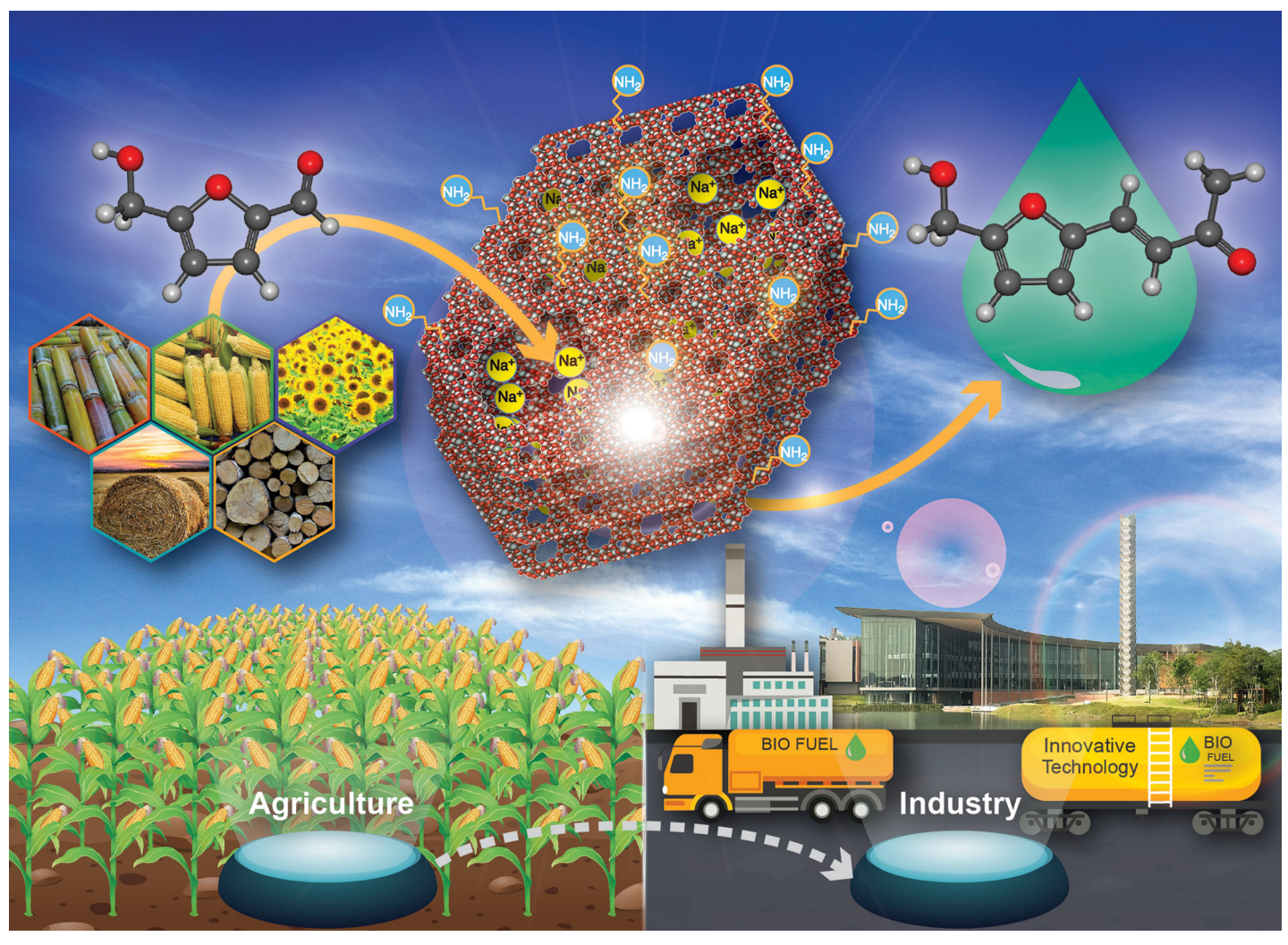
Competing interests: The authors declare no competing financial interests.

Reprints and permission information is available online at http://npg.nature.com/reprintsandpermissions/

Publisher's note: Springer Nature remains neutral with regard to jurisdictional claims in published maps and institutional affiliations.

Open Access This article is licensed under a Creative Commons Attribution 4.0 International License, which permits use, sharing, adaptation, distribution and reproduction in any medium or format, as long as you give appropriate credit to the original author(s) and the source, provide a link to the Creative Commons license, and indicate if changes were made. The images or other third party material in this article are included in the article's Creative Commons license, unless indicated otherwise in a credit line to the material. If material is not included in the article's Creative Commons license and your intended use is not permitted by statutory regulation or exceeds the permitted use, you will need to obtain permission directly from the copyright holder. To view a copy of this license, visit https://creativecommons.org/licenses/by/4.0/.

© The Author(s) 2017



Showcasing research from the laboratory of Dr Chularat Wattanakit, School of Energy Science and Engineering, Vidyasirimedhi Institute of Science and Technology (VISTEC), Thailand.

Aldol condensation of biomass-derived platform molecules over amine-grafted hierarchical FAU-type zeolite nanosheets (Zeolean) featuring basic sites

Amine-grafted FAU nanosheets exhibited the superior catalytic performance for the aldol condensation of biomass feedstocks yielding the desired product close to 100%. This example revealed the development of surface-modified catalysts for applications regarding the conversion of renewable sources to chemicals.





ChemComm



COMMUNICATION

View Article Online



Cite this: Chem. Commun., 2017, 53 12185

Received 15th August 2017, Accepted 20th October 2017

DOI: 10.1039/c7cc06375i

rsc.li/chemcomm

Aldol condensation of biomass-derived platform molecules over amine-grafted hierarchical FAU-type zeolite nanosheets (Zeolean) featuring basic sites†

Thittaya Yutthalekha, 🕩 a Duangkamon Suttipat, 🕩 a Saros Salakhum, 🕩 a Anawat Thivasasith, 🕩 a Somkiat Nokbin, 🕩 b Jumras Limtrakul 🕩 c and Chularat Wattanakit ***

The superior catalytic performance of amine-grafted hierarchical basic FAU-type zeolite nanosheets for the aldol condensation of 5hydroxymethylfurfural (5-HMF) and acetone (Ac) has been achieved due to the synergistic effect of hierarchical structures, featuring basic active sites together with surface modification. This results in an unprecedented yield of 4-[5-(hydroxymethyl)furan-2-yl]but-3en-2-one (HMB) close to 100%. The catalytic activity can be easily tuned by changing the degree of basicity corresponding to the nature of basic sites and surface modification.

The conversion of renewable feedstocks to chemicals is one of the most fascinating research topics, especially in catalysis. Aldol condensation is a well-known reaction forming a carbon-carbon bond between two aldehyde/ketone molecules. To combine this reaction together with biomass-derived platform molecules, the direct condensation of 5-hydroxymethylfurfural (5-HMF) with acetone (Ac), which is also available from renewable biomass via fermentation, is proposed to be a promising approach to increase the number of the carbon chain length (from C₇ to C₁₅) of biomass precursors in order to obtain biofuels.^{2,3}

Base-catalysed aldol condensation is a typical reaction generating an enolate intermediate, which is subsequently transformed to a C-C condensation product.⁴ However, there are drawbacks with homogeneous mineral base catalysts as they cannot undergo the reaction because of the formation of an alkoxide ion and they are very difficult to recover from the reaction mixtures.⁵ Therefore, heterogeneous solid catalysts have significant advantages;

however, they often suffer from rapid catalyst deactivation when using solid bases due to the presence of acids,6 which have a large portion of fermented biomass, for example, acetic acid. To overcome these limitations, the development of alternative highly efficient solid-base catalysts is still a great challenge.⁷

The application of zeolites as heterogeneous base catalysts has been attracting tremendous interest over the past few decades due to their outstanding selectivity in fine-chemistry related reactions,8 simplified process, and waste treatment. Moreover, their moderate basicity made them more attractive in aldol-type condensation, while stronger bases (e.g., NaOH, MgO) promote the formation of undesired side-products. 9-11

Since this type of reaction always deals with bulky molecules, aluminum-rich FAU-type zeolites have been considered as one of the most suitable candidates. Although there are many advantages, such as shape selectivity to bulky reactants and high ion exchange capacity due to their large pores and low Si/Al ratio, 12 conventional FAU zeolites often suffer from diffusion limitation of their sole microporous structures. 10,13 Therefore, hierarchical zeolite nanosheets have become more interesting for the aldol condensation of bulky molecules. 14-16 Recently, our group demonstrated that the hierarchical acid zeolite nanosheets exhibit superior performances in various catalytic reactions dealing with bulky molecules, such as alkylation and aromatization of hydrocarbons. 17-19 However, a very limited number of studies regarding the catalytic behavior of hierarchical base zeolite nanosheets have been reported, 17 and in particular, such catalysts have not yet been demonstrated for the aldol-type condensation involving bulky reactants.

Surface modification is also an alternative way to fine-tune the surface properties of catalysts. To further increase the efficiency of basic zeolite, amine functionalized surfaces can enhance the basicity of catalysts. In this work, we present the benefits of hierarchical FAU-type zeolite nanosheets featuring basic sites, which are obtained by ion-exchange with various alkaline metals together with amine-grafted surface modification for potential application of the aldol condensation of 5-HMF and Ac. The synergistic effects of hierarchical porosity,

^a Department of Chemical and Biomolecular Engineering, School of Energy Science and Engineering, Vidyasirimedhi Institute of Science and Technology, Rayong 21210. Thailand. E-mail: chularat.w@vistec.ac.th

^b Department of Chemistry, NANOTEC Center for Nanoscale Materials Design for Green Nanotechnology, and Center for Advanced Studies in Nanotechnology and Its Applications in Chemical, Food and Agricultural Industries, Faculty of Science, Kasetsart University, Bangkok 10900, Thailand

^c Department of Materials Science and Engineering, School of Molecular Science and Engineering, Vidyasirimedhi Institute of Science and Technology, Rayong 21210,

[†] Electronic supplementary information (ESI) available. See DOI: 10.1039/c7cc06375j

Communication ChemComm

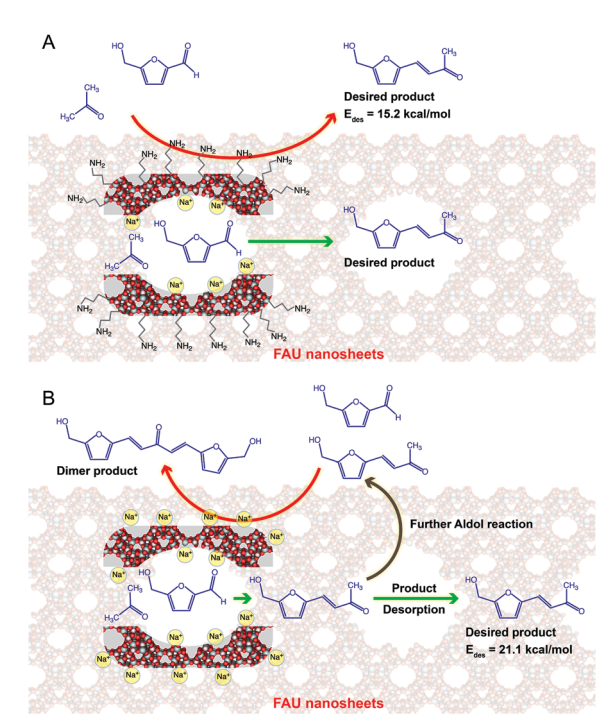


Fig. 1 Illustration showing (A) the amine-grafted surface modification of FAU nanosheets featuring ion-exchanged basic sites to promote the selective production of HMB via the aldol condensation of 5-HMF and Ac, (B) the non-selective reaction over unmodified zeolite surfaces.

the basicity of various alkaline metals and amine surface modification on catalytic performances in terms of the catalytic activity, desired product selectivity, and coke resistance of a nanosheet zeolite were also demonstrated.

Fig. 1A presents the selective production of HMB as confirmed by the mass spectra (see Fig. S1, ESI†) via the aldol condensation of 5-HMF and Ac over amine-grafted surfaces of FAU nanosheets featuring ion-exchange basic sites. The amine modified surfaces not only promote the basic sites for the reaction but also weaken the adsorption of HMB, resulting in suppression of dimerization as a side reaction (Fig. 1). In strong contrast to this, unmodified zeolite surfaces facilitate the dimerization of products, eventually leading to a low selectivity of HMB (Fig. 1B). The production pathway of HMB is described by the base-catalysed mechanisms as illustrated in Fig. S2 (ESI†). The enolate adduct can be formed and then converted to α,β -unsaturated carbonyl compounds.

To provide high ion-exchange capacity of catalysts, hierarchical X-type zeolite nanosheets after complete removal of the organosilane template (see Fig. S3, ESI†) have been used because they have high aluminum content. In this case, various alkaline active sites (Na, Ca and Ba) have been successfully prepared with a high ion exchange degree (%IED) (~95%, see Table S1, ESI†). In addition, the catalyst surfaces were modified by amine grafting of 3-aminopropyltriethoxysilane (APTES) in an ethanol solution at room temperature. All prepared zeolite X samples maintain their FAU structures (black pattern in Fig. 2A) without any competing crystalline impurity (e.g., GIS as shown in the red pattern) together with the same Si/Al ratio (1.3-1.4) even after several repeated ion exchange and amino grafting processes (see Table S1, ESI†).

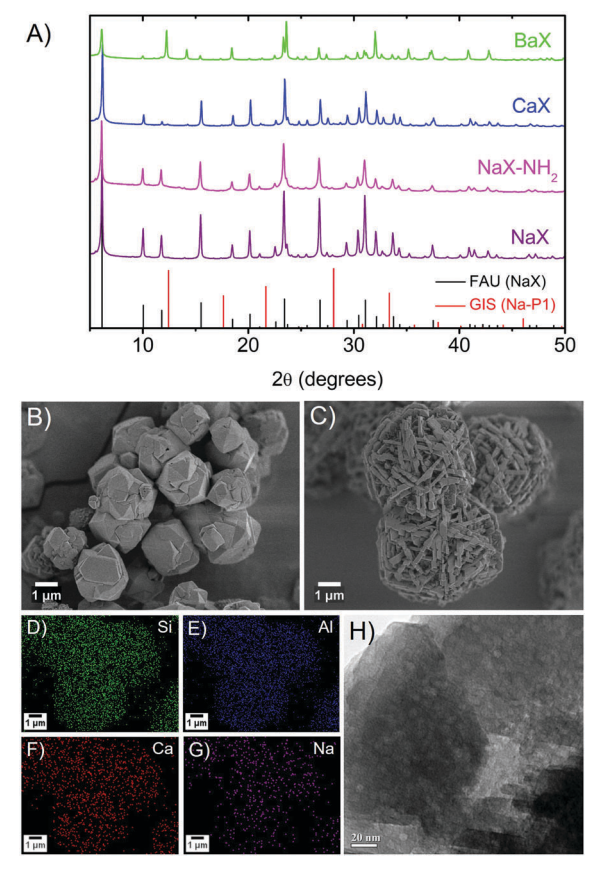


Fig. 2 Characterization of zeolite catalysts featuring basic sites including (A) XRD patterns of various hierarchical basic zeolite nanosheets; NaX (purple), amine grafted NaX (NaX-NH₂, pink), CaX (blue) and BaX (green) together with standard XRD of FAU (black) and GIS (red) structures, SEM images of (B) conventional NaX and (C) hierarchical NaX nanosheets, (D-G) EDS elemental mapping of ion-exchanged hierarchical nanosheets and (H) the TEM image of hierarchical NaX nanosheets.

However, the ratio of the diffraction peak intensities was significantly changed in the case of the zeolite exchanged with larger cations. The reason for this phenomenon might be explained by the lower X-ray adsorption coefficient of large cations.²⁰ For instance, the sample obtained by ion exchange with Ba exhibits weaker peak intensities and the disappearance of diffraction peaks at 2Θ of 10, 15, 20° was observed, while some intense peaks at 2Θ of 12, 14, 24° appeared instead. This relates to the fact that the structural distortion of the zeolite framework occurs due to the strong interaction of the larger cations and oxygen atoms in the framework.21

Compared with the conventional zeolite, the morphologies of the ion-exchanged hierarchical nanosheets were obviously different (Fig. 2B and C) and similar to those demonstrated in the previous report. 17 The elemental mapping revealed a very uniform distribution of the alkaline cations in the zeolite framework (Fig. 2D-G). The existence of amine groups on the surface of catalysts was also confirmed by ATR-FTIR and ¹³C NMR spectroscopy (see details in the ESI† and Fig. S4). The intracrystalline mesopores were also found in the nanosheet structure as can be seen in Fig. 2H.

ChemComm Communication

The physicochemical properties of catalysts were measured using N₂ sorption measurements. The isotherms of all conventional zeolites (Fig. S5A, ESI†) exhibit adsorption only at a relatively low pressure $(P/P_0 < 0.2)$ with a long horizontal plateau due to micropore filling, corresponding to the type-I isotherm, confirming the microporous characteristic. On the other hand, all hierarchical nanosheet catalysts (Fig. S5B, ESI†) exhibit adsorption at a relatively low pressure together with a hysteresis loop at $P/P_0 \sim 0.45$ due to capillary condensation in the mesopores, which is characteristic of the mesoporous structure. The combination of type-I and IV isotherms observed in the nanosheet catalysts confirms the hierarchical porous structure of catalysts. The hierarchical zeolite exchanged with Ca cations slightly alters the physicochemical properties compared with the NaX nanosheet (Table S2, ESI†). In contrast, the zeolite samples exchanged with the Ba cation and the amine-grafted zeolite could eventually lead to a significant reduction of the specific surface area and pore volume (about 30% and 25% decrease compared with the NaX nanosheet for BaX-NS and NaX-NS-NH₂, respectively). The reason for this decrease in the surface area and pore volume of the Ba-exchanged zeolite related to the fact that Ba obstructs the accessible pore windows due to its large size and also occupies the zeolite pore. In the case of amine-grafted zeolite, the large number of amine-grafted moieties at the zeolite pore mouth also restricts the accessible site of the zeolite pores, resulting in the blockage of zeolite openings.

CO₂-TPD was used to determine the basicity of catalysts. Theoretically, the basic strength of ion-exchanged zeolite could be related to the electrostatic potential of alkaline metal cations in the zeolite framework.²² From the CO₂-TPD profiles (Fig. S6, ESI†), it was observed that all catalysts are composed of two distinct peaks centered at \sim 170 °C and \sim 320 °C. These results indicate that the basic strength of all exchanged zeolites is nearly similar. The number of accessible basic sites was increased noticeably from alkali cations (NaX) to alkaline earth cations (CaX) and decreased upon increasing the cation size (Ca²⁺ to Ba²⁺) (see Table S2, ESI†). This may be explained by the fact that large alkaline cations preferentially occupied the inaccessible sites or they formed reduced metal clustered species. 23-25 Therefore, it becomes evident that the degree of basicity of the exchanged zeolite can be simply tuned depending on the type of alkaline cations.

To demonstrate the catalytic performance, in this study the direct condensation of 5-HMF and Ac was carried out using a batch-type reactor at 130 °C. Typically, HMB and 4-hydroxy-4methyl-2-pentanone (HMP) were formed as the desired and self-condensation products, respectively. For comparison with modified catalysts, the conventional NaX (CON-NaX) was used as the reference sample and the catalytic data are shown in Table S3 (ESI†). As expected, the desired product (HMB) was significantly reduced at a longer reaction time (from 100% at 6 h to 86.47% at 48 h, entries 1-4). Interestingly, the catalytic activity also changes depending on the type of alkaline cation. For example, in the case of a conventional alkaline exchange catalyst, the yield of HMB significantly increases from 29.32% to 38.05% when conventional CaX is used instead of NaX (Fig. 3A). However, the activity decreases when the alkaline

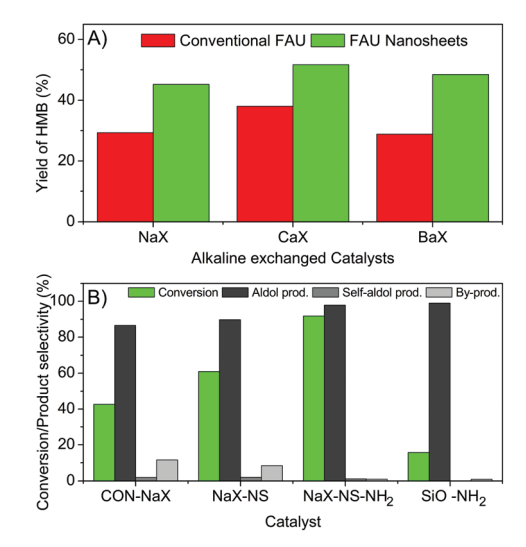


Fig. 3 Catalytic activity of conventional zeolite and hierarchical zeolite nanosheets to demonstrate; (A) the accessibility of molecules to basic sites of alkaline exchanged zeolites and (B) comparison with various solid base catalysts.

earth metal size is increased. The yield of HMB was 28.84% in the case of the conventional BaX. This makes it clear that the catalytic activity towards HMB is directly related to the degree of basicity of the exchanged zeolite.

To further confirm the beneficial effect of hierarchical structures, the catalytic performances of conventional and hierarchical zeolite X nanosheets with various alkaline cations were compared (Fig. 3A). As expected, a significantly higher yield of HMB was observed in all cases of hierarchical zeolites. Although the yield of HMB as a function of the degree of basicity over nanosheet samples was also observed with a similar tendency, the effect of the type of alkaline cation is much less pronounced compared with that of the conventional one. The moderate yield of HMB was approximately 50% in all cases. It is reasonable to assume that the hierarchical structure benefits the increase of the accessible ability of large guest species.

In addition, the recyclability of the catalysts was examined by performing several cycles of the reaction. After the completion of each reaction cycle, the catalysts were regenerated by calcination to remove the deposited cokes before being reused in the next cycle. The O2-TPO profiles of such cokes indicated that the deactivation process of conventional zeolite was not the same as that of the nanosheet one (see details in the ESI† and Fig. S7). The catalytic activity of the regenerated nanosheet and conventional catalysts was unaffected after two or three reaction cycles exhibiting almost constant conversion of 5-HMF and desired product selectivity (Table S3, ESI†). Moreover, the reproducibility of these catalytic results was also demonstrated again. These results clearly confirm the comparable stability of the conventional and nanosheet structures of the catalysts.

Interestingly, the amine-grafted zeolites exhibited a dramatically high conversion of 5-HMF (91.74%) as shown in Fig. 3B. This makes it clear that such amine functionalized surfaces can be considered as additional basic sites. In addition, not only an Communication ChemComm

improved activity but also a significantly higher selectivity of HMB was observed (89.67 and 97.81% for NaX-NS, NaX-NS-NH $_2$, respectively). In strong contrast to this, amine-grafted silica (SiO $_2$ -NH $_2$) showed a very low conversion of only 15.69%, and it is related to a very low external surface area of the support, eventually resulting in a low number of active basic sites (see Table S2, ESI †). Therefore, the hierarchical structure of the NaX zeolite can provide a large portion of additional basic sites compared to amorphous silica.

To verify the effect of amine-grafted surface modification on the catalytic selectivity towards HMB, DFT calculations were performed to investigate the interaction between the product (HMB) and catalytic sites as shown in Fig. S8 (ESI†) for optimized structures of HMB on unmodified surfaces (Fig. S8B, ESI†) and the amine-grafted zeolite X (Fig. S8C, ESI†) (see details in the ESI† and Fig. S8 and S9). It was found that in the case of unmodified NaX, the HMB molecule can be adsorbed on active sites via interaction between the oxygen of HMB (O_{HMB}) and the alkaline sites (Na⁺) with a distance of 2.44 Å, providing a calculated adsorption energy of -21.1 kcal mol⁻¹. In contrast, the adsorption energy of HMB on the amine-grafted surfaces was 6 kcal mol⁻¹ lower than that of the unmodified NaX via interactions between the oxygen of HMB (OHMB) and the amine functional group. It is therefore reasonable to assume that the HMB product on amine grafted zeolite X can be somewhat easily desorbed compared with the unmodified system, resulting in suppression of the formation of dimeric by-products. This is consistent with the view that the HMB selectivity increases after the modification of surfaces with aminosilane molecules.

In summary, the superior catalytic performance in aldol condensation of 5-HMF and Ac has been reported using amine-grafted basic FAU-type zeolite nanosheets for the first time. The synergistic effect of hierarchical structures, featuring basic active sites together with surface modification results in an increase in the catalytic performances due to the following factors: (i) hierarchical structures can improve the accessibility of bulky molecules to catalytically basic sites, especially in the case of large cationic sizes; (ii) the catalytic activity can be easily tuned by changing the degree of basicity of accessible basic active sites; (iii) the introduction of basicity by amine-grafted surfaces provides exceptional catalytic activity and HMB selectivity due to the additional basic sites and the weakening of the interaction of HMB and the zeolite surface. This example opens up very interesting perspectives for the development of surface modified hierarchical zeolite nanosheets for applications regarding conversion of bulky biomass feedstocks to biofuels/ chemicals.

This work was supported by the Research Fellowship from the Vidyasirimedhi Institute of Science and Technology and the Frontier Research Center. C.W would like to thank the Thailand Research Fund (TRF) (MRG5980114), the Office of Higher Education Commission (OHEC), and the Junior Research Fellowship Program of the French Embassy in Thailand.

Conflicts of interest

There are no conflicts to declare.

Notes and references

- D. M. Alonso, J. Q. Bond and J. A. Dumesic, Green Chem., 2010, 12, 1493.
- 2 R. Xing, A. V. Subrahmanyam, H. Olcay, W. Qi, G. P. van Walsum, H. Pendse and G. W. Huber, *Green Chem.*, 2010, **12**, 1933.
- 3 G. W. Huber, J. N. Chheda, C. J. Barrett and J. A. Dumesic, *Science*, 2005, 308, 1446.
- 4 S. Van de Vyver, C. Odermatt, K. Romero, T. Prasomsri and Y. Román-Leshkov, ACS Catal., 2015, 5, 972.
- 5 A. V. Subrahmanyam, S. Thayumanavan and G. W. Huber, *ChemSusChem*, 2010, 3, 1158.
- 6 K. Tanabe, New solid acids and bases: their catalytic properties, Kodansha, 1989.
- 7 J. Li, A. Corma and J. Yu, Chem. Soc. Rev., 2015, 44, 7112.
- 8 J. Weitkamp, M. Hunger and U. Rymsa, *Microporous Mesoporous Mater.*, 2001, **48**, 255.
- 9 L. Faba, E. Díaz and S. Ordóñez, Appl. Catal., B, 2012, 113-114, 201.
- 10 T. C. Keller, S. Isabettini, D. Verboekend, E. G. Rodrigues and J. Perez-Ramirez, Chem. Sci., 2014, 5, 677.
- 11 A. Corma, V. Fornés, R. M. Martín-Aranda, H. García and J. Primo, Appl. Catal., 1990, 59, 237.
- 12 Y. Watanabe, H. Yamada, J. Tanaka, Y. Komatsu and Y. Moriyoshi, Sep. Sci. Technol., 2005, 39, 2091.
- 13 O. Kikhtyanin, V. Kelbichová, D. Vitvarová, M. Kubů and D. Kubička, Catal. Today, 2014, 227, 154.
- 14 A. Inayat, I. Knoke, E. Spiecker and W. Schwieger, Angew. Chem., Int. Ed., 2012, 51, 1962.
- 15 M. Choi, K. Na, J. Kim, Y. Sakamoto, O. Terasaki and R. Ryoo, Nature, 2009, 461, 246.
- 16 X. Zhang, D. Liu, D. Xu, S. Asahina, K. A. Cychosz, K. V. Agrawal, Y. Al Wahedi, A. Bhan, S. Al Hashimi, O. Terasaki, M. Thommes and M. Tsapatsis, *Science*, 2012, 336, 1684.
- 17 T. Yutthalekha, C. Wattanakit, C. Warakulwit, W. Wannapakdee, K. Rodponthukwaji, T. Witoon and J. Limtrakul, J. Cleaner Prod., 2017, 142, 1244.
- 18 P. Wuamprakhon, C. Wattanakit, C. Warakulwit, T. Yutthalekha, W. Wannapakdee, S. Ittisanronnachai and J. Limtrakul, *Microporous Mesoporous Mater.*, 2016, 219, 1.
- W. Wannapakdee, C. Wattanakit, V. Paluka, T. Yutthalekha and J. Limtrakul, RSC Adv., 2016, 6, 2875.
- 20 A. Borgna, S. Magni, J. Sepúlveda, C. L. Padró and C. R. Apesteguía, Catal. Lett., 2005, 102, 15.
- 21 Y. H. Yeom, S. B. Jang, Y. Kim, S. H. Song and K. Seff, J. Phys. Chem. B, 1997, 101, 6914.
- 22 S.-T. Yang, J. Kim and W.-S. Ahn, Microporous Mesoporous Mater., 2010, 135, 90.
- 23 G. M. Lari, K. Desai, C. Mondelli and J. Perez-Ramirez, *Catal. Sci. Technol.*, 2016, 6, 2706.
- 24 T. C. Keller, E. G. Rodrigues and J. Pérez-Ramírez, ChemSusChem, 2014, 7, 1729.
- 25 T. C. Keller, J. Arras, S. Wershofen and J. Pérez-Ramírez, ACS Catal., 2015, 5, 734.



ScienceDirect

Current Opinion in Electrochemistry

Review Article Chiral metals as electrodes Chularat Wattanakit*



Chirality is one of the most fascinating issues in chemical researches. In this review, the development of chiral metals is summarized from the past to the present. Several very recent concepts for generating chiral metals, such as the design of chiral imprinted cavities at mesoporous metal surfaces, are also presented. The application of chiral metals as electrodes in the enantioselective recognition and asymmetric synthesis of chiral compounds reveals that these designer surfaces open up potential perspectives for the development of new materials for chiral technologies.

Address

Department of Chemical and Biomolecular Engineering, School of Energy Science and Engineering, Vidyasirimedhi Institute of Science and Technology, Rayong, 21210, Thailand

*Corresponding author: Wattanakit, Chularat (chularat.w@vistec.ac.th)

Current Opinion in Electrochemistry 2018, 7:54-60

This review comes from a themed issue on **Physical and Nanoelectrochemistry**

Edited by Alexander Kuhn, Neso Sojic and Laurent Bouffier

For a complete overview see the Issue and the Editorial

Available online 12 October 2017

https://doi.org/10.1016/j.coelec.2017.09.027

2451-9103/© 2017 Elsevier B.V. All rights reserved.

Introduction

The introduction of chiral features on solid surfaces has become an important research issue and has seen some original evolutions in recent years because such surfaces might be used in many applications ranging from pharmaceutics [1] and catalysis [2] to sensing [3] and separation science [4]. Over the past decades, the chirality on solid surfaces has been extensively studied due to the benefits of surface properties compared with homogeneous chiral systems. To date, the synthesis of chiral solid surfaces has been achieved by several approaches, including generating an intrinsically chiral surface on a crystal, the adsorption of molecules on a surface or the elaboration of polymeric chiral interfaces based on surface-grafting and molecular imprinting [5–9]. Among them, metals with chiral features have become increasingly popular due to the versatile surface modification of metals and limitations of other materials, such as too flexible molecular structures [10], and low thermal and/or chemical stability [11°].

In the past, the development of chiral metal surfaces has mostly been focused on the design of chiral surfaces by the adsorption of chiral molecules on achiral metal surfaces [12°,13°°]. However, this strategy sometimes suffers from disadvantages, such as losing chirality due to the leaching of adsorbed molecules [14°]. An alternative way to overcome these problems is the design of intrinsically chiral metal surfaces, which can be achieved by cleaving of metal crystals [15**-17**]. In this review, we present a brief overview of the development of chiral metal surfaces and phases. In particular, the concepts of imprinting metal surfaces with chiral molecules, allowing to retain geometric chiral information even after dissolution of the chiral templates, are described [18**-24**]. Furthermore, new potential applications of chiral metals as electrodes in electrochemical analysis and asymmetric synthesis are also discussed, including the development of an electrochemical method for tuning the enantioselective properties of the designer surfaces [23°°].

Development of chiral metal surfaces

Concerning the development of chiral metal surfaces, several concepts have been used by following one of the five approaches: (i) adsorption of chiral molecules on surfaces to produce chiral metals [12°,13°°,25°,26°]; (ii) binding of chiral ligands to metal surfaces [27°]; (iii) cleaving bulk crystals of metals [16°°,28°,29°]; (iv) distortion of symmetrical metal structures [30°]; (v) molecular imprinting with chiral molecules as templates [21°°-23°°,31°°,32°].

First, chiral metal interfaces have been introduced by the molecular adsorption on crystalline surfaces. To obtain chiral features on metal surfaces by the molecular adsorption approach, various modified systems, including achiral molecules adsorbed on achiral surfaces [33°] and chiral molecules adsorbed on achiral/chiral surfaces [26°,34°] are able to generate chiral surfaces. Interestingly, a chiral surface can be obtained by an achiral molecule adsorbed on an achiral surface due to a reduction of the symmetry of the adsorption system compared to the isolated system [33°,35°]. For instance, the adsorption of the achiral molecule, 2,5,8,11,14,17-hexa-tertbutylhexabenzo [bc,ef,hi,kl,no, qr]coronene (HtB-HBC) on a Cu(110) substrate can produce chiral surfaces [33]. The reason for the existence of these chiral surfaces relates to the van der Waals (vdW) interactions between the substrate and the surface, eventually leading to a rotation of the symmetry axis of the self-assembled molecules in a close-packed geometry [25°,33°]. Unsurprisingly, chiral surfaces have been successfully designed by the adsorption of chiral

molecules on achiral surfaces, because of the retention of the conformation of chiral molecules on achiral surfaces [26°,34°]. However, this concept often suffers from losing the chirality on surfaces due to the leaching of adsorbed molecules [36°].

Recently, the encapsulation of metallic nanoclusters in the environment of chiral self-assembled monolayers (SAM) has been demonstrated to improve the efficiency of enantioselective heterogeneous catalysis [27°]. In this case, chiral supramolecular homogeneous catalysts are self-assembled to form a chiral environment immobilized on mesoporous silica as shown in Figure 1A. Gold nanoparticles have been successfully encapsulated inside the chiral matrix without any other stabilizing agent. These materials exhibit outstanding enantioselective catalysis due to the synergetic effect of the catalytically active metal sites and the surrounding chiral matrix.

In addition to such chiral surfaces, intrinsically chiral surfaces can be produced, by creating high Miller index surfaces of metals (e.g., Cu{531}, Pt{643}). This is achieved by cutting a bulk crystal along a specific high index plane [16°,28°,29°]. The asymmetric structure is composed of kinks, vacancies, and adatoms constituting specific adsorption site. Although the low population and limited stability of the chiral sites might be a problem of this approach, these surfaces exhibit significantly different adsorption/desorption rates for two enantiomers $[15^{\circ\circ},29^{\circ},37^{\circ}-43^{\circ}]$. For example, Pt(643) and Pt(431) sites provide different rates for the electrooxidation of Dand L-glucose [16**]. Furthermore, it was also possible to enhance the degree of chirality on metal surfaces by the distortion of metal structures [30°]. Interestingly, the thiol-passivation of gold clusters can also induce and increase chirality when using an intermediate size of gold clusters due to a significant distortion of the structures [30°].

Molecular imprinting with chiral molecules as template is a popular approach to obtain chiral imprinted polymers. However, it is also possible to apply an analog concept to metal and metal oxide surfaces. CuO films have been successfully deposited onto achiral Au(001) $[18^{\bullet\bullet}, 20^{\bullet\bullet}]$ and Cu(111) $[19^{\bullet\bullet}]$ surfaces by the electrodeposition in the presence of chiral compounds, such as chiral tartrate molecules as shown in Figure 1B. Interestingly, the conformation of the chiral molecules was mimicked in the CuO film and this eventually leads to different rates of electrooxidation of (R,R)- and (S,S)-tartrate according to the imprinted chiral configuration as shown in Figure 1C. This work was the first example for generating a chiral metal oxide surface in the presence of a chiral organic molecule.

Not only metal oxides but also metallic materials with modified chiral surfaces have been successfully prepared [31°]. The chiral information can be retained on imprinted Pd nanoparticles even after removable of chiral organic molecules [31°]. To enhance the degree of chirality of molecular imprinted metals, the combination of the chiral imprinting approach together with mesoporous structures has been studied by the electrodeposition of metal in a matrix of self-assembled non-ionic surfactants [44°] and chiral molecules as shown in Figure 2 [21°°]. The columnar structure of a lyotropic liquid crystal is used as a mesoporogen (A). The interaction between chiral molecules and the hydrophilic outer part of the surfactant columns allows electrodeposition of metal around the oriented chiral template (B), and finally chiral cavities at the internal surface of the mesopores can be created after removal of the template molecules (C). This concept can be generalized for various chiral template molecules such as DOPA, and mandelic acid [21**-23**].

Chiral recognition at metal surfaces

To illustrate the application of chiral metal surfaces, chiral recognition is an important aspect, especially from a pharmaceutical and biological point of view. Currently, efforts are devoted to the development of chiral recognition technologies based on electrode surfaces because there are many advantages of these methods, such as a rapid detection by an electrochemical signal. The SAM of chiral molecules on a metal electrode surface can be widely applied for chiral recognition because they are very versatile, allowing to introduce different chemical functionalities, resulting in various chiral surface properties [45°-49°°].

In addition to molecular assemblies at metal electrode surfaces, the imprinting of chiral molecules in a metal or metal oxide matrix is also interesting [18**-23°,31°,32°,50°]. Switzer et al. demonstrated that it was also possible to create chiral recognition sites on several low symmetry materials, such as CuO [18°,20°] and AgO [19**]. These materials exhibit chiral recognition abilities when used as electrodes. For example, an electrodeposited CuO film imprinted with (S,S)-tartrate molecules shows a higher electrooxidation current for (S,S)-tartrate and vice versa for the (R)-imprinted surfaces [18°-20°]. As stated above, an enhanced effect of chirality can be obtained when the active surface area is increased. Enantioselective recognition of chiral molecules has been reported for chiral cavities generated in mesoporous electrode materials [21**,51**]. Significant differences in the electrooxidation currents of two enantiomers are observed by differential pulse voltammetry (DPV). For example, chiral mesoporous platinum imprinted by D-DOPA exhibits higher activity for the electro-oxidation of the D-enantiomer with respect to oxidation of the other (see Figure 4 in Ref. [21**]). The concept of imprinting chirality in mesoporous metals is rather versatile and can be employed for different chiral templates [22**,23**].

Figure 1

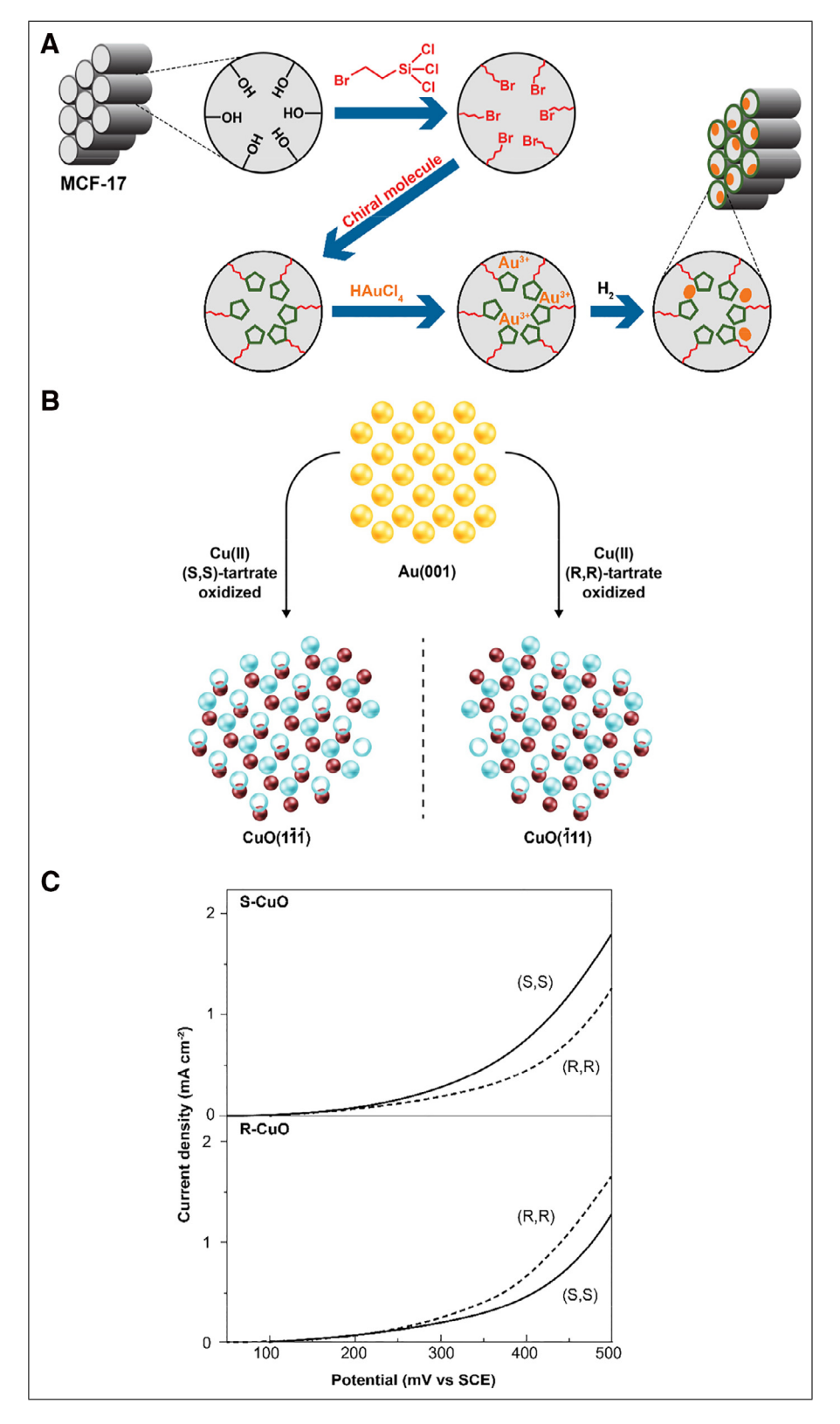


Illustration of: (A) preparation of gold nanoclusters encapsulated inside a chiral matrix, (B) two configurations of electrodeposited chiral CuO films ([111] and [111]) onto achiral Au (001), (C) linear sweep voltammograms of the electrooxidation of (R,R)-tartate and (S,S)-tartate on S-CuO and R-CuO films grown in Cu(II) (S,S-tartrate) and Cu(II) (R,R-tartrate), respectively. Adapted from Refs. [27°] and [18°°].

Figure 2

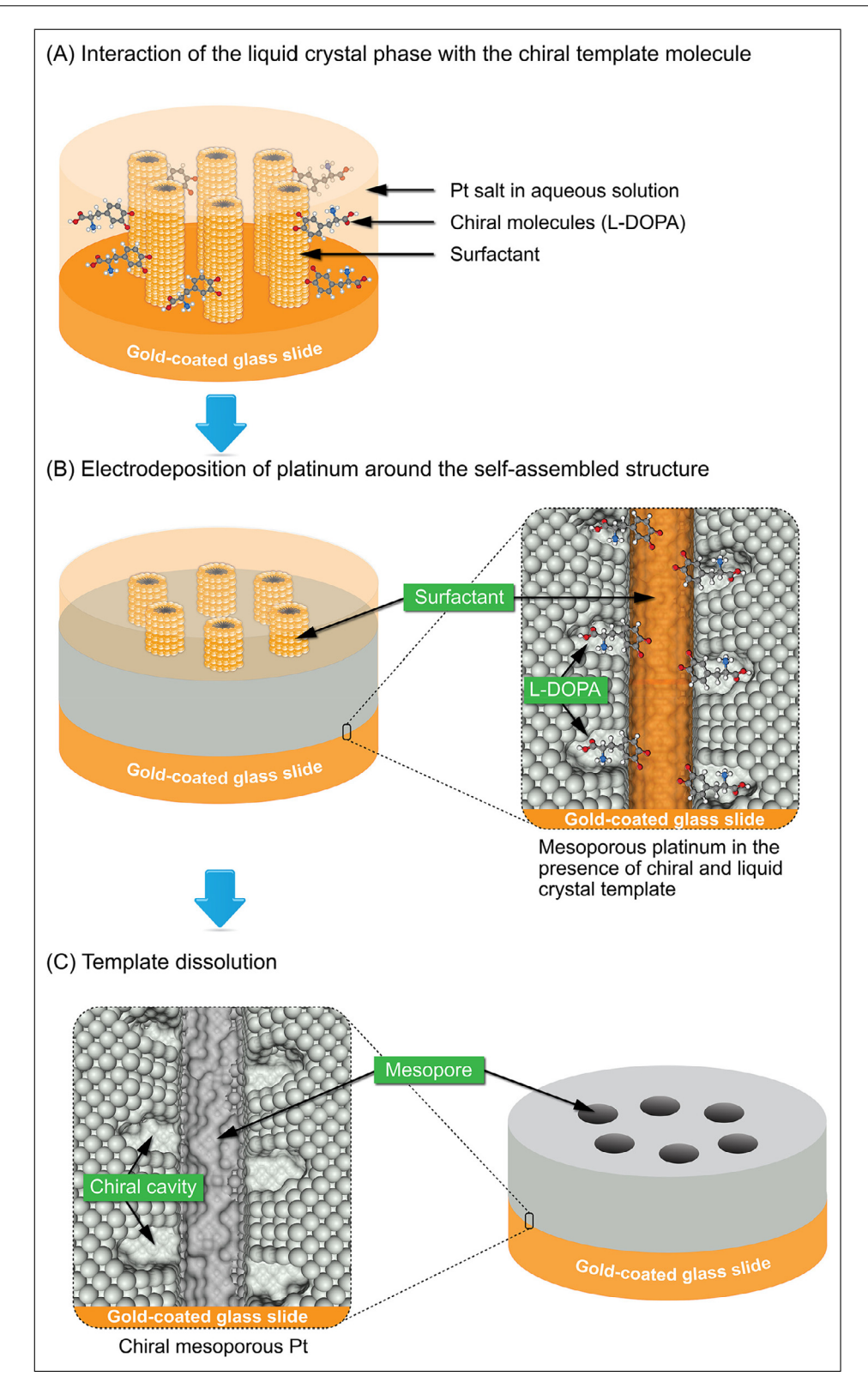


Illustration of the fabrication process of chiral imprinted mesoporous metals in the simultaneous presence of a lyotropic liquid crystal and chiral templates: (A) interaction of lyotropic liquid crystal with the chiral template molecules, (B) reduction of metal around templates, and (C) structures after the removable of templates. Adapted from Ref. [21**].

Asymmetric synthesis at chiral metal surfaces

Another important challenge for chiral technologies is the selective synthesis of a single enantiomer. Although there are many reports demonstrating the development of asymmetric catalysts, most of them are based on the concepts of homogeneous catalysis. Herein, we present a brief overview of the perspectives of asymmetric synthesis using heterogeneous reaction schemes based on chiral metals, in particular when using them in the context of electrochemical synthesis.

Typically, chiral metals lead to low enantioselectivity compared to homogeneous catalysts due to the weak interaction between the surface and the reactants. However, it is possible to overcome this problem. Recently, several chiral metal nanoparticle systems have been reported as novel heterogeneous chiral catalysts [52°-56°]. For example, the excellent yield of chiral arylated product obtained from the asymmetric 1,4-addition of arylboronic acids has been achieved using chiral diene-modified Rh/Ag NP systems [52°]. In addition, the concepts of using chirally imprinted metallo-organic hybrid materials as heterogeneous catalysts have been extensively developed [24**,31**]. Durán Pachón et al. reported that imprinted Pd-alkaloid hybrid materials can be produced by the reduction of a metal salt in the presence of cinchona alkaloid and the resulting compound shows catalytic activity with a certain degree of enantioselectivity for the hydrogenation of acetophenone and isophorone.

Apart from the development of asymmetric synthesis based on chiral metal nanoparticles, recently the concept of using mesoporous metals encoded with chiral information has been introduced for the stereoselective transformation of an achiral starting compound [23**]. As mentioned above, the chiral mesoporous metal matrix can be easily prepared by the reduction of metal ions in the simultaneous presence of a liquid crystal phase and chiral template molecules and perfectly retains the chiral information even after the removable of template. Using these designer surfaces as electrodes leads to significant enantiomeric excess in the product mixture. For example, an electrode imprinted with (R)-mandelic acid eventually enhances the enantiomeric excess of the (R)-enantiomer when converting phenylglyoxylic acid by electroreduction. In addition, the degree of enantiomeric excess can be easily tuned by changing the density of chiral cavities in the material. The enantiomeric excess relates to the fact that the spatial orientation of the prochiral precursor in the asymmetric environment of the imprinted cavities favors hydrogenation of the prochiral carbonyl carbon atom from one side (Figure 3).

However, the simultaneous presence of non-imprinted sites at the external part of the electrode is a limiting factor for the enantiomeric excess so far.

Figure 3

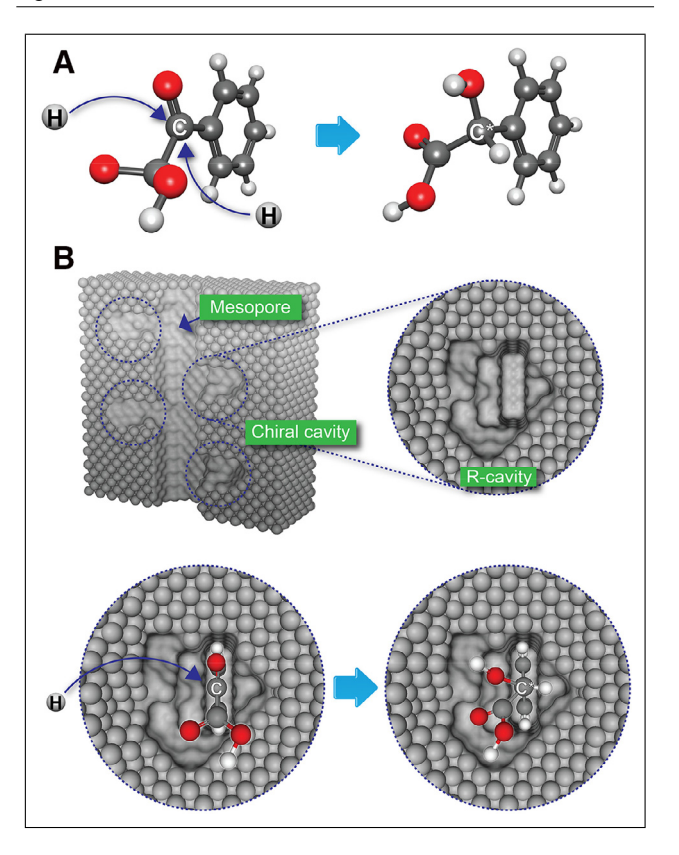


Illustration of (A) the reduction of phenylglyoxylic acid (PGA) to mandelic acid (MA) and (B) the concept of enantioselectivity for the asymmetric electrochemical reduction of PGA to MA. Adapted from Ref. [23**].

Concluding remarks

The development of chiral metals for the enantioselective recognition and asymmetric synthesis has been explored over the past decade. This short review illustrates several promising approaches to elaborate metal surfaces with chiral features. These designer surfaces not only exhibit significant enantioselective recognition, which is an important factor for the development of sensing and separation technologies, but their specific properties also allow asymmetric electrochemical synthesis. These findings open promising perspectives for the application of chiral electrodes in analysis and synthesis.

Acknowledgments

We would like to thank the support from the Vidyasirimedhi Institute of Science and Technology (VISTEC), the Junior Research Fellowship Program of the French Embassy in Thailand, sponsored by the French Ministry Foreign Affairs and the Thailand Research Fund (TRF) (MRG5980114) and the Office of Higher Education Commission (OHEC).

References and recommended reading

Papers of particular interest, published within the period of review, have been highlighted as:

- Paper of special interest.
- Paper of outstanding interest.

- Farina V, Reeves JT, Senanayake CH, Song JJ: Asymmetric synthesis of active pharmaceutical ingredients. Chem Rev 2006, 106:2734-2793
- Blaser H-U, Pugin B, Spindler F: Progress in enantioselective catalysis assessed from an industrial point of view. J Mol Catal A 2005, 231:1-20.
- Bodenhofer K, Hierlemann A, Seemann J, Gauglitz G, Koppenhoefer B, Gpel W: **Chiral discrimination using** piezoelectric and optical gas sensors. Nature 1997,
- Cichelli J, Zharov I: Chiral permselectivity in surface-modified nanoporous opal films. J Am Chem Soc 2006, 128:8130-8131.
- Pernites RB, Venkata SK, Tiu BDB, Yago ACC, Advincula RC: Nanostructured, molecularly imprinted, and template-patterned polythiophenes for chiral sensing and differentiation. Small 2012, 8:1669-1674.
- Vlatakis G, Andersson LI, Muller R, Mosbach K: Drug assay using antibody mimics made by molecular imprinting. Nature 1993, **361**:645-647.
- Ramström O, Ansell RJ: Molecular imprinting technology: challenges and prospects for the future. Chirality 1998,
- Pietrzyk A, Kutner W, Chitta R, Zandler ME, D'Souza F, Sannicolò F, Mussini PR: Melamine acoustic chemosensor based on molecularly imprinted polymer film. Anal Chem 2009, **81**:10061-10070.
- Zhang M, Qing G, Sun T: Chiral biointerface materials. Chem Soc Rev 2012, 41:1972-1984.
- Valluzzi R., Liu L., Sprout C., Chaloner-Gill B. Particulate chiral separation material. U.S. Patent US20100230339 A1, 2005.
- 11. Chen L, Xu S, Li J: Recent advances in molecular imprinting technology: current status, challenges and highlighted applications. Chem Soc Rev 2011, 40:2922-2942
- 12. Barlow SM, Raval R: Complex organic molecules at metal surfaces: bonding, organisation and chirality. Surf Sci Rep 2003, 50:201-341
- 13. Humblot V, Lorenzo MO, Baddeley CJ, Haq S, Raval R: Local and
 global chirality at surfaces: succinic acid versus tartaric acid on Cu(110). J Am Chem Soc 2004, 126:6460-6469

This work describes the the adsorption properties of chiral molecules on an achiral metal crystal.

- 14. Burk MJ, Harper TGP, Kalberg CS: Highly enantioselective hydrogenation of β -keto esters under mild conditions. J Am
- Chem Soc 1995, 117:4423-4424. 15. McFadden CF, Cremer PS, Gellman AJ: Adsorption of chiral
- alcohols on "chiral" metal surfaces. Langmuir 1996, **12**:2483-2487

This article reports different rates of adsorption of enantiomeric alcohols on chiral metal surfaces due to the effect of different kink sites on high miller index surfaces (left or right hand relationship of the two surfaces).

- 16. Attard GA: Electrochemical studies of enantioselectivity at
- Attail metal surfaces. J Phys Chem B 2001, 105:3158–3167.
 This article describes enantioselective recognition on intrinsically chiral metal electrodes.
- Ahmadi A, Attard G, Feliu J, Rodes A: Surface reactivity at "chiral" platinum surfaces. Langmuir 1999, 15:2420-2424 This article demonstrated that the different rate of the electro-oxidation of D- and L-glucose on the chiral electrode Pt{643}R and its enantiomorph, Pt{643}S.
- Switzer JA, Kothari HM, Poizot P, Nakanishi S, Bohannan EW:
- Enantiospecific electrodeposition of a chiral catalyst. Nature 2003, **425**:490-493

The first report demonstrated the possibility to create chiral metal surfaces by electrodeposition of CuO films using chiral tartate enantiomers as chiral template molecules.

- 19. Bohannan EW, Kothari HM, Nicic IM, Switzer JA: Enantiospecific
- electrodeposition of chiral CuO films on single-crystal Cu(111). J Am Chem Soc 2004, 126:488-489.

This article reported that chiral films of CuO have been successfully successfully deposited onto single-crystal Cu(111) and show the discrimination of the enantiomer of tartate ion.

Kothari HM, Kulp EA, Boonsalee S, Nikiforov MP, Bohannan EW, Poizot P, Nakanishi S, Switzer JA: Enantiospecific electrodeposition of chiral CuO films from copper(II)

complexes of tartaric and amino acids on single-crystal Au(001). Chem Mater 2004, 16:4232-4244.

This article reported that deposited chiral films of CuO on Au(001) in the presence of tartaric acid and the amino acids alanine and valine to complex the Cu(II) exhibit the chiral properties on their surfaces for the discrimination of chiral recognition for the electrochemical oxidation of tartaric acid.

- Wattanakit C, Côme YBS, Lapeyre V, Bopp PA, Heim M,
 Yadnum S, Nokbin S, Warakulwit C, Limtrakul J, Kuhn A:
 Enantioselective recognition at mesoporous chiral metal surfaces. Nat Commun 2014, 5:3325.
 This work demonstrated the synthesis of chiral imprinted mesoporous

metals obtained by an electrodeposition of metals in the simultaneous presence of a lyotropic liquid crystalline phase and chiral template molecules. These electrodes exhibit a large active surface area and also show significant enantioselective recognition of DOPA molecules.

- 22. Yutthalekha T, Warakulwit C, Limtrakul J, Kuhn A:
- Enantioselective recognition of DOPA by mesoporous platinum imprinted with mandelic acid. Electroanalysis 2015, 27:2209-2213

This article demonstrated that the chiral imprinted mesoporous platinum can be used to distinguish the electro-oxidation of DOPA enantiomers when using the electrodes imprinted by corresponding mandelic acid enantiomers.

- 23. Yutthalekha T, Wattanakit C, Lapeyre V, Nokbin S, Warakulwit C,
- Limtrakul J, Kuhn A: Asymmetric synthesis using chiral-encoded metal. Nat Commun 2016, 7:12678

This first observation demonstrated the use of chiral imprinted mesoporous metals in the asymmetric synthesis. Chiral-encoded metal induces stereoselectivity in the electrochemical synthesis of mandelic acid from a prochiral compound.

- Behar-Levy H, Neumann O, Naaman R, Avnir D: Chirality
- induction in bulk gold and silver. Adv Mater 2007, 19:1207-

This article described the development of chirality on the metal surface of gold or silver and the evidence for consistent chiral asymmetry in the photoemission of electrons from gold and silver embedded with various chiral biomolecules.

- 25. Ohmann R, Levita G, Vitali L, De Vita A, Kern K: Influence of subsurface layers on the adsorption of large organic molecules on close-packed metal surfaces. ACS Nano 2011, 5:1360-
- 26. Lorenzo MO, Haq S, Bertrams T, Murray P, Raval R, Baddeley CJ: Creating chiral surfaces for enantioselective heterogeneous catalysis: R,R-tartaric acid on Cu(110). J Phys Chem B 1999, **103**:10661-10669.
- 27. Gross E, Liu JH, Alayoglu S, Marcus MA, Fakra SC, Toste FD,
 Somorjai GA: Asymmetric catalysis at the mesoscale: gold nanoclusters embedded in chiral self-assembled monolayer as heterogeneous catalyst for asymmetric reactions. J Am Chem Soc 2013, 135:3881-3886.
- 28. Hazzazi OA, Attard GA, Wells PB: Molecular recognition in adsorption and electro-oxidation at chiral platinum surfaces. J Mol Catal A 2004, 216:247-255
- 29. Sholl DS, Asthagiri A, Power TD: Naturally chiral metal surfaces as enantiospecific adsorbents. J Phys Chem B 2001, 105:4771-4782
- Garzón IL, Beltrán MR, González G, Gutterrez-González I, Michaelian K, Reyes-Nava JA, Rodriguez Hernández JI: **Chirality**, defects, and disorder in gold clusters. Eur Phys J D 2003, **24**:105-109.
- 31. Durán Pachón L, Yosef I, Markus TZ, Naaman R, Avnir D,
 Rothenberg G: Chiral imprinting of palladium with cinchona alkaloids. Nat Chem 2009, 1:160-164.

This article described the properties of chiral imprintinedimprinted metal obtained by a simple and efficient synthesis strategy.

- 32. Lawton TJ, Pushkarev V, Wei D, Lucci FR, Sholl DS, Gellman AJ, Sykes ECH: Long range chiral imprinting of Cu(110) by tartaric acid. J Phys Chem C 2013, 117:22290-22297
- 33. Schöck M, Otero R, Stojkovic S, Hümmelink F, Gourdon A,
 Stensgaard I, Joachim C, Besenbacher F: Chiral close-packing of achiral star-shaped molecules on solid surfaces. J Phys Chem B 2006, 110:12835-12838.
- 34. Humblot V, Raval R: Chiral metal surfaces from the adsorption
- of chiral and achiral molecules. Appl Surf Sci 2005, 241:150-156.
- 35. Xu B, Tao C, Cullen WG, Reutt-Robey JE, Williams ED: Chiral symmetry breaking in two-dimensional C₆₀-ACA intermixed systems. Nano Lett 2005, 5:2207-2211.
- 36. Izumi Y: Modified raney nickel (MRNi) catalyst: heterogeneous enantio-differentiating (asymmetric) catalyst. Adv Catal 1983,
- 37. Attard GA, Ahmadi A, Feliu J, Rodes A, Herrero E, Blais S. Jerkiewicz G: Temperature effects in the enantiomeric electro-oxidation of D- and L-Glucose on Pt{643}S. J Phys Chem B 1999, 103:1381-1385.
- 38. Gellman AJ, Horvath JD, Buelow MT: Chiral single crystal surface chemistry. J Mol Catal A 2001, 167:3-11.
- 39. Horvath JD, Gellman AJ: Enantiospecific desorption of R- and
- S-propylene oxide from a chiral Cu(643) surface. J Am Chem Soc 2001, 123:7953-7954.
- 40. Horvath JD, Gellman AJ: Enantiospecific desorption of chiral compounds from chiral Cu(643) and achiral Cu(111) surfaces. J Am Chem Soc 2002, 124:2384-2392.
- 41. Hazen RM, Sholl DS: Chiral selection on inorganic crystalline
- •• surfaces. Nat Mater 2003. 2:367-374.

This review article focused on both experimental and theoretical approaches to chiral selection on inorganic crystalline surfaces.

- 42. Sholl DS: Adsorption of chiral hydrocarbons on chiral platinum surfaces. Langmuir 1998, 14:862-867
- 43. Asthagiri A, Feibelman PJ, Sholl DS: Thermal fluctuations in the structure of naturally chiral Pt surfaces. Top Catal 2002, **18**:193-200.
- Attard GS, Bartlett PN, Coleman NRB, Elliott JM, Owen JR, Wang JH: Mesoporous platinum films from lyotropic liquid
- crystalline phases. Science 1997, 278:838-840.
- 45. Matsunaga M, Nakanishi T, Asahi T, Osaka T: Highly enantioselective discrimination of amino acids using copper deposition on a gold electrode modified with homocysteine monolayer. Electrochem Commun 2007, 9:725-728.
- 46. Nakanishi T, Matsunaga M, Nagasaka M, Asahi T, Osaka T:
- Enantioselectivity of redox reaction of DOPA at the gold electrode modified with a self-assembled monolayer of homocysteine. J Am Chem Soc 2006, 128:13322-13323.

- 47. Matsunaga M, Nakanishi T, Asahi T, Osaka T: Effect of surface coverage of gold(111) electrode with cysteine on the chiral
- discrimination of DOPA. Chirality 2007, 19:295-299.
- Yang F, Kong N, Conlan XA, Wang H, Barrow CJ, Yan F, Guo J, Yang W: Electrochemical evidences of chiral molecule recognition using L/D-cysteine modified gold electrodes. Electrochim Acta 2017, 237:22-28.
- 49. Kang Y-J, Oh J-W, Kim Y-R, Kim JS, Kim H: Chiral gold
 •• nanoparticle-based electrochemical sensor for enantioselective recognition of 3,4-dihydroxyphenylalanine. Chem Commun 2010. 46:5665-5667.

This article focused on the enantioselective recognition of 3,4-dihydroxyphenylalanine using penicillamine-modified gold nanoparticles as electrode. Gold nanoparticles with one enantiomeric ligand can be an enatioselective recognition site in the redox reaction of the coresponding corresponding enantiomer of 3,4-dihydroxyphenylalanine.

- 50. Chen C, Shi H, Zhao G: Chiral recognition and enantioselective photoelectrochemical oxidation toward amino acids on single-crystalline ZnO. J Phys Chem C 2014, 118:12041–12049.
- 51. Fang Y, Li C, Bo J, Henzie J, Yamauchi Y, Asahi T: Chiral sensing
- with mesoporous Pd@Pt nanoparticles. ChemElectroChem 2017, 4:1832-1835

This article reported the first case of mesoporous bimetalicbimetallic nanoparticles for enantioselective recognition of chiral compounds.

- Yasukawa T, Suzuki A, Miyamura H, Nishino K, Kobayashi S:
- Chiral metal nanoparticle systems as heterogeneous catalysts beyond homogeneous metal complex catalysts for asymmetric addition of arylboronic acids to α, β -unsaturated carbonyl compounds. J Am Chem Soc 2015, 137:6616-6623.
- 53. Savitha G, Saha R, Sekar G: Bimetallic chiral nanoparticles as catalysts for asymmetric synthesis. Tetrahedron Lett 2016, **57**:5168-5178.
- 54. Zhan P, Wang Z-G, Li N, Ding B: Engineering gold nanoparticles
- with DNA ligands for selective catalytic oxidation of chiral substrates. ACS Catal 2015, 5:1489-1498.
- 55. Wang Y, Wan X-K, Ren L, Su H, Li G, Malola S, Lin S, Tang Z,
- Häkkinen H, Teo BK, et al.: Atomically precise alkynyl-protected metal nanoclusters as model catalyst: observation of promoting effect of surface ligands on catalysis by metal nanoparticles. J Am Chem Soc 2016, 138:3278-3281.
- 56. Cheng H-G, Miguelez J, Miyamura H, Yoo W-J, Kobayashi S:
- Integration of aerobic oxidation and intramolecular asymmetric aza-friedel-crafts reactions with a chiral bifunctional heterogeneous catalyst. Chem Sci 2017, 8:1356-1359.



Contents lists available at ScienceDirect

Microporous and Mesoporous Materials

journal homepage: www.elsevier.com/locate/micromeso



Synthesis of hierarchical faujasite nanosheets from corn cob ash-derived nanosilica as efficient catalysts for hydrogenation of lignin-derived alkylphenols



Saros Salakhum ^a, Thittaya Yutthalekha ^a, Metta Chareonpanich ^b, Jumras Limtrakul ^c, Chularat Wattanakit ^{a, *}

- ^a Department of Chemical Engineering, School of Energy Science and Engineering, Vidyasirimedhi Institute of Science and Technology, Rayong 21210, Thailand
- ^b Department of Chemical Engineering, Faculty of Engineering, Kasetsart University, Bangkok 10900, Thailand
- ^c Department of Materials Science and Engineering, School of Molecular Science and Engineering, Vidyasirimedhi Institute of Science and Technology, Rayong 21210, Thailand

ARTICLE INFO

Article history: Received 11 July 2017 Received in revised form 28 August 2017 Accepted 10 September 2017 Available online 13 September 2017

Keywords: Corn cob ash Green synthesis Nanosilica Fauiasite nanosheets

ABSTRACT

The development of green synthesis using renewable resources is of crucial importance in various applications, including adsorption and catalysis. In this work, hierarchical faujasite nanosheets have been successfully prepared by a hydrothermal process in the presence of a dimethyloctadecyl-(3-(trimethoxysilyl)propyl) ammonium chloride (TPOAC) as a hierarchical porogen using an extracted silica derived from renewable resources. The extracted nanosilica was obtained from a corn cob ash by the solgel method without adding any dispersing agent. The TPOAC content and crystallization temperature have a great effect on tuning the morphologies and textural properties of hierarchical faujasite nanosheets. Interestingly, the obtained materials also exhibit outstanding catalytic properties in terms of activity, desired product selectivity, and catalyst lifetime for the hydrogenation of lignin-derived alkylphenols, which is an important step of bio-oil upgrading. The high yield of 4-propylcyclohexanol over novel designed catalysts is about 2.14 times compared with the conventional faujasite. The first presented approach, thus not only demonstrates a highly efficient way to produce zeolites with hierarchical nanosheet structures via a green synthesis method, but also opens up interesting perspectives for the development of heterogeneous catalysts for bio-oil upgrading applications.

© 2017 Elsevier Inc. All rights reserved.

1. Introduction

As a lot of wastes from agricultural products, such as rice husks, rice hulls, bagasses, and corn cobs are generated, especially in an agricultural country as well as an environmental problem has been considered as an international security issue, the conversion of such wastes is the most promising way to increase the value of products. Interestingly, one of the most abundant components in agricultural wastes is silica. The natural silica, which was extracted from agricultural wastes, can provide an alternative silica source [1–4]. According to the United States Department of Agriculture (USDA), for example, Thailand corn manufacture was about

5,200,000 million tons per year in 2016 and it was increased approximately by 10.64% from the previous year, resulting in a mass production of corn cob wastes. In addition, the corn cob ash (CCA) can be considered as a by-product waste from the combustion process after using corn cob as fuels to increase an energy efficiency. Consequently, the conversion of such wastes is an interesting choice to produce higher value-added products. However, there have been a few reports on the preparation of an amorphous silica derived from corn cob wastes. For example, the extracted amorphous silica was prepared in a high yield from corn cob ash by the sol-gel method and it was found that the CCA-extracted silica exhibits a good potential property for the adsorption of methylene blue [5,6]. To the best of our knowledge, there are so far no reports on the use of the extracted silica obtained from CCA as a raw material for the synthesis of zeolites, in particular, hierarchical zeolites.

E-mail address: chularat.w@vistec.ac.th (C. Wattanakit).

^{*} Corresponding author.

Such designed materials would allow not only reducing agricultural wastes but also opening up their benefits for potential applications.

The FAU-type zeolite is one of the most important catalysts for various catalytic applications, such as catalytic cracking, hydrocracking, hydrogenation, alkylation, and deoxygenation [7-11]. In particular, the hydrogenation of lignin-derived alkylphenols, which is an important step of bio-oil upgrading, is one of the most promising ways to produce green fuels. However, the conventional FAU, which consists of sole micropores, diminishes the catalytic performance of the catalyst because of the diffusion limitation of bulky molecules of bio-oil through small microporous channels of FAU. The most promising way to improve the hydrogenation reaction of conventional FAU is to use the designed hierarchical FAU because it is expected to improve the diffusion limitation [7,12], reduce a metal size and increase a metal dispersion [13], which can enhance the hydrogenation ability of metals in order to increase the catalytic activity. Moreover, not only hierarchical zeolites, which have been possible to exhibit a superior and promising catalytic performance over conventional materials, but also some other hierarchically support materials or catalysts, for example, the hierarchically ordered macroporous-mesoporous SBA-15 silica [14], the 3D hierarchical foam-like monolith catalyst [15,16], the hierarchically macro-mesoporous metal oxide catalyst [17], and the hierarchical nanosheets of transition-metal vanadate on metal meshes [18] also reveal the promising results for various applications in the catalysis field. FAU zeolites have been successfully synthesized by a hydrothermal process with the aid of an organic structure directing agents (OSDA) [19–22]. To reduce the synthesis cost and the emission of toxic species, there are several efforts to synthesize FAU zeolites in the free OSDA system, including the use of silica source derived from rice husk, and fly ash as raw materials [23,24]. For example, the micron-size NaY zeolite has been successfully prepared by using a rice husk ash as a renewable source by the two-step process (aging and crystallization steps) to improve a degree of crystallinity [24].

Because of low catalytic performances of a conventional zeolite in many applications, there is an increasing demand to develop such materials [25–28]. Although various hierarchical zeolites have been successfully prepared by different methods, the most popular one is based on the bottom-up synthesis approach because it preciously controls hierarchical structures, mesoporosities, and chemical compositions [7,29–39]. Until now, such materials having hierarchical nanosheet structures have only been obtained using commercial chemicals as a raw material [7,29,30], but have not been synthesized so far by using renewable resources, even though this strategy would be considered as a very green and highly efficient synthesis method. In addition, modified zeolites would give many advantages, such as increasing external surface areas of materials, prolonging a catalyst lifetime and overcoming the diffusion limitation of bulky molecules [7,33,40,41].

As the above-mentioned benefits of reducing agricultural wastes and introducing hierarchical structures of zeolites, in the present study, we demonstrate the synthesis of hierarchical FAU-type zeolite nanosheets using a natural silica source derived from a corn cob ash (CCA). Interestingly, the nanosilica with the size of about 40 nm can be prepared without adding any dispersing agent. Subsequently, the hierarchical FAU nanosheets have been synthesized via a hydrothermal synthesis using the extracted nanosilica in the simultaneous presence of a dimethyloctadecyl(3-(trimethoxysilyl) propyl) ammonium chloride (TPOAC) as a hierarchical porogen. Furthermore, the effects of TPOAC content and crystallization temperature on their surface morphologies and textural properties are systematically investigated. To illustrate the benefits of our designed catalysts in heterogeneous catalytic applications, the hydrogenation activity of lignin-derived alkylphenols over

hierarchical samples is compared with the corresponding conventional zeolite under a mild operating condition at an atmospheric pressure of H_2 and low temperature (<150 °C).

2. Experimental section

2.1. Reagents and materials

A corn cob was obtained from Kanchanaburi, Thailand. Sodium hydroxide anhydrous (NaOH: minimum assay 98%, Carlo Erba), hydrochloric acid (HCl: 37%, QRec), sodium aluminate (NaAlO₂: 40-45% Na₂O and 50-56% Al₂O₃, Sigma-Aldrich), sodium silicate (Na₂Si₃O₇: 26.5 wt% SiO₂, and 10.6 wt% Na₂O, Merck), dimethyloctadecyl (3- (trimethoxysilyl) propyl) ammonium chloride (TPOAC, 42% in methanol, Sigma-Aldrich), chloroplatinic acid hexahydrate (H_2 Cl₆Pt.6 H_2 O: $\geq 37.50\%$ Pt basis, Sigma-Aldrich), 4-propylphenol (C_9H_4 OH: 99%, Sigma-Aldrich), octane (C_6H_{18} : 98%, Sigma-Aldrich) were used as received without further purification.

2.2. Preparation of nanosilica from corn cob ash (CCA)

Silica was extracted from a corn cob ash (CCA) by applying the method developed by Mohanraj et al. [42] and Velmurugan et al. [6] with some modifications. Typically, the corn cob waste was washed with deionized (DI) water and then dried at 100 °C overnight. The cleaned corn cob was calcined at 650 °C for 2 h. A 10 g of a CCA was boiled under vigorous stirring in 80 ml of 3 N NaOH at 70 °C for 4 h to dissolve a silica from a CCA. After that, the sodium silicate solution was obtained after filtration and then washed with a 50 ml of boiled deionized water. The filtrate was cooled down to room temperature and a silica was then precipitated by adjusting the pH of the solution from 14 to 7 with 3 N HCl. The gels started to precipitate when the pH of the solution was less than 11. When the pH of solution reached to 7, the aging precipitation was kept for 18 h. The obtained gel was centrifuged at 4000 rpm for 5 min to separate from the supernatant and dried at 75 °C for 24 h to produce xerogels. The dried silica xerogels were washed with deionized water to remove other impurities and minerals from the silica. Finally, the washed silica xerogels were dried at 100 °C overnight to obtain nanosilica.

2.3. Synthesis of hierarchical FAU-type zeolite nanosheets

In order to use the nanosilica as a silica source to synthesize FAU nanosheets, the nanosilica was dissolved in NaOH solution to form the sodium silicate solution. In this case, a 2 g of nanosilica was dissolved in NaOH solution containing a 1.03 g of NaOH and a 4.50 g of HaO

The FAU nanosheets were prepared by applying our synthesis method with some modifications [7]. In a typical procedure, the sodium aluminate solution was prepared by mixing a 1.0 g of NaAlO₂, a 0.7 g of NaOH and a 14.4 g of H₂O and then stirred for 5 min to obtain the homogenous mixture. Subsequently, the sodium aluminate solution was added dropwise into a 3.7 g of the sodium silicate solution. The obtained mixture was vigorously stirred at room temperature for 1 h and the desired amount of TPOAC was then added to the sodium silicate aluminate solution, and the mixture was stirred at room temperature for 24 h. The gel was crystallized at 75 or 85 °C for 4 days. The obtained solution was collected and washed with a large amount of deionized water until the supernatant with a pH of less than 8 was observed. Finally, assynthesized samples were dried at 100 °C overnight and calcined at 350 °C for 8 h.

For the synthesis of the conventional FAU, above-mentioned procedures were applied except without adding TPOAC into the

solution mixture. The FAU-CON-*x*C-*y*T and FAU-NS-*x*C-*y*T represent the conventional FAU and the hierarchical FAU sample, respectively. *X* and *y* refer to the crystallization temperature and the mole fraction of SDA, respectively.

To prepare hydrogenation catalysts, a 1 wt% of Pt was loaded onto FAU supports via wet impregnation method using $\rm H_2Cl_6Pt.6H_2O$ as Pt precursors. The solvent was then removed by either conventional static drying (CSD) process or under vacuum-rotating drying (VRD). Finally, as-prepared samples were calcined at 350 °C for 5 h. The Pt/FAU-CON-CSD and Pt/FAU-CON-VRD refer to Pt nanoparticles (1 wt%) supported on the conventional FAU prepared by the CSD and VRD, respectively. In addition, the Pt/FAU-NS-CCA-CSD, and the Pt/FAU-NS-CCA-VRD refer to Pt nanoparticles (1 wt%) supported on the hierarchical FAU synthesized from CCA prepared by the CSD and VRD, respectively and the Pt/FAU-NS-SS-VRD is Pt nanoparticles (1 wt%) supported on the hierarchical FAU synthesized from sodium silicate prepared by the VRD.

2.4. Characterization of the extracted silica and hierarchical FAU-type zeolite nanosheets

X-ray powder diffraction (XRD, Bruker D8 ADVANCE diffractometer with Cu K- ∝ radiation (30 kV, 40 mA)) was used to investigate the phase of silica and the crystalline structure of synthesized samples. The scanning rate was 1° .min⁻¹ in the 2θ diffraction angle in the range of 5° – 60° . The relative crystallinity of zeolite samples was calculated by the following equation: (% XRD relative crystallinity of the desired sample = $(H_x/H_r) \times 100$, where H_x and H_r are the height of the most intense peak for the desired samples and the reference sample, respectively. X-ray fluorescence analysis (XRF, Bruker model S8 TIGER sequential WDXRF) was used to determine the chemical compositions of corn cob ash, and extracted silica. Surface area analysis was determined through a N2 adsorption/desorption technique at -196 °C by using a MicrotracBEL, BELSORP-max model. The specific surface area (S_{BET}), micropore surface area/pore volume, and mesopore size distribution were calculated by BET method, t-plot method and BJH model, respectively. The total pore volume (Vtotal) was estimated at P/Po at 0.99. Scanning electron microscopy (SEM) and transmission electron microscopy (TEM) images were recorded by the JEOL microscope, JSM-7610F and JEM-ARM200F models, respectively. Pt dispersion was determined by the H₂ pulse chemisorption technique performed on a chemisorption analyzer (MicrotracBEL, BELCAT II model). The acid sites of the zeolite samples were examined by a temperature-programed desorption of ammonia (NH₃-TPD). ²⁷Al MAS NMR spectroscopy operated on an AVANCE 300 MHZ Digital NMR spectrometer by using Bruker Biospin; DPX-300 was used to distinguish the nature of aluminium species of zeolite samples.

2.5. Catalytic testing

To illustrate the benefits of designed catalysts, the hydrogenation of 4-propylphenol to 4-propylcyclohexanol was performed using a two-necked round-bottom flask equipped with a reflux condenser under an atmospheric H₂ pressure [43]. In a typical procedure, a 5 ml of octane, a 20 µl of decane, and a 0.14 ml of 4-propylphenol as solvent, internal standard and reactant, respectively, were added to a 0.1 g of Na-formed catalysts and the reaction mixture was stirred continuously at 110 °C. For the reaction product analysis, the organic phase was analyzed at a certain reaction time by a gas/mass chromatography (Agilent, GC system 7890 B) performed on gas-mass spectrometer (Agilent, system 5977A MSD) with a HP-5 column (30 m, 0.32 mm i.d., a stationary phase

thickness of 0.25 μm). The mass balance was in the range of $93.0 \pm 3.0\%$.

3. Results and discussion

3.1. Preparation of nanosilica from corn cob ash (CCA)

The chemical compositions of the CCA and the extracted silica obtained from CCA are shown in Table 1. It was found that after the extraction of CCA via a sol-gel method, the silica content obviously increased from 37.3 to 97.0%, whereas impurities in CCA were almost completely removed. This makes it clear that a highly efficient extraction process has been successfully employed to produce pure silica. The silica yield obtained from the CCA was about 20% compared to the starting CCA.

A Fig. 1A shows XRD diffraction patterns of the CCA and the extracted nanosilica obtained from the CCA. The XRD patterns of the calcined corn cob ash at 650 °C for 2 h are attributed to the characteristics of quartz and tridymite [42]. In strong contrast to this, the extracted silica composes of an amorphous phase exhibiting a board hump at 2θ in the range of 15–35°, which was also found in the case of the commercial amorphous silica [44]. Fig. 1B demonstrates the surface morphology of the extracted silica. Interestingly, the obtained particle size of amorphous silica is in the nanometer range (40 nm) and very uniform over the entire area. The nanosilica was prepared by the precipitation of the silicate solution in the alkaline media by adjusting a pH with an acid solution. Typically, at high silicate concentration condition ($>10^{-3}$ M), the silanol groups condense to produce oligomers of silica by creating a disiloxy bond. Subsequently, the oligomers grow into larger fragments of nanosilica particles [45].

3.2. Synthesis of hierarchical FAU obtained from extracted nanosilica

3.2.1. Effect of crystallization temperature

The extracted nanosilica obtained from the CCA was used as a silica source for the synthesis of FAU zeolite. To optimize the synthesis condition, the effect of crystallization temperature on the formation of faujasite nanosheets was examined. A Fig. 2A shows XRD patterns of as-synthesized samples including the conventional FAU (FAU-CON-75C-0T and FAU-CON-85C-0T), and the hierarchical FAU nanosheets obtained at different crystallization temperatures (FAU-NS-75C-0.030T and FAU-NS-85C-0.030T). All of assynthesized samples exhibit the characteristic peaks of faujasite structure. It indicates that the faujasite zeolite can be synthesized using the crystallization temperature in the range of 75–85 °C without adding the zeolite structure-directing agent (SDA). In addition, the crystallinity of FAU samples obtained at a higher

Table 1Chemical composition of a corn cob ash (CCA) and an extracted silica derived from a corn cob ash.

Components expressed as oxides	Samples				
	Corn cob ash	Extracted silica			
K ₂ O	48.0	1.1			
SiO ₂	34.3	97.0			
P_2O_5	6.9	_			
MgO	4.5	0.7			
CaO	3.2	_			
SO ₃	2.1	_			
Al_2O_3	0.4	0.3			
ZnO	0.3	0.2			
Fe ₂ O ₃	0.3	_			
Na ₂ O	_	0.5			

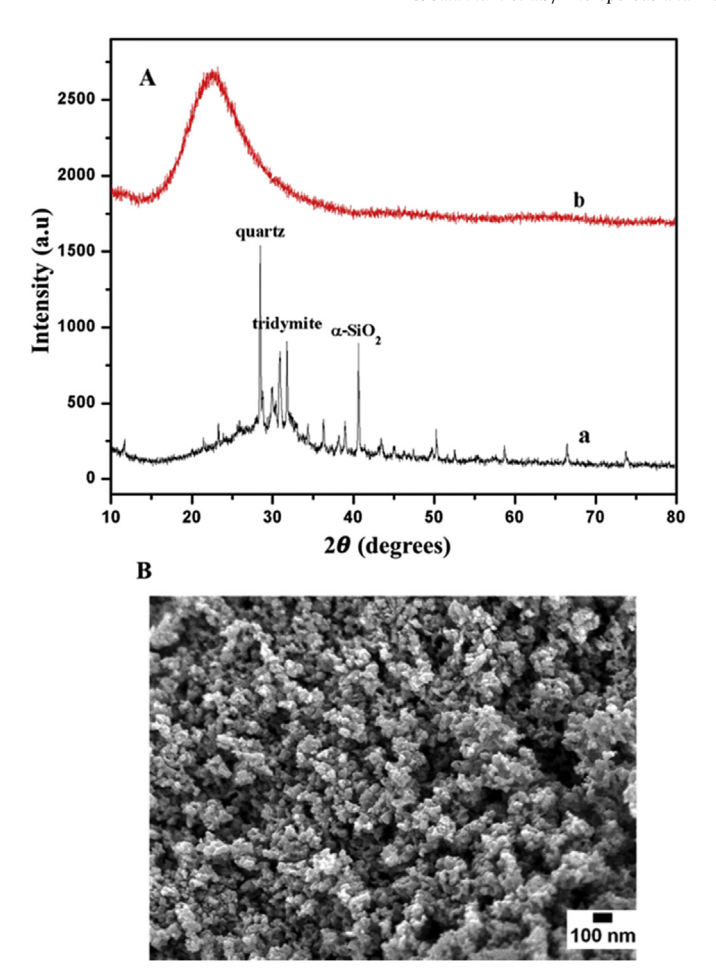


Fig. 1. (A) XRD patterns of (a) a corn cob ash (CCA), and (b) an extracted nanosilica, and (B) SEM images of an extracted nanosilica.

crystallization temperature slightly increases for both conventional FAU and FAU nanosheets. For example, the relative crystallinity is increased by approximately 5% when increasing the crystallization temperature from 75 to 85 °C in the case of FAU nanosheets synthesized by adding 0.030 mol fraction of TPOAC. This behavior can be attributed to the fact that the crystal growth rate at 85 °C is, as expected, larger than that of the lower temperature. In addition, it obviously shows that the microporosity of crystals is directly proportional to the crystallization temperature. The micropore surface area increases as a function of crystallization temperature (Fig. 2B and Table 2), confirming that the microporous structure is preferable to be grown at 85 °C. In addition, the uniform nanosheet structure can be observed at 85 °C as shown in Fig. 2C.

3.2.2. Effect of hierarchical porogen content

To further study the effect of synthesis parameters on morphologies and textural properties of zeolites, FAU samples were crystallized at various contents of TPOAC at the crystallization temperature of 75 and 85 °C. Fig. 3A shows XRD patterns of FAU-CON-85C-0T, FAU-NS-85C-0.015T, FAU-NS-85C-0.030T, FAU-NS-85C-0.045T, and FAU-NS-85C-0.060T, which were the assynthesized samples with TPOAC in the mole fraction of 0, 0.015, 0.030, 0.045, and 0.060, respectively (see Fig. S1 for the XRD patterns of samples crystallized at 75 °C). In the absence of TPOAC, a high crystallinity of FAU can be observed. However, the crystallinity significantly decreases as a function of the TPOAC content. For example, the crystallinity of FAU samples declines from 100 to

92.39. 86.51. and 84.31% for FAU-CON-85C-0T. FAU-NS-85C-0.015T. FAU-NS-85C-0.030T, and FAU-NS-85C-0.045T, respectively. Typically, the relative crystallinity is calculated from the ratio of the height of the most intense peak for the desired samples and the height of the most intense peak for the reference sample. To further increase the amount of TPOAC to 0.06 mole fraction, the characteristic peak of faujasite zeolite disappears, while the NaP zeolite is a major component. According to XRD patterns, all abovementioned samples obtained at the synthesis temperature of 75 and 85 °C show pure phase of faujasite zeolite except the one with the 0.060 mole fraction of TPOAC (See Fig. 3A(e)). This confirms that the formation of the FAU framework obviously depends on the amount of TPOAC, and it is limited in the range of 0.015-0.045 mole fraction. To further confirm the phase transformation of the extracted nanosilica to the FAU framework structure, FTIR spectra illustrate the characteristic of structures (Fig. S2). In a typical amorphous silica, the bands at 1000, 780, and 450 cm⁻¹ can be assigned to the asymmetric stretching vibration of the siloxane bonds (Si-O-Si), the network Si-O-Si symmetric stretching vibration, and network O-Si-O bending vibration modes, respectively, indicating that the extracted silica obtained from the CCA is an amorphous structure [5,6]. However, in the case of faujasite samples, the different characteristics obviously appear as described by the peaks around 450, 560, 660, 750, and 960 cm⁻¹ attributing to the T-O symmetric bending mode (where T = Si or Al), the double six membered rings T-O-T symmetric stretching, the Si-O-Al symmetric stretching, the T-O-T symmetric stretching, and the Si-O-Al antisymmetric stretching vibration mode of T-O bonds. respectively [46]. In particular, the peak around 560 cm⁻¹ belongs to the double six membered rings T-O-T symmetric stretching, which is a special characteristic structure of the FAU-type framework (Fig. S2 (b-e)) [47,48]. These observations again confirm the formation of FAU structure even in the presence of TPOAC.

As for textural properties, the N₂ adsorption-desorption isotherm of the conventional bulk FAU (FAU-CON-85C-0T) can be attributed to the type I, confirming that the FAU sample composes of the sole microporous structure in the framework. Another confirmation of the presence of sole microporous structure of bulk FAU is the BJH pore size distribution (Fig. S3A (a,b)). As expected, there are no obvious peaks appeared in the mesoporous size range (2–50 nm). Interestingly, different isotherms having high sorption at low relative pressure and hysteresis loop at P/P₀ of 0.45-0.8 represent to the simultaneous presence of mesoporous structures and microporous networks for samples obtained by adding TPOAC. In addition, the mesoporous character of FAU nanosheet samples is further verified by the mesoporous size distribution derived from the adsorption branch data using the BJH model (Fig. S3B (b-d)). The explicit BJH curve demonstrates the mesoporous size ranging from 5 to 9 nm for all hierarchical FAU nanosheet samples. The presence of hierarchical porous structures might be explained by the self-assembly of the nanosheet structure. To further confirm this explanation, the surface morphologies of synthesized samples analyzed by SEM are shown in Fig. 3C. Interestingly, the formation of FAU nanosheets strongly depends on the amount of TPOAC content. The presence of smooth surfaces with high microporosity and low mesoporosity can be attributed to the feature of conventional zeolite (Fig. 3B and C (a)). However, the surface morphologies obviously change when adding TPOAC. For example, the smooth surface of zeolites changes to rough spherical crystals in the presence of a small and suitable amount of TPOAC (0.015-0.030 mole fraction).

However, the degree of a uniform structure becomes smaller when adding a higher amount of TPOAC, resulting in a decrease of external surface areas of the FAU-NS-85C-0.045T sample. This indicates that an excess amount of TPOAC can disturb the self-

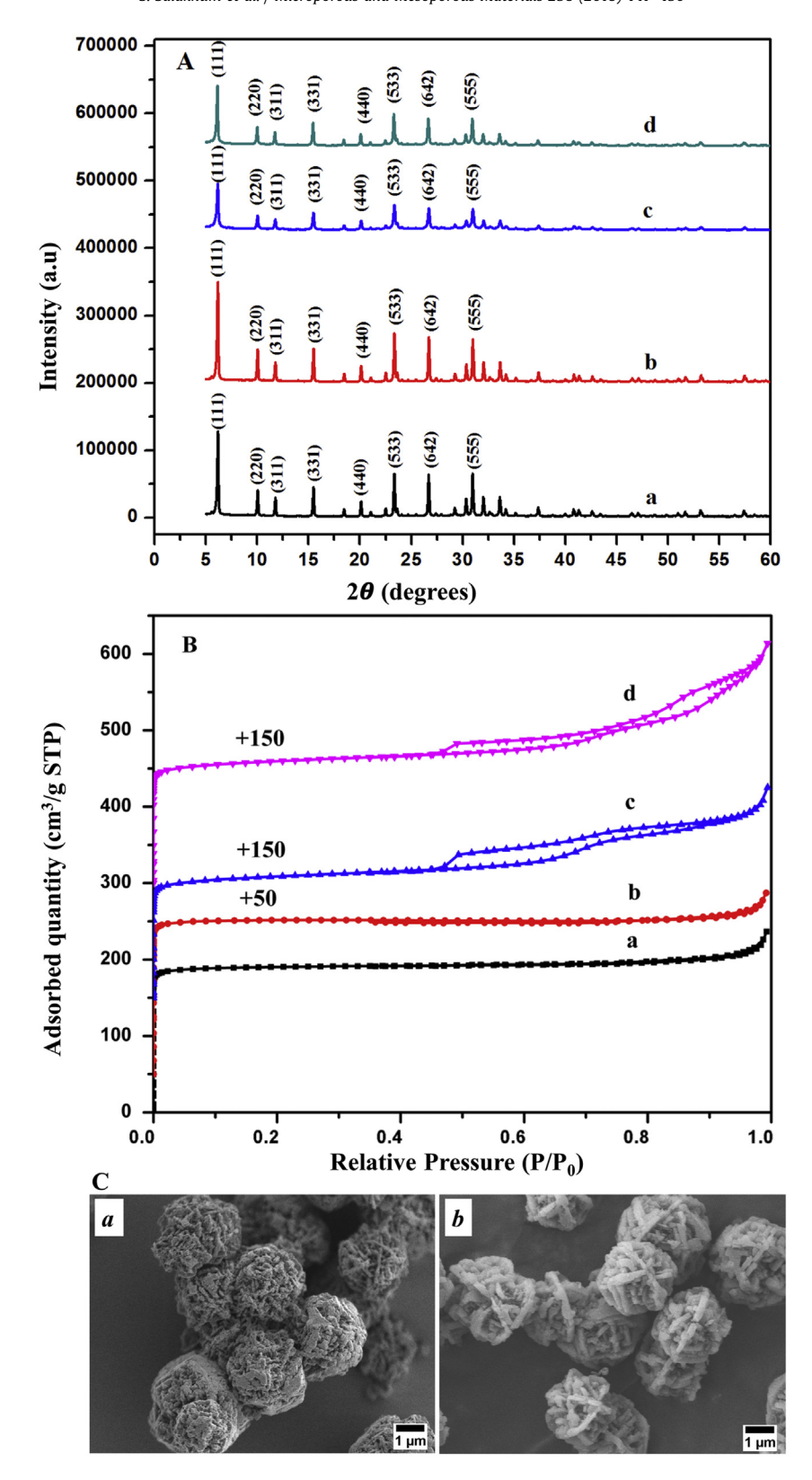


Fig. 2. (A) XRD patterns, (B) N_2 adsorption-desorption isotherms of (a) FAU-CON-75C-0T, (b) FAU-CON-85C-0T, (c) FAU-NS-75C-0.030T, and (d) FAU-NS-85C-0.030T, and (b) FAU-NS-85C-0.030T, and (c) SEM images of (a) FAU-NS-75C-0.030T, and (b) FAU-NS-85C-0.030T.

formation of nanosheet assemblies. From these observations, the proposed formation process of FAU crystals is therefore demonstrated in Scheme 1. In the case of the small TPOAC content (0.015), the large portion of bulk FAU crystals is still observed, suggesting

that the template does not so much affect the crystal growth of zeolites (Scheme 1, path a). Interestingly, when increasing the TPOAC content to the suitable value, the intergrowth of nanolayer is predominant to form the nanosheet assembly (Scheme 1, path b).

Table 2Textural properties of synthesized FAU samples obtained by N₂ physisorption.

Sample	S _{BET} ^a	S _{micro} ^b	$S_{\rm ext}^{\rm c}$	$V_{\rm total}^{\rm d}$	V _{micro} ^e	$V_{\rm ext}^{\rm f}$	S _{ext/} S _{BET} ^g
Fau-CON-75C-0T	787	690	97	0.36	0.28	0.08	0.12
Fau-NS-75C-0.015T	623	445	178	0.48	0.18	0.30	0.28
Fau-NS-75C-0.030T	536	350	186	0.50	0.17	0.33	0.35
Fau-NS-75C-0.045T	437	329	108	0.44	0.16	0.28	0.25
Fau-CON-85C-0T	839	724	115	0.38	0.29	0.09	0.14
Fau-NS-85C-0.015T	700	568	132	0.40	0.23	0.17	0.19
Fau-NS-85C-0.030T	625	473	152	0.47	0.20	0.27	0.24
Fau-NS-85C-0.045T	573	430	143	0.45	0.19	0.26	0.25

- ^a S_{BET}: BET specific surface area.
- ^b S_{micro}: micropore surface area.
- ^c S_{ext}: external surface area.
- ^d V_{total}: total pore volume.
- ^e V_{micro}: micropore volume.
- f $V_{ext} = V_{total} V_{micro}$; All surface areas and pore volumes are in the units of m^2/g and cm^3/g , respectively.
 - g Fraction of mesopore volume.

However, at a higher amount of TPOAC, the simultaneous presence of non-uniform nanosheets together with nanoparticles in the structure is observed (Fig. S3), suggesting inhibiting crystal growth by a high content of TPOAC and therefore obstructing self-assemblies of nanosheets (Scheme 1, path c). This behavior relates to the fact that the excess amount of TPOAC leads to the reduction of the long-range ordered structure of zeolite, and eventually produces the growth of zeolite nanoparticles on nanosheet surfaces [49,50]. At an excess amount of TPOAC (Fig. S4), the surfactant has a strong impact on the crystal growth of FAU zeolite so that the NaP species start to appear (Scheme 1, path d).

To confirm the nature species of aluminum sites in the zeolite framework, Fig. S5 shows the ²⁷Al NMR spectra of synthesized FAU samples. It is clear that the distinct peak at the chemical shift about 65 ppm, attributing to the characteristic peak of tetrahedral coordinated aluminum species in the framework, is observed with a very small portion of extra-framework, octahedrally coordinated aluminum species [34]. It suggests that most aluminum active sites are occupied in the zeolite framework.

3.3. Catalytic activity: application of hierarchical FAU nanosheets in the hydrogenation of lignin-derived alkylphenols

The hydrogenation of lignin-derived alkylphenols is an important step in the bio-oil upgrading process. In this case, the Pt nanoparticles are a well-known Lewis acid site for the hydrogenation of aromatic compounds, and therefore they were supported on the designed synthesized zeolites. In order to illustrate the benefits of hierarchical zeolite nanosheet assemblies in heterogeneous catalysis, the hydrogenation of lignin-derived 4-propylphenol to 4-propylcyclohexanol as a model reaction was used in this study as shown in Scheme 2.

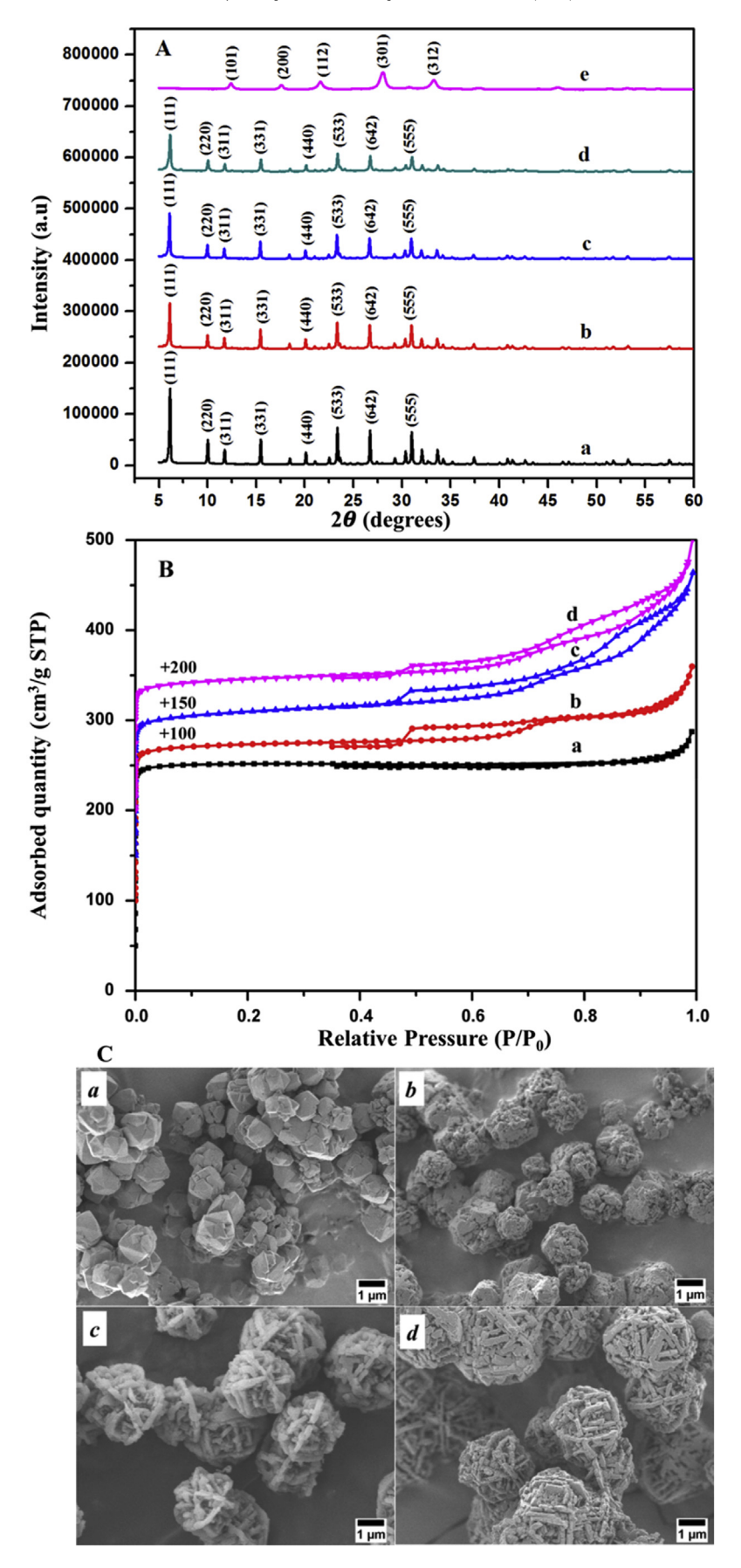
To verify that the hierarchical structure also benefits not only improving the diffusion limitation of substrates inside the porous network [7,40,41], but also enhancing the metal distribution on zeolite supports, which is one of the most important parameters to control the catalytic activity. In this case, the yield of 4-propylcy-clohexanol can greatly increase over Pt (1 wt%) supported on the designed hierarchical FAU nanosheets obtained from CCA prepared by the VRD method (Pt/FAU-NS-CCA-VRD, Fig. 4A(c)) compared with the conventional catalyst prepared by the same method (Pt/FAU-CON-VRD, Fig. 4A(b)). This makes it clear that the catalytic activity over hierarchical FAU nanosheets extremely enhances compared with a conventional FAU and the turnover frequency (TOF) can be increased from 565 to 877 h⁻¹ when using the designed hierarchical zeolite (Table S3, Entries 2 and 4).

Interestingly, the hierarchical Pt/FAU nanosheets also exhibit an improved catalytic activity compared to the Pt supported on the conventional FAU even though they were prepared by the conventional static drying (CSD) method, which gives the lower metal distribution compared to those of the VRD (Table S3, Entries 1 and 3).

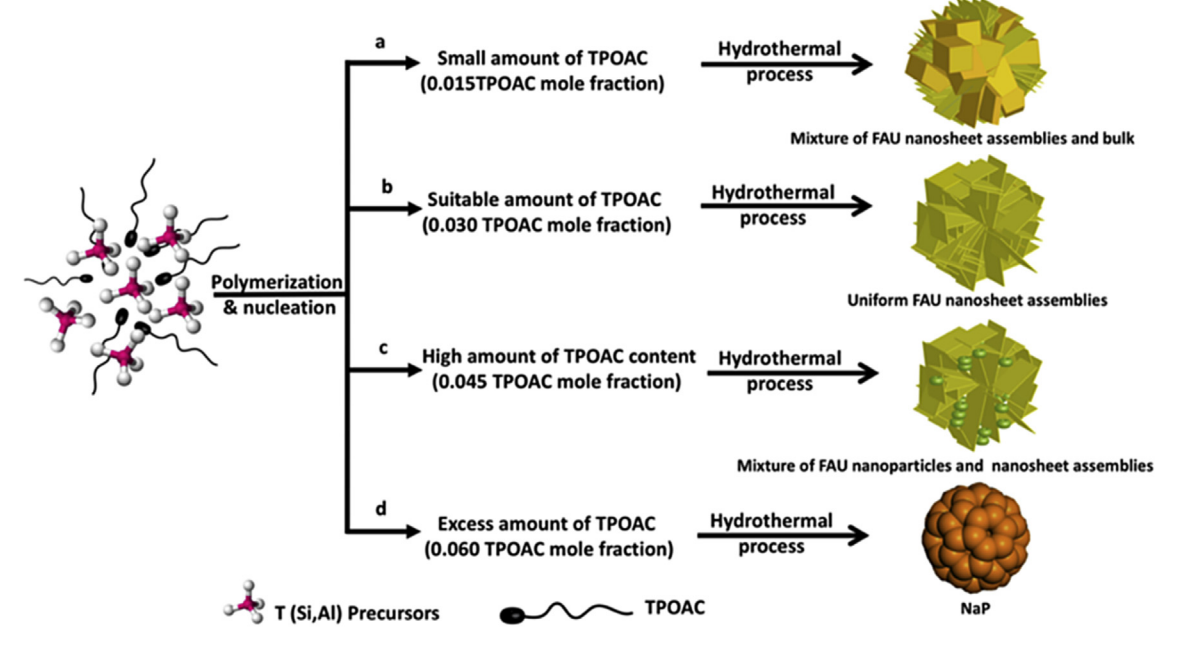
Compared with the hierarchical FAU nanosheets synthesized by using a commercial sodium silicate (Pt/FAU-NS-SS-VRD) as a raw material, Fig. 4A(c and d) illustrates that the designed hierarchical nanosheets obtained from CCA (Pt/FAU-NS-CCA-VRD) exhibit comparable performances with producing a high yield of 4-propylphenol almost 80%. To investigate the reaction mechanism, the product distribution as a function of reaction time is plotted as shown in Fig. 4B. In the first step of the reaction, propylcyclohexanone is produced due to the partial hydrogenation of 4-propylphenol and it is subsequently further hydrogenated to propylcyclohexanol. This is consistent with that at the beginning of reaction the high amount of propylcyclohexanone is produced; however, propylcyclohexanol greatly increases whereas propylcyclohexanone disappears after 5 h. It is also important to note that propylphenol can be directly dehydrated to propylbenzene or propylcyclohexane as by-products due to the significant presence of acid sites on the external surface of FAU (see Fig. S6 for NH₃-TPD

Fig. 5A and B shows TEM images of Pt dispersion on the conventional FAU and the hierarchical FAU nanosheets, respectively. Compared with the conventional FAU, the dispersion of Pt nanoparticles over the hierarchical FAU nanosheets can be greatly improved as shown in Tables S1 and S2. The uniform particle size distribution of Pt on hierarchical FAU nanosheets can be clearly seen from the TEM image (Fig. S7), confirming the high dispersion of Pt particle size in the range of 2.00 ± 0.26 nm. The Pt dispersion is one of the most important reasons for the improved catalytic activity of FAU nanosheets compared with the bulk FAU. In addition, the Pt dispersion obviously depends on the TPOAC content, which used as a hierarchical porogen in the synthesis process. Unsurprisingly, the sample obtained at a very small amount of TPOAC (0.015 mole fraction) exhibits insignificant different values of metal dispersion compared with the conventional one. However, when increasing the TPOAC content the metal dispersion obviously enhances. This is consistent with the view that the Pt dispersion over solid supports relates to their surface area (Fig. 5C). An increase of Pt dispersion is also directly proportional to its particle size on the hierarchical structure. For example, the Pt size over the hierarchical sample and conventional zeolite is approximately by 2.00±0.26 and 2.52 ± 0.21 , respectively (see Table S2). This makes it clear that the hierarchical structure exhibits remarkably a higher fraction of exposed metal active sites compared with the conventional microporous structure.

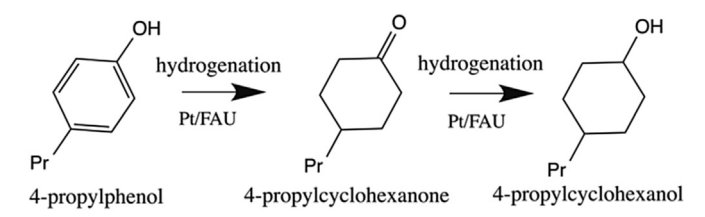
To further explain the enhanced catalytic activity of catalysts, the efficiency of catalysts should theoretically depend on the nature and amount of exposed active metal areas. Catalyst samples having a different Pt dispersion were prepared by different methods. As for the low Pt dispersion sample, the conventional static drying (CSD) process was applied for removal of solvent after the impregnation and it exhibited a very poor dispersion of metals (Table S3, Entries 1 and 3). To improve the efficiency of metal species, the solvent was removed under vacuum and rotating drying condition (VRD). It clearly shows that the Pt dispersion over the hierarchical FAU increased from 17.29 to 27.23% compared with those prepared by the conventional method (CSD). As stated above, the fraction of exposed metal active sites directly related to the metal dispersion. It is therefore reasonable to assume that in the case of the CSD method the catalytic activity of catalyst for the hydrogenation of 4propylphenol is significantly decreased due to the presence of a



 $\textbf{Fig. 3.} \ \ (A) \ \ \text{XRD patterns of sample a-e, (B) N}_2 \ \ \text{adsorption-desorption isotherms of samples a-d, and (C) SEM images of samples a-d: (a) FAU-CON-85C-0T, (b) FAU-NS-85C-0.015T, (c) FAU-NS-85C-0.030T, and (d) FAU-NS-85C-0.045T, and (e) FAU-NS-85C-0.06T (NaP).}$



Scheme 1. Proposed formation process of FAU crystals obtained at different TPOAC content.



Scheme 2. Illustration of the hydrogenation of 4-propylphenol on Pt supported on a zeolite catalyst.

lower fraction of exposed active sites compared with the one obtained by the VRD method (Fig. 4A (a and b) and Table S3, Entries 3–5). This allows the rise of the turnover frequency (TOF) from 485 to 880 $\,\mathrm{h}^{-1}$ when increasing the metal dispersion (Table S3, Entries 3–5).

To illustrate the reusability of catalysts, the insignificant change of activity was observed even after three cycles. The percentage of conversion is 100, 98.45 and 94.78% for the first, second, and third cycles, respectively (Fig. 6). Interestingly, the product selectivity of the desired product does not significantly reduce. In other words, the designed hierarchical FAU nanosheet catalysts can be repeatedly used as the active species for the hydrogenation of hydrogenation of lignin-derived alkylphenol.

4. Conclusions

The highly purified extracted nanosilica obtained from a corn cob ash (CCA) without using any dispersing agent has been successfully prepared. FAU nanosheets have also been synthesized via a hydrothermal process using the obtained nanosilica with the aid of TPOAC as a hierarchical porogen. Interestingly, the morphologies and textural properties of FAU nanosheets can be easily tuned by changing the synthesis parameters, such as crystallization temperature and TPOAC content. At the optimized condition, very uniform FAU nanosheet assemblies can be observed under the crystallization temperature of 85 °C and the molar fraction of TPOAC of 0.030. The hierarchical factor directly improves the metal dispersion, resulting in an increase of the fraction of exposed active species, which can enhance the catalytic activity of hydrogenation of lignin-derived alkylphenol.

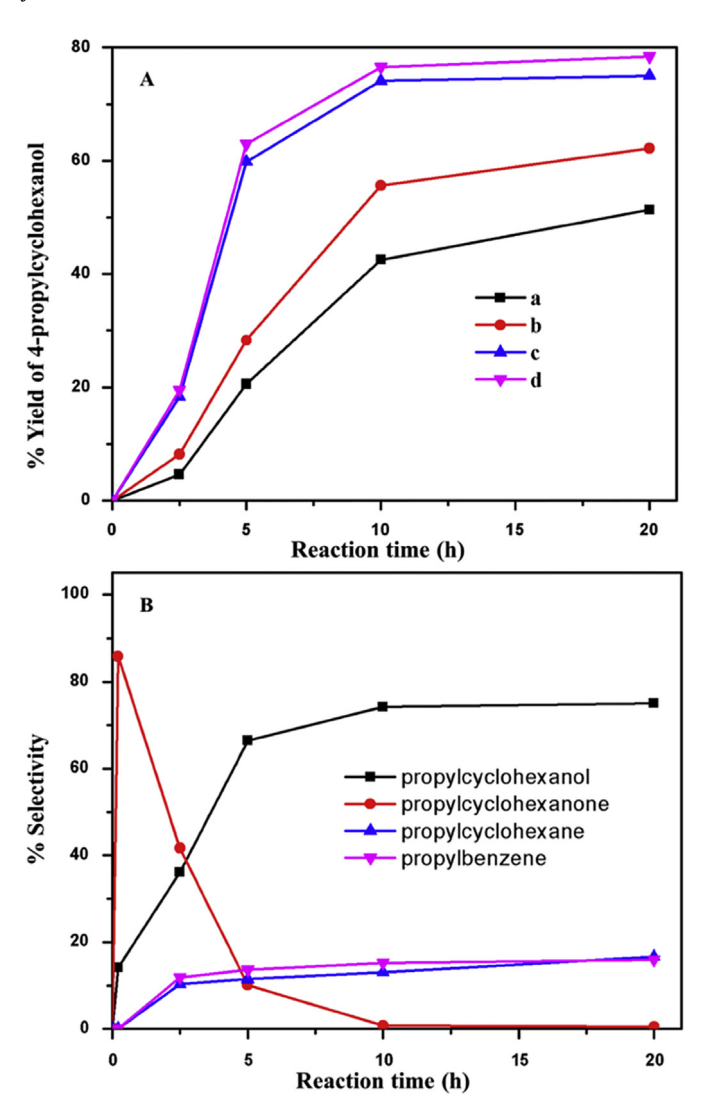


Fig. 4. (A) Yield of 4-propylcyclohexanol as a function of reaction time on (a) Pt/FAU-CON-CSD, (b) Pt/FAU-CON-VRD, (c) Pt/FAU-NS-CCA-VRD, and (d) Pt/FAU-NS-SS-VRD, (B) product selectivity over Pt/FAU-NS-CCA-VRD.

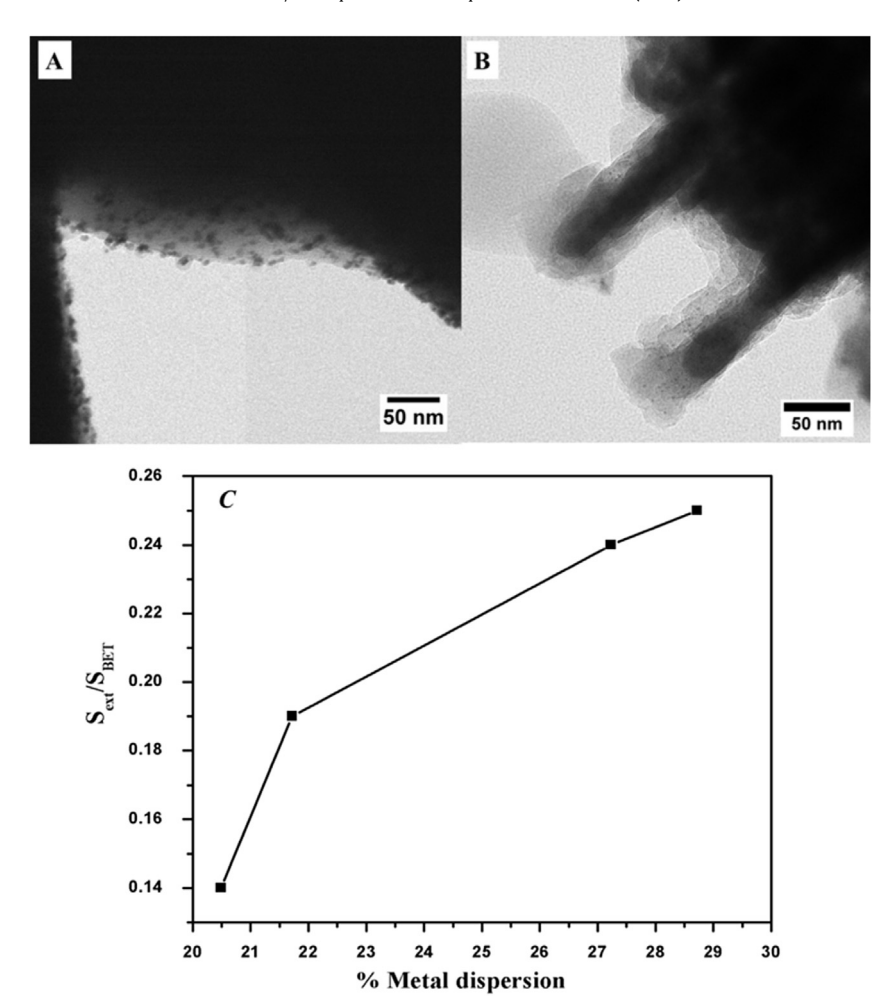


Fig. 5. Representative TEM images of Pt dispersion on (a) Pt/FAU-CON-CSD, (b) Pt/FAU-NS-CCA-VRD, and (c) the relationship of Pt dispersion and external surface areas.

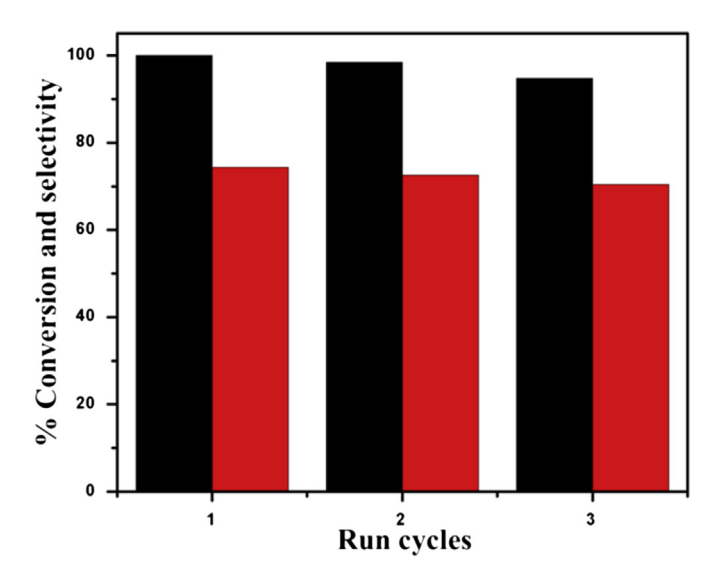


Fig. 6. Recycle ability of Pt/FAU-NS-CCA-VRD: (black bar) conversion and (red bar) product selectivity. (For interpretation of the references to colour in this figure legend, the reader is referred to the web version of this article.)

The first presented approach thus not only demonstrates highly efficient way to produce zeolites with hierarchical nanosheet structures using renewable resources but also opens up interesting

perspectives for the development of heterogeneous catalysts for the part of bio-oil upgrading application, and future work will be focused on generalizing this approach by applying for the synthesis of other zeolites and extending the scope of the development of hierarchical bifunctional catalysts for the bio-oil upgrading to transportation fuels.

Acknowledgements

This work was financially supported by the Vidyasirimedhi Institute of Science and Technology (VISTEC), the Thailand Research Fund (TRF) (MRG5980114) and the Office of Higher Education Commission (OHEC). Furthermore, the authors would like to acknowledge the PTT group (PTT Global Chemical) and the NANOTEC Center of Excellence on Nanoscale Materials Design for Green Nanotechnology at Kasetsart University.

Appendix A. Supplementary data

Supplementary data related to this article can be found at http://dx.doi.org/10.1016/j.micromeso.2017.09.009.

References

[1] I. Cornejo, S. Ramalingam, J. Fish, I. Reimanis, Hidden treasures: turning food waste into glass, Am. Ceram. Soc. Bull. 93 (2014) 24–27.

- [2] S.S. Danewalia, G. Sharma, S. Thakur, K. Singh, Agricultural wastes as a resource of raw materials for developing low-dielectric glass-ceramics, Sci. Rep. 6 (2016) 24617.
- [3] N. Yalcin, V. Sevinc, Studies on silica obtained from rice husk, Ceram. Int. 27 (2001) 219–224.
- [4] N. Nazriati, H. Setyawan, S. Affandi, M. Yuwana, S. Winardi, Using bagasse ash as a silica source when preparing silica aerogels via ambient pressure drying, J. Non-Cryst. Solids 400 (2014) 6–11.
- [5] E. Okoronkwo, P. Imoisili, S. Olusunle, Extraction and characterization of amorphous silica from corn cob ash by sol-gel-method, J. Chem. Mater. Res. 3 (2013) 68–72.
- [6] P. Velmurugan, J. Shim, K.-J. Lee, M. Cho, S.-S. Lim, S.-K. Seo, K.-M. Cho, K.-S. Bang, B.-T. Oh, Extraction, characterization, and catalytic potential of amorphous silica from corn cobs by sol-gel method, J. Ind. Eng. Chem. 29 (2015) 298–303.
- [7] T. Yutthalekha, C. Wattanakit, C. Warakulwit, W. Wannapakdee, K. Rodponthukwaji, T. Witoon, J. Limtrakul, Hierarchical FAU-type zeolite nanosheets as green and sustainable catalysts for benzylation of toluene, J. Clean. Prod. 142 (2017) 1244–1251.
- [8] C.H. Tempelman, X. Zhu, K. Gudun, B. Mezari, B. Shen, E.J. Hensen, Texture, acidity and fluid catalytic cracking performance of hierarchical faujasite zeolite prepared by an amphiphilic organosilane, Fuel Process. Technol. 139 (2015) 248–258.
- [9] K. Motazedi, N. Mahinpey, D. Karami, Preparation and application of faujasite-type Y zeolite-based catalysts for coal pyrolysis using sodium silicate solution and colloidal silica as silicon source, Chem. Eng. Commun. 203 (2016) 300–317.
- [10] T. Rørvik, H. Mostad, O.H. Ellestad, M. Stöcker, Isobutane/2-butene alkylation over faujasite type zeolites in a slurry reactor. Effect of operating conditions and catalyst regeneration, Appl. Catal. A 137 (1996) 235–253.
- [11] A.M. Yusof, N.A. Nizam, N.A.A. Rashid, Hydrothermal conversion of rice husk ash to faujasite-types and NaA-type of zeolites, J. Porous Mater. 17 (2010) 39–47.
- [12] H.W. Lee, B.R. Jun, H. Kim, D.H. Kim, J.-K. Jeon, S.H. Park, C.H. Ko, T.-W. Kim, Y.-K. Park, Catalytic hydrodeoxygenation of 2-methoxy phenol and dibenzofuran over Pt/mesoporous zeolites, Energy 81 (2015) 33–40.
- [13] A. Śrębowata, K. Tarach, V. Girman, K. Góra-Marek, Catalytic removal of trichloroethylene from water over palladium loaded microporous and hierarchical zeolites, Appl. Catal. B 181 (2016) 550–560.
- [14] C.M. Parlett, M.A. Isaacs, S.K. Beaumont, L.M. Bingham, N.S. Hondow, K. Wilson, A.F. Lee, Spatially orthogonal chemical functionalization of a hierarchical pore network for catalytic cascade reactions, Nat. Mater. 15 (2016) 178–182
- [15] S. Cai, D. Zhang, L. Shi, J. Xu, L. Zhang, L. Huang, H. Li, J. Zhang, Porous Ni–Mn oxide nanosheets in situ formed on nickel foam as 3D hierarchical monolith de-NO_x catalysts, Nanoscale 6 (2014) 7346–7353.
- [16] C. Fang, L. Shi, H. Hu, J. Zhang, D. Zhang, Rational design of 3D hierarchical foam-like Fe₂ O₃@ CuO_x monolith catalysts for selective catalytic reduction of NO with NH₃, RSC Adv. 5 (2015) 11013—11022.
- [17] C. Fang, L. Shi, H. Li, L. Huang, J. Zhang, D. Zhang, Creating hierarchically macro-/mesoporous Sn/CeO ₂ for the selective catalytic reduction of NO with NH₃, RSC Adv. 6 (2016) 78727—78736.
- [18] L. Huang, X. Zhao, L. Zhang, L. Shi, J. Zhang, D. Zhang, Large-scale growth of hierarchical transition-metal vanadate nanosheets on metal meshes as monolith catalysts for De-NO_x reaction, Nanoscale 7 (2015) 2743–2749.
- [19] D. Yuan, D. He, S. Xu, Z. Song, M. Zhang, Y. Wei, Y. He, S. Xu, Z. Liu, Y. Xu, Imidazolium-based ionic liquids as novel organic SDA to synthesize high-silica Y zeolite, Microporous Mesoporous Mater. 204 (2015) 1–7.
- [20] B.A. Holmberg, H. Wang, J.M. Norbeck, Y. Yan, Controlling size and yield of zeolite Y nanocrystals using tetramethylammonium bromide, Microporous Mesoporous Mater. 59 (2003) 13–28.
- [21] L. Zhu, L. Ren, S. Zeng, C. Yang, H. Zhang, X. Meng, M. Rigutto, A. van der Made, F.-S. Xiao, High temperature synthesis of high silica zeolite Y with good crystallinity in the presence of N-methylpyridinium iodide, Chem. Commun. 49 (2013) 10495–10497.
- [22] N. Taufiqurrahmi, A.R. Mohamed, S. Bhatia, Nanocrystalline zeolite beta and zeolite Y as catalysts in used palm oil cracking for the production of biofuel, J. Nanopart. Res. 13 (2011) 3177–3189.
- [23] P. Thuadaij, A. Nuntiya, Preparation and characterization of faujasite using fly ash and amorphous silica from rice husk ash, Procedia Eng. 32 (2012)
- [24] R. Mohamed, I. Mkhalid, M. Barakat, Rice husk ash as a renewable source for the production of zeolite NaY and its characterization, Arab. J. Chem. 8 (2015) 48–53
- [25] J. Pérez-Ramírez, C.H. Christensen, K. Egeblad, C.H. Christensen, J.C. Groen, Hierarchical zeolites: enhanced utilisation of microporous crystals in catalysis by advances in materials design, Chem. Soc. Rev. 37 (2008) 2530–2542.
- [26] M.S. Holm, E. Taarning, K. Egeblad, C.H. Christensen, Catalysis with hierarchical zeolites, Catal. Today 168 (2011) 3–16.

- [27] C.H. Christensen, K. Johannsen, E. Törnqvist, I. Schmidt, H. Topsøe, C.H. Christensen, Mesoporous zeolite single crystal catalysts: diffusion and catalysis in hierarchical zeolites, Catal. Today 128 (2007) 117–122.
- [28] L.-H. Chen, X.-Y. Li, J.C. Rooke, Y.-H. Zhang, X.-Y. Yang, Y. Tang, F.-S. Xiao, B.-L. Su, Hierarchically structured zeolites: synthesis, mass transport properties and applications, J. Mater. Chem. 22 (2012) 17381–17403.
- [29] A. Inayat, I. Knoke, E. Spiecker, W. Schwieger, Assemblies of mesoporous FAU-type zeolite nanosheets, Angew. Chem. Int. Ed. 51 (2012) 1962–1965.
 [30] M. Khaleel, A.J. Wagner, K.A. Mkhoyan, M. Tsapatsis, On the rotational inter-
- [30] M. Khaleel, A.J. Wagner, K.A. Mkhoyan, M. Tsapatsis, On the rotational intergrowth of hierarchical FAU/EMT zeolites, Angew. Chem. Int. Ed. 53 (2014) 9456–9461.
- [31] X. Zhang, D. Liu, D. Xu, S. Asahina, K.A. Cychosz, K.V. Agrawal, Y. Al Wahedi, A. Bhan, S. Al Hashimi, O. Terasaki, Synthesis of self-pillared zeolite nanosheets by repetitive branching, Science 336 (2012) 1684–1687.
- [32] D. Xu, G.R. Swindlehurst, H. Wu, D.H. Olson, X. Zhang, M. Tsapatsis, On the synthesis and adsorption properties of single-unit-cell hierarchical zeolites made by rotational intergrowths, Adv. Funct. Mater. 24 (2014) 201–208.
- [33] H.W. Lee, S.H. Park, J.-K. Jeon, R. Ryoo, W. Kim, D.J. Suh, Y.-K. Park, Upgrading of bio-oil derived from biomass constituents over hierarchical unilamellar mesoporous MFI nanosheets, Catal. Today 232 (2014) 119–126.
- [34] W. Wannapakdee, C. Wattanakit, V. Paluka, T. Yutthalekha, J. Limtrakul, One-pot synthesis of novel hierarchical bifunctional Ga/HZSM-5 nanosheets for propane aromatization, RSC Adv. 6 (2016) 2875–2881.
- [35] P. Wuamprakhon, C. Wattanakit, C. Warakulwit, T. Yutthalekha, W. Wannapakdee, S. Ittisanronnachai, J. Limtrakul, Direct synthesis of hierarchical ferrierite nanosheet assemblies via an organosilane template approach and determination of their catalytic activity, Micropor. Mesopor. Mat. 219 (2016) 1–9.
- [36] K. Cho, H.S. Cho, L.-C. De Menorval, R. Ryoo, Generation of mesoporosity in LTA zeolites by organosilane surfactant for rapid molecular transport in catalytic application, Chem. Mater. 21 (2009) 5664–5673.
- [37] M. Choi, H.S. Cho, R. Srivastava, C. Venkatesan, D.-H. Choi, R. Ryoo, Amphiphilic organosilane-directed synthesis of crystalline zeolite with tunable mesoporosity, Nat. Mater. 5 (2006) 718–723.
- [38] G.V. Shanbhag, M. Choi, J. Kim, R. Ryoo, Mesoporous sodalite: a novel, stable solid catalyst for base-catalyzed organic transformations, J. Catal. 264 (2009) 88–92
- [39] R.R. Mukti, H. Hirahara, A. Sugawara, A. Shimojima, T. Okubo, Direct hydrothermal synthesis of hierarchically porous siliceous zeolite by using alkoxysilylated nonionic surfactant, Langmuir 26 (2009) 2731–2735.
- [40] L. Wang, J. Zhang, X. Yi, A. Zheng, F. Deng, C. Chen, Y. Ji, F. Liu, X. Meng, F.-S. Xiao, Mesoporous ZSM-5 zeolite-supported Ru nanoparticles as highly efficient catalysts for upgrading phenolic biomolecules, ACS Catal. 5 (2015) 2727–2734.
- [41] Y. Wang, J. Wu, S. Wang, Hydrodeoxygenation of bio-oil over Pt-based supported catalysts: importance of mesopores and acidity of the support to compounds with different oxygen contents, RSC Adv. 3 (2013) 12635–12640.
- [42] K. Mohanraj, S. Kannan, S. Barathan, G. Sivakumar, Preparation and characterization of nano SiO_2 from corn cob ash by precipitation method, Adv. Mat. 4.6 (2012) 394–397.
- [43] H. Ohta, K. Yamamoto, M. Hayashi, G. Hamasaka, Y. Uozumi, Y. Watanabe, Low temperature hydrodeoxygenation of phenols under ambient hydrogen pressure to form cyclohexanes catalysed by Pt nanoparticles supported on H-ZSM-5, Chem. Commun. 51 (2015) 17000–17003.
- [44] N. Thuadaij, A. Nuntiya, Synthesis and characterization of nanosilica from rice husk ash prepared by precipitation method, J. Nat. Sci. Spec. Issue Nanotechnol. 7 (2008) 59–65.
- [45] P. Jal, M. Sudarshan, A. Saha, S. Patel, B. Mishra, Synthesis and characterization of nanosilica prepared by precipitation method, Colloids Surf. A Physicochem. Eng. Asp. 240 (2004) 173–178.
- [46] N. Thuadaij, A. Nuntiya, Preparation of nanosilica powder from rice husk ash by precipitation method, Chiang Mai J. Sci. 35 (2008) 206–211.
- [47] K.P. Dey, S. Ghosh, M.K. Naskar, Organic template-free synthesis of ZSM-5 zeolite particles using rice husk ash as silica source, Ceram. Int. 39 (2013) 2153–2157.
- [48] W. Panpa, S. Jinawath, Synthesis of ZSM-5 zeolite and silicalite from rice husk ash, Appl. Catal. B 90 (2009) 389–394.
- [49] L. Emdadi, Y. Wu, G. Zhu, C.-C. Chang, W. Fan, T. Pham, R.F. Lobo, D. Liu, Dual template synthesis of meso-and microporous MFI zeolite nanosheet assemblies with tailored activity in catalytic reactions, Chem. Mater. 26 (2014) 1345–1355.
- [50] C. Wang, M. Yang, P. Tian, S. Xu, Y. Yang, D. Wang, Y. Yuan, Z. Liu, Dual template-directed synthesis of SAPO-34 nanosheet assemblies with improved stability in the methanol to olefins reaction, J. Mater. Chem. A 3 (2015) 5608–5616.
- [51] J. Datka, O. Vogt, J. Rakoczy, A. Kubacka, Heterogeneity of acid sites in ZSM-5 zeolites and boralites studied by IRspectroscopy and a catalytic method, Stud. Surf. Sci. Catal. 94 (1995) 240–245.

RSC Advances



PAPER

View Article Online



Cite this: RSC Adv., 2017, 7, 35581

Catalytic upgrading of carboxylic acids as bio-oil models over hierarchical ZSM-5 obtained *via* an organosilane approach†

Kamonlatth Rodponthukwaji,^a Chularat Wattanakit, ^b Thittaya Yutthalekha,^b Sunpet Assavapanumat,^b Chompunuch Warakulwit,^a Wannaruedee Wannapakdee^b and Jumras Limtrakul^c

Biomass is an interesting renewable energy resource as it is widespread in nature and low cost. The development of bio-oil derived from biomass as a fuel is still a scientific and industrial challenge. In this context, we demonstrate the synthetic method of bio-oil upgrading catalysts based on hierarchical zeolites and open up interesting perspectives for bio-oil upgrading processes. The hierarchical ZSM-5 zeolite has been successfully prepared via a direct hydrothermal synthesis with the aid of a commercial organosilane surfactant (TPOAC). The influences of TPOAC content and Si/Al ratio on hierarchical structures were also systematically studied. To illustrate their catalytic performances, an esterification reaction of various organic acids such as (acetic acid and levulinic acid) and alcohols was performed as the model reaction representing the bio-oil upgrading application. The synergic effect of acidity and the hierarchical structure of catalysts can greatly enhance the catalytic performance in terms of activity, product yield, coke formation, and reusability of the catalysts. For example, they can convert almost 100% of reactant in 8 h in the esterification of acetic acid and alcohols, whereas the conventional zeolite reveals significantly lower activity (<20%). Interestingly, the hierarchical zeolite can also greatly improve the catalytic activity of the esterification of levulinic acid and ethanol to produce ethyl levulinate that can be used as a diesel miscible biofuel (DMB). In addition, the efficiency of hierarchical catalysts obtained by different synthesis methods is also discussed. This first example demonstrates that the hierarchical zeolite obtained via a direct synthesis approach can benefit bio-oil upgrading applications via the esterification of various carboxylic acids.

Received 5th April 2017 Accepted 11th July 2017

DOI: 10.1039/c7ra03890a

rsc.li/rsc-advances

Introduction

The development of renewable energy sources has attracted a great deal of attention from both academic and industrial points of view due to the shortage of fossil fuels. Although renewable energy can be obtained from many sources, such as solar, wind, geothermal, hydroelectric, and biomass, the

conversion of biomass is one of the most fascinating methods because it is widespread in nature and low cost. Typically, biomass resources can be divided into one of the following three groups: (i) wastes; (ii) forest products; (iii) energy crops.2 The lignocellulosic biomass is one of the most abundant sources to be used for the production of liquid fuels or bio-oils. Although the bio-oil derived from the lignocellulosic biomass is a good candidate to replace a petroleum fuel, it typically consists of high oxygen content (20-50 wt%) and acidity (pH = 2.5-3), resulting in undesirable properties, such as low heating value, high viscosity, thermal instability, and corrosiveness.3 To overcome these problems, the upgrading of bio-oils is crucial to improve their properties. In general, the bio-oil upgrading processes can be obtained by hydrodeoxygenation (HDO),4 ketonisation,⁵ aldol condensation,⁶ and esterification.⁷ The most popular one is based on the catalytic upgrading via an esterification of organic acids in the presence of alcohol molecules, resulting in the reduction of oxygen content and acidity, thus improving the oil stability.8

Although a common acid catalyst, such as sulfuric acid (H₂SO₄), exhibits an excellent catalytic activity in an

^aDepartment of Chemistry, NANOTEC Center for Nanoscale Materials Design for Green Nanotechnology, Kasetsart University, Bangkok 10900, Thailand

^bDepartment of Chemical and Biomolecular Engineering, School of Energy Science and Engineering, Vidyasirimedhi Institution of Science and Technology, Rayong 21210, Thailand. E-mail: Chularat.w@vistec.ac.th; Fax: +66 3301 4445 extn 2176

Department of Materials Science and Engineering, School of Molecular Science and Engineering, Vidyasirimedhi Institution of Science and Technology, Rayong 21210, Thailand

 $[\]dagger$ Electronic supplementary information (ESI) available: Calibration curves (S1), particle size distribution (S2), XRD patterns (S3), ^{27}Al MAS NMR spectra (S4), IR spectra of pyridine adsorption experiments (S5), weight loss profiles (S6), O2 TPO profiles (S7), Raman spectra (S8), benzyl alcohol conversion (%) on different samples obtained by different methods (S9), Tables S1–S4. See DOI: 10.1039/c7ra03890a

RSC Advances Paper

esterification, such an acid is not recommended as it is corrosive and non-environmentally-friendly. Alternatively, various solid acid catalysts, such as sulfated zirconia,⁹ functionalized mesoporous silica,¹⁰ heteropoly acid,¹¹ and zeolite^{12,13} have been applied. In particular, zeolites have been widely used for an esterification due to their outstanding properties, such as high surface area, high thermal/chemical stability, suitable acidity, and shape selective property.

Over the past decade, zeolites have played an important role in various potential applications, especially in petrochemical reactions, such as aromatization, 14,15 isomerization, 16,17 alkylation,18,19 dehydration,20 and esterification.21,22 However, the presence of sole micropores in their structures often suffers from the transportation limitation of guest molecules, including reactants, intermediates, and products. As a consequence, the catalyst deactivation can be easily observed due to the coke formation inside micropores. To improve the efficiency of a conventional zeolite, many researchers have paid a lot of effort to develop the zeolite structure by either reducing the crystal size²³ or introducing the hierarchical pores into its structures.24-26 In the latter case, the fabrication of hierarchical zeolites has been successfully obtained by one of the following two major routes: (i) post-treatment;27-29 (ii) direct synthesis.30-37 In the direct synthesis, a secondary template was applied by either hard or soft templates to control the hierarchical structure. According to the soft templating approach, an organosilane surfactant has been widely used as the mesoporedirecting agent because it provides a strong interaction with the zeolitic gels, thus preventing the phase separation between zeolite precursors and mesoporous template molecules. However, it sometimes also suffers from the disadvantage because it requires many complicated steps of the synthesis of a designed organosilane template, 38 while there are only a few hierarchical zeolites which have been successfully produced by using a commercial organosilane surfactant as a mesoporous structure-directing agent.35,39-41

Recently, hierarchical zeolites have been applied as an interesting catalyst for an esterification. For example, the mesoporous ZSM-5 and H-ZSM-5 monolith were prepared by an alkali treatment and using corn or sorghum stem piths as sacrificial solid templates, respectively. Interestingly, the obtained ZSM-5 can significantly improve catalytic performances of the esterification of benzyl alcohol and hexanoic acid. In addition, the esterification of *o*-cresol with acetic acid over mesoporous ZSM-5 zeolites obtained by an alkaline treatment or post treatment has been reported. The remarkably improved activity in the liquid-phase esterification of alcohol and acid was observed over the mesoporous ZSM-5 *via* demetallation in alkaline media.

An alternative way to produce the ordered mesoporous zeolite has been achieved by a direct synthesis or a templating approach. This strategy can obviously solve several limitations of hierarchical zeolites obtained from a post-treatment and in particular it can be used to synthesize hierarchical zeolites with a wide range of Si/Al ratios.⁴⁴ In contrast to this, a post-treatment has been applied to the limited initial Si/Al ratio of parent zeolites. Typically, the zeolite having the Si/Al ratio in the

range of 25–50 is the most favourable by a post-treatment, while a low mesoporosity and a loss of crystallinity are obtained in the case of higher and lower Si/Al ratios, respectively. ^{45,46} To the best of our knowledge, the development of hierarchical zeolites by a direct synthesis based on an organosilane approach for the bio-oil upgrading application has not yet been demonstrated, even though it is one of the most interesting alternative ways to extend the scope of hierarchical zeolite researches.

Herein, we demonstrate not only the synthesis of hierarchical ZSM-5 by a direct synthesis approach with the aid of a commercial organosilane surfactant, dimethyloctadecyl[3-(trimethoxysilyl)propyl] ammonium chloride (TPOAC), as a hierarchical pore-directing agent but also its catalytic perspectives for the bio-oil upgrading application using a model reaction. The catalytic performances in terms of activity, product selectivity, and coke formation were explored *via* the esterification of various carboxylic acids such as acetic acid and levulinic acid and alcohols. Complementary, the reusability of hierarchical catalysts was also examined and compared with that of the conventional one. In addition, the catalytic activity of the hierarchical catalyst obtained by different synthesis methods including direct- and post synthesis approaches was discussed in details.

Experimental

Preparation of catalysts

The hierarchical ZSM-5 was hydrothermally synthesized by using the dimethyloctadecyl[3-(trimethoxysilyl)propyl] ammonium chloride (TPOAC) (42 wt% in methanol, Sigma-Aldrich) as a mesopore structure-directing agent. For a typical procedure, we developed the synthesis method from our previous work by using the TPOAC instead of carbon material as the hierarchical mesopore-directing agent.⁴⁷ In the modified mixture, a 1 g of silica gel (SiO2, Merck), 0.02 g of sodium aluminate (53 wt% Al₂O₃, 43 wt% Na₂O; Riedel-deHaën), 0.26 g of tetrapropylammonium bromide, TPABr, (98% C₁₂H₂₈BrN, Sigma-Aldrich), 0.11 g of sodium hydroxide (98% NaOH, Carlo Erba), and 7 ml of deionized (DI) water were mixed and stirred at room temperature for 1 h. Then, the desired amount of TPOAC was dropped slowly into the solution. The final molar composition was $178 \text{ SiO}_2/1 \text{ Al}_2\text{O}_3/16 \text{ NaO}_2/9 \text{ TPABr}/4251\text{H}_2\text{O}/x \text{ TPOAC}$ which x refers to the amount of TPOAC. The mixture was stirred further for 2 h and transferred to a Teflon-coated stainless steel autoclave. Then, it was heated at 453 K for 3 days. The product was filtered and washed with deionized water until the pH of filtrate less than 9. It was then dried in an oven at 373 K overnight and subsequently calcined in air at 823 K for 9 h. The obtained samples were designated as ZSM-5_(x)TPOAC in which x refers to an amount of TPOAC in molar composition. To compare the benefits of modified and unmodified structures, a conventional sample, the ZSM-5 was also synthesized in the absence of TPOAC and the commercial ZSM-5 (SH-55 from ALSI-PENTA Zeolithe GmbH, Si/Al ratio of 24) was also used to compare with the synthesized samples. They are designated as C_ZSM-5 and Commercial ZSM-5, respectively.

RSC Advances Paper

To prepare the acid catalyst, all synthesized samples were ion-exchanged into the proton-formed ZSM-5 by repeating the treatment three times with 1 M of NH₄NO₃ at 353 K for 2 h. Then, the sample was dried at 373 K and calcined at 823 K for

To evaluate the influence of the number of acid sites, we therefore prepared the hierarchical ZSM-5 samples with various Si/Al ratios. For a typical synthesis, the above-mentioned procedure with varying the amount of sodium aluminate was used. The amount of Al₂O₃ was varied in the range of 1 to 3.6 molar ratio. The samples are designated as Hierarchical ZSM-5(A) in which A refers to the Si/Al ratio.

To compare the effect of hierarchical structures obtained by different synthesis approaches on their catalytic performances, an alkaline post treatment was also chosen for the preparation of hierarchical ZSM-5 as a representative of a top-down synthesis approach. A 1 g of the commercial zeolite (SH-55 from ALSI-PENTA Zeolithe GmbH, Si/Al ratio of 24) was mixed with 30 ml of 0.5 M NaOH and it was stirred at 353 K for 1 h. Then, the product was washed with DI water until the pH of filtrate less than 8. The filtered product was dried and subsequently ionexchanged into the proton-formed catalyst. The alkaline treated sample is designated as the Hierarchical ZSM-5_AT.

Characterization of catalysts

Powder X-ray diffraction (XRD) patterns were recorded by a Bruker D8 ADVANCE instrument using CuKα radiation (30 kV, 40 mA) with step size of 0.02° and scan rate of 10° min⁻¹ in the 2θ range of 5-50°. The relative crystallinity of zeolite samples was calculated by the following equation: (% XRD relative crystallinity of the desired sample = $(Hx/Hr) \times 100$), where Hx and Hr are the height of the most intense peak for the desired samples and the reference sample, respectively. The morphologies of materials were examined by a scanning electron microscopy (SEM) performed with a Hitachi-3400 instrument. The samples for SEM studies were dispersed on carbon tape and coated with a thin layer of gold.

Nitrogen adsorption-desorption isotherms were measured at 77 K performed on a Micromeritics ASAP 2020 physisorption analyzer. Before the measurement, the samples were evacuated at 575 K for 20 h. The specific surface area was calculated by using the Brunauer-Emmett-Teller (BET) theory ($S_{\rm BET}$).⁴⁸ The total pore volume (V_{tot}) was calculated at $P/P_0=0.98$. The t-plot method was used to calculate the micropore volume (V_{micro}) , and external surface area (Sext).49 The mesopore size distributions were examined by using the Barrett-Joyner-Halenda (BJH) model derived from the adsorption branch of isotherms.⁵⁰

The aluminum structures were determined by using ²⁷Al MAS NMR spectroscopy performed on an AVANCE 300 MHz Digital NMR spectrometer (Bruker Biospin; DPX-300) at 78 MHz. The Al_2O_3 was used as a reference (set to 0 ppm). The Si/Al ratio of products was investigated by ICP-OES technique performed on the Agilent Technologies 715 model.

The NH₃ temperature-programmed desorption (NH₃-TPD) curves were recorded by using a fixed-bed reactor system equipped with a TCD detector. Typically, a 1 g of zeolite sample was pretreated at 823 K for 2 h under the flow of N2 (30 ml

min⁻¹) and it was subsequently cooled down to 323 K. The sample was equilibrated with 5 vol% of NH3 in He for 60 min and then purged under the flow of He (30 ml min⁻¹) for 1 h. To record NH₃ TPD profiles, the temperature was increased from 323 K to 1073 K with the heating rate of 10 K min $^{-1}$. To determine the density of acid sites in zeolites, FTIR spectra of pyridine adsorption were recorded at a 2 cm⁻¹ resolution and averaged over 64 scans performed on a Bruker Vertex V70v instrument. Firstly, the zeolite sample was heated to 823 K with the heating rate of 2 K min⁻¹ under 20 vol% O₂ in He. Pyridine was then introduced for 10 min into the chamber at its vapor pressure at room temperature. Subsequently, pyridine was removed by evacuation for 1 h at 573 K. To calculate the number of Brønsted and Lewis acid sites, molar extinction coefficient values of 0.73 and 1.11 cm μ mol⁻¹ were applied, respectively.

The amount of coke formation in the zeolite network after catalytic tests was evaluated by the thermogravimetric analysis (TGA) and the O₂ temperature-programmed desorption (O₂-TPO). As for TGA experiments, it was performed on a Perkin Elmer Pyris 1 TGA instrument in the temperature range of 373-1073 K with a heating rate of 10 K min⁻¹ under an oxygen (O₂, 99.99% purity, Praxair, Thailand) with the flow rate of 40 ml min⁻¹. Prior to the O₂-TPO measurement, used catalysts were pretreated at 523 K for 2 h under the flow of He. The catalysts were then heated under the flow of 5% (v/v) O₂ in He. The TPO profiles were recorded in the temperature range of 373-1073 K with the ramp rate of 5 K min⁻¹. The Raman spectra of spent catalysts were collected at room temperature, performing at least 3 different positions. A laser beam was used at 532 nm focused on the sample by a microscope.

Esterification of benzyl alcohol with acetic acid

Prior to the catalytic test, the proton-formed ZSM-5 samples were activated at 823 K for 6 h. For the experimental procedure, the reaction was performed in a three-necked round bottom flask with a reflux condenser at 373 K under an atmospheric pressure. A 15 ml of toluene was added into the reactor following by 0.10 ml of decane as a solvent and an internal standard, respectively. A 3.10 ml of benzyl alcohol and 2.06 ml of acetic acid were added. A 0.45 g of catalyst was then placed into the reactor. The reaction mixtures were collected at a desired time and analyzed by gas chromatography (GC) performed on an Agilent 7820A GC instrument using a FID detector and a DB-1 capillary column (100 m \times 0.5 μ m \times 0.25 mm). The percentage of conversion was calculated based on the total percentage of benzyl alcohol converted into the product. The quantitative analysis was investigated by using the individual calibration curves of benzyl alcohol and its products as shown in Fig. S1 in ESI.† The mass balance was checked for all experiments (97.29 \pm 1.50%).

Results and discussion

Characterization of catalysts

Effect of TPOAC content. According to the XRD results in Fig. 1, the patterns reveal that all samples contain characteristic **RSC Advances**

Fig. 1 XRD patterns of all ZSM-5 samples obtained at various TPOAC contents: (a) Commercial ZSM-5, (b) C_ZSM-5, (c) ZSM-5_(4.8) TPOAC, (d) ZSM-5_(9.6)TPOAC, and (e) ZSM-5_(38.4)TPOAC.

peaks of the MFI zeolite structure with high crystallinity, while no crystalline impurity phase is observed. It suggests that zeolite samples were successfully synthesized under a simple hydrothermal process even in the presence of a mesopore structure-directing agent. For example, the samples obtained by adding a small amount of TPOAC (ZSM-5_(4.8)TPOAC and ZSM-5_(9.6)TPOAC) exhibit high intense peaks comparable to the reference sample (C_ZSM-5), having the relative crystallinity of 61.5% and 69.5%, respectively (see Table S1 in the ESI†). However, when the TPOAC was further added with higher content, the relative crystallinity of samples, ZSM-5 (38.4) TPOAC, is significantly decreased (about 40%). A large amount of surfactant directly causes the significant reduction of crystallinity, suggesting the incompatibility of surfactant and zeolite gels to hinder the crystallization process (from 9.6 to 38.4 mol of TPOAC). This makes it clear that the amount of a mesoporous structure-directing agent strongly affects the formation of zeolite structures.

To verify the morphologies of synthesized zeolites, the scanning electron microscopy (SEM) images reveal that the TPOAC apparently affects the morphology of products (Fig. 2). In the absence of TPOAC, the C_ZSM-5 sample exhibits smooth surface morphology, having particle sizes of 3.6 \pm 0.5 μm (see the particle size distribution in Fig. S2 in the ESI†). In strong contrast to this, the sample obtained in the presence of low TPOAC content, ZSM-5_(4.8)TPOAC, shows non-uniform particles with various shapes, including coffin-like and spherical morphologies. Due to the variety of shapes and non-uniform particle size distribution (8.8 \pm 2.0 μm see in Fig. S2 in the ESI†), this would allow us to increase the TPOAC content to produce more uniform particles. Consequently, the ZSM-5_(9.6) TPOAC product was fabricated by increasing the amount of TPOAC. The sample exhibits stacking plate-like shapes, providing a high surface areas with average crystal sizes of 10.6 \pm 2.0 μm (Fig. S2 in the ESI†). To examine the limitation of TPOAC content, the ZSM-5_(38.4)TPOAC was also synthesized by further increasing the amount of TPOAC by the fourfold compared with the ZSM-5_(9.6)TPOAC. The mixture of crystalline and amorphous phases is observed, when an excess amount of TPOAC is added. This is consistent with the XRD

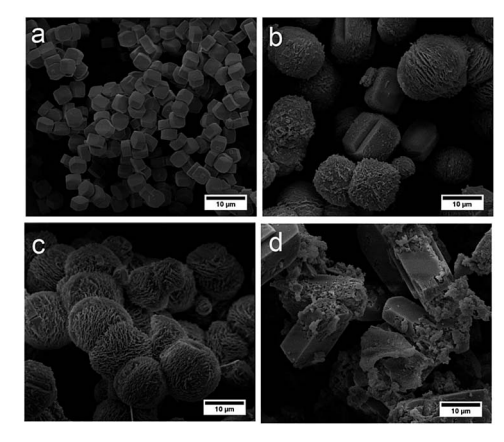


Fig. 2 SEM images of ZSM-5 samples obtained at various amounts of TPOAC: (a) C_ZSM-5, (b) ZSM-5_(4.8)TPOAC, (c) ZSM-5_(9.6)TPOAC, and (d) ZSM-5_(38.4)TPOAC.

data, showing a dramatic decrease in crystallinity compared with the reference sample (C_ZSM-5). In particular, the simultaneous presence of the coffin-like crystals and the amorphous phase is observed in the case of the ZSM-5_(38.4)TPOAC sample due to the use of overdosed TPOAC.

To confirm the presence of mesoporosity, the textural properties of all samples were measured by N2 physisorption technique. N2 adsorption/desorption isotherms (Fig. 3) demonstrate that synthesized ZSM-5 products show the isotherms with hysteresis loop at P/P_0 in the range of 0.4-0.8 due to the mesopore filling, indicating the presence of additional mesopores. In contrast to the synthesized samples, the hysteresis loop does not exist in the isotherm of the commercial ZSM-5 and the C_ZSM-5, while the adsorption at the relatively low pressure $(P/P_0 \sim 0.2)$ with a long horizontal plateau is clearly observed due to the micropore filling, suggesting the presence of sole micropores in the zeolite structure. Moreover, the BJH mesopore size distribution in Fig. 4 reveals the presence of a mesoporous structure in the hierarchical ZSM-5 samples. The BJH curve of ZSM-5_(9.6)TPOAC sample shows a wide distribution in the range of 10-20 nm. However, when the TPOAC is

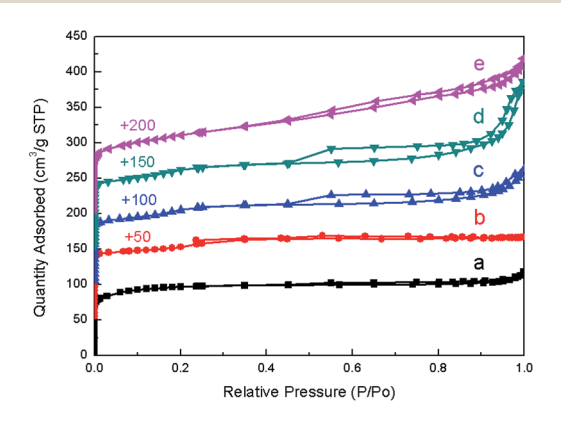


Fig. 3 N_2 adsorption/desorption isotherms of synthesized ZSM-5 samples obtained at various TPOAC contents: (a) Commercial ZSM-5, (b) C_ZSM-5, (c) ZSM-5_(4.8)TPOAC, (d) ZSM-5_(9.6)TPOAC, and (e) ZSM-5_(38.4)TPOAC.

Paper RSC Advances

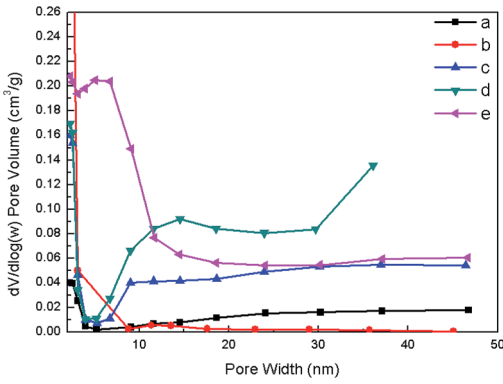


Fig. 4 Mesopore size distribution derived from BJH adsorption branch of synthesized ZSM-5 samples obtained at various TPOAC contents: (a) Commercial ZSM-5, (b) C_ZSM-5, (c) ZSM-5_(4.8)TPOAC, (d) ZSM-5_(9.6)TPOAC, and (e) ZSM-5_(38.4)TPOAC.

increased to 38.4 mol, the pore size distribution becomes narrow in the range of 5–10 nm. In contrast, the porous structure in the range of mesopore size was not observed in the cases of the commercial ZSM-5 and the C_ZSM-5. This result again confirms the presence of hierarchical mesopores in the hierarchical ZSM-5 samples and the presence of sole micropores in the conventional ZSM-5, which is consistent with the $\rm N_2$ sorption isotherm results.

From these observations, the results indicate that a suitable amount of TPOAC is equal to 9.6 mol, which produces excellent textural properties (Table 1), providing the highest mesoporosity. It is therefore reasonable to assume that in the case of the catalytic study, it should be possible to be used as a candidate catalyst.

Effect of Si/Al ratios

To verify the role of acidity on the catalytic performances, we also carried out several additional experiments to prepare the hierarchical ZSM-5 samples with various Si/Al ratios via a direct synthesis. The catalysts, having low Si/Al ratio, Si/Al = 34 (hierarchical ZSM-5(34)), and high Si/Al ratio, Si/Al = 90, (ZSM-5_(9.6)TPOAC or hierarchical ZSM-5(90)), were also synthesized by using the suitable amount of TPOAC obtained from the previous section to generate secondary mesopores. The hierarchical ZSM-5(34) also shows characteristic peaks of the MFI



Fig. 5 SEM images of: (a) Commercial ZSM-5, and (b) Hierarchical ZSM-5(34), the representative sample having low Si/Al ratio: (c) Hierarchical ZSM-5(90), the representative sample having high Si/Al ratio.

structure as shown in Fig. S3 in the ESI.† However, its crystal-linity is lower than that of the commercial ZSM-5 due to the effect of TPOAC template on the morphology of crystal growth. SEM images in Fig. 5 also confirm the differences in morphologies of three catalysts, the commercial ZSM-5, the hierarchical ZSM-5(34), and the hierarchical ZSM-5(90). Interestingly, the hierarchical ZSM-5(34) sample exhibits the self-assemblies of stick-like nanocrystals, while the hierarchical ZSM-5(90) sample consists of stacking plate-like crystals. Both samples are expected to show high catalytic performance due to their high surface areas and mesoporosity as shown in Table 1.

In addition to the number of acid sites, the nature of Al sites was also monitored by ²⁷Al MAS NMR spectroscopy (as shown in Fig. S4 in the ESI†). As the presence of the single peak at about 54 ppm of all samples, it clearly shows that the samples contain only tetrahedral coordinated Al in frameworks, whereas the presence of the octahedrally extra-framework Al species can be excluded.

The acidity of catalysts was also examined by NH₃-TPD technique. From NH₃-TPD profiles (Fig. 6), all curves were fitted and obtained with two visible peaks, appearing at low temperature, LT (*ca.* 493 K) and high temperature, HT (*ca.* 723 K). The LT peak is assigned to weak acid sites due to the interaction between NH₃ molecules desorbed from weakly acidic hydroxyl sites, which also refer to the defect and external silanol groups. However, the HT peak corresponds to the desorption of NH₃ from strong acid sites, which are Brønsted acid sites (BAS) and Lewis acid sites (LAS).⁵¹ Among synthesized samples, the hierarchical ZSM-5(34) sample exhibits the lower acidity, which is of 35.5% compared with the commercial ZSM-5. As expected, the hierarchical ZSM-5(90) shows the lowest acidity due to a small number of acid sites and it decreases approximately by 35%

Table 1 Textural properties and Si/Al ratios of all synthesized ZSM-5 samples

Samples	Si/Al ^a	S_{BET}^{b}	$S_{ m micro}^{c}$	S_{ext}^{d}	$V_{ m total}^{e}$	V_{micro}^{f}	$V_{ m ext/meso}^{\ \ g}$	$V_{ m meso}/V_{ m total}^{\ \ h}$
Commercial ZSM-5	19	363	276	87	0.171	0.110	0.060	0.351
C_ZSM-5	115	387	249	137	0.180	0.099	0.081	0.450
ZSM-5_(4.8)TPOAC	88	374	162	212	0.240	0.066	0.174	0.725
ZSM-5_(9.6)TPOAC	90	396	176	220	0.346	0.072	0.273	0.789
ZSM-5_(38.4)TPOAC	97	393	163	229	0.321	0.068	0.253	0.788
Hierarchical ZSM-5(34)	34	434	287	147	0.338	0.115	0.223	0.660

^a Si/Al ratio obtained by ICP-OES technique. ^b $S_{\rm BET}$: BET specific surface area. ^c $S_{\rm micro}$: micropore surface area. ^d $S_{\rm ext}$: external surface area. ^e $V_{\rm total}$: total pore volume. ^f $V_{\rm micro}$: micropore volume. ^g $V_{\rm ext/meso} = V_{\rm total} - V_{\rm micro}$; all surface areas and pore volumes are in the units of m² g⁻¹ and cm³ g⁻¹, respectively. ^h Fraction of mesopore volume.

RSC Advances Paper

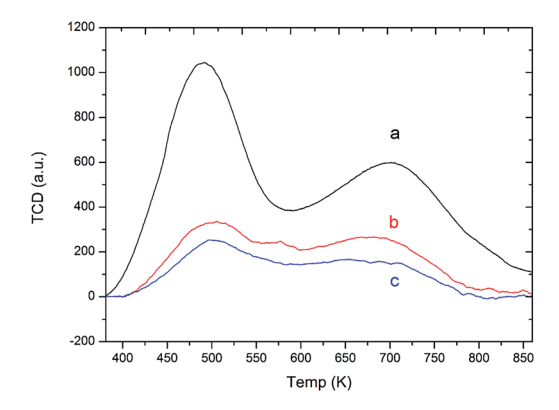


Fig. 6 NH₃-TPD curves obtained on different samples: (a) Commercial ZSM-5, (b) Hierarchical ZSM-5(34), and (c) Hierarchical ZSM-5(90).

compared with the hierarchical ZSM-5(34) sample. The amount of acid sites is known to relate to Al atoms in a framework in which the charge is compensated by acidic protons.52

To further investigate the amount of BAS and LAS, FTIR spectra of pyridine adsorption are shown in Fig. S5 and Table S2.† The peak at around 1545 cm⁻¹ is assigned to pyridinium ions formed by protonation at BAS, while a band at 1455 cm⁻¹ corresponds to pyridine adsorbed on LAS. It was found that the contribution of BAS of both catalysts is very high compared with LAS. This parameter strongly affects many potential catalytic applications, especially in an esterification.53 Consequently, this catalyst is expected to lead to enhancing the catalytic activity of the esterification.

Catalytic performance of catalysts

To illustrate the benefits of hierarchical catalysts for the catalytic upgrading of carboxylic acids, the prepared samples were tested with an esterification of benzyl alcohol and acetic acid as a model study (as shown in Scheme 1). As shown in Fig. 7, the catalytic activities of an esterification of different catalysts are demonstrated as a function of reaction time. The major product of this reaction is benzylacetate, which is almost 100% selectivity for all catalysts (Fig. 7). Interestingly, the hierarchical ZSM-5(34) sample exhibits an excellent activity compared with the other catalysts. It can convert the reactant into product about 90% in 8 h. In contrast, the commercial ZSM-5 shows very low activity, which gives only 22% of the conversion of alcohol, although it contains higher acidic density compared with the hierarchical ZSM-5(34). The different activities between two catalysts can be attributed to the fact that the presence of the



Scheme 1 Esterification reaction of benzyl alcohol and acetic acid on zeolite catalysts.

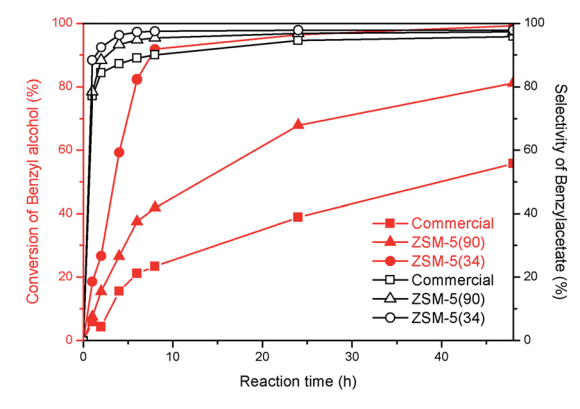


Fig. 7 Benzyl alcohol conversion (%) (red) and benzylacetate selectivity (%) (black) as a function of reaction time on different samples: Commercial ZSM-5, Hierarchical ZSM-(90), and Hierarchical ZSM-5(34)

hierarchical porous network can reduce the diffusion constraints inside micropores. Interestingly, the hierarchical sample containing the lower amount of acidic density (high Si/ Al ratio) also exhibits higher catalytic activity than that of the commercial ZSM-5, implying that the higher catalytic activity can be contributed by the hierarchical porous network. This result again confirms that the promising property of hierarchical structures can promote the catalytic activity of an esterification of carboxylic acid.

To demonstrate the efficiency of catalysts, the reusability studies of the hierarchical ZSM-5 and the corresponding conventional zeolite were also carried out at various reaction cycles (Fig. 8). The conversion of alcohol is about 90% at 8 h when the hierarchical ZSM-5(34) sample was used as a catalyst for the first cycle. In contrast, the commercial sample only converts the reactant into the product by 22%. For the second cycle, the hierarchical ZSM-5(34) sample still exhibits an excellent performance by showing about 85% of alcohol conversion. However, the commercial catalyst performs similarly low catalytic activity compared to itself in the first cycle. In the third cycle, the hierarchical catalyst still shows, as expected, a good catalytic performance (80% conversion of alcohol), while the

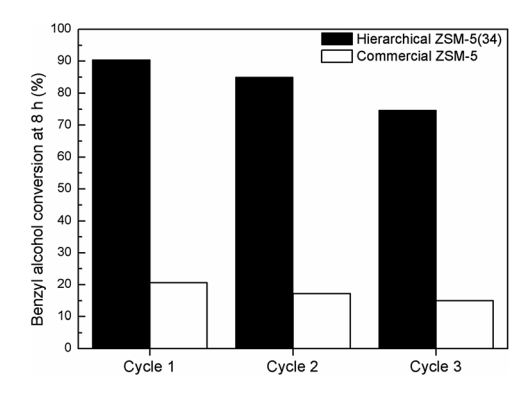


Fig. 8 Reusability experiments of Hierarchical ZSM-5(34) and Commercial ZSM-5 catalysts for three cycles (catalytic test condition: 373 K and 1 atm).

Paper **RSC Advances**

commercial one only converts about 15% of the alcohol toward the product. It is noteworthy that the inferior catalytic activity of the commercial sample is due to the presence of sole micropores in the structure and this could eventually lead to accelerate the coke formation.

To further verify in the term of catalyst deactivation, the amount of deposited coke was also measured by the temperature thermogravimetric analysis (TGA) and the O₂ temperatureprogrammed oxidation (O2-TPO) as shown in Fig. S6 and S7 in the ESI.† From TGA profiles, it was found that a carbon weight loss over the hierarchical ZSM-5(34) sample is much less than that of the commercial one (11.5% and 32.4% for the hierarchical ZSM-5(34) and the commercial ZSM-5, respectively) after the reaction time of 24 h. As expected, the presence of hierarchical pores obviously improves the catalytic activity by rendering molecular transportation, resulting in a reduction in coke formation.

In contrast, the commercial sample contains a large amount of deposited coke due to the presence of sole micropores in its structure, causing the pore blocking. Besides, O₂-TPO profiles demonstrate the location and the type of carbonaceous species. At the low temperature about 673 K, it is attributed to the lowest aromatic condensation, which are easily oxidized and mostly located on the outermost surface of zeolite (coke I). Meanwhile, at higher temperature about 773-873 K, it is ascribed to the high aromatic condensation, the polynuclear aromatic coke species or graphitic like coke (cokes II and III), which are originated from the microporous zeolite structure. 54-56 The deconvolution of TPO curves shows an amount of coke content of three different species. The significant decrease of cokes I and II over the hierarchical ZSM-5 sample was observed, indicating a lower degree of condensation of coke species. The commercial sample exhibits a large amount of developed polynuclear aromatic coke/ graphitic species deposited on external surfaces and inside zeolite structures with the total coke content of 10 mmol g^{-1} . In contrast, the hierarchical ZSM-5 sample dramatically reduces the coke formation of all types with the total coke content of 3 mmol g^{-1} due to shortening the diffusion path length. On the other hand, a large content of coke II and III species in the commercial sample indicates that the fast deactivation of catalyst is the results of pore blockage by high aromatic condensation. This is also consistent with the TGA results, revealing that the hierarchical samples can significantly reduce the content, resulting in an increase of catalytic activity. Fig. S8† shows Raman spectra of coke species deposited on catalysts after the reaction. It was found that two visible peaks appearing at 1610 and 1389 cm⁻¹ are assigned to the G band corresponding to the presence of graphitic materials⁵⁷ and the D band due to disordered carbon structures, respectively. Obviously, both catalysts exhibit the presence of both graphite-like carbon species and disordered amorphous polyaromatic species. Interestingly, the ratio of area of D band and G band (I_D/I_G) of commercial ZSM-5 and hierarchical ZSM-5(34) is 0.52 and 0.39, respectively. These correspond well with O2-TPO results that the higher ratio of coke II to coke III content was observed in the deposited coke obtained by a commercial catalyst.

This makes it clear that the catalytic activity for the esterification of carboxylic acids can be greatly improved in the case of hierarchical ZSM-5 samples even though they exhibit lower Brønsted acid density. Together with the presence of mesoporous networks connected to the microporous framework, it gives the benefits to improve the catalytic performances in terms of catalytic activity, desired product yield, and catalyst stability/reusability, due to the improved accessibility to active sites. On the other hand, the sole microporous structure of commercial ZSM-5 does not show the advantage for the reaction because of not only inhibiting the diffusion of molecules to active sites but also facilitating the coke formation inside microporous network, especially for catalysts with very high Brønsted acid density, which is required for the acid catalysed reaction, such as an esterification of organic acids.

To compare the catalytic performances of hierarchical zeolites obtained by various synthesis approaches (Fig. S9 in the ESI†), the hierarchical ZSM-5 sample obtained by a direct synthesis, hierarchical ZSM-5(34), shows a significantly improved catalytic activity compared with those obtained by using a conventional alkaline treatment, even though both samples contain the similarity in textural properties, such as micro- and mesoporosity (as shown in Table S3 in the ESI†). The hierarchical ZSM-5(34) sample exhibits an excellent conversion of alcohol (about 90% and high selectivity of benzylacetate almost 100%).

In order to further illustrate the benefits of hierarchical zeolites for the catalytic upgrading of carboxylic acids, an esterification of levulinic acid, which can be formed by the acidcatalyzed dehydration of monosaccharide, and ethanol has also been investigated (Table S4 in the ESI†). Interestingly, the hierarchical zeolite can greatly improve the catalytic activity to produce the ethyl levulinate that can be used as diesel miscible biofuel (DMB). The hierarchical ZSM-5 have the two-three fold advantage of the catalytic conversion of levulinic acid compared with the conventional zeolite as well as preserved shape selectivity of zeolite framework. This work opens up interesting perspectives for the development of hierarchical mesoporous zeolites via a direct synthesis approach using an organosilane template for the catalytic upgrading of various carboxylic acids.

Conclusions

The hierarchical ZSM-5 samples have been successfully synthesized under a simple direct hydrothermal method. With the aid of TPOAC, the synthesized hierarchical ZSM-5 products exhibit promising catalytic performances in terms of increasing activity, desired product yield, and catalyst reusability for an esterification of carboxylic acids. In particular, the hierarchical ZSM-5(34) sample performs a remarkable activity by converting almost 90% of benzylalcohol to benzylacetate for an esterification of acetic acid and benzylalcohol within 8 h corresponding to the presence of hierarchical porous networks in the zeolite structure.

To illustrate the ability of hierarchical structures, the sample with a low content of acidic density also shows a good performance by catalyzing 70% of reactant in 24 h. This might be **RSC Advances**

explained by the hierarchical pores rendering the catalyst's performance. In the view of catalyst reusability, the hierarchical catalyst, hierarchical ZSM-5(34), exhibits an excellent performance compared with the commercial catalyst with almost fivefold catalytic activity even after three cycles.

To evaluate the efficiency of catalysts obtained by different synthesis methods, it was also found that the catalyst prepared by a direct synthesis shows a significantly improved activity compared with the one obtained by a conventional posttreatment method. Interestingly, not only different catalytic performances can be observed for hierarchical zeolites obtained by different methods, but also a wider range of framework Si/Al ratios of catalysts can be prepared by a direct synthesis. For these reasons, the developed hierarchical zeolites by a direct synthesis approach can benefit to many applications, in particular, the bio-oil upgrading via an esterification of various carboxylic acids for the development of renewable energy resources in future.

Acknowledgements

This work was supported in part by grants from the National Science and Technology Development Agency (NANOTEC Center for Nanoscale Materials Design for Green Nanotechnology funded by the National Nanotechnology Center), the Commission on Higher Education, Ministry of Education (the National Research University Project of Thailand), the Vidyasirimedhi Institute of Science and Technology, the PTT group (PTT Public Company Limited, PTT Exploration & Production, PTT Global Chemical, IRPC and Thaioil). K. R. would like to thank to the Development and Promotion of Science and Technology Talents Project (DPST). C. W. would like to acknowledge funding from the Thailand Research Fund (TRF) (MRG5980114), the Office of Higher Education Commission (OHEC), the Junior Research Fellowship Program of the French Embassy in Thailand, and the support of scientific instrument by the Frontier Research Center, Vidyasirimedhi Institute of Science and Technology and Schuit Institute of Catalysis, Department of Chemical Engineering and Chemistry, Eindhoven University of Technology.

- 1 M. Stöcker, Angew. Chem., Int. Ed., 2008, 47, 9200-9211.
- 2 H. B. Goyal, D. Seal and R. C. Saxena, Renewable Sustainable Energy Rev., 2008, 12, 504-517.
- 3 S. Czernik and A. V. Bridgwater, Energy Fuels, 2004, 18, 590-
- 4 P. M. Mortensen, J. D. Grunwaldt, P. A. Jensen, K. G. Knudsen and A. D. Jensen, Appl. Catal., A, 2011, 407, 1-19.
- 5 C. A. Gärtner, J. C. Serrano-Ruiz, D. J. Braden and J. A. Dumesic, ChemSusChem, 2009, 2, 1121-1124.
- 6 R. W. Snell, E. Combs and B. H. Shanks, Top. Catal., 2010, 53,
- 7 Y. Liu, Z. Li, J. J. Leahy and W. Kwapinski, Energy Fuels, 2015, 29, 3691-3698.

- 8 L. Ciddor, J. A. Bennett, J. A. Hunns, K. Wilson and A. F. Lee, J. Chem. Technol. Biotechnol., 2015, 90, 780-795.
- 9 S. Furuta, H. Matsuhashi and K. Arata, Catal. Commun., 2004, 5, 721-723.
- 10 E. Cano-Serrano, G. Blanco-Brieva, J. M. Campos-Martin and J. L. G. Fierro, Langmuir, 2003, 19, 7621-7627.
- 11 H. Liu, N. Xue, L. Peng, X. Guo, W. Ding and Y. Chen, Catal. Commun., 2009, 10, 1734-1737.
- 12 A. Corma, H. Garcia, S. Iborra and J. Primo, J. Catal., 1989, **120**, 78-87.
- 13 J. Bedard, H. Chiang and A. Bhan, J. Catal., 2012, 290, 210-
- 14 H. Katsuno, T. Fukunaga and M. Sugimoto, in Studies in Surface Science and Catalysis, ed. F. Solymosi, L. Guczi and P. Tétényi, Elsevier, 1993, vol. 75, pp. 2419–2422.
- 15 W. Wannapakdee, C. Wattanakit, V. Paluka, T. Yutthalekha and J. Limtrakul, RSC Adv., 2016, 6, 2875-2881.
- 16 P. Cañizares, A. de Lucas, F. Dorado and D. Pérez, Appl. Catal., A, 2000, 190, 233-239.
- 17 C. Wattanakit, S. Nokbin, B. Boekfa, P. Pantu and J. Limtrakul, J. Phys. Chem. C, 2012, 116, 5654-5663.
- 18 C. H. Christensen, K. Johannsen, I. Schmidt and C. H. Christensen, J. Am. Chem. Soc., 2003, 125, 13370-13371.
- 19 P. Wuamprakhon, C. Wattanakit, C. Warakulwit, T. Yutthalekha, W. Wannapakdee, S. Ittisanronnachai and J. Limtrakul, Microporous Mesoporous Mater., 2016, 219, 1-9.
- 20 G. M. Lari, B. Puértolas, M. S. Frei, C. Mondelli and J. Pérez-Ramírez, ChemCatChem, 2016, 8, 1507-1514.
- 21 S. R. Kirumakki, N. Nagaraju and K. V. R. Chary, Appl. Catal., A, 2006, 299, 185-192.
- 22 K. H. Chung and B. G. Park, J. Ind. Eng. Chem., 2009, 15, 388-
- 23 C. J. H. Jacobsen, C. Madsen, T. V. W. Janssens, H. J. Jakobsen and J. Skibsted, Microporous Mesoporous Mater., 2000, 39, 393-401.
- 24 W. Chaikittisilp, Y. Suzuki, R. R. Mukti, T. Suzuki, K. Sugita, K. Itabashi, A. Shimojima and T. Okubo, Angew. Chem., Int. Ed., 2013, 52, 3355-3359.
- 25 P. Kumar, K. V. Agrawal, M. Tsapatsis and K. A. Mkhoyan, Nat. Commun., 2015, 6, 7128.
- 26 B. M. Weckhuysen and J. Yu, Chem. Soc. Rev., 2015, 44, 7022-7024.
- 27 J. C. Groen, T. Bach, U. Ziese, A. M. Paulaime-van Donk, K. P. de Jong, J. A. Moulijn and J. Pérez-Ramírez, J. Am. Chem. Soc., 2005, 127, 10792-10793.
- 28 D. Verboekend, S. Mitchell, M. Milina, J. C. Groen and J. Pérez-Ramírez, J. Phys. Chem. C, 2011, 115, 14193-14203.
- 29 H. Mochizuki, T. Yokoi, H. Imai, S. Namba, J. N. Kondo and T. Tatsumi, Appl. Catal., A, 2012, 449, 188–197.
- 30 I. Schmidt, A. Boisen, E. Gustavsson, K. Ståhl, S. Pehrson, S. Dahl, A. Carlsson and C. J. H. Jacobsen, Chem. Mater., 2001, 13, 4416-4418.
- 31 A. H. Janssen, I. Schmidt, C. J. H. Jacobsen, A. J. Koster and K. P. de Jong, Microporous Mesoporous Mater., 2003, 65, 59-
- 32 M. Y. Kustova, P. Hasselriis and C. H. Christensen, Catal. Lett., 2004, 96, 205-211.

Paper

33 F.-S. Xiao, L. Wang, C. Yin, K. Lin, Y. Di, J. Li, R. Xu, D. S. Su,

- R. Schlögl, T. Yokoi and T. Tatsumi, Angew. Chem., Int. Ed., 2006, 45, 3090-3093.
- 34 H. Zhu, Z. Liu, D. Kong, Y. Wang, X. Yuan and Z. Xie, J. Colloid Interface Sci., 2009, 331, 432-438.
- 35 Y. Cheneviere, F. Chieux, V. Caps and A. Tuel, J. Catal., 2010, 269, 161-168,
- 36 W. Park, D. Yu, K. Na, K. E. Jelfs, B. Slater, Y. Sakamoto and R. Ryoo, Chem. Mater., 2011, 23, 5131-5137.
- 37 K. Cho, K. Na, J. Kim, O. Terasaki and R. Ryoo, Chem. Mater., 2012, 24, 2733-2738.
- 38 M. Choi, H. S. Cho, R. Srivastava, C. Venkatesan, D.-H. Choi and R. Ryoo, Nat. Mater., 2006, 5, 718-723.
- 39 Z. Zhao, Y. Liu, H. Wu, X. Li, M. He and P. Wu, Microporous Mesoporous Mater., 2009, 123, 324-330,
- 40 A. J. J. Koekkoek, H. Xin, Q. Yang, C. Li and E. J. M. Hensen, Microporous Mesoporous Mater., 2011, 145, 172-181.
- 41 L. Wu, V. Degirmenci, P. C. M. M. N. J. H. G. M. Lousberg and E. J. M. Hensen, J. Catal., 2013, 298, 27-40.
- 42 M. Krishnamurthy, K. Msm and C. Kanakkampalayam Krishnan, Microporous Mesoporous Mater., 2016, 221, 23-31.
- 43 M. Milina, S. Mitchell and J. Pérez-Ramírez, Catal. Today, 2014, 235, 176-183.
- 44 D. Verboekend and J. Perez-Ramirez, Catal. Sci. Technol., 2011, 1, 879-890.
- 45 J. C. Groen, J. C. Jansen, J. A. Moulijn and J. Pérez-Ramírez, J. Phys. Chem. B, 2004, 108, 13062-13065.

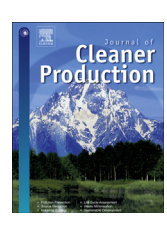
- 46 J. C. Groen, J. A. Moulijn and J. Pérez-Ramírez, Microporous Mesoporous Mater., 2005, 87, 153-161.
- 47 C. Wattanakit, C. Warakulwit, P. Pantu, B. Sunpetch, M. Charoenpanich and J. Limtrakul, Can. J. Chem. Eng., 2012, 90, 873-880.
- 48 S. Brunauer, P. H. Emmett and E. Teller, J. Am. Chem. Soc., 1938, 60, 309-319.
- 49 B. C. Lippens and J. H. de Boer, J. Catal., 1965, 4, 319–323.
- 50 E. P. Barrett, L. G. Joyner and P. P. Halenda, J. Am. Chem. Soc., 1951, 73, 373-380.
- 51 J. N. Kondo, R. Nishitani, E. Yoda, T. Yokoi, T. Tatsumi and K. Domen, Phys. Chem. Chem. Phys., 2010, 12, 11576-11586.
- 52 K. Mlekodaj, K. Tarach, J. Datka, K. Góra-Marek and W. Makowski, Microporous Mesoporous Mater., 2014, 183,
- 53 V. N. Shetti, J. Kim, R. Srivastava, M. Choi and R. Ryoo, J. Catal., 2008, 254, 296-303.
- 54 F. Bauer and H. G. Karge, Characterization II, ed. H. G. Karge and J. Weitkamp, Springer Berlin Heidelberg, Berlin, Heidelberg, 2007, pp. 249-364.
- 55 I. H. Son, S. J. Lee, I. Y. Song, W. S. Jeon, I. Jung, D. J. Yun, D.-W. Jeong, J.-O. Shim, W.-J. Jang and H.-S. Roh, Fuel, 2014, 136, 194-200.
- 56 W. B. Widayatno, G. Guan, J. Rizkiana, J. Yang, X. Hao, A. Tsutsumi and A. Abudula, Appl. Catal., B, 2016, 186, 166 - 172.
- 57 J. Guo, H. Lou and X. Zheng, Carbon, 2007, 45, 1314-1321.



Contents lists available at ScienceDirect

Journal of Cleaner Production

journal homepage: www.elsevier.com/locate/jclepro



Hierarchical FAU-type zeolite nanosheets as green and sustainable catalysts for benzylation of toluene



Thittaya Yutthalekha ^{a, b, c}, Chularat Wattanakit ^a, Chompunuch Warakulwit ^{b, c}, Wannaruedee Wannapakdee ^a, Kamonlatth Rodponthukwaji ^{b, c}, Thongthai Witoon ^{c, d}, Jumras Limtrakul ^{e, *}

- ^a Department of Chemical and Biomolecular Engineering, School of Energy Science and Engineering, Vidyasirimedhi Institute of Science and Technology, Rayong 21210, Thailand
- ^b Department of Chemistry and NANOTEC Center for Nanoscale Materials Design for Green Nanotechnology, Faculty of Science, Kasetsart University, Bangkok 10900, Thailand
- ^c Center for Advanced Studies in Nanotechnology and Its Applications in Chemical, Food and Agricultural Industries, Kasetsart University, Bangkok 10900, Thailand
- ^d Department of Chemical Engineering, Faculty of Engineering, Kasetsart University, Bangkok 10900, Thailand
- ^e Department of Materials Science and Engineering, School of Molecular Science and Engineering, Vidyasirimedhi Institute of Science and Technology, Rayong 21210, Thailand

ARTICLE INFO

Article history: Received 28 December 2015 Received in revised form 8 July 2016 Accepted 1 August 2016 Available online 3 August 2016

Keywords:
Green catalyst
Hierarchical zeolite
Organosilane
Clean benzylation
Recyclable synthesized precursor

ABSTRACT

The development of recyclable solid acids is of major industrial importance and challenging in many reactions, for instance, the Friedel-Crafts alkylation as one of the most prevalent examples, which generally requires the presence of acid catalysts. However, not only the replacement of traditional toxic acid catalyst by solid acidic zeolites but also the improvement such catalysts in term of high efficiency has been addressed through environmental technologies. Our present study explores the use of hierarchical faujasite zeolite nanosheets as catalysts in industrial applications with the frame of development of green and sustainable technologies. The simple and efficient route to prepare the faujasite zeolite with the nanosheet-assembled structure together with the roles of synthetic parameters on the characteristics and properties are systematically investigated. This first example of hierarchical zeolite, which has uniform mesoporous features derived from the interstitial pores between the nanosheet assemblies, exhibits a superior catalytic activity in terms of conversion and selectivity for the benzylation of toluene with benzyl chloride. In conclusion, the fine-tuning of structural characteristics of zeolites by a simple optimization of surfactant contents and crystallization temperatures allows the design of the candidate catalyst for a green and sustainable future. This work also demonstrates the next step forward in the development of an industrial catalyst based on the concept of cleaner production.

© 2016 Elsevier Ltd. All rights reserved.

1. Introduction

Currently, many chemical processes have suffered from highenergy consumption, large amount of wastes and pollution. Therefore, sustainable innovation with energy saving, green processes, and environmental concerns is a desired goal for the chemical industry (Díaz López and Montalvo, 2015). The development of existing industrial catalysts with the intention of increasing their performances in order to efficiently use natural resources, including raw materials, energy and water, while reducing the generation of waste is one of the major goals of the cleaner production concepts (Glavič and Lukman, 2007; Jegatheesan et al., 2009). This is portrayed in the new patterns of industrial production, which is gaining widespread and increasing interest from national society (Zeng et al., 2010).

The use of an environmentally friendly chemical process is currently gaining popularity because the use of conventional Lewis and mineral acid catalysts (e.g., AlCl₃, HF, H₂SO₄) has led to environmental problems, especially in large-scale production. Great efforts have been made to replace such conventional catalysts with solid acid catalysts. Among them, zeolites have attracted increasing

Corresponding author.

E-mail address: jumras.limtrakul@vistec.ac.th (J. Limtrakul).

interest due to their benefits of heterogeneous catalyst, which can be easily separated from the reaction mixtures and also be recycled. Moreover, their well-known special features such as high micropore surface area, acidity, shape selectivity, and good thermal/hydrothermal stability, zeolites are considered as green catalysts in the petrochemical manufacture of fine chemicals and chemical intermediates.

However, in some cases, the presence of sole micropores limits the catalytic performance of zeolites. Conventionally, the pores or cavities of zeolites are size related to molecular dimensions or micropores (<2 nm). Bulky molecules with the molecular dimension larger than the micropore dimension, then cannot adsorb and undergo any reactions in the pores. In addition, the diffusion of the molecules may be slow, resulting in a relatively low catalytic activity and a fast catalytic deactivation, especially in the refining processes dealing with heavy feedstock molecules. Thus, the development of highly active zeolite catalysts that can be applied for a large number of potential applications in various industrially important reactions remains as a challenge.

The improvement of zeolite efficiency has been extensively studied. Most of such developments concern the design of hierarchical zeolites in order to overcome the problems of small pore sizes and diffusion limitations in conventional zeolites. Both the introduction of larger pores, such as mesopores (2-50 nm) and macropores (>50 nm), interconnected to the conventional micropores (Egeblad et al., 2007; Na et al., 2013) and the size reduction of zeolite crystals (Tosheva and Valtchev, 2005), especially to nanoscale, have been investigated by many researchers. Among hierarchical zeolites, zeolite nanosheets have attracted considerable attention. As a result of their sheet-like crystals and their thickness in the nanometer range, the nanosheets exhibit high external surface areas and a large number of pore volumes derived from mesoand/or macropores in addition to micropores (Choi et al., 2009). To prepare nanosheet zeolites, organosilanes were used as structure directing agent (SDA) because of the stable interaction between the organosilane molecules and the growing zeolite crystals preventing phase separation. This leads to the efficient formation of the nanosheets (Inayat et al., 2012; Khaleel et al., 2014).

Zeolites having a faujasite (FAU) framework structure are one of the most industrially important catalysts. They are commonly used in a wide range of potential catalytic reactions, including fluid catalytic cracking to convert heavy petroleum crude oils to high value-added products, such as gasoline (Garcia-Martinez et al., 2012), and in the transesterification of sugars or fatty acids (Davis, 2003; Luz Martínez et al., 2010). The FAU nanosheet assemblies were successfully synthesized using organosilane surfactants with 16- and 18-carbon alkyl chains. However, it is still in an early stage of development and the catalytic behaviors of the FAU nanosheets as well as the roles of synthetic parameters on the product characteristics and properties have never been systematically investigated.

In this work, a simple and practical strategy to prepare hierarchical FAU zeolite nanosheet assemblies using 3-(trimethoxysilyl) propyl octadecyl dimethyl ammonium chloride or TPOAC, an organosilane surfactant with an 18-carbon alkyl chain, as SDA, has been demonstrated. The roles of the synthetic parameters, including the surfactant content in the synthesis gel and the crystallization temperature, on the product characteristics were systematically investigated. Moreover, the recycling waste motherliquid, which is composed of non-reacted species, including Si, Al, and TPOAC surfactant from the first batch synthesis, can be used to synthesize hierarchical FAU zeolite nanosheet assemblies. The obtained insight into the synthetic parameters together with the recyclable synthesis strategy allow us to prepare the FAU zeolite nanosheets with huge saving on energy and cost of production. Our

study clearly demonstrates, for the first time, the superior catalytic behaviors of the hierarchical FAU nanosheets compared with the conventional FAU zeolite for the benzylation of toluene, which is one of the most important reactions in the fine chemical industry. These would be applicable for a green and sustainable catalytic process.

2. Materials and methods

In the present study, we divided the experiments into three sections including synthesis of FAU nanosheets, characterization and catalytic testing as per the following details:

2.1. Synthesis of FAU nanosheets

Sodium hydroxide (NaOH: 97%, Carlo Erba), sodium aluminate (NaAlO₂: 44 wt% Na₂O and 56 wt% Al₂O₃, Riedel-de Haën) and sodium silicate (Na₂Si₃O₇: 26.5 wt% SiO₂ and 10.6 wt% Na₂O, Merck) were used as the mineralizing agent, alumina and silica sources, respectively. 3-(trimethoxysilyl) propyl octadecyl-dimethylammonium chloride (TPOAC, 42 wt% in methanol, Aldrich) was used as the SDA.

The FAU samples were prepared according to the literature with slight modifications, (Inayat et al., 2012; Khaleel et al., 2014). In a typical synthesis, the freshly prepared sodium aluminate solution containing 1.0 g of NaAlO₂, 0.5 g of NaOH and 3.2 g of DI water was dropwisely added into the sodium silicate solution containing 3.7 g of Na₂Si₃O₇, 0.2 g of NaOH and 11.2 g of DI water. The obtained mixture was vigorously stirred for 1 h. Subsequently, the desired amount of TPOAC was added. The resulting mixture was further stirred for 1 h. The molar composition of the synthesis gel was 3 SiO_2 : 3.5 Na₂O: 1 Al₂O₃: 180 H₂O: x TPOAC, where x = 0.01, 0.02, 0.04, 0.06 and 0.08. The gel was aged at 30 °C for 24 h and then crystallized for 4 days within a desired temperature range (65–85 °C) in static mode. The product and its waste mother-liquid were collected by filtration. Then, the product was washed with DI water until the pH of the filtrate was less than 8. After drying overnight at 100 °C, the product was calcined in air at 350 °C for 15 h to remove the SDA. The waste mother-liquid was used to synthesize FAU zeolite in the subsequent recycle experiment.

In comparison, the conventional FAU zeolite samples were also prepared under the same conditions, but without the addition of the surfactant. The samples prepared in this study are designated as "xT-nC" according to the content of TPOAC in the synthesis gel (x) and the crystallization temperature $(n, \, ^{\circ}C)$.

2.2. Characterizations

X-ray diffraction (XRD) was performed using a Bruker D8 ADVANCE instrument with CuK_{α} radiation (30 kV, 40 mA). The data were collected in the 2θ range of $5-50^{\circ}$ with a step size of 0.02° and a scan rate of 1° /min. The average crystallite size was estimated from the Scherrer equation using the full-width at half maximum (fwhm) of the peaks at 6° [111], 16° [331], and 27° [642] (Zhan et al., 2002).

The morphology of the products was observed by scanning electron microscopy (SEM) performed on a Hitachi-3400 instrument with an accelerating voltage of 5 kV. Prior to each measurement, the sample was sputtered with a layer of platinum with the thickness of 2.3 nm. The average particle size and the nanosheet thickness of the products were estimated from at least 200 particles. The transmission electron microscopy (TEM) was performed on a JEOL JEM-2100 microscope at 200 kV. Prior to each measurement, the sample was dispersed in absolute ethanol, dropped and dried on a copper grid.

The textural properties of the products were analyzed by the measurement of the N_2 adsorption-desorption isotherms using a Micromeritics ASAP 2020 apparatus performed at $-196\,^{\circ}$ C. Prior to each measurement, the sample was degassed at 300 $^{\circ}$ C for 20 h. The specific surface area (S_{BET}) was determined by using the Brunauer–Emmett–Teller (BET) theory. The micropore volume (V_{micro}), the micropore area (S_{micro}) and the external surface area (S_{ext}) were determined by the t-plot method. The mesopore size distribution was derived from the adsorption and desorption branches by using a Barrett-Joyner-Halendat (BJH) model. The total pore volume (V_{total}) was estimated at P/P0 = 0.98 (Storck et al., 1998).

The Si/Al ratio of the products was estimated by X-ray fluorescence (XRF) spectrometry performed with a Bruker AXS S4 Pioneer instrument equipped with a rhodium X-ray source. The nature of the Al atoms incorporated in the zeolite framework was examined by the ²⁷Al magic angle spinning nuclear magnetic resonance (²⁷Al MAS NMR) spectroscopy. The spectra were recorded at 130.322 MHz with an acquisition delay of 4 s, an acquisition time of 0.012 s and 640 scans by using an INOVA-500 spectrometer. The acidity of catalysts was determined by temperature-programmed desorption of ammonia (NH3-TPD) performed on a BELCAT II instrument equipped with thermal conductivity detectors (TCD). Prior to the measurement, the catalyst was preheated at 300 °C for 1 h under the flow of He. Then the catalyst was saturated with NH₃ at 100 °C for 30 min and subsequently flushed under the flow of He for 30 min to remove the physically adsorbed NH₃. The TPD profiles were recorded in the temperature range of 100–550 °C with ramp rate of 10 $^{\circ}$ Cmin⁻¹.

2.3. Catalytic testing

The benzylation of toluene with benzyl chloride was performed by using a three-necked round-bottom flask equipped with a reflux condenser at 110 °C. Typically, 25 ml of toluene was added to 0.5 g of the proton-formed catalysts, which were activated in $\rm N_2$ atmosphere at 350 °C for 1 h. The obtained mixture was stirred for 10 min. Then, 5 ml of benzyl chloride was added. The reaction products were analyzed at certain predetermined times (6, 24 and 30 h) by gas chromatography (GC) performed on an Agilent 7820A GC instrument equipped with a FID detector and a DB-1 column. Based on the consumption of benzyl chloride, which acts as the benzylating agent, as the amount of toluene was in excess, the conversion and product selectivity were calculated by the following equations.

$$\textit{Conversion} \ (\%) \ = \ \left(\frac{\textit{wt\% of consumed benzylchloride}}{\textit{wt\% of initial benzylchloride}} \right) \ \times \ 100$$

$$Selectivity~(\%) = \frac{(wt\%~of~desired~product) \times 100}{(wt\%~of~total~products)}$$

3. Results and discussion

This section provides a step-by-step explanation starting from

the effect of crystallization temperatures on the formation of conventional FAU zeolite, the roles of the crystallization temperature and the surfactant content for the formation of hierarchical FAU zeolite nanosheet assemblies to the catalytic activity.

3.1. Synthesis of conventional FAU zeolite at various crystallization temperatures

The FAU zeolites obtained from the synthesis without the addition of the TPOAC surfactant are shown in Fig. 1. Conventional FAU crystals with uniform size and shape are observed. The measurement of the average particle size from the low-magnification image (Fig. 1-a) indicates a narrow size distribution of the particles. The high-magnification image (Fig. 1-b) reveals an octahedral crystal shape. The average particle size of the products $(2.0-2.5~\mu\text{m})$ is found to slightly increase with the increase of the crystallization temperature (see Table 1 and Fig. S1).

The XRD data delivered evidence of the formation of FAU crystals and agree well with the standard XRD data in JCPDS file no. 39-0218 as shown in Fig. 2. The XRD pattern and the high intensity peaks of the synthesized samples indicate the characteristics of FAU with high crystallinity (see Fig. S2, OT-65C, OT-75C and OT-85C). The samples crystallized at higher temperatures exhibit slightly sharper peaks with higher intensities compared to the products crystallized at lower temperatures. This result is in good agreement with those observed by SEM, indicating that the products crystallized at the higher temperature have a more well-defined octahedral shape than those crystallized at lower temperatures (see Fig. 1-b, S1-b and S1-d). Moreover, the crystallite size of the products calculated by the Scherrer equation slightly increases with the increase of the crystallization temperature in the range of 81–98 nm (see Table 1). This range corresponds well with the typical values of bulk FAU zeolites (Chaves et al., 2012).

The variation of the crystallization temperature induces the change of the product morphology and the textural properties. The N₂ sorption isotherms of the bulk samples prepared without the addition of TPOAC do not show any hysteresis loop. Only adsorption at relatively low pressure $(P/P_0 < 0.2)$ with a long horizontal plateau due to the micropore filling, corresponding to the type-I isotherm, can be observed (Fig. 3a). This finding confirms the presence of sole micropores, which is of the nature of conventional zeolites. The micropore size distribution was observed by the micropore analysis (MP) method as shown in Fig. S3. The average micropore size is 0.7 nm, that confirms the structural pore of FAU zeolite (theoretical pore diameter of ~0.74 nm). Additionally, the micropore surface area increases with the increase of crystallization temperature $(777-842 \text{ m}^2/\text{g} \text{ at a rising temperature from 65 to 85 °C})$, whereas the external surface area does not significantly change, leading to the enhancement of the total specific surface area (see Table 2). The suggested reason is the increase of the crystallization rate due to the increase of temperature (Li et al., 2002; Zhan et al., 2002). This clearly confirms that the crystallization temperature is an important parameter controlling the product characteristics and textural properties.

3.2. Synthesis of hierarchical FAU zeolite nanosheet assemblies: roles of the crystallization temperature and the surfactant content in the synthesis gel

The data regarding the characteristics of the products prepared by using TPOAC at various crystallization temperatures are also summarized in Table 1. The results show that the TPOAC is able to modulate the product characteristics. FAU products with spherical assemblies (see Fig. 4-a), composing the compact nanosheet-assembled structure (see Fig. 4-b), were successfully prepared

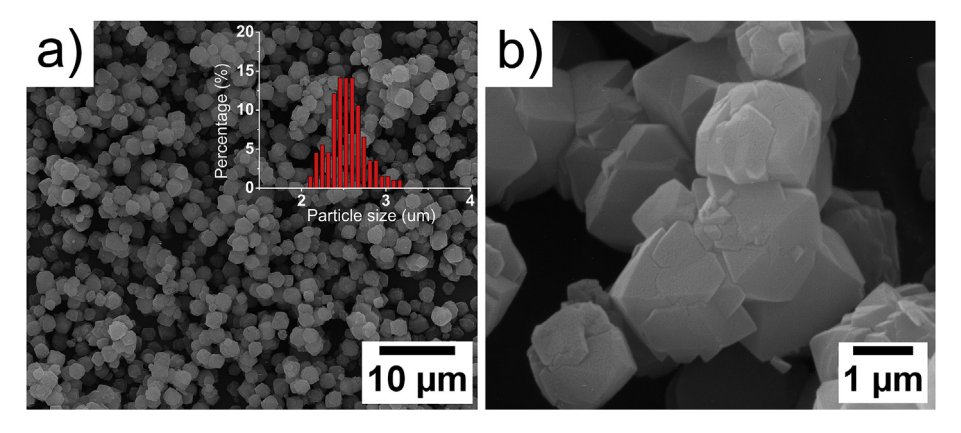


Fig. 1. SEM images with a) low and b) high magnifications of the FAU zeolite products prepared without the addition of the TPOAC surfactant. The images are of an 0T-85C sample.

Table 1Summary of the characteristics of products prepared at various crystallization temperatures.

Sample	Morphology	Particle size ^a (μm)	Thickness ^a (nm)	Crystallite size ^b (nm)
0T-65C	Bulk NaX	2.0 ± 0.2	NA	81
0.01T-65C	Nanosheet	3.1 ± 0.3	201 ± 29	59
0.02T-65C	Nanosheet	3.6 ± 0.5	199 ± 11	59
0.04T-65C	Nanosheet	3.8 ± 0.4	175 ± 27	47
0.06T-65C	Amorphous	NA	NA	NA
0.08T-65C	Amorphous	NA	NA	NA
0T-75C	Bulk NaX	2.2 ± 0.1	NA	98
0.01T-75C	Nanosheet	3.2 ± 0.2	NA	87
0.02T-75C	Nanosheet	3.5 ± 0.1	196 ± 25	72
0.04T-75C	Nanosheet	3.7 ± 0.7	141 ± 24	62
0.06T-75C	Nanosheet	5.0 ± 0.1	134 ± 17	60
0.08T-75C	Amorphous	NA	NA	NA
0T-85C	Bulk NaX	2.5 ± 0.3	NA	92
0.01T-85C	Bulk NaX	3.2 + 0.3	NA	97
0.02T-85C	Bulk NaX	3.2 ± 0.2	NA	93
0.04T-85C	Nanosheet	3.7 ± 0.2	216 ± 25	96
0.06T-85C	Nanosheet	4.1 ± 0.3	375 ± 83	90
0.08T-85C	Bulk NaP	NA	NA	NA

^a Estimated from SEM images.

depending on the TPOAC content and the crystallization temperature. By controlling such parameters, the obtained samples can be prepared with various morphologies, particle sizes, crystallite sizes, and textural properties. In the case of nanosheet products, the thickness of the sheet assemblies can also be tuned. The powder-XRD patterns reveal that the samples prepared with the addition of TPOAC compose of the FAU framework without any crystalline impurities (see Fig. 2). Compared with the conventional FAU zeolite, the lower peak intensity of the nanosheet samples indicates lower crystallinity. In addition, when the content of TPOAC is increased, the peak intensity of nanosheet samples significantly decreases.

The N_2 sorption isotherms of the FAU products having the nanosheet-assembled structure (see Fig. 3b–d, left) typically exhibit the adsorption at relatively low pressure (P/P₀ ~ 0.2) due to the micropore filling and the hysteresis loop at P/P₀ ~ 0.45 due to the capillary condensation in the mesopores. The step-down in the desorption branch associated with the hysteresis loop closure was observed in all nanosheet samples. The loop demonstrates the coexistence of H2 and H3 types, corresponding to the ink-bottle and slit-shaped mesoporous (or plate-like particle) characteristics, respectively. The pore size distribution data of all nanosheet samples exhibit both characteristics of the slit-shaped and inkbottle-type pores with 7–10 nm diameter resulted from the pore network effect (Fig. 3b–d, right). The contribution of the slit-

shaped and inkbottle pore types in the products depends on the synthesis conditions.

TEM images also confirm the multilayer stacking of nanosheets indicating the interstitial mesopores between sheets with slit shape (Fig. 4c). This result corresponds well with those slit shaped

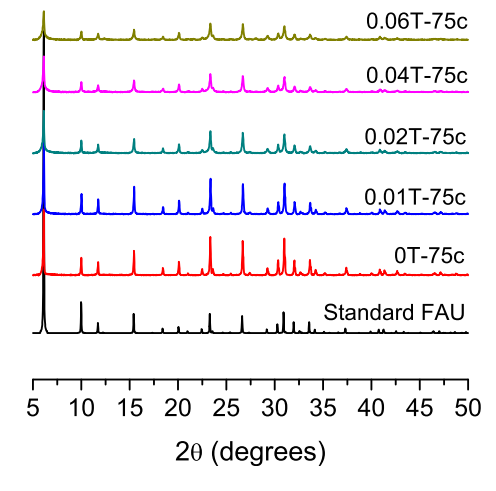


Fig. 2. XRD patterns of standard and synthesized FAU zeolites at the crystallization temperature of 75 $^{\circ}\text{C}.$

b Analyzed by XRD.

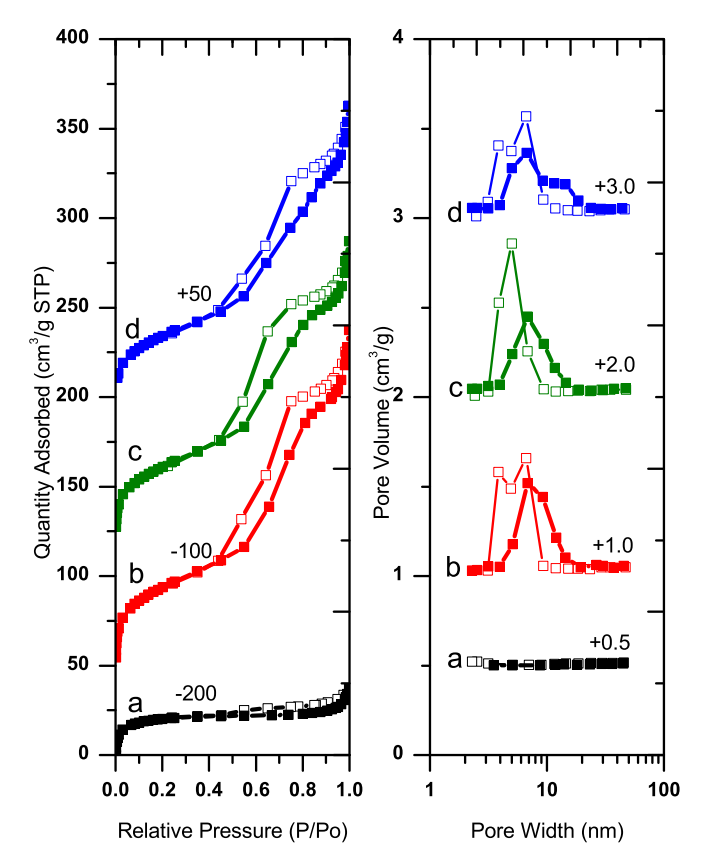


Fig. 3. N₂ adsorption-desorption isotherms (left) and BJH pore size distribution (right) data derived from the adsorption (solid symbol) and desorption branches (open symbol) of the FAU products with the a) conventional zeolite and b-d) nanosheet-assembled structures in which the dominant b) slit-shaped and c-d) inkbottle-type pores with different sizes of cavity and pore entrance are illustrated. The data are taken from a) 0T-75C, b) 0.01T-65C, c) 0.02T-65C, and d) 0.06T-75C samples.

Table 2Textural data^a of the FAU products prepared with and without the addition of TPOAC in the synthesis gel at various crystallization temperatures.

				•		
Sample	S _{BET}	S _{micro}	S _{ext}	V_{total}	V_{micro}	V _{meso}
0T-65C	810	777	34	0.35	0.30	0.05
0.01T-65C	734	560	174	0.50	0.22	0.28
0.02T-65C	606	441	165	0.43	0.17	0.26
0.04T-65C	566	407	160	0.43	0.16	0.27
0T-75C	865	819	46	0.36	0.32	0.04
0.01T-75C	698	571	127	0.41	0.22	0.19
0.02T-75C	645	497	148	0.43	0.20	0.23
0.04T-75C	665	504	161	0.46	0.20	0.26
0.06T-75C	699	540	159	0.46	0.21	0.25
0T-85C	870	842	28	0.35	0.33	0.02
0.01T-85C	789	736	52	0.33	0.29	0.04
0.02T-85C	819	759	60	0.36	0.30	0.06
0.04T-85C	769	681	88	0.38	0.27	0.11
0.06T-85C	787	686	101	0.42	0.27	0.15

^a S_{BET} (BET specific surface area); S_{micro} (micropore surface area) by t-plot method; S_{ext} (external surface area) by t-plot method; V_{total} (total pore volume); V_{micro} (micropore volume) by t-plot method, $V_{ext} = V_{total} - V_{micro}$; The surface areas and pore volumes are in units of m^2/g and cm^3/g , respectively.

mesopores observed with ~7 nm diameter by N_2 sorption isotherms. In addition, the presence of another kind of mesopores was also observed (bright spot in Fig. 4d) that could be ascribed to the filling of the surfactants and then transformed into meso-cavities after their removal. This result corresponds well with that reported in the literature (Inayat et al., 2012).

Among the samples crystallized at 65 °C, the average particle size slightly increases from 3.1 to 3.8 µm when the TPOAC amount is increased from 0.01 to 0.04 (see Table 1 and Fig. S4) whereas the thickness of the sheet assemblies and the crystallite sizes are slightly decreased. In addition, the increase of the TPOAC amount results in the change of textural properties in which significant decreases of the total surface area and micropore volume are observed, whereas the external surface area does not significantly alter. Apparently, the surface area derived from micropores significantly decreases from 560 to 407 m²/g, resulting in the significant decrease of the total surface area from 734 to 566 m²/g (Table 2).

In contrast to the conventional zeolite, the micropore volumes of nanosheet-assemblies decrease by 1.4 times, whereas their external surface areas increase by up to 5 times compared to those of the conventional one. Due to the fact that the crystallite size of FAU nanosheets is significantly smaller than that of the bulk one, it is not surprising that the microporosity of nanosheet assembled structures is decreased. However, the factor of an increase in external surface areas of the nanosheet zeolite is much higher than that of a decline in the microporous feature. Therefore, it is noteworthy that the introduction of the nanosheet structure can greatly improve the external surface area of the materials due to the additional mesopores/macropores, while the large amount of microporosity is still preserved.

The further increase of the TPOAC amount to 0.06 leads to the formation of amorphous materials, which can be clearly observed from SEM images by their sponge-like appearance (Fig. S4), and revealed by the absence of crystalline XRD peaks. The result shows that this amount is in excess, thus disrupting the zeolite crystallization. This may be explained by the adsorptive competition of the surfactant to the zeolite precursors, which are forming the crystalline framework (Li et al., 2013).

At the crystallization temperature of 75 °C, the nanosheet-assembled products are obtained by the addition of TPOAC in the range of 0.02–0.06, while the TPOAC amount of 0.01, the FAU zeolite with rough surface was observed (see Fig. S4). As the TPOAC amount is increased, the average particle size is increased, whereas the thickness of the sheet assemblies and the crystallite sizes are decreased (Table 1). With the further increase of the TPOAC amount to 0.04, the nanosheet structure still prevails, but the thickness of the sheet significantly decreases, resulting in the noticeable increase of the external surface area and the total pore volume (Table 2). With the TPOAC amount of 0.06, the average particle size of the products considerably increases from ~3.7 to ~5.0 μ m. However, this behavior does not have much influence on the textural properties. The further addition of the amount of TPOAC to 0.08 leads to the formation of amorphous materials.

To illustrate the benefits of the recyclable synthesis, the waste mother-liquid from the first batch synthesis was also used to synthesize hierarchical FAU zeolite nanosheet assemblies at the crystallization temperature of 75 °C in order to reuse the non-reacted species, such as Si, Al, and TPOAC surfactant remained in the mother liquid. The XRD pattern of zeolite product obtained by recycling the mother liquid reveals a significant presence of FAU crystalline phase as shown in Fig. S5a. However, the GIS crystalline structure (a competitive crystalline phase of FAU) also appears. The SEM image exhibits two different morphologies of crystals. Although the coexistence of nanosheet assemblies and large spherical crystal morphology of GIS zeolite was observed (Fig. S5b), the recyclable synthesis would be possible and it is considered as an eco-friendly synthetic strategy. However, this strategy needs to be further optimized including exact supplementary compensation of the consumed zeolite precursors and the corrected pH adjustment in order to get the hierarchical FAU zeolite nanosheet assemblies without the presence of GIS structure.

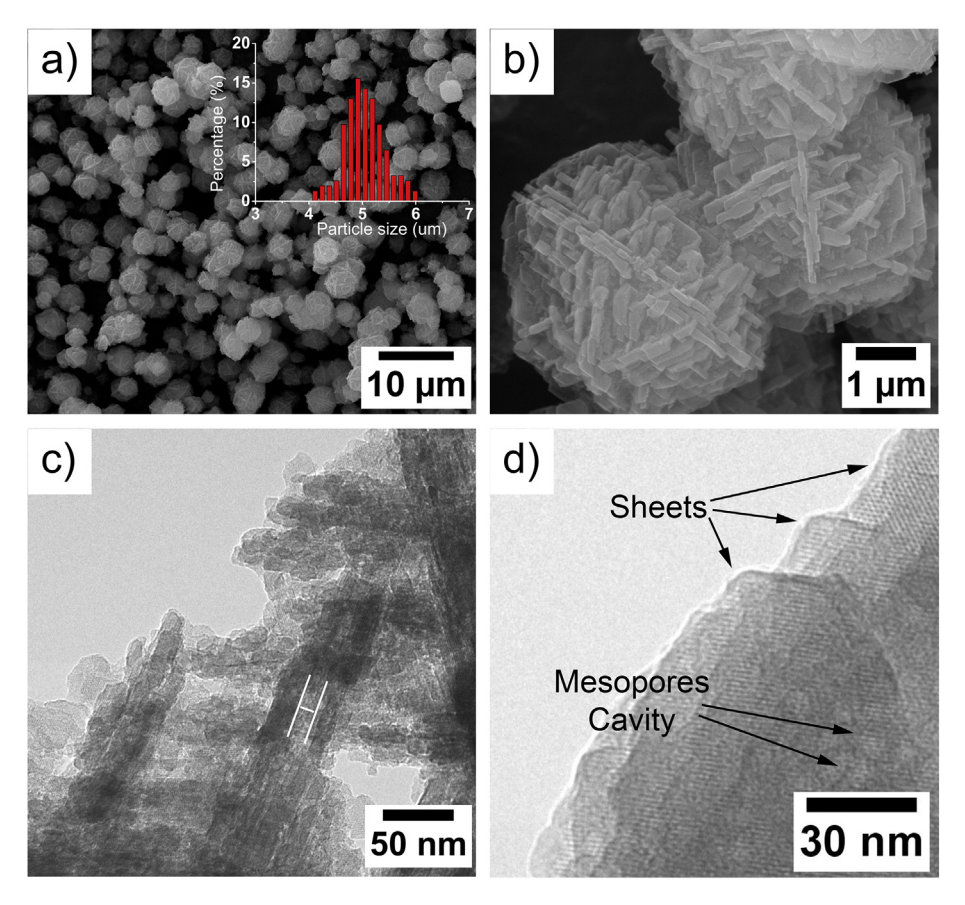


Fig. 4. SEM images with a) low and b) high magnifications and c-d) TEM images of the nanosheet-assembled FAU products. The images are taken from the 0.06T-75C samples.

For the samples crystallized at 85 °C, with the addition of TPOAC in the range of 0.01–0.02 only the formation of FAU products with normal conventional crystal appearance (octahedral shape) is obtained (see Table 1 and Fig. S4). It should be noted that such a small addition of TPOAC cannot bring about the formation of FAU nanosheets, unlike in the case of the lower temperatures (65 and 75 °C) in which the nanosheets start to be formed when the TPOAC amount is 0.01. This finding shows that at a relatively high crystallization temperature, a high amount of surfactant is required to tailor the nanosheet structure. The reason for this is suggested in two ways. Firstly, because at the higher temperature (85 °C) crystal growth occurs more rapidly compared with that at the lower temperatures and thus the formation of bulk zeolites tends to occur. Therefore, a larger amount of the surfactant is required for preventing the formation of bulk products, and yielding the nanosheet products. Secondly, the formation of the lamellar structure is less favorable when the temperature is increased (Li et al., 2013).

The further addition of TPOAC in the range of 0.04–0.06 successfully yields the FAU nanosheets (see Fig. S4). The increase of the TPOAC amount results in the increase of the average particle size of the products and the thickness of the sheets (see Table 1). These alterations signify the gradual structural change to the bulk crystals. The average thickness is increased by ~2 times compared with the case of 65 and 75 °C. The reason is due to the fact that the faster crystal growth-rate at high temperature influences the enlargement of the crystal size. Moreover, the increase of the average sheet thickness with the increase of the amount of TPOAC is only found in this case. This result corresponds to that in the case of the TPOAC amount being 0.08 in which bulk GIS is achieved instead of amorphous material. Therefore, it can be deduced that at the relatively

high crystallization temperature of 85 °C where the bulk materials tend to be crystallized, together with a high amount of TPOAC leads to the formation of another more stable zeolite framework.

All of the products in this study are prepared to a constant Si/Al ratio of ~1.24 (see Table S1). This value agrees well with the typical values reported for FAU type zeolite X (Si/Al ~ 1.0—1.5) (Inayat et al., 2012; Zhan et al., 2002). The results show that TPOAC is able to modulate the product characteristics while the Si/Al ratio of the products (~1.24) is independent (see Table S1). The ²⁷Al MAS NMR spectra of the products are typically composed of a strong peak at the chemical shift of ~65 ppm (see Fig. S6), corresponding to the tetrahedrally coordinated Al in the zeolite framework. A peak at the chemical shift of 0 ppm that corresponds to the extra-framework, octahedrally coordinated Al was not observed. The findings indicate that all Al atoms were completely incorporated into the framework.

The acidity of conventional and nanosheet zeolites was investigated by the NH₃-TPD. As a comparison, the TPD profiles of Naform and H-exchanged zeolites were shown in Fig. S7. The TPD profile of Na-form zeolite exhibits a major desorption peak at 230 °C with shoulder at 300 °C indicating the presence of weak Lewis acid site resulted from Na cations located at different sites in FAU zeolite (Song et al., 2012). The TPD profiles of exchanged conventional and nanosheet zeolites consist of two major desorption peaks, indicating the existence of two types of acid sites. The peak centered at 250 °C is attributed to the weak Lewis acid sites and the high-temperature desorption peaking at 450 °C corresponds to the strong Brønsted acid sites. The total amount of desorbed NH₃ molecules derived from integral areas of NH₃-TPD curves for conventional and nanosheet zeolites are 1.47 and 1.49 mmol/g, respectively. Such results clearly indicate that the acid

strength and acid density of both catalysts are comparable.

In summary, our simple optimization of the surfactant content in the synthesis gel and the crystallization temperature shows that hierarchical FAU nanosheet assemblies can be prepared at the low temperature of 65 °C with a low content of SDA of about 0.01. Moreover, such FAU nanosheets exhibit high external surface areas (174 m²/g) and high pore volumes (0.50 cm³/g) that might be the promising aspect for using them as catalysts in the catalytic reactions involving bulky molecules. Considering the preparation procedures of hierarchical nanosheets that are very simple as well as of relatively low temperature synthesis and low use of SDA, a huge saving on energy and cost of production would be great benefits to industry.

3.3. Catalytic activity

To evaluate the catalytic activity of hierarchical FAU nanosheets, the benzylation of toluene with benzyl chloride, which involves the bulky molecules as reactants and products (Scheme 1) was used as the model reaction. The main products of this reaction are three isomers of benzyltoluene (BTol), *o-*, *m-* and *p-*benzyltoluene and the by-products are dibenzyltoluene (dBtols) and tribenzyltoluene (tBtols). The conversion and product selectivity of the reaction over four catalysts prepared with various synthesis conditions (0T-75C, 0.01T-75C, 0.06T-75C and 0.01T-65C) owing to their different textural properties (ratio of micropore volume to mesopore volume) are summarized in Table 3.

In the early period of the reaction (<6 h), the conventional FAU zeolite (0T-75C with the highest $V_{\rm micro}/V_{\rm meso}$ ratio of 8.00) shows a very low catalytic activity with the conversion of only 8.78%. This is the result of excellent micropore characteristics (high BET specific surface area of up to 865 m²/g, mainly derived from the micropores, see Table 2). In contrast, the zeolite nanosheets in which the $V_{\rm micro}/V_{\rm meso}$ ratio are in range of 0.79–1.16, exhibit relatively higher catalytic activity under the same reaction conditions, even though they have relatively lower BET specific surface area (698–734 m²/

Scheme 1. Benzylation of toluene with benzyl chloride.

g). Because there is a higher mesoporous feature in nanosheet zeolite compared with the conventional zeolite while the acidic property is comparable as demonstrated by NH_3 -TPD. This makes it clear that the improvement in the catalytic activity of the zeolite nanosheets is due to the increase of mesoporosity, and consequently, the possible accessibility of molecules to the active sites is enhanced.

With the reaction time of 24 h, the percentage of conversion increases to 18.30% in the case of conventional FAU zeolite. However, when the reaction time is further prolonged to 30 h, the reaction conversion remains almost the same (18.83%). In strong contrast to this, the catalytic activities of the zeolite nanosheets are 3–4 times higher than that of the conventional zeolite. These findings strongly point out that zeolite nanosheets deliver superior catalytic activity over conventional one for the benzylation of toluene with benzyl chloride. Among the zeolite nanosheet samples, their catalytic activity depends on their mesoporosity, especially the 0.01T-65C sample (with lowest $V_{\rm micro}/V_{\rm meso}$ ratio of 0.79) has significantly higher catalytic activity compared with the other ones.

The product selectivity towards BTol of up to 90% for all FAU samples, irrespective of reaction time indicates that the FAU zeolite typically exhibits high selectivity to two benzylated products where *p*-BTol is more dominant than the others. The distribution of BTol isomers is similar in all samples with the ratio of *p*-to *o*-isomers of about 1.5, which is higher than our previous work on the FER nanosheets with the lack of shape selectivity (Wuamprakhon et al., 2016), in which the ratio of *p*-to *o*-isomers is close to 1 due to the small pore size of the FER framework that allows the reaction to take place only on the external surface area of FER zeolite. These results signify that the benzylation of toluene takes place on the acidic sites inside the pores of FAU zeolites resulting in the molecular shape selectivity to the *p*-isomer (Coq et al., 1993).

All of the results indicate that FAU zeolite nanosheets can greatly enhance the catalytic activities of benzylation of toluene with benzyl chloride compared to conventional FAU zeolite, while the selectivity of the product due to the shape selectivity of the zeolite framework can be preserved. This would be a benefit of using such zeolite nanosheets in the clean synthesis of fine chemicals that allows the reduction of undesirable products. Compared to conventional catalysts such as HF and H₂SO₄, a greener process through reducing wastes and avoiding the use of toxic chemicals can be achieved by using the zeolite nanosheet catalysts. From this view, this well-designed catalyst has great potential to be used in clean technologies in the fine chemical industry. In this way, the

 Table 3

 Catalytic performances of the conventional and nanosheet FAU zeolite samples with different mesopore contents for the benzylation of toluene with benzylchloride.

Catalyst	Ratio of V_{micro}/V_{meso}	Time (h)	%Conversion ^a (%)	%Selectivity ^b (%)				
				BTol	Isomer			
					m-	0-	p-	
0T-75C	8.00	6	8.78	90.55	6.72	34.62	49.20	
		24	18.30	94.64	6.89	35.25	52.51	
		30	18.83	95.01	6.90	35.42	52.68	
0.01T-75C	1.16	6	13.34	95.35	6.97	36.21	52.17	
		24	32.45	95.93	6.63	35.19	54.11	
		30	36.53	95.81	6.60	35.07	54.15	
0.06T-75C	0.84	6	19.90	93.93	6.73	35.83	54.37	
		24	57.51	93.57	6.16	33.89	53.52	
		30	68.36	92.25	6.04	33.24	52.97	
0.01T-65C	0.79	6	26.74	95.81	6.47	35.34	54.00	
		24	71.32	92.57	5.97	33.57	53.03	
		30	75.08	92.25	5.94	33.43	52.88	

 $^{^{\}rm a}$ %Conversion = (wt% of consumed benzylchloride/wt% of initial benzylchloride) \times 100 (%).

 $^{^{\}rm b}$ %Selectivity = (wt% of desired product/wt %of total products) \times 100 (%).

advantages in terms of economic and environmental points of view are accomplished.

4. Conclusions

The nanosheet-assembled FAU zeolites with the tunable textural properties were successfully prepared by using an organosilane surfactant, TPOAC, as a structure directing agent. The morphologies and textural properties of the products are tailored by controlling the synthesis parameters, including the surfactant content in the synthesis gel and the crystallization temperature. The particle size, the thickness of the sheet assemblies, the crystallite size and the textural properties of the nanosheet products are varied depending on both synthesis parameters. Moreover, a greener synthesis would be possible by recycling the waste motherliquid, which effectively reduces environmental pollution.

The catalytic study reveals that the nanosheet nature brings not only the relatively higher conversion for the benzylation of toluene with benzylchloride compared with the conventional FAU, but also preserved the product selectivity due to the shape-selective zeolite framework. All FAU samples exhibit high selectivity to BTol isomers in which the *p*-BTol is the most predominant. This first example demonstrates that FAU nanosheets have been successfully prepared and simply controlled by adjustments of the SDA content and crystallization temperature as well as it opens up interesting perspectives for the design of new industrial catalysts for potential catalytic reactions. This also demonstrates the next step forward in the development of an industrial catalyst based on the concept of cleaner production.

Acknowledgment

This work was supported in part by grants from the National Science and Technology Development Agency (NANOTEC Center of Excellence funded by the National Nanotechnology Center), the Development and Promotion of Science and Technology Talents Project (DPST) and the Thailand Research Fund (TRF) (MRG5980114). The Research Fellowship from Vidyasirimedhi Institute of Science and Technology are also acknowledged.

Appendix A. Supplementary data

Supplementary data related to this article can be found at http://dx.doi.org/10.1016/j.jclepro.2016.08.001.

- Chaves, T.F., Pastore, H.O., Cardoso, D., 2012. A simple synthesis procedure to prepare nanosized faujasite crystals. Microporous Mesoporous Mater. 161, 67–75.
- Choi, M., Na, K., Kim, J., Sakamoto, Y., Terasaki, O., Ryoo, R., 2009. Stable single-unitcell nanosheets of zeolite MFI as active and long-lived catalysts. Nature 461, 246–249.
- Coq, B., Gourves, V., Figuéras, F., 1993. Benzylation of toluene by benzyl chloride over protonic zeolites. Appl. Catal. A 100, 69–75.
- Davis, R.J., 2003. New perspectives on basic zeolites as catalysts and catalyst supports. J. Catal. 216, 396–405.
- Díaz López, F.J., Montalvo, C., 2015. A comprehensive review of the evolving and cumulative nature of eco-innovation in the chemical industry. J. Clean. Prod. 102. 30–43.
- Egeblad, K., Christensen, C.H., Kustova, M., Christensen, C.H., 2007. Templating mesoporous zeolites†. Chem. Mater. 20, 946–960.
- Garcia-Martinez, J., Li, K., Krishnaiah, G., 2012. A mesostructured Y zeolite as a superior FCC catalyst from lab to refinery. Chem. Commun. 48, 11841–11843. Glavič, P., Lukman, R., 2007. Review of sustainability terms and their definitions.
- J. Clean. Prod. 15, 1875–1885. Inayat, A., Knoke, I., Spiecker, E., Schwieger, W., 2012. Assemblies of mesoporous FAU-type zeolite nanosheets. Angew. Chem. Int. Ed. 51, 1962–1965.
- Jegatheesan, V., Liow, J.L., Shu, L., Kim, S.H., Visvanathan, C., 2009. The need for global coordination in sustainable development. J. Clean. Prod. 17, 637–643.
- Khaleel, M., Wagner, A.J., Mkhoyan, K.A., Tsapatsis, M., 2014. On the rotational intergrowth of hierarchical FAU/EMT zeolites. Angew. Chem. Int. Ed. 53, 9456–9461.
- Li, H., Wu, H., Shi, J.-l, 2013. Competition balance between mesoporous self-assembly and crystallization of zeolite: a key to the formation of mesoporous zeolite. J. Alloys Compd. 556, 71–78.
- Li, Q., Creaser, D., Sterte, J., 2002. An investigation of the nucleation/crystallization kinetics of nanosized colloidal faujasite zeolites. Chem. Mater. 14, 1319–1324.
- Luz Martínez, S., Romero, R., López, J.C., Romero, A., Sánchez Mendieta, V.c., Natividad, R., 2010. Preparation and characterization of CaO nanoparticles/NaX zeolite catalysts for the transesterification of sunflower oil. Ind. Eng. Chem. Res. 50, 2665–2670.
- Na, K., Choi, M., Ryoo, R., 2013. Recent advances in the synthesis of hierarchically nanoporous zeolites. Microporous Mesoporous Mater. 166, 3–19.
- Song, L., Li, Z., Zhang, R., Zhao, L., Li, W., 2012. Alkylation of toluene with methanol: the effect of K exchange degree on the direction to ring or side-chain alkylation. Catal. Commun. 19, 90—95.
- Storck, S., Bretinger, H., Maier, W.F., 1998. Characterization of micro- and mesoporous solids by physisorption methods and pore-size analysis. Appl. Catal. A 174. 137–146.
- Tosheva, L., Valtchev, V.P., 2005. Nanozeolites: synthesis, crystallization mechanism, and applications. Chem. Mater. 17, 2494–2513.
- Wuamprakhon, P., Wattanakit, C., Warakulwit, C., Yutthalekha, T., Wannapakdee, W., Ittisanronnachai, S., Limtrakul, J., 2016. Direct synthesis of hierarchical ferrierite nanosheet assemblies via an organosilane template approach and determination of their catalytic activity. Microporous Mesoporous Mater. 219, 1–9.
- Zeng, S.X., Meng, X.H., Yin, H.T., Tam, C.M., Sun, L., 2010. Impact of cleaner production on business performance. J. Clean. Prod. 18, 975–983.
- Zhan, B.-Z., White, M.A., Lumsden, M., Mueller-Neuhaus, J., Robertson, K.N., Cameron, T.S., Gharghouri, M., 2002. Control of particle size and surface properties of crystals of NaX zeolite. Chem. Mater. 14, 3636–3642.



Catalytic conversion of bioethanol to light olefins over hierarchical zeolites catalysts

Sirawit Shetsiri¹, Wannaruedee Wannapakdee¹, Saros Salakhum¹, and Chularat Wattanakit^{1*}

¹Department of Chemical and Biomolecular Engineering, School of Energy Science and Engineering, Vidyasirimedhi Institute of Science and Technology, Rayong 21210, Thailand.

*e-mail: chularat.w@vistec.ac.th

Abstract: The conversion of bioethanol to light olefins is one of the most promising reactions in green catalytic processes. Here we report the application of novel designed hierarchical zeolites in the light olefin production from bioethanol. The hierarchical zeolites have been successfully prepared by a one-pot hydrothermal synthesis. The designed hierarchical zeolites exhibit the superior physicochemical properties with an increase of mesoporosity (~30 %) compared with a commercial one. To illustrate the beneficial effect of hierarchical structures on the catalytic performance of bioethanol conversion, the catalytic study was carried out using a fixed-bed reactor at 300-500 °C under an atmospheric pressure. Interestingly, the hierarchical zeolite exhibits the outstanding catalytic activity with the high yield of light olefins approximately by 90%. In addition, the catalyst lifetime of hierarchical zeolite can be significantly improved, whereas the rapid catalyst deactivation of a conventional catalyst is observed after 10 hours of time-on-stream (TOS). This example opens up interesting perspectives for the application of hierarchical zeolites in the transformation of substrates-derived from biomass to high value-added chemicals via a green chemistry approach.

1. Introduction

Light olefins (e.g. ethylene, propylene, and butylene) are important intermediates substantial produce derivative compounds such as polyethylene and polypolylene. One of the most popular processes to produce light olefins, in particular ethylene, is based on the naphtha thermal cracking process. However, it often suffers from many disadvantages such as high operating cost and energy consumption because it operates at very high temperature (700-850°C).² Moreover, a non-environmentally friendly process is a concerning issue due to the release of toxic gases.3

An alternative way to produce light olefins is the catalytic conversion of bioethanol to light olefins, which is considered as a greener process because biomass renewable resources are

transformed into high value-added products at much lower energy consumption.⁴

Although this reaction can be catalyzed by various solid-acid catalysts, the most popular one is based on using zeolites as catalysts.⁴ They aluminosilicate are compounds with three-dimensional regular framework and microporous structures.⁵ Among them, the HZSM-5 having the MFI zeolitic framework has been widely used in many potential catalytic applications due to its unique acid-base properties and high mechanical-thermal stability.⁶ However, the conventional HZSM-5 catalyst suffers from many drawbacks, in particular, a short catalyst lifetime due to the pore blockage of cokes.⁷ The hierarchical HZSM-5 catalyst is one of the most interesting developed catalysts to improve the catalytic stability of many reactions⁸.

There are many synthesis approaches that can be used to create the hierarchical



structure, in particular, the synthesis of hierarchical zeolites via a soft template approach using a one-pot hydrothermal process in the presence of self-assembly of organosilane template as a hierarchical porogen. 9-11

In the present study, we synthesize the hierarchical HZSM-5 via a one-pot hydrothermal process by a soft-template approach to improve physicochemical properties of catalysts. In addition, catalytic performances of the bioethanol conversion to light olefins over synthesized hierarchical zeolites are compared with that of the conventional HZSM-5 having similar acidity.

2. Materials and Methods2.1 Catalyst Preparation

conventional ZSM-5 and hierarchical ZSM-5 were synthesized by a hydrothermal method. The one-pot conventional zeolite was crystallized at 180 °C for 72 hours using the mixture of 3.50 g 0.014 TEOS. g of aluminum isopropoxide and 2.02 g of TPAOH. Finally, the solid products were calcined at 650 °C for 8 hours.

As for the synthesis of hierarchical ZSM-5, the above-procedure was modified by using a soft template approach.¹² Finally, HZSM-5 samples were prepared via a conventional ion-exchange by using 0.1 M of NH₄Cl solution and subsequently calcined at 650 °C for 6 hours.

2.2 Catalyst Characterization

The physical and chemical properties of the prepared catalysts were investigated by various characterization techniques. For instance, powder X-ray diffraction (XRD) patterns were used to identify crystalline phases. Chemical compositions were analyzed by Wavelength-Dispersive X-ray Fluorescence Spectrometer (WDXRF). Physisorption measurements were used to

analyze specific surface area micropore surface area/pore volume, and mesopore size distribution, which are calculated by the Brunauer-Emmett-Teller (BET) method, t-plot method and Barrett-Joyner-Halenda (BJH) model, respectively. Chemisorption analysis via NH₃-TPD technique was used to investigate aciditybasicity properties of the catalysts and the morphology of the synthesized samples was investigated by scanning electron (SEM) and transmission microscopy electron microscopy (TEM) technique.

2.2 Catalytic testing of bioethanol conversion

To investigate the beneficial effect of catalysts, the ethanol conversion was performed using a down-flow fixed-bed reactor. Prior to the catalytic study, the prepared catalysts were activated under N₂ stream at 50 ml/min for 2 hours at 500 °C. After that, the reactor temperature was cooled down to the reaction temperature (300-500 °C) under an atmospheric with pressure the N_2 carrier gas. Subsequently, the ethanol feed introduced into the reactor with the weight hourly space velocities (WHSV) of 23.3 h⁻¹. The products were detected by an online gas chromatograph (GC) (Agilent 7820A) equipped with a FID detector and a PoraBOND Q Capillary GC Columns (10 m 0.25 mm) at an interval time of 1 h

3. Results & Discussion3.1 Characterization of hierarchical HZSM-5 catalysts

Fig.1 reveals XRD patterns of the synthesized samples (CON-HZSM-5 (A) and Hie-HZSM-5 (B) representing the conventional zeolite and hierarchical HZSM-5, respectively). It clearly shows that the synthesized samples compose of highly crystalline MFI framework without



the contamination of any other crystalline phases.

The morphology and structure of the synthesized catalysts are obtained as shown in Fig. 2. Interestingly, the different morphologies of the conventional zeolite and hierarchical HZSM-5 can be observed. For example, the conventional HZSM-5 exhibits cubic-shaped crystalline structures, while the shape of hierarchical HZSM-5 is spherical crystals with self-assemblies of nanolayers. The regular stack of layered assembly generates secondary porous structures in the zeolite crystals. ¹⁰

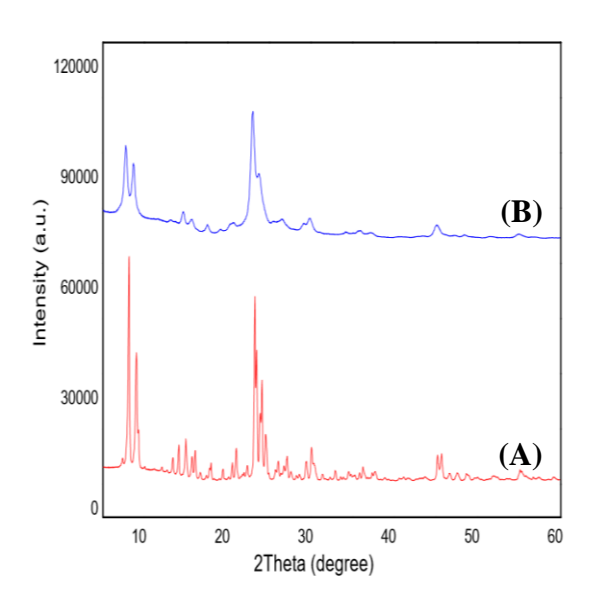


Figure 1. XRD patterns of the synthesized samples (A) CON-HZSM-5 and (B) Hie-HZSM-5.

The textural properties of the synthesized catalysts were investigated by N_2 physisorption technique. According to the adsorption-desorption isotherm for the conventional HZSM-5 sample, it exhibited the type I isotherm due to a micopore filling (Fig. 3). In strong contrast to this, the hierarchical HZSM-5 sample displayed the presence of hysteresis loop at a high relative pressure due to a capillary condensation effect into mesopores and macropores.

The table 1 demonstrates summarized physical and textural properties of the synthesized catalysts. The results indicate that the hierarchical structure can greatly enhance the external surface area

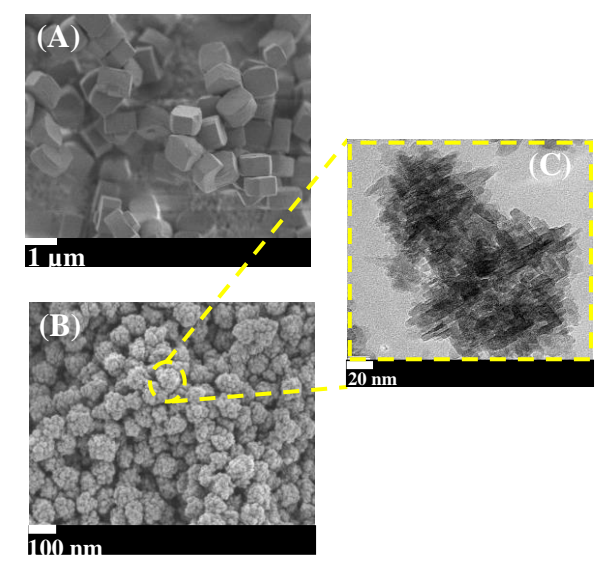


Figure 2. SEM images of (A) CON-HZSM-5 and (B) Hie-HZSM-5 and (C) TEM image of Hie-HZSM-5.

and total pore volume due to the assemblies of nanolayers and interparticle voids, which are also confirmed the presence of mesopores in the range of 26 – 30 nm obtained from BJH method (Fig. 4).

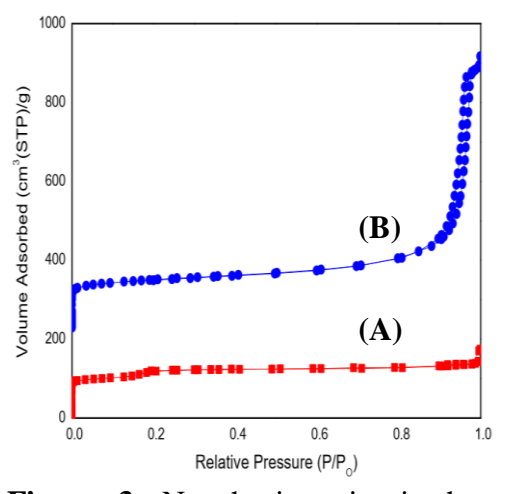


Figure 3. N₂ physisorption-isotherms of (A) CON-HZSM-5 and (B) Hie-HZSM-5.



Table 1. Physical and textural properties of the synthesized catalysts obtained from N_2 adsorption measurement.

Samples	Si/Ala	S_{BET}^{b}	$S_{\text{micro}}^{}c}$	S_{ext}^{d}	V_{total}^{e}	$V_{\text{micro}}{}^{\mathrm{f}}$	$V_{\text{ext}}^{\text{g}}$	$S_{\text{ext}}\!/\!S_{\text{BET}}{}^{h}$
CON-HZSM-5	38	408	385	23	0.22	0.18	0.04	0.06
Hie- HZSM-5	37	448	287	161	1.02	0.12	0.90	0.36

^aSi/Al obtained by WXRF. ^bBET specific surface area (m²/g). ^cmicropore surface area (m²/g). ^dexternal surface area (m²/g). ^e total pore volume obtained at P/P_O=0.99 (cm³/g). ^fmicropore volume (cm³/g). ^gexternal pore volume (cm³/g). ^hexternal surface area proportion.

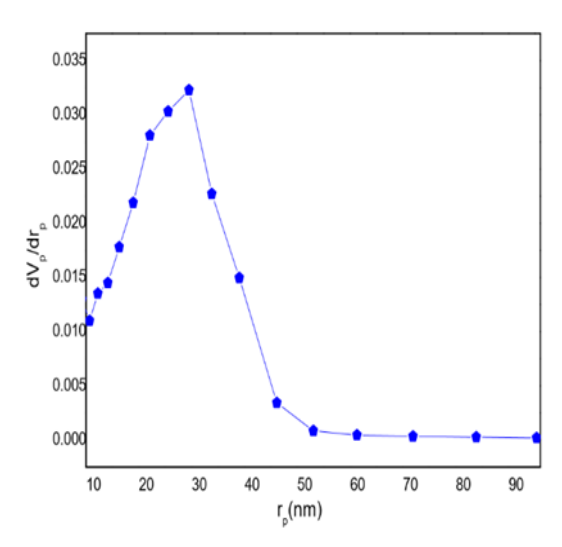


Figure 4. BJH pore size distribution of Hie-HZSM-5 sample.

The acidic properties of the synthesized catalysts were analyzed via chemisorption technique with NH₃-TPD method as shown in Fig. 5. It was found that both samples compose of weak acid sites and strong acid sites for which the peak at 220 and 450 °C can be observed, respectively. It was also mentioned that the amount of the acid density of both samples is comparable (~0.20 mmol/g obtained by the deconvolution technique).

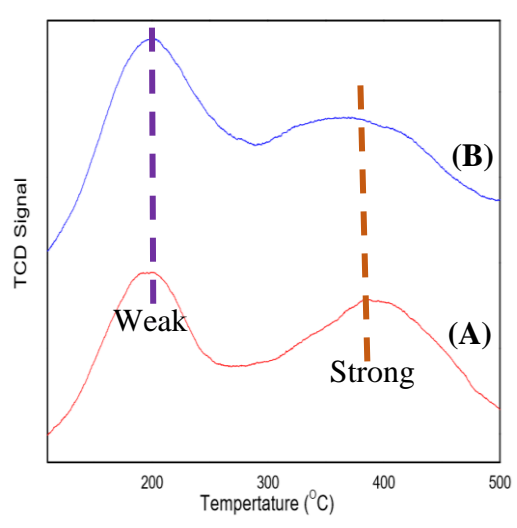


Figure 5. NH₃-TPD profiles of (A) CON-HZSM-5and (B) Hie-HZSM-5.

3.2 Catalytic activity in the bioethanol dehydration process

To illustrate the benefits of hierarchical structures of HZSM-5, the catalytic conversion of bioethanol to light olefins as a function of time-on stream (TOS) was studied as shown in Fig.6. Compared with the conventional HZSM-5 having similar acidic property, the hierarchical HZSM-5 can greatly improve the catalytic activity of the ethanol conversion. Interestingly, the catalyst lifetime of hierarchical zeolite was also improved as shown that the catalytic stability is still very high even after 15 hours of TOS, whereas the rapid deactivation of a conventional zeolite was observed after 4 hours of TOS. This makes it clear that the hierarchical samples can



prevent the catalyst deactivation due to the reduction of diffusion path length, resulting in a decrease of coke formation into the microporous structures. ¹³⁻¹⁵

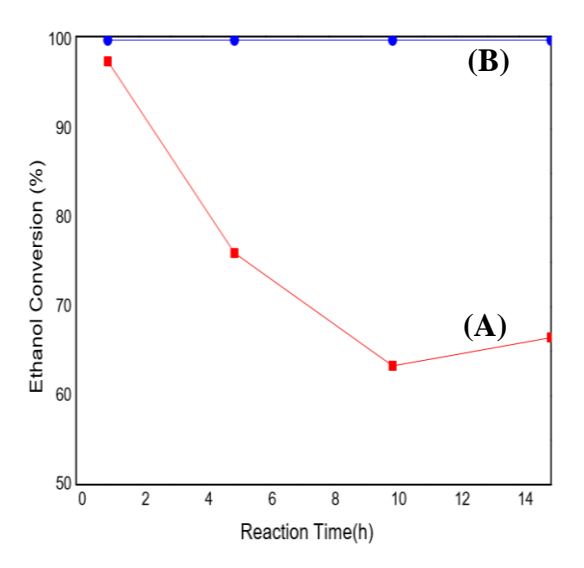


Figure 6. Ethanol conversion over (A) CON-HZSM-5 and (B) Hie-HZSM-5 catalysts having a similar Si/Al ratio obtained under the same reaction condition: 300 °C, 1 atm, 23.30 h⁻¹ and 15 hours of TOS.

Not only the catalytic activity but also the light olefin yield over the hierarchical HZSM-5 increases compared with the conventional HZSM-5 as shown in Fig. 7. In particular, the yield of ethylene over the hierarchical HZSM-5 is almost 90%. However, the yield of diethyl-ether (DEE) slightly decreases over the hierarchical sample.

4. Conclusion

Compared with the conventional zeolite, the physicochemical properties of hierarchical HZSM-5 catalyst obtained by a one-pot hydrothermal synthesis using a soft template approach can be greatly improved. This modified catalyst, as expected, leads to increase the

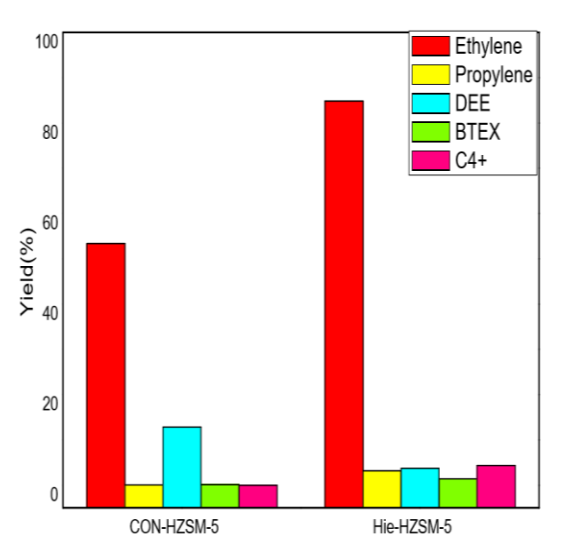


Figure 7. Yield of desired products obtained over the conventional HZSM-5 (CON-HZSM-5) and the hierarchical HZSM-5 (Hie-HZSM-5) having the similar Si/Al ratio obtained under the same reaction conditions: 300 °C, 1 atm, and 23.30 h⁻¹ and 15 hours of TOS.

catalytic activity and the catalyst lifetime of the ethanol dehydration to ethylene.

Furthermore, the yield of light olefins, especially, ethylene can be dramatically enhanced (85 % and 55% for the hierarchical zeolite and the conventional one, respectively). This example opens up interesting perspectives for the application of hierarchical zeolites in the transformation of substrates-derived from biomass to high value-added chemicals.

Acknowledgements

This work was supported by Vidyasirimedhi Institute of Science and Technology (VISTEC), the Thailand Research Fund (TRF) (MRG5980114), the NANOTEC Center of Excellence on Nanoscale Materials Design for Green Nanotechnology at Kasetsart University, and Frontier Research Center (FRCs) at VISTEC.



- 1. Nicholas, C. P.; Laipert, L.; Prabhakar, S., Oligomerization of Light Olefins to Gasoline: An Advanced NMR Characterization of Liquid Products. *Industrial & Engineering Chemistry Research* **2016**, *55* (34), 9140-9146.
- 2. Joo, E.; Park, S.; Lee, M., Pyrolysis Reaction Mechanism for Industrial Naphtha Cracking Furnaces. *Industrial & Engineering Chemistry Research* **2001**, *40* (11), 2409-2415.
- 3. Meng, X.; Xu, C.; Li, L.; Gao, J., Cracking Performance and Feed Characterization Study of Catalytic Pyrolysis for Light Olefin Production. *Energy & Fuels* **2011**, *25* (4), 1357-1363.
- 4. Zhang, M.; Yu, Y., Dehydration of Ethanol to Ethylene. *Industrial & Engineering Chemistry Research* **2013**, *52* (28), 9505-9514.
- 5. Migues, A. N.; Muskat, A.; Auerbach, S. M.; Sherman, W.; Vaitheeswaran, S., On the Rational Design of Zeolite Clusters. *ACS Catalysis* **2015**, *5* (5), 2859-2865.
- 6. Kordatos, K.; Gavela, S.; Ntziouni, A.; Pistiolas, K. N.; Kyritsi, A.; Kasselouri-Rigopoulou, V., Synthesis of highly siliceous ZSM-5 zeolite using silica from rice husk ash. *Microporous and Mesoporous Materials* **2008**, *115* (1–2), 189-196.
- 7. Inaba, M.; Murata, K.; Saito, M.; Takahara, I., Ethanol conversion to aromatic hydrocarbons over several zeolite catalysts *Reaction Kinetics and Catalysis Letters* **2006**, 88 (1), 135-141.
- 8. Ramasamy, K. K.; Zhang, H.; Sun, J.; Wang, Y., Conversion of ethanol to hydrocarbons on hierarchical HZSM-5 zeolites. *Catalysis Today* **2014**, *238*, 103-110.
- 9. Na, K.; Choi, M.; Park, W.; Sakamoto, Y.; Terasaki, O.; Ryoo, R.,

- Pillared MFI Zeolite Nanosheets of a Single-Unit-Cell Thickness. *Journal of the American Chemical Society* **2010**, *132* (12), 4169-4177.
- 10. Wannapakdee, W.; Wattanakit, C.; Paluka, V.; Yutthalekha, T.; Limtrakul, J., One-pot synthesis of novel hierarchical bifunctional Ga/HZSM-5 nanosheets for propane aromatization. *RSC Advances* **2016**, *6* (4), 2875-2881.
- 11. Emdadi, L.; Wu, Y.; Zhu, G.; Chang, C.-C.; Fan, W.; Pham, T.; Lobo, R. F.; Liu, D., Dual Template Synthesis of Meso- and Microporous MFI Zeolite Nanosheet Assemblies with Tailored Activity in Catalytic Reactions. *Chemistry of Materials* **2014**, *26* (3), 1345-1355.
- 12. Zhang, X.; Liu, D.; Xu, D.; Asahina, S.; Cychosz, K. A.; Agrawal, K. V.; Al Wahedi, Y.; Bhan, A.; Al Hashimi, S.; Terasaki, O.; Thommes, M.; Tsapatsis, M., Synthesis of Self-Pillared Zeolite Nanosheets by Repetitive Branching. *Science* **2012**, *336* (6089), 1684-1687.
- 13. Phung, T. K.; Radikapratama, R.; Garbarino, G.; Lagazzo, A.; Riani, P.; Busca, G., Tuning of product selectivity in the conversion of ethanol to hydrocarbons over H-ZSM-5 based zeolite catalysts. *Fuel Processing Technology* **2015**, *137*, 290-297.
- 14. Tarach, K. A.; Tekla, J.; Makowski, W.; Filek, U.; Mlekodaj, K.; Girman, V.; Choi, M.; Gora-Marek, K., Catalytic dehydration of ethanol over hierarchical ZSM-5 zeolites: studies of their acidity and porosity properties. *Catalysis Science & Technology* **2016**, 6 (10), 3568-3584.
- 15. Xin, H.; Li, X.; Fang, Y.; Yi, X.; Hu, W.; Chu, Y.; Zhang, F.; Zheng, A.; Zhang, H.; Li, X., Catalytic dehydration of ethanol over post-treated ZSM-5 zeolites. *Journal of Catalysis* **2014**, *312*, 204-215.

Synthesis and applications of various hierarchical zeolite nanosheets for potential petrochemical reactions

<u>Chularat Wattanakit</u>, ^{a,*} Wannaruedee Wannapakdee, ^a Thittaya Yutthalekha, ^a Phatsawit Wuamprakhon, ^b Kamonlatth Rodponthukwaji, ^b Jumras Limtrakul^c

^aSchool of Energy Science and Engineering, Vidyasirimedhi Institute of Science and Technology, Rayong, 21210, Thailand ^bDepartment of Chemistry and NANOTEC Center for Nanoscale Materials Design for Green Nanotechnology, Kasetsart University, Bangkok, 10900, Thailand

^cSchool of Molecular Science and Engineering, Vidyasirimedhi Institution of Science and Technology, Rayong, 21210, Thailand *Corresponding author: chularat.w@vistec.ac.th

ABSTRACT

The development of hierarchical zeolites is a major scientific and industrial challenge due to their outstanding properties, such as high surface area, high thermal/chemical stability, high acidity, and appropriate shape selectivity so that they have been applied for a large number of potential applications¹⁻⁴. Here we report the fabrication of various hierarchical zeolite nanosheets (e.g., FER, Ga-HZSM5, FAU, Pt/Silicalite-1 etc.) obtained by a one-pot hydrothermal process^{1,3}. The obtained zeolites exhibit not only a different morphology, but also a higher hierarchy factor (HF) compared with that obtained in the case of conventional zeolites. This results in an improvement of the catalytic performances in terms of activities, product selectivity, and catalyst stability for various potential petrochemical catalytic applications, such as alkylation, aromatization and dehydrogenation of propane. For example, significantly improved catalytic activity of benzylation of toluene with benzyl chloride was observed over the FER nanosheet (82% and 14% conversion efficiency in the cases of the FER nanosheet and the conventional FER, respectively)³. In addition to a monofunctional zeolite, the galloaluminosilicate nanosheets also exhibit outstanding catalytic properties, in terms of activity (60 and 20% for propane conversion over the hierarchical Ga/HZSM-5 and the conventional zeolite, respectively), BTX selectivity (almost three times higher compared with conventional zeolite), and significant reduction of deposited coke for conversion of propane². These are complementary to the nanolayered-materials design on various types of zeolite structures and open up the development of heterogeneous catalysts for various petrochemical reactions.



Figure 1. Propane aromatization over hierarchical bifunctional zeolite nanosheets as an example application.

- 1) T. Yutthalekha, C. Wattanakit, C. Warakulwit, W. Wannapakdee, K. Rodponthukwaji, T. Witoon, J. Limtrakul*, *J. Clean Prod.* **2016**, doi: 10.1016/j.jclepro.2016.08.001.
- 2) W. Wannapakdee, C. Wattanakit*, V. Paluka, T. Yutthalekha, J. Limtrakul, RSC Adv. 2016, 6, 2875-2881.
- 3) P. Wuamprakhon, C. Wattanakit, C. Warakulwit, T. Yutthalekha, W. Wannapakdee, S. Ittisanronnachai, J. Limtrakul*, Micropor. Mas. 2016, 219, 1-9.

4) C. Wattanakit, C. Warakulwit, P. Pantu, B. Sunpetch, M. Charoenpanich, J. Limtrakul*, Can. J. Chem. Eng. 2012, 90 (4), 873-880.

FAU-type zeolite nanosheets as superior basic catalysts for aldol condensation

Thittaya Yutthalekha, a Saros Salakhum, Jumras Limtrakul, Chularat Wattanakita,*

^aSchool of Energy Science and Engineering, Vidyasirimedhi Institute of Science and Technology, Rayong, 21210, Thailand ^bSchool of Molecular Science and Engineering, Vidyasirimedhi Institute of Science and Technology, Rayong, 21210, Thailand *Corresponding author: chularat.w@vistec.ac.th

ABSTRACT

Hierarchical zeolite nanosheets have emerged as an effective technology in the field of industrial applications owing to their improved diffusion efficiency. Many types of hierarchical zeolite nanosheets (e.g., FER, MFI, MOR, FAU, etc.) have been successfully prepared and exhibit outstanding performances in various catalytic applications.^{1,2} However, the opening perspectives of catalytic reactions over FAU-type zeolite nanosheets have been rarely reported.¹ Herein, we present a potential application of hierarchical FAU-type zeolite nanosheets featuring basic sites in Aldol condensation which is one of the most important steps for the upgrading of biomass to biofuel. The FAU-type zeolite nanosheets were synthesized via an amphiphilic organosilane as a structure-directing agent (SDA) and transformed as a basic catalyst by ionexchange with alkaline earth metals. The structural and physicochemical properties were extensively characterized by means of XRD, SEM-EDS, TEM, N2-sorption and CO2-TPD. To illustrate the beneficial effect of the hierarchical structure, the aldol condensation of various aldehydes, including the selfcondensation of acetaldehyde and the aldol condensation of 5-(Hydroxymethyl)furfural (5-HMF) with acetone was tested over alkaline-earth exchanged FAU nanosheets. It was found that the catalytic activity in the self-condensation of acetaldehyde over FAU nanosheets and their corresponding conventional zeolite is comparable. Interestingly, FAU nanosheets exhibit superior performances over the conventional one in the condensation of 5-HMF with acetone. These results signified that the hierarchical structure overcomes the diffusion limitation resulting from the large molecular size of aldehyde reactants. In addition, the reusability experiment also exhibited that zeolite nanosheets are able to restore their activity even after several reaction cycles.

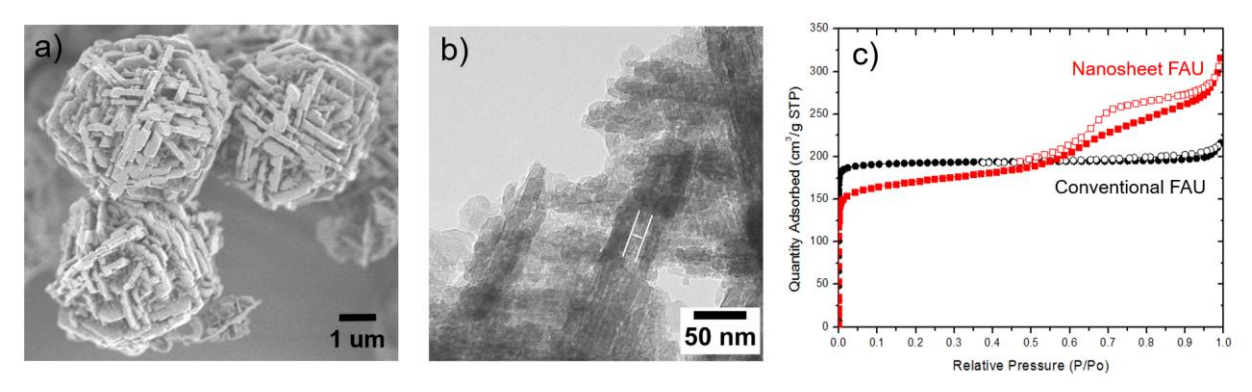


Figure 1. Characterizations of hierarchical FAU-type zeolite nanosheets: a) SEM, b) TEM and c) N₂ sorption

- 1) T. Yutthalekha, C. Wattanakit, C. Warakulwit, W. Wannapakdee, K. Rodponthukwaji, T. Witoon, J. Limtrakul, *J. Clean. Prod.* **2016**, doi: 10.1016/j.jclepro.2016.08.001.
- 2) W. Wannapakdee, C. Wattanakit*, V. Paluka, T. Yutthalekha, J. Limtrakul, RSC Adv. 2016, 6, 2875-2881.

Novel Design of Hierarchical Zeolite Nanosheets Using Renewable Resources

Saros Salakhum, Thittaya Yutthalekha, Jumras Limtrakul, Chularat Wattanakita,*

^aSchool of Energy Science and Engineering, Vidyasirimedhi Institute of Science and Technology, Rayong, 21210, Thailand ^bSchool of Molecular Science and Engineering, Vidyasirimedhi Institute of Science and Technology, Rayong, 21210, Thailand *Corresponding author: chularat.w@vistec.ac.th

ABSTRACT

The design of hierarchical zeolites is of crucial importance because of their advantages such as, high external surface area, high thermal stability, and excellent catalytic performance. Unfortunately, they are often obtained by the high cost of synthesis method. In order to overcome such a problem, the zeolite has been successfully prepared using a silica raw material derived from available renewable resources such as fly ash and rice husk.^{1,2} However, the synthesis of hierarchical zeolite nanosheets using renewable resources has not been demonstrated so far.³ Herein, we demonstrate the novel design of the hierarchical faujasite (FAU) nanosheets using a silica source obtained from a corn cob ash (CCA). An extracted silica with very high purity (>99.5 %) has been prepared from a corn cob ash by the sol-gel method.⁴ Subsequently, the hierarchical faujasite nanosheets have been synthesized via a hydrothermal synthesis using an organosilane, dimethyloctadecyl [3- (trimethoxysilyl) propyl] ammonium chloride (TPOAC) as a structure-directing agent (SDA) together with the obtained extracted amorphous silica. Interestingly, a surface morphology of the hierarchical FAU nanosheets can be easily tuned by changing the SDA content and the crystallization temperature. For example, when increasing the crystallization temperature from 75°C to 85°C, the crystal growth was improved significantly confirmed by means of XRD and SEM. Interestingly, the nanosheets morphologies can be straightforwardly adjusted by changing the SDA content in the range of 0.015-0.045 mole fraction. Moreover, the obtained hierarchical FAU samples exhibit outstanding catalytic properties for the hydrogenation of alkylphenols compared with the conventional materials.

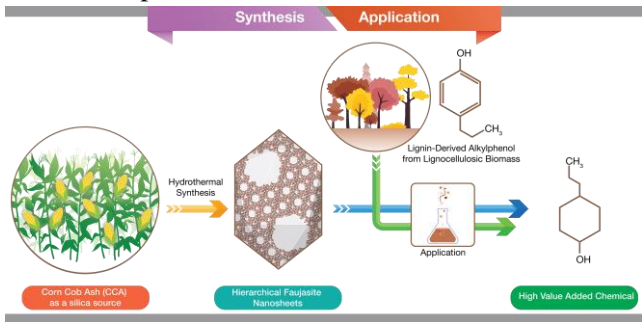


Figure 1. Schematic illustration of the synthetic process for hierarchical faujasite nanosheets using green renewable resources as silica source and its application.

- 1) P. Thuadaij, and A. Nuntiya, Procedia Engineering. 2012, 32, 1026-1032.
- 2) R.M. Mohamed, I.A. Mkhalid, and M.A. Barakat, Arabian Journal of Chemistry. 2015, 8.1, 48-53.
- 3) T. Yutthalekha, C. Warakulwit, C. Wattanakit, W. Wannapakdee, K. Rodponthukwaji, T. Witoon, J. Limtrakul,
- J. Clean Prod. 2016, doi: 10.1016/j.jclepro.2016.08.001.
- 4) E.A. Okoronkwo, P.E. Imoisili, S.O.O Olusunle, Chemistry Materials Research. 2013, 3, 68-72.

Ethylene production from dehydration of bioethanol over MFI zeolite nanosheets

Sirawit Shetsiri¹, Wannruedee Wannapakdee¹, Saros Salakhum¹, and Chularat Wattanakit^{1*}

¹Department of Chemical and Biomolecular Engineering, School of Energy Science and Engineering, Vidyasirimedhi Institute of Science and Technology, Rayong 21210, Thailand.

*Email of presenting Author: s15_sirawit.s@vistec.ac.th

ABSTRACT

The bioethanol dehydration via solid acid catalysts such as zeolites and heteropoly acid catalysts is one of the most important ways to produe the ethylene as the important intermediate for petrochemical industry. Although a conventional MFI zeolite has been widely used in the process, it often suffers from the mass transfer limitation, exhibiting low activity and high coke formation rate. To overcome these problems, the hierarchical MFI zeolite nanosheet can be applied. In this work, hierarchical MFI zeolite nanosheets having various Si/Al ratios have been successfully prepared by a hydrothermal synthesis using tetra(*n*-butyl) phosphonium hydroxide (TBPOH) as a dual template. The designed hierarchical zeolites exhibit the preferable physicochemical properties with an increase of mesoporosity (~30 %) compared with a corresponding commercial zeolite. To demonstrate the application of hierarchical zeolite in the bioethanol conversion, the catalytic tests were carried out using a fixed-bed reactor at 350-450 °C under an atmospheric pressure. The hierarchical MFI exhibits the superior catalytic activity with yielding light olefins over 80% due to their hierarchical structure that can greatly improve the mass transfer limitation and the thermal stability of catalysts. Furthermore, the effect of Si/Al ratios of hierarchical zeolites on catalytic mechanisms will be systematically discussed.

Keywords: Ethylene, Bioethanol, MFI nanosheets

One-pot synthesis of novel hierarchical bifunctional Ga/HZSM-5 nanosheets for propane aromatization

Wannaruedee Wannapakdee, ¹ Chularat Wattanakita^{1,*}, Veerachart Paluka², Thittaya Yutthalekha^{1,2} and Jumrus limtrakul¹

 ¹Department/Research Institute, University, Country a Department of Chemical and Biomolecular Engineering, School of Energy Science and Engineering, Vidyasirimedhi Institute of Science and Technology, Rayong 21210, Thailand.
 ²Department of Chemistry and NANOTEC Center for Nanoscale Materials Design for Green Nanotechnology, Kasetsart University, Bangkok 10900, Thailand

*Corresponding author: chularat.w@vistec.ac.th

Scientific topic: 1) Green Energy, 2) Green industrial processes and Molecular innovation

Keywords: Hierarchical zeolite, Galloaluminosilicate zeolite, Natural gas

Abstract

Natural gases (i.e., methane, ethane, propane, etc.) have been discovered in large quantities throughout the world. The conversion of natural gases to high value-added chemicals can be more economically sustainable. One technique for converting natural gases has been achieved by a zeolite -based process as green catalyst (i.e. non-toxic, environmentally friendly). Herein, we have been successfully prepared H-galloaluminosilicate (MFI) zeolite nonosheets by using a tetrabutylphosphonium ion (TBPOH) in a one-pot reaction via a hydrothermal synthesis. A molecular highway mesoporous structure has been created due to the house-of-card assembly of nanosheets^{1,2}, resulting in a decrease of the microporous diffusion length and an increase of the external surface area. The obtained samples were characterized by means of X-ray diffraction (XRD), Scanning Electron Microscopy (SEM), Transmission Electron Microscopy (TEM), N₂ sorption technique, NH₃ Temperature Programmed Desorption (NH₃-TPD) and ²⁷Al NMR spectroscopy. Because of the benefits of bifunctional metalloaluminosilicate zeolites compared with an aluminosilicate zeolite, for example, the presence of Ga active sites leads to high selectivity of the dehydrogenation and reduction of a coke formation, the catalytic performances of the H-galloaluminosilicate (MFI) zeolite nonosheets can be greatly improved for the conversion of natural gas in terms of the activity and the stability of catalysts.

- [1] X. Zhang, D. Liu, D. Xu, S. Asahina, K. A. Cychosz, K. V. Agrawal, Y. Al Wahedi, A. Bhan, S. Al Hashimi, O. Terasaki, M. Thommes and M. Tsapatsis, Science, 2012, 336, 1684–1687
- [2] W. Wannapakdee, C. Wattanakit, V. Paluka, T. Yutthalekha and J. Limtrakul, RSC Adv., 2016, 6, 2875-2881

Novel Design of FAU@ ZIF-8 Composite in Core/Shell Structures via a Layer-by-

Layer Method

D. Suttipat¹, S. Bureekaew¹, W. Wannapakdee¹, and C. Wattanakit¹*

¹ Department of Chemical and Biomolecular Engineering, School of Energy Science and Engineering, Vidyasirimedhi Institute of Science and Technology, Rayong 21210, Thailand.

*Corresponding author: Chularat.w@vistec.ac.th

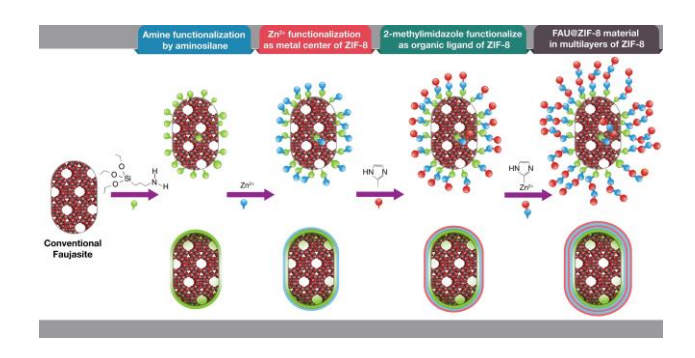
Scientific topic: 1) Green industrial processes and Molecular innovation, 2) Green Materials

Keywords: Zeolite, Metal Organic Framework, Zeolite@MOF composite, Core/Shell structure

Abstract

The novel composite of faujasite and zeolitic imidazolate framework (FAU@ZIF-8) in core/shell structures has been successfully prepared via a layer-by-layer method. The ZIF-8 nanospheres were attached on the external surfaces of the amine-grafted FAU crystals. The synthesized FAU@ZIF-8 composite was characterized by means of XRD, FT-IR, TGA, SEM, TEM, N₂ adsorption technique, NH₃-TPD and CA equipment. Compared to the direct growth of MOF materials on the zeolite surfaces [1-4], the ZIF-8 particle size and the thickness of shell obtained by this method can be easily controlled by adjusting the number of deposited MOF layers. For example, a size of ZIF-8 nanospheres is approximately 37 nm when a number of deposited MOF layers are 15 layers. The novel designed FAU@ZIF-8 composite can also enhance the hydrophobicity of zeolite surface due to the MOF surface-layer characteristics whereas its acidity does not significantly change. This first example demonstrates the simple and controllable synthesis method of zeolite@MOF composite and it is expected to be useful for the aqueousphase reactions which are green chemistry.

Scheme 1. Schematic illustration of the synthetic process for FAU@ZIF-8 composite obtained by a



layer-by-layer method.

References

[1] G. Zhu, R. Graver, L. Emdadi, B. Liu, K. Y. Choi and D. Liu, RSC Adv. 2014, 4, 30673-30676.

- [2] T. Zhang, X. Zhang, X. Yan, L. Lin, H. Liu, J. Qiu and K. L. Yeung, Catal. Today 2014, 236, 41-48.
- [3] G. Zhang, T. Zhang, X. Zhang and K. L. Yeung, Catal. Commun 2015, 68, 93-96.
- [4] F. Gao, Y. Li, Z. Bian, J. Hu and H. Liu, J. Mater. Chem. A **2015**, 3, 8091–8097.

CHIRAL RECOGNITION AND ASYMMETRIC SYNTHESIS AT MESOPOROUS CHIRAL METAL SURFACES

<u>Chularat Wattanakit^{1,2}</u>, Thittaya Yutthalekha², Veronique Lapeyre¹, Somkiat Nokbin³, Chompunuch Warakulwit³, Jumras Limtrakul² and Alexander Kuhn^{1*}

¹Univ. de Bordeaux, CNRS, ISM, UMR 5255, Pessac, France ²Vidyasirimedhi Institute of Science and Technology, Rayong 21210, Thailand ³Department of Chemistry, Faculty of Science, Kasetsart University, Bangkok 10900, Thailand

e-mail: chularat.w@vistec.ac.th

Keywords: Enantioselective recognition, Asymmetric synthesis, Mesoporous chiral metal

The development of materials with chiral features is a major scientific challenge due to a large number of potential applications ranging from sensing to catalysis and separation. Although the molecular imprinting approach has been successfully employed using polymers for generating materials with enantioselective properties, it is particularly difficult to synthesize chiral metal matrices by this method. We report here the elaboration of chiral imprinted mesoporous metal, obtained by the electrochemical reduction of platinum salts in the simultaneous presence of a liquid crystal phase and chiral template molecules [1, 2]. The chiral encoded mesoporous metal perfectly retains the chiral information after removal of the template and shows a very significant discrimination between two enantiomers when using these materials as electrodes in Differential Pulse Voltammetry. Interestingly, such nanostructured metals are also able to break the symmetry during the electrochemical synthesis of mandelic acid as model molecule [3]. It was found that the R/S ratio of the synthesis product is higher than unity when using (R)-imprinted electrodes and vice versa for the (S)-imprinted ones. In order to illustrate the general validity of this approach, we were able to extend the concept also to other chiral template molecules, which lead to chiral encoded nanostructures. Therefore these designer surfaces open new horizons not only for electroanalysis and separation science, but also for enantioselective electrosynthesis.

- [1] C. Wattanakit, Y. Bon Saint Côme, V. Lapeyre, P. A. Bopp, M. Heim, S. Yadnum, S. Nokbin, C. Warakulwit, J. Limtrakul, A. Kuhn, *Nat. Comm.* 2014, 5:3325.
- [2] T. Yutthalekha, C. Warakulwit, J. Limtrakul, A. Kuhn, Electroanalysis, 2015, 27: 2209.
- [3] T. Yutthalekha, C. Wattanakit, V. Lapeyre, S. Nokbin, C. Warakulwit, J. Limtrakul, A. Kuhn, *Nat. Comm.* 2016, 7:12678.